Diffusion and perfusion magnetic resonance imaging in human ischaemic stroke – analysis strategies and measurement issues in the assessment of lesion evolution

Carly Shaen Rivers

PhD Clinical Neuroscience

The University of Edinburgh

2005

EX DIST. UNIV. EDINBURGH

Declaration

I hereby declare that:

- I composed this thesis
- I made a substantial contribution to the work: I co-developed the analysis strategies with Professor J. Wardlaw, I performed the literature reviews, I performed the lesion measurements, and analysed and interpreted the lesion measurement data in conjunction with patient demographic data where appropriate. Dr. P. Hand and Dr. V. Cvoro recruited, examined, and performed clinical assessment and follow-up of the patients in this study. Dr. P. Armitage, Dr. M. Bastin, and Dr. T. Carpenter developed the image processing algorithms and processed the magnetic resonance imaging data. Dr. P. Armitage also wrote the code for the grid-based analysis program.
- This thesis has not been submitted for any other degree or professional qualification

Signed:

Acknowledgements

I would like to thank the Royal Society of Edinburgh and the Lloyds TSB Foundation for Scotland for their generous funding of my PhD. The source of funding for the imaging studies was the Chief Scientist Office for Scotland. I am grateful to all the patients who took part in this study.

I received invaluable help and guidance from the members of the Division of Clinical Neurosciences, particularly the members of the SHEFC Brain Imaging Research Centre. I thank Dr. P. Hand and Dr. V. Cvoro for recruiting and assessing the patients in this study, and the radiographers – Mrs. A. Blane, Mrs. E. Cowie, Ms. L. Cunningham, Ms. T. Eiffe, and Ms. K. Gee – for performing the imaging and providing help with organising the patient data. I thank Mr. L. Murray and Ms. A. Deary for their administrative support, and Ms. S. Lewis for her statistical advice. Dr. P. Armitage, Dr. M. Bastin, and Dr. T. Carpenter developed and performed the MR data processing, have always helped me to understand the finer points of DWI and PWI, and have prevented me from single-handedly rewriting the laws of physics. Dr. P. Armitage designed the SGAT lesion analysis program, for which I am grateful (though not for the suggestion of voxel-by-voxel analysis).

I would especially like to thank my supervisors: Dr. Mark Bastin, who has always willingly answered my many questions and provided invaluable feedback; and Professor Joanna Wardlaw, who has been a source of ideas, answers, inspiration, motivation, and personal support.

for mom, dad, and uncle dave from the blm

Abstract

Stroke is the third most common cause of death in the developed world, and is the major cause of long term disability in the U.K. Eighty percent of strokes are ischaemic, or caused by vascular occlusion. Magnetic resonance imaging (MRI) provides stroke researchers with an invaluable tool to visualise ischaemic processes non-invasively from very early times after stroke onset. However, despite major progress, it is still unclear to what degree particular appearances on MRI relate to the underlying pathophysiological state of the ischaemic lesion, or the clinical outcome of the stroke patient.

The aim of this thesis is to explore the evolution and issues affecting the analysis of ischaemic lesions on diffusion- and perfusion-weighted MRI (DWI and PWI) from acute (< 24 hours) to chronic (90 days) times after stroke onset. This thesis includes a review of previous human studies of acute DWI and PWI appearance versus final lesion outcome, a review of the 'DWI/PWI mismatch' model (thought to represent the ischaemic penumbra, or 'tissue at risk' of infarction), and a systematic review of previous animal studies of the pathophysiology associated with particular lesion appearances on DWI.

The methodological problems raised by these reviews are addressed in this thesis using a large cohort of stroke patients with serial DWI and PWI. The interrater variability of manual lesion measurements on acute DWI is investigated, and factors affecting this variability are discussed. The effect of lesion oedema (swelling) on measurements of ischaemic lesions on MRI is investigated. This thesis also investigates the tissue state underlying persistent hyperintensity on late DWI, and whether this is just T_2 'shine through', or indicates distinct features in the evolution

of the lesion. A novel grid-based analysis method is developed and employed to track serial DWI and PWI changes more effectively, and the effect of observer variability on diffusion and perfusion parameters measured by this method is assessed. Lastly, this thesis discusses the concept of using 'threshold' values to predict tissue infarction or survival.

Note – The scans reproduced in this thesis are represented in conventional medical imaging format, i.e. with the patient's right on the left, and left on the right.

Table of Contents

Table of Figures

Table of Tables

1. Introduction

Aim of thesis

The aim of this thesis is to explore the evolution and issues affecting the analysis of ischaemic lesions on diffusion- and perfusion-weighted magnetic resonance imaging (DWI and PWI respectively) from acute (< 24 hours) to chronic (90 days) times after stroke onset using a large group of patients with serial DWI and PWI scanning data.

Scope of thesis

This thesis is organised into 12 chapters:

Chapter 1 provides background information on ischaemic stroke, including clinical features, causes, pathophysiology, and treatment. The basic principles of magnetic resonance imaging (MRI) are also reviewed.

Chapter 2 discusses the appearance of ischaemic lesions on DWI and how they are measured. Problems with measuring lesions on DWI, including ill-defined lesions, T_2 'shine through', and tissue swelling are discussed. The use of the 'DWI/PWI mismatch' and thresholds of DWI and PWI values to identify 'tissue at risk' of infarction are examined. The issues raised in Chapter 2 form the basis of subsequent analyses in the thesis.

Chapter 3 comprises of a systematic review of the use of DWI and PWI in animal models of ischaemic stroke, investigating what particular appearances on DWI mean in terms of the underlying pathophysiology of ischaemic tissue.

Chapter 4 presents the methods for the recruitment, imaging, and basic lesion measurement of the large cohort of patients used for the analyses in this thesis.

Results of basic lesion analysis, including DWI and PWI parameter values from the visible DWI and PWI abnormalities from baseline (< 24 hours after stroke onset) to final (90 days after stroke onset) imaging are presented.

Chapter 5 assesses factors that affect lesion volume measurement on DWI by examining the differences in measured lesion volumes between two observers, and how the differences relate to lesion morphology and observer experience.

Chapter 6 explores which baseline PWI parameter, if any, identifies 'tissue at risk' of infarction, and whether the presence of an acute 'DWI/PWI mismatch' as discussed in Chapter 2 is related to lesion growth.

Chapter 7 investigates ischaemic lesion regions that remain hyperintense on late (≥ 30 days after stroke onset) DWI, and whether these regions are merely the effect of T_2 'shine through' as discussed in Chapter 2, or if they indicate important underlying differences in the pathophysiology of the ischaemic tissue.

Chapter 8 consists of the development of a novel grid-based method to investigate regions of heterogeneity of DWI and PWI parameters within ischaemic lesions. A manual grid-based analysis method is developed and tested in a small group of patients to determine if different degrees of abnormality on baseline DWI indicate different degrees of underlying tissue damage.

Chapter 9 concerns the development of a more efficient grid-based analysis program for analysis of a larger sample of patients. The effect of observer differences on lesion volume and extracted DWI and PWI values from lesion analysis with the grid-based program is assessed.

Chapter 10 investigates the evolution of DWI and PWI parameters in ischaemic lesions in a large group of patients, including whether differences in lesion

appearance on baseline DWI are associated with differences in underlying DWI and PWI parameter values using the grid-based analysis method as developed and tested in Chapter 9. Differences in DWI and PWI parameter values at baseline and over time between patients whose lesions grow, stay the same size, or shrink between baseline and final imaging are also assessed.

Chapter 11 investigates both general and localised tissue distortion due to swelling and tissue cavitation after ischaemic stroke. A novel swelling analysis program is developed and tested to quantify tissue distortion at key stages after onset of ischaemic stroke.

Chapter 12 is a summary and discussion of the results of this thesis.

Introduction

The rest of this chapter presents background information on ischaemic stroke and the basic principles of MRI.

What is 'stroke'?

Stroke is defined as a sudden onset of neurological deficit, often manifested as hemiparesis or hemianaesthesia, and/or loss of higher cerebral functions such as speech or spatial awareness, caused by cerebral haemorrhage or ischaemia[1,2]. A stroke is further defined as causing symptoms that last longer than 24 hours,

distinguishing stroke from a transient ischaemic attack (TIA), where stroke-like symptoms resolve within 24 hours of onset[3].

Although the correct mechanism of stroke (as a disorder of the blood vessels) was not determined until the late 17th century, being variously attributed to causes like a blow to the head, an imbalance of the 'humours', and fright, the disease itself has been described since ancient times[3,4]. Hippocrates (460 - 370 B.C., Figure 1.1) described apoplexia, literally 'to strike down' in ancient Greek[4], as an affliction characterised by numbness and anaesthesia particularly affecting people between the ages of 40 - 60 years[5]. Hippocrates noted that 'to get over a strong attack is impossible, over a weak one, not easy'[4], still poignant today where 1/3 of the annual 15 million stroke sufferers worldwide die, and 1/3 remain dependent on others for daily care[6].

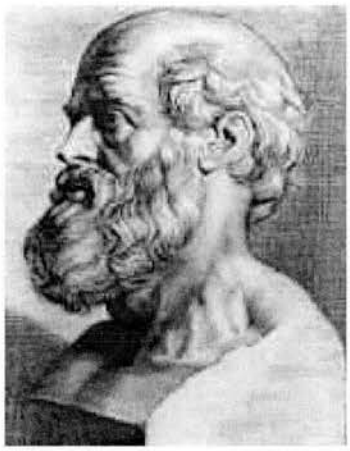

Figure 1.1 Hippocrates (460 – 370 B.C.)

What is the burden of stroke?

Stroke remains the third most common cause of death in developed countries, and is the major cause of long term disability in the UK[6]. Stroke causes 10% of all deaths worldwide, and carries a heavy economic burden. Approximately 4% of the National Health Service spending in the UK goes towards stroke services, covering the care costs for both short and long term follow-up care for stroke patients. Furthermore, short and long term disability of patients after stroke puts immense pressure on family members and society[6].

How prevalent is stroke?

Epidemiology

The incidence of stroke rises sharply with age, affecting only 0.1 - 0.5 per thousand people under the age of 55, rising to 10 - 20 per thousand people over the age of 75[8]. Men and women are equally affected by stroke; men are slightly more likely to have a stroke in younger age groups, and women more likely to have a stroke in older age groups (probably due to the increasing percentage of women in older populations caused by the younger average age of mortality of men)[8]. Stroke, unlike other cardiovascular diseases such as ischaemic heart disease, is prevalent in both developing and developed countries, but is particularly problematic in developed countries[6,8]. In the developed world, regional and ethnic differences in stroke incidence occur, with areas in Finland, Japan, and Scotland showing high rates of

incidence, which have been attributed to factors such as cold winters, low economic status, and a high proportion of people with the known risk factors for stroke[8,9].

The diagnosis of 'stroke' currently includes patients presenting with clinical signs of cerebral ischaemia, intracerebral haemorrhage, and subarachnoid haemorrhage[10]. Ischaemic stroke results from vascular occlusion and is the cause of approximately 80% of strokes[11,12]. Intracerebral haemorrhage, caused by bleeding in the brain parenchyma, and subarachnoid haemorrhage, caused by bleeding in the sub-arachnoid space, cause approximately 15% and 5% of strokes respectively[3,11,12]. This study will focus on ischaemic stroke and will not consider strokes caused by intracerebral and subarachnoid haemorrhages further.

Risk factors

Previous stroke (or TIA) represents the biggest risk factor for ischaemic stroke, with 10 - 15% of all strokes being recurrent[8]. High blood pressure is another strong risk factor; it is estimated that 4/10 deaths caused by stroke could have been prevented with blood pressure management[6]. Other common risk factors echo those for other cardiovascular diseases, including diabetes, high blood cholesterol levels, high salt intake, obesity, and smoking[6,9].

Clinical features of stroke

The presentation of an acute stroke depends on where in the cerebral circulation the blockage has occurred. Stroke patients present with varying degrees of focal neurological symptoms: motor symptoms such as weakness and imbalance; speech

and language disturbances such as slurred speech or difficulty reading; sensory symptoms such as numbness or visual disturbances; and often general confusion and forgetfulness[2]. Because of the functional organisation of the brain, it is possible to pinpoint the probable location of the arterial blockage[2], however due to the complexity of the brain, infarcts are usually initially classified as syndromes of symptoms that point to the likely affected arterial territory[3,13]. For example, ischaemia of the dominant frontal cortex (associated with speech and language) usually causes expressive aphasia, leading clinicians to diagnose ischaemia of the middle cerebral artery which supplies this area of the brain[2].

Causes of ischaemic stroke

Cerebral ischaemia, or ischaemic stroke, is caused by occlusion of an intracerebral artery, usually by thrombosis or an embolism[9]. Ischaemic stroke has three main causes, large artery atherothromboembolism, cardiac emboli, and intracranial small vessel disease[3].

Atherothromboembolism

Atherothromboembolism, the cause of approximately 50% of ischaemic strokes, results from atheroma of large and medium sized intracranial and extracranial arteries[3]. Atheroma develops over long periods of time, from the early formation of fatty streaks through a long term process of injury to the endothelium that ultimately results in the thickening of the vessel wall (and thus narrowing of the vessel) caused by fibrolipid plaque formation[3]. Thrombosis occurs when a plaque grows to occlude

the vessel completely, or ruptures, presenting an acutely thrombogenic surface to the blood[3]. Embolism occurs when fragments of atheroma or emboli forming at the plaque surface dislodge from the plaque surface and travel through the circulation to become lodged in a smaller vessel in the brain[3].

Cardiac emboli

Emboli from the heart that travel into the cerebral circulation and occlude a cerebral vessel account for about 20% of ischaemic stroke cases[3]. Emboli from the heart vary greatly in age, size, and composition (e.g. fibrin, calcium, platelets)[3]. There is some evidence that cardiac emboli are more likely to cause larger cortical infarcts versus (vs.) smaller cortical infarcts[3]. Some patients may have cardiac as well as large artery embolic sources.

Intracranial small vessel disease

Intracranial small vessel disease accounts for approximately 25% of ischaemic stroke cases[3]. The cause of intracranial small vessel disease is subject to much debate, but many attribute it to intrinsic changes and abnormalities of small vessels, which often cause lacunar ischaemic lesions[3]. Lacunar infarctions are rarely fatal, and may go undetected clinically[3]. As this work will focus on large artery stroke, lacunar infarctions will not be discussed further, although the same principles discussed in this thesis may apply to the study of lacunar ischaemic lesions.

Other causes

The causes of the last 5% of ischaemic stroke are varied and include cancer, vasospasm, trauma, snakebites, and complications of pregnancy, but these are rare, and will not be discussed further[3].

Pathophysiology of ischaemic stroke

Ischaemic stroke causes a decrease or cessation of blood flow to the part of the brain supplied by the affected artery[3]. Cerebral ischaemia eventually leads to cell death in the affected area, termed infarction, if the affected part of the brain is not adequately supplied by collateral blood supply or blood flow is not quickly restored[14]. The severity of a stroke depends on the volume, and to some extent the location, of brain tissue affected. In the past, all tissue in the territory of the affected artery was thought to die immediately after the onset of ischaemia. However, it is now clear that there are stages of blood flow decline, and some cells may survive for periods of decreased blood flow.

Despite comprising only 2% of the body's mass, the brain uses about 20% of the blood oxygen used by the body[9]. The brain uses only glucose and oxygen for fuel, and their consumption is closely coupled to the density of neurons and functional activity of the tissue. Via the Krebs cycle[15], cells use oxygen and glucose to produce adenosine triphosphate (ATP), the energy source for vital cell processes, and the by-products carbon dioxide and water.

Despite the high energy consumption of the brain, glucose reserves in the brain are only sufficient for about one minute, so continuous delivery of glucose and oxygen via the cerebral circulation is required to keep the brain functioning normally[9]. Although the brain is vulnerable to disturbances in blood flow, there are several 'safety mechanisms' that can protect the brain from damage.

Autoregulation of cerebral blood flow

The arteries of the cerebral circulation have an autoregulatory capacity to maintain the cerebral perfusion pressure when cerebral blood pressure is decreased[14].

Decreases in systemic blood pressure cause cerebral vasodilation in an attempt to maintain the cerebral blood flow (CBF) and thus delivery of oxygen and glucose to the tissue. However, the capacity for vasodilation is finite, and when the blood pressure is decreased below a certain level (systemic pressure of approximately 50 mmHg, Figure 1.2), the CBF becomes pressure-passive and falls with further reduction in blood pressure, and the brain may not receive enough oxygen and glucose to operate properly[9,14]. Maximal vasodilation for a period of time can cause vasoparalysis, where the autoregulatory capacity of the artery fails and oxygen extraction is decreased despite increased blood flow (termed 'luxury perfusion', i.e. blood flow in excess of oxygen demand)[9,14].

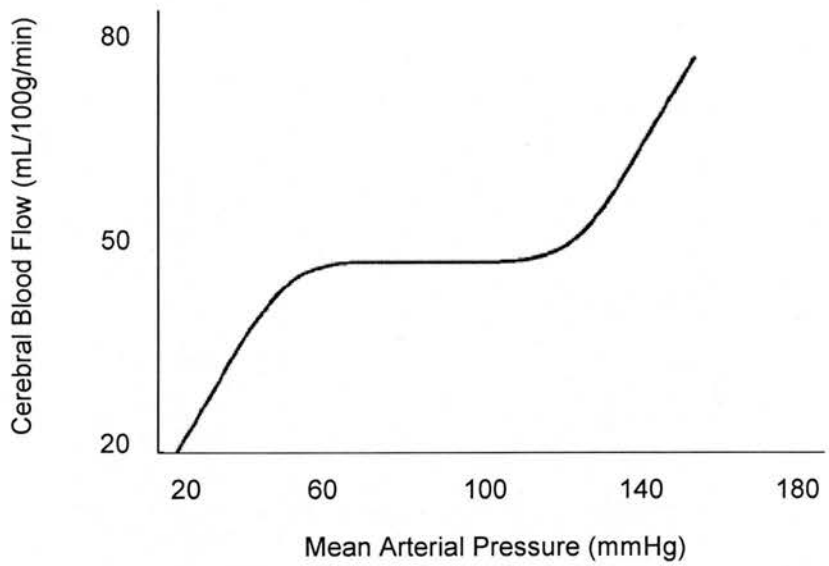

Figure 1.2 Cerebral autoregulation.

Collateral blood supply

Focal disturbances in CBF due to arterial abnormality may be reduced by the presence of collateral blood supply whereby a neighbouring artery can supply an

adjacent arterial territory that is under ischaemic stress[14]. However, collateral potential varies between individuals, and may not be adequate to supply more than the periphery of an ischaemic territory so that the tissue at the core of the arterial territory still becomes infarcted[9,14].

Tissue death is no longer considered an instant process after an ischaemic insult. If autoregulation or collateral blood flow are insufficient to support the tissue undergoing the ischaemic insult, the cells of the brain can still survive by reverting to vital maintenance functions only, sacrificing electrical 'functional' activity for 'survival' activity.

The 'ischaemic cascade'

Electrical failure

Remarkably, the brain can withstand reductions in blood flow of about 40% of normal (approximately 20 mL/100g/min) before it starts to be adversely affected[14]. At this first critical blood flow threshold of approximately 40% of normal (Figure 1.3), ATP can be produced in small quantities anaerobically, but this yields much less ATP than normal aerobic production so a reduction of energy expenditure is required[7].

The affected area of the brain begins to shut down electrical activities such as spontaneous action potentials (observable by the absence of electroencephalogram activity) in an attempt to conserve energy for vital cell processes[14]. The reduced ATP energy supplies are used to maintain an ion homeostasis that produces the membrane

potential (meaning the cell is still viable) by powering the ion pumps that actively pump sodium ions out of the cell and potassium ions into the cell[15]. At this stage, cell death is not inevitable; restoration of blood flow will result in a return to normal cell function[9]. There is currently some question on how long brain cells can remain viable in this state of 'suspended animation'; animal studies have shown that even short periods of ischaemia (e.g. 30 minutes of vascular occlusion) cause cell death[16-19].

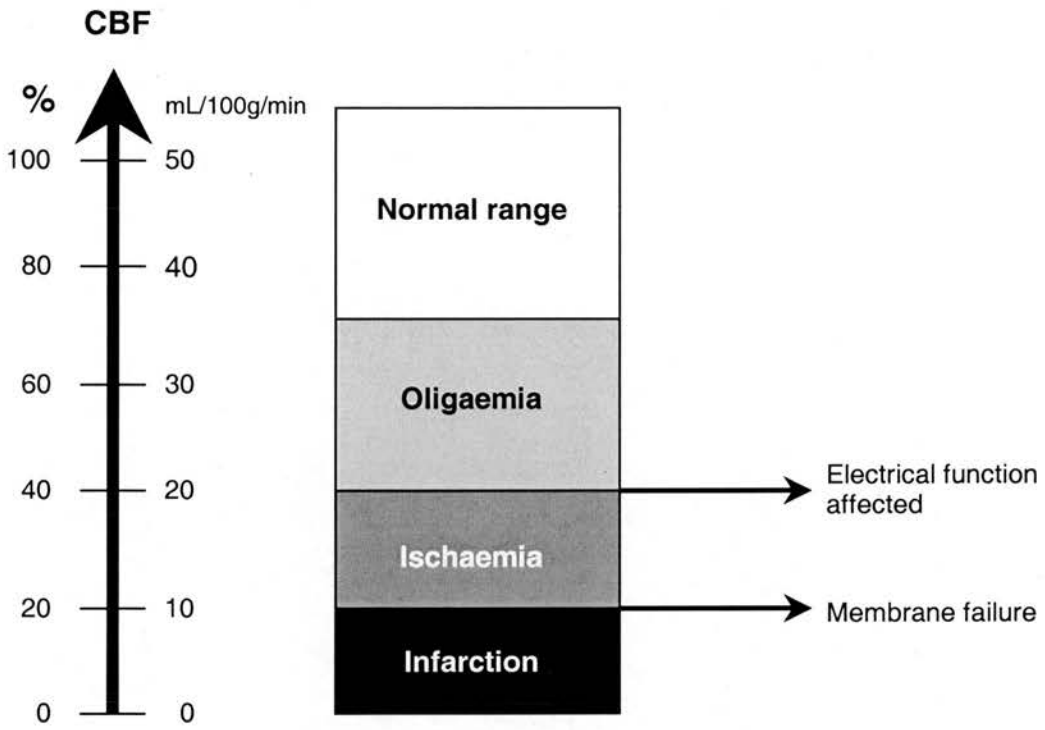

Figure 1.3 Approximate ischaemic blood flow thresholds. Adapted from Astrup et al.[7]

Energy failure

Further CBF decreases to ≤ 20% of normal blood flow (approximately 10 mL/100g/min) causes energy failure: ATP supplies deplete rapidly, and a massive increase in extracellular potassium ions indicates failure of the ion pumps and

subsequent ion homeostasis disruption (Figure 1.3)[7]. The failure of the ion pumps causes sodium, calcium, magnesium, and hydrogen ions to accumulate in the cell, instigating ionic imbalance and acidosis in the cell. Furthermore, anaerobic ATP production yields lactic acid, which accumulates and causes intracellular and extracellular acidosis[15]. The cell's attempts to regulate its lowered intracellular pH, together with the failure of ion pumps, causes a massive influx of sodium ions into the cell. There is a subsequent influx of water into the cell via osmosis from the extracellular space, causing cytotoxic oedema[3,9].

Cell death

Failure of the membrane potential for any amount of time begins a cascade that will result in cell death, whether by necrosis or apoptosis[7]. The increased intracellular concentration of calcium ions cause the release of toxic concentrations of excitatory neurotransmitters such as glutamate and aspartate[20], as well as activating proteases that lyse the structural proteins of the cell membrane and facilitate the release of free radicals that further damage membrane lipids[20]. Increased intracellular calcium ion concentrations appear to be the key factor in the initiation of necrosis[3]. In parallel with cell death by necrosis, active cell death, or apoptosis, is triggered in some cells[3]. Lowered intracellular calcium ion and increased zinc ion concentrations appear to favour apoptotic cell death, but there is a continuum of necrosis and apoptosis in ischaemic tissue[3]. If ischaemia continues even longer, the membranes of the blood-brain barrier (BBB) become compromised and allow plasma constituents to leak into the extracellular space, causing vasogenic oedema[9]. Once damage to the BBB has occurred, the risks of reperfusion causing further injury rather than being beneficial may rise considerably[9].

The 'ischaemic penumbra'

It is not just the severity of blood flow interruption, but also the length of time that the blood flow is compromised that determines the fate of the affected tissue. The 'ischaemic penumbra', or area at risk of infarction, captures the notion that brain tissue may be saved from death if blood flow can be restored in time, either by spontaneous reperfusion or medical intervention. The concept of the 'ischaemic penumbra' was first postulated by Astrup et al.[21] in 1981, and is defined as a region of tissue with compromised CBF that is not yet dead surrounding an inner core of irreversibly damaged tissue (Figure 1.4). Schematically, the 'ischaemic penumbra' is thought of as a 'shell' of tissue surrounding the 'core' of the infarct (Figure 1.4), but it is likely these regions are patchy and unevenly distributed in the infarct. It is this tissue that is the focus of much stroke research: how can we identify this 'tissue at risk' and salvage it from infarction?

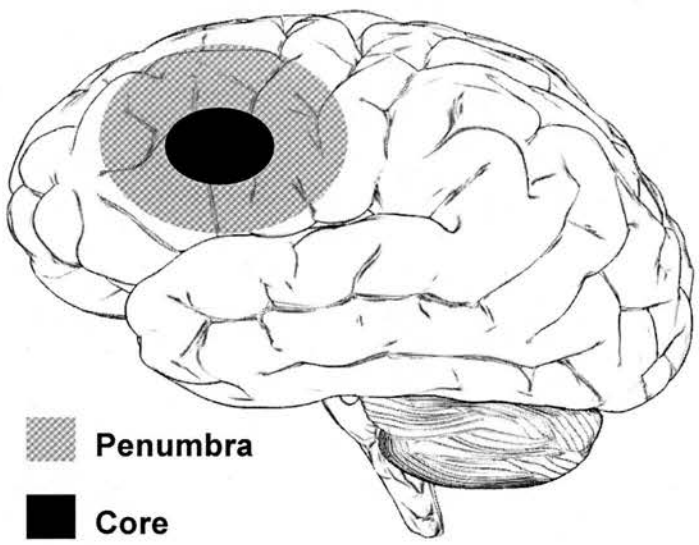

Figure 1.4 Schematic diagram of the ischaemic penumbra. Note the penumbra is not considered to necessarily be an even 'shell' around an infarct core.

Treatments for stroke

There are many preventative treatments that reduce the risk of ischaemic stroke, such as lowering blood pressure and cholesterol and antithrombotic drugs like aspirin, which remains the cheapest drug available worldwide for stroke prevention[22]. Clinicians have a number of available acute treatments for ischaemic stroke, however, many of these require further clinical trials to confirm benefit and safety. Ideally, an acute stroke treatment should clearly reduce mortality and long term disability and be safe to administer to all stroke patients[22]. No treatment currently fulfils all these ideals, although aspirin is a well established and widely used treatment - having modest effects but being safe for most ischaemic stroke patients[3]. Unproven therapies such as neuroprotective compounds, calcium antagonists, and haemodilution require further large clinical trials to provide proof of benefit and safety, although it is likely that these therapies will only be useful and safe in small subgroups of patients[3]. Currently the most promising therapy being tested in several large clinical trials is treatment with thrombolytic or 'clot-busting' agents[3].

Thrombolytic agents

Intravenous thrombolytic agents, such as recombinant tissue plasminogen activator (rtPA), lyse thrombi and improve clinical outcome[23]. However, thrombolytic agents carry a high risk of intracerebral haemorrhage for some patients, so rtPA administration must be selective and patients must be rigorously monitored - further large clinical trials are ongoing to improve patient selection[3]. Currently, licensing guidelines for rtPA mean that only highly selected suitable patients that arrive at the hospital within 3 hours of stroke onset may be treated with rtPA, although some trials are currently testing the benefit of rtPA up to 6 hours after stroke onset[24]. Newly

developed plasminogen activators, including desmoteplase (engineered from the saliva of the vampire bat) are said to be more fibrin specific, dissolving clots locally without affecting the blood clotting mechanisms, theoretically lowering the risk of haemorrhage[25] - but further clinical trials are needed to determine patient benefit and safety. The use of these agents might be improved if it was possible to identify patients with significant amounts of 'ischaemic penumbra', or salvageable 'tissue at risk' of infarction, quickly and accurately.

Imaging in stroke

With the development of computed tomography (CT) imaging by Cormack and Hounsfield in the 1970s, clinicians were provided with a means of non-invasively visualising the brain, leading Cormack and Hounsfield to be awarded the 1979 Nobel Prize in Physiology or Medicine. CT was, and remains, particularly useful in distinguishing cerebral infarction from stroke 'mimics' (e.g. intracranial tumours), and is vital in screening patients for thrombolytic therapy to ensure the absence of haemorrhage[3]. However, the positive signs of ischaemia on CT are less obvious than with DWI, especially for small lesions, so most research interest in stroke imaging is focused on MRI[26,27]. The development of advanced MRI techniques like DWI has given stroke researchers a tool to visualise ischaemic changes within minutes of stroke onset[28].

Magnetic resonance imaging

MRI, in particular DWI and PWI, offers the possibility of determining the underlying pathophysiological state of ischaemic tissue, and thus might lead to the development of possible appropriate therapeutic interventions. In fact, MRI has proven so useful in medicine that Lauterbur and Mansfield, who were foremost in development of ultrafast magnetic resonance (MR) sequences, shared the 2003 Nobel Prize in Physiology or Medicine.

Basic MRI

MRI relies on the physical properties of nuclei, in particular hydrogen nuclei (protons), and their behaviour in the presence of a magnetic field and applied radiofrequency (RF) pulse. At the atomic level, nuclei can be said to spin about their own axes, generating a tiny magnetic field (Figure 1.5)[29].

Protons, and other nuclei sharing the spin quantum number ½, align themselves in one of two orientations in the presence of a magnetic field (B_0; Figure 1.5)[29].

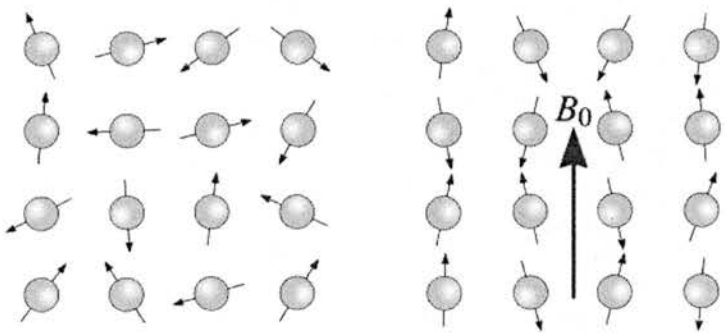

Figure 1.5 Nuclei spin about their own axes and produce a small magnetic moment (left). In the presence of a magnetic field, nuclei align either parallel or antiparallel to the magnetic field B_0 (right).

One orientation is of slightly less energy than the other, so a few more nuclei align in this direction, causing a net magnetisation in the direction of the applied magnetic field (Figure 1.6).

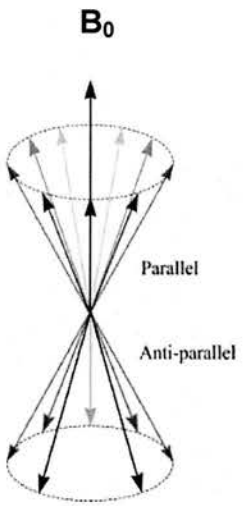

Figure 1.6 Net magnetisation of nuclei.

Nuclei do not align themselves directly parallel or anti-parallel to B_0; instead they precess, or follow a circular path about B_0 (Figure 1.7) with a characteristic angular frequency, called the Larmor frequency (ω)[29].

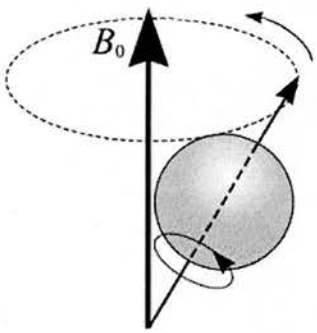

Figure 1.7 Precession of nuclei about the magnetic field B_0.

ω is proportional to the strength B_0 multiplied by a 'gyromagnetic ratio' (γ) that is constant for any particular type of nuclei, like protons, as described by the Larmor equation[29]:

$$\omega = B_0 \gamma$$

With the application of a RF pulse of frequency ω, the net magnetisation can be tilted into a different plane, after which the magnetisation will return, or *relax*, to its original value[29]. Two important 'relaxation' times can be measured as the tilted magnetisation both recovers along the original direction of magnetisation (T_1 relaxation time) and decays along the perpendicular direction of magnetisation (T_2 relaxation time). Due to magnetic field inhomogeneity, nuclei in different places in the sample will experience a slightly different magnetic field strength, making them precess at different frequencies, causing phase differences (T_2*). These phase differences can be 'refocused' using a further 180° RF pulse, which flips the dephased precessions and focuses them back into a single signal, called a spin echo (SE) which can then be detected by a receiver coil (Figure 1.8).

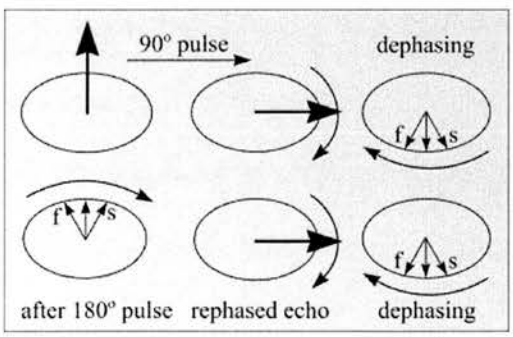

Figure 1.8 Refocusing of dephased spins. f = fast, s = slow.

A pulse sequence comprising of a combination of several RF pulses at a particular repetition time (TR) and time to echo (TE) allows for some amount of control of the

contrast between tissues. To select a 'slice' through the sample, a magnetic field gradient can be set up by supplying current to two coils inside the scanner. This gradient causes one end of the magnet to have a slightly higher field strength than the other, meaning only a narrow area of the sample aligned longitudinally to B_0 will respond to a particular RF pulse (as ω of the nuclei will change with distance from, and current supplied to, the gradient coil)[29].

The use of three orthogonal, in-bore magnetic field imaging gradients allows for imaging in three dimensions. Once a 'slice' of the sample is selected with one of the magnetic field imaging gradients, one of the other two gradients is turned on to spatially encode the slice along one axis. A signal of amplitude vs. time is detected in the receiver coil: this signal is called a free induction decay (FID), so named because it decays to zero with a characteristic time constant, T_2^*. To obtain an interpretable signal, a series of FIDs are acquired and mathematically manipulated by a method known as Fourier transformation, which converts the time-dependent FIDs into a frequency-dependent spectrum[29].

Another 'phase encoding' step must be performed to obtain an image of, for instance, 256 × 256 pixels (two-dimensional picture elements). Repeating the pulse sequence 256 times changing only the 'phase encoding gradient' gives 256 signals of different frequencies that can be used to assign a signal intensity (SI) to each pixel, from which a grey-scale image can be created.

SE sequences are used to obtain T_1- and T_2-weighted (T_1W and T_2W respectively) images. In T_1W imaging, tissues with short T_1 relaxation times (e.g. fat) appear bright, while tissues with a long T_1 relaxation time (e.g. cerebrospinal fluid [CSF])

appear dark (Figure 1.9). In T_2W imaging (T_2WI), the signal intensities are reversed, with CSF appearing bright (Figure 1.9).

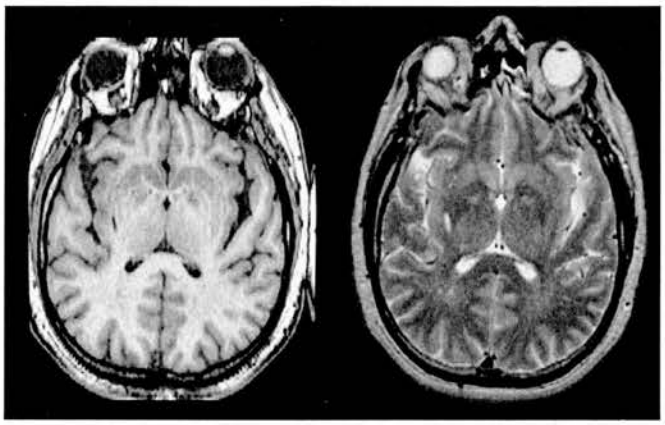

Figure 1.9 Example of T_1W and T_2W images.

In general, T_1W images provide excellent anatomical detail, while T_2W images are frequently used for examination of pathology (Figure 1.9).

Images can be obtained more quickly than standard SE imaging using echo planar (EP) imaging sequences, at the sacrifice of increased signal-to-noise and more image artefacts. However, ultrafast imaging techniques are invaluable in diffusion, perfusion, and functional MRI, as they reduce the influence of motion, can catch rapid responses, and reduce the time that patients are in the scanner.

Diffusion-weighted MRI

Molecules in a sample experience thermal translational random motion, called Brownian motion, which can cause signal loss because phases of different spins vary randomly. This signal loss would seem undesirable, but it can actually be manipulated to provide diffusion-weighted (DW) images (Figure 1.10).

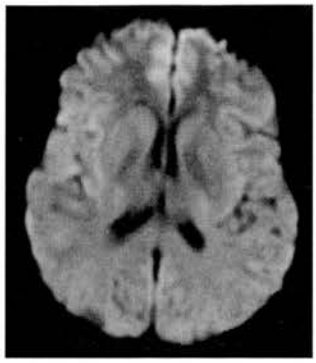

Figure 1.10 Example of a DW image.

In the 1960s, Stejskal and Tanner developed an eponymous sequence to obtain DW images. As the scale of the movement of a water molecule (approximately 60 μm/s) is of the order of the size of cells, differences in the diffusion of water in a sample can inform on the density, integrity, and pathology of the sampled tissue[29]. DWI is achieved by adding strong pulsed magnetic field gradients to a standard SE-EP imaging sequence. These strong pulsed gradients make the images sensitive to small displacements of water molecules, and the 'weighting', or sensitivity of imaging to the diffusion of water, is described by a value known as *b*. The larger the *b*, the stronger the diffusion weighting[30]; T_2W images have a $b \approx 0$ s/mm^2 and receive only a tiny amount (approximately 2%) of signal loss due to diffusion, whereas clinical DW images typically have a $b = 1000$ s/mm^2. The signal (S) in a voxel (three-dimensional volume element) in a DW image is calculated using the signal without diffusion effects (S_0) by the Stejskal-Tanner diffusion equation[31]:

$$S = S_0 \, e^{-b \, ADC}$$

where *e* is the base of the natural logarithm (Euler's constant), and ADC is the apparent diffusion coefficient, which measures the movement of a water molecule due to self-diffusion in a given time, measured in mm^2/s. ADC is termed 'apparent'

as it represents the diffusion of water in biological tissue where water molecules are restricted by cell membranes and fibre tracts. Typical ADC values in the brain range from 0.7×10^{-3} mm^2/s in the corpus callosum to 3.0×10^{-3} mm^2/s in the cerebrospinal fluid[30]. The restriction of water diffusion in biological tissues such as the brain also necessitates sampling diffusion images in three orthogonal gradient directions in order to obtain reproducible, reliable, quantifiable DW images[32]. White matter tracts and other restricting membranes in the brain can cause the diffusion to be anisotropic, or directionally restricted, and the orientation of the pulsed magnetic field gradient in relation to this anisotropic diffusion can influence the appearance of the diffusion images. Therefore, DWI is now commonly performed in three orthogonal directions which are then averaged to obtain an 'isotropic' diffusion image with minimal effects from the anisotropy of the tissue[32]. As ADC values are scalar, they can only describe the magnitude of diffusion. The development of diffusion tensor (DT) imaging, with sampling in at least six gradient directions, allows for the measurement of the directionality of diffusion.

As DWI is exquisitely sensitive to the small diffusional motion of water, it is excellent at visualising some aspects of the pathology of ischaemic stroke, where fluid balance is compromised in acute stages by cytotoxic oedema and in chronic stages by vasogenic oedema. Acute DW images generally show a hyperintense ('bright') lesion against a dark background, which is easier to pick out than dark lesions on a grey background as on ADC images (Figure 1.11). However, there are several downsides to DWI in comparison to more conventional imaging such as T_2WI and CT. Firstly, because DWI is so sensitive to small diffusional motion, it is also subject to image artefacts caused by other types of motion, such as pulsatile

movement in the heart and lungs (though not a problem in the comparatively 'rigid' brain) and gross patient movement. Secondly, DWI is subject to T_2 'shine through', where the signal intensity from T_2WI can show through on the DW image and make it unclear how much of the altered signal (e.g. the 'bright' lesion) is due to real diffusion restrictions[30].

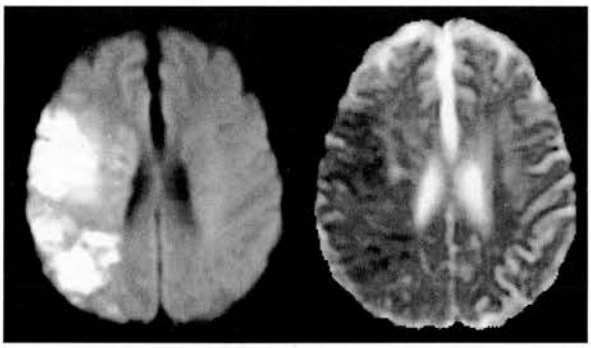

Figure 1.11 DWI and ADC image of a patient with a right hemisphere ischaemic lesion at 22 hours after stroke onset.

Perfusion-weighted MRI

The perfusion of blood through tissue is commonly measured with MRI in two ways: arterial spin labelling (ASL) and dynamic susceptibility contrast (DSC) PWI. ASL PWI involves magnetically 'labelling' the water in blood as it enters the brain with pulsed RF energy, and is appealing as it involves no exogenous contract agent[30]. However, ASL PWI is technically highly demanding, is very susceptible to patient movement artefacts, has difficulty in measuring long blood transit times (which are prevalent in stroke patients), and has poor signal-to-noise ratio[33]. Thus, ASL is a much less commonly used approach for PWI in acute stroke than DSC PWI, and will not be discussed further. In DSC PWI, an injection of paramagnetic contrast agent

(usually gadolinium-based) is traced using classical indicator dilution principles[30]. After the injection of the bolus of contrast agent, a volume is imaged repeatedly with a T_2^*-weighted sequence which has a high sensitivity to magnetic susceptibility effects. The presence of the contrast agent in the sample causes a transient decrease in SI, and the time course of this change is recorded for all voxels in the volume, which are compiled to produce a SI vs. time plot (Figure 1.12)[30].

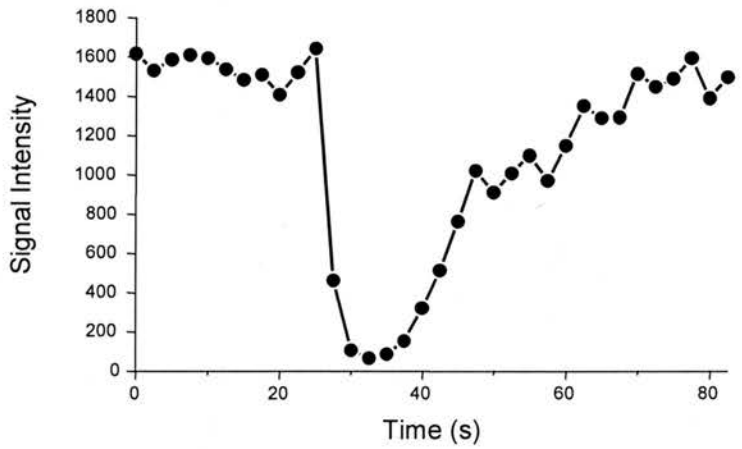

Figure 1.12 Signal intensity vs. time graph.

The tracer concentration is estimated from the change in T_2^* SI to obtain a tracer concentration vs. time curve (Figure 1.13).

Perfusion information obtained from the SI or concentration vs. time curves can be either 'non-quantitative' (including 'summary' and 'index' measures) or 'quantitative' (also described as 'absolute' in the literature)[33].

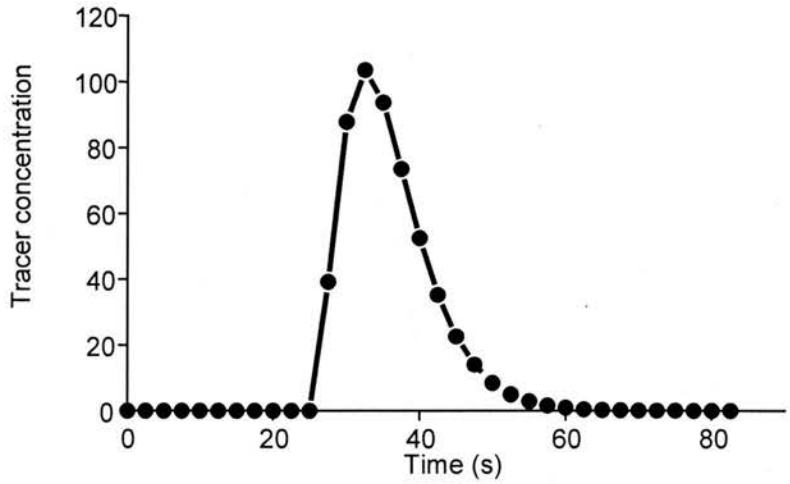

Figure 1.13 Tracer concentration vs. time graph.

'Non-quantitative' perfusion measures can be used to obtain 'summary' perfusion parameters, which can be quickly and easily obtained directly from either the SI or concentration vs. time curves, and may even be calculated automatically at the time of examination using software on some MR consoles. 'Summary' PWI parameters, such as tracer bolus arrival time, time-to-peak (TTP, measured as the time from tracer bolus arrival to peak concentration), and peak concentration height are commonly used in MR stroke research[33]. Though easily obtained and useful for distinguishing general pathology, 'summary' parameters have no clear relationship to actual underlying cerebral haemodynamics, so interpretation should be cautious[33]. In particular, 'summary' parameters do not account for bolus delay and dispersion or cardiac output – to account for these factors and obtain a more direct measure of CBF, complex and technically demanding image processing must be performed[33].

'Non-quantitative' perfusion measures can also be used to calculate 'index' values of CBF, cerebral blood volume (CBV), and mean transit time (MTT). These 'index'

perfusion parameters require complex 'offline' processing, including correction of the concentration vs. time curves using gamma-variate curve-fitting procedures to isolate the 'first pass' of the tracer and eliminate the influences of 'subsequent pass' tracer recirculation. From these corrected concentration vs. time curves, 'index' perfusion measures of CBV (CBV_i), MTT (MTT_i), and CBF (CBF_i), are calculated. CBV_i is proportional to the area under the concentration vs. time curve, and MTT_i is obtained by calculating the first moment of the concentration vs. time curve. Once CBV_i and MTT_i have been calculated, CBF_i can be obtained by applying the Central Volume Principle[34,35]:

$$CBF = CBV/MTT$$

'Index' perfusion parameters are superior to 'summary' perfusion parameters as they attempt to model only one of the underlying parameters, however, they do not have either the correct units or the correct scale. For example, CBF_i is not quantified in 'absolute' units (e.g. mL/100g/min), so an 'absolute' CBF_i threshold of tissue viability cannot be calculated.

It is important to note that 'relative' measures must be calculated in order to analyse 'non-quantitative' perfusion parameters. 'Relative' CBF (CBFr), CBV (CBVr), and MTT (MTTr) are obtained by normalising the values of a region of interest to a homologous contralateral region to allow for comparison of values both between patients and between different scan times within the same patient. Note CBFr, CBVr, and MTTr have no units. Obtaining quantitative measures of perfusion would theoretically eliminate these problems[33].

'Quantitative', or 'absolute' measures of perfusion require even further complex processing. An arterial input function (AIF) that records the appearance of the tracer

bolus as it enters the neurovascular circulation is used in conjunction with the individual voxel concentration vs. time curves to estimate a property termed the residue function. The residue function describes the rate at which the contrast leaves a voxel as if an ideal (instantaneous and infinitely thin) tracer bolus is delivered to the voxel; i.e. the voxel is instantaneously filled with contrast that then leaves the voxel over time. The AIF is typically estimated from an intracerebral artery, and is used to 'deconvolve' the voxel concentration vs. time curve in order to estimate the residue function - this estimation represents one of the big challenges in obtaining quantitative PWI[33]. 'Absolute' CBF (CBF_a) is assumed to be equal to the maximum value of the estimated deconvolved residue function[36]. 'Absolute' CBV (CBV_a) is obtained by dividing the area under the voxel concentration vs. time curve by the area under the AIF concentration vs. time curve[36]. 'Absolute' MTT (MTT_a) can be obtained by applying the Central Volume Principle[34,35]:

$$MTT = CBV/CBF$$

Although in theory the perfusion parameters obtained by deconvolution are quantitative, difficulties in quantifying the contrast concentration in voxels in different physiological environments *in vivo* mean these values should be interpreted with caution[37]. 'Absolute' parameters have the correct units and will have the same scaling between serial scans in the same patient, however 'absolute' and 'true' CBF, CBV, and MTT are almost certainly not equivalent, and are instead related by an unknown scaling factor[33,37].

The complex nature of image processing and the many assumptions made as to the tracer haemodynamics mean that even 'quantitative' perfusion values are only approximate[37]. Furthermore, greatly varying individual haemodynamics in imaging

subjects mean it is unwise to compare measures between patients – for example, 'baseline' CBF may be lower in a patient with atheroma in the arteries of the head and neck than in a healthy patient. Thus, it is advisable to calculate and compare 'relative' perfusion parameters even for the current 'quantitative' perfusion measures.

To MRI, or not to MRI?

MRI is a valuable tool for safely scanning most patients as it does not involve ionizing radiation. However, there are some contraindications for MRI, for instance metal implants, pacemakers, and the presence of other magnetic material in the patient. Furthermore, the narrow cylindrical shape of the bore of the MRI machine itself (Figure 1.14) means claustrophobic patients often ask to abandon scans early or refuse imaging to start with, and makes access for patient monitoring difficult.

Figure 1.14 GE Signa 1.5 T MRI scanner in the SHEFC Brain Imaging Research Centre for Scotland.

Some acutely ill stroke patients are unable to keep still enough, or have impaired protection of their airways making it unsafe for them to lay supine for the duration of the imaging sequences[3]. These contraindications (among others) are not inconsiderable – up to 20% of acute stroke patients may not be suitable for MRI[38,39]. However, MRI does present potential benefits, namely the high sensitivity of detecting ischaemic lesions even at hyperacute stages[26]. MRI can provide images of excellent anatomical detail, as well as information about water diffusion, blood perfusion, and even functional data, all within one imaging session. Although CT is conventionally used as the 'gold standard' for detection of haemorrhage in stroke patients[40,41], information that is vital in treatment decision-making[42,43], many studies show that MRI is more accurate at haemorrhage detection, and is more specific in determining the age of the haemorrhage[40,44-48]. The high sensitivity of MRI diffusion and perfusion imaging to the pathology of ischaemic stroke make it an ideal tool to further understand the mechanisms and processes involved in ischaemic stroke - information that could be used to develop more effective treatments for stroke patients.

2. Ischaemic stroke lesions on MRI

Introduction

This chapter will discuss the appearance of ischaemic lesions on DWI, and how they are measured. Problems with measuring lesions on DWI, including ill-defined lesions, T_2 'shine through', and tissue swelling are also discussed. The use of the 'DWI/PWI mismatch' and thresholds of DWI and PWI values to identify 'tissue at risk' of infarction are examined.

The appearance of ischaemic stroke lesions on MRI

The sensitivity of MRI in detecting changes in water diffusion and blood perfusion in brain tissue means that many studies have investigated the appearances of ischaemic stroke from acute to chronic stages in an effort to further understand the underlying pathology of ischaemic tissue and perhaps identify 'tissue at risk' of infarction that might benefit from treatment.

Early studies in acute stroke demonstrate that ischaemic changes could be detected as an increased signal on T_2WI at approximately 8 hours after stroke onset[49,50]. Although Bryan et al.[51] reported superiority of T_2WI over CT imaging in detecting ischaemic lesions, others found that T_2WI did not perform better than CT imaging in diagnosing acute ischaemic stroke[52]. However, the advent of DWI provided stroke researchers with an ideal tool to investigate early ischaemic changes due to its excellent sensitivity to changes in the diffusivity of water.

DWI in ischaemic stroke

DWI vs. T_2WI and CT imaging

DWI sequences developed in the 1980s enabled visualisation of the self-diffusion of water *in vivo*[53,54]. In early experimental ischaemic stroke research in animals, ischaemic changes on DWI were seen within minutes, whereas ischaemic changes on T_2WI did not appear until > 2 hours after stroke onset[55-57]. Early studies in human acute ischaemic stroke found that DWI detected infarcts at earlier times after ischaemic stroke than T_2WI (Figure 2.1), probably because of the higher signal contrast between normal and abnormal tissue of DWI compared to T_2WI at early time points[58], and could help distinguish old from new ischaemic lesions[59-63].

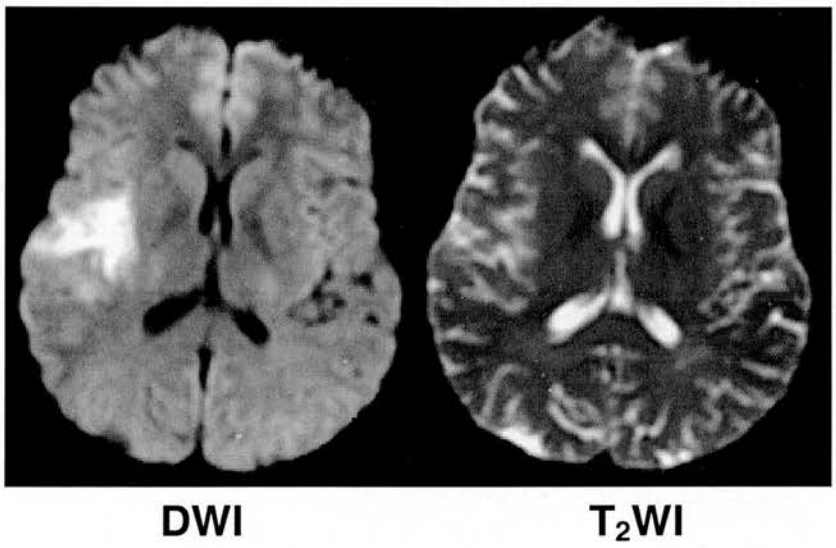

Figure 2.1 DWI and T_2WI from a patient with a right hemisphere ischaemic lesion at 6 hours after stroke onset. Note the hyperintense DWI lesion, and minimal (if any) visible T_2WI lesion.

Comparative studies show DWI to be more sensitive, have similar specificity, and higher accuracy for the detection of acute ischaemic lesions compared to T_2WI and CT imaging[52,64-67].

Acute appearance of ischaemic lesions on DWI

New ischaemic lesions appear as a hyperintense ('bright') area relative to surrounding tissue on DWI within minutes of stroke onset (Figure 2.1). The underlying ADC images show a hypointense ('dark') lesion reflecting the decrease in the ADC of ischaemic tissue (Figure 2.2).

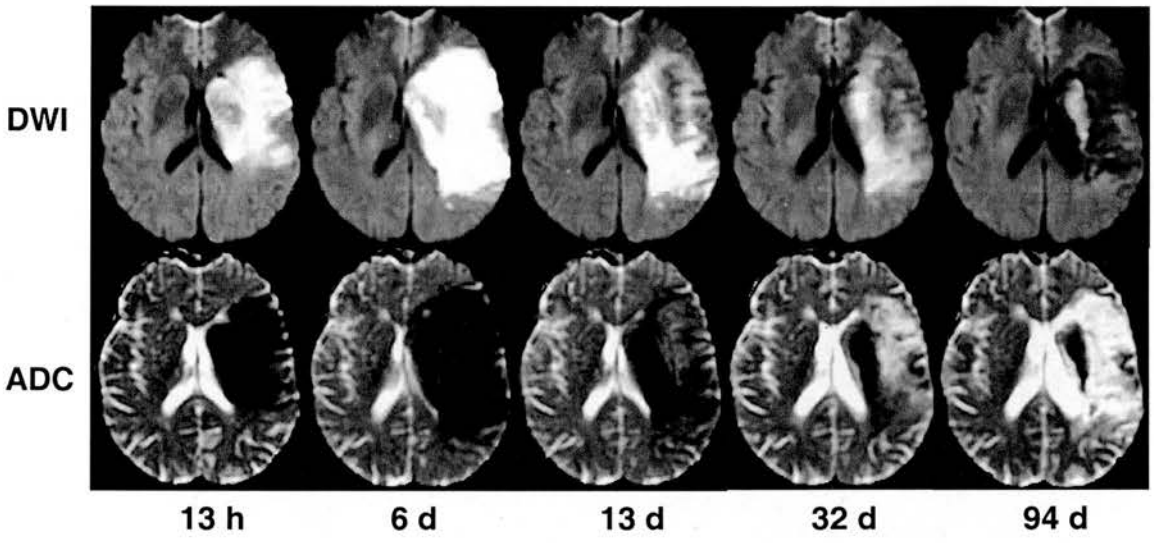

Figure 2.2 DWI and ADC images from a patient with a left hemisphere ischaemic lesion from 13 hours (h) to 95 days (d) after stroke onset. Note the compression of the left lateral ventricle between 13 hours and 13 days and subsequent *ex vacuo* effect at 94 days after stroke onset.

Evolution of ischaemic lesions on DWI

Ischaemic stroke is a variable condition: some patients have large areas of brain affected by ischaemia, some small; some patients have early spontaneous resolution of perfusion deficits, while others may have slower, possibly incomplete, restoration of blood flow. The range of individual differences in stroke severity and recovery in ischaemic stroke patients means that studies involving small numbers of patients are likely skewed by individual differences amongst patients. Furthermore, to establish

the pattern of ischaemic changes over time, the same patients must be serially scanned within distinct time points after stroke onset. What does the current literature say about the evolution of ischaemic lesions on DWI, and do these studies use adequate numbers of patients and appropriate serial scanning?

The hyperintensity of the DWI lesion persists for variously reported times from 48 hours - 14 days after stroke onset[60,62,68-71], and decreases in ADC for 18 hours - 85 days after stroke onset[59-61,70,72-78]. Subacutely, ADC becomes less hypointense, seeming to return to normal ('pseudonormalisation'[60,61]), and lesions on DWI become more isointense. However, this 'pseudonormalisation' does not indicate a resolution of the lesion; ADC values subsequently become increased relative to normal, showing as a hypointensity on DWI and a hyperintensity on ADC images at late times after stroke onset[60-62,70] (Figure 2.2).

Typically these studies used groups of approximately 20 patients with acute and follow-up scanning to assess the time course of DWI changes. Several studies used larger groups of patients (e.g. number of subjects [n] = 30[79] – 147[73]), but each patient had only one scan within a large range of times (e.g. from 2 hours - 417 days after stroke onset[74]) that were assembled to create models of lesion evolution on DWI. Using 'snapshot' images from different patients at a wide range of different times to form a composite pattern of lesion evolution is problematic due to the small number of patients at each time point and large degree of variability between patients.

To measure the 'final' lesion appearance and extent, many studies used a scan from ≤ 7 days after stroke onset[80-89]. However, as mentioned above, there is clear evidence that lesion evolution on MRI persists well beyond 7 days after stroke onset. Furthermore, the lesion can seem to disappear on T_2WI (the 'gold standard' for

measuring chronic ischaemic lesions[77,90,91]) at < 30 days after stroke onset[92,93], a phenomenon known as 'fogging', which can cause underestimation of lesion volume, or a false negative for lesion presence[77,93]. Thus, measurements of lesion extent on T_2WI from < 30 days after stroke onset do not accurately express, and will not be considered to measure, final infarct extent.

What does lesion appearance on DWI indicate about tissue state?

Stroke researchers are interested in trying to use acute (< 24 hours after stroke onset) DWI lesion appearance to determine final infarct extent and clinical outcome.

If acute DWI appearance is to be used to predict the final infarct extent and guide patient treatment decisions, the pathophysiological state of tissue of a particular appearance on DWI must be determined.

Experimental models of ischaemic stroke in animals indicate that lesion appearance on DWI closely correlates with the infarct as determined by histological analysis[55-57], and one study in human stroke patients (n = 11) shows that DWI lesions accurately predict the presence of a pathologically verified lesion on autopsy within 5 days of DWI[94]. However, the pathophysiology underlying ischaemic changes on DWI are still unclear. Hyperacute changes in DWI are not attributed to a change in water *content* (as there is no accompanying change on T_2WI, which is acutely sensitive to changes in water content), but rather a change in the *distribution* of water content[61]. The early hyperintensity on DWI (and corresponding hypointensity on ADC) is

thought to represent cytotoxic oedema, or the influx of water from the extracellular into the intracellular space[55,57]. The increase in intracellular water content causes restriction of the extracellular space, which is thought to cause the decrease in water diffusion that shows up on acute DWI and ADC images (Figure 2.3)[56,57,61].

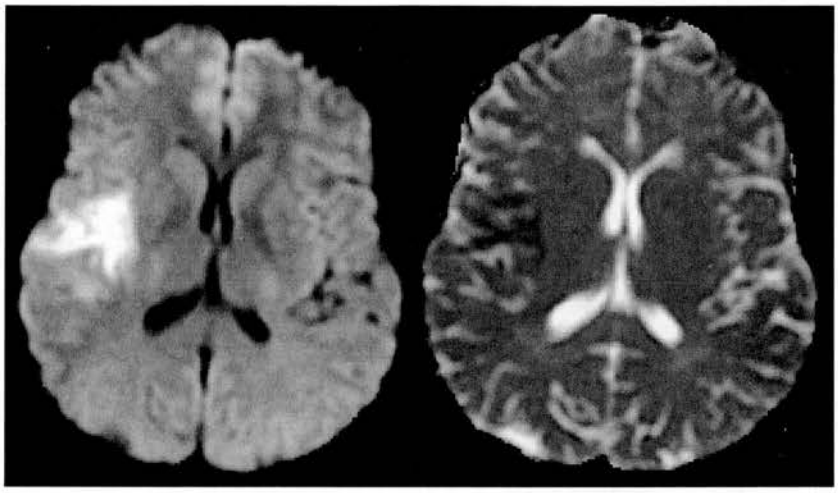

Figure 2.3 DWI and ADC images from a patient with a right hemisphere ischaemic lesion at 6 hours after stroke onset. Note the hyperintense DWI lesion is easily visible, while the hypointense ADC lesion is less easily distinguished (particularly at the lesion edges).

The pathophysiology underlying subacute patterns on DWI and ADC is even less well understood, although processes involved in the evolution of acute ischaemic damage, including membrane failure (with associated disturbances in ion homeostasis), cell death, cell lysis, and vasogenic oedema have been postulated as probable causes[61,62,70]. Chronic hypointensity on DWI and hyperintensity on ADC images are thought to represent areas of vasogenic oedema caused by cell death and resulting tissue cavitation[60,69,70,95].

The pathophysiological correlates of DWI appearance will be explored further in Chapter 3.

Measuring ischaemic lesions on DWI

Acute DWI lesion volume may predict clinical outcome and could help guide treatment decisions[96-98], but factors influencing DWI lesion measurement have not been widely assessed. Acute DWI lesions are 'bright' against the 'dark' grey of the rest of the brain, and are easier to distinguish visually (i.e. greater contrast between normal and abnormal tissue) than a 'dark' ADC lesion against the slightly lighter grey of the rest of the brain (Figure 2.3); thus DWI is much more commonly used for measurement and analysis of ischaemic lesions[89,99,100].

However, there is no consensus on the best way to measure lesions on acute DWI. The most common method of lesion measurement is manual outlining the visible DWI lesion.

Manual lesion outlining

Manual outlining of the visible DWI lesion has been performed in previous studies by one observer (often with explicit mention of blinding to clinical and other imaging details)[62,83,84,101-103], or several experienced observers (generally blinded to clinical and other imaging details), often on more than one occasion, which have been averaged to obtain a DWI lesion 'region of interest'[85,99,100,104-106]. Although some studies report high levels of intraobserver and interobserver reliability for manual outlining of DWI lesions[99,100,104], these studies measured DWI lesions from widely

variable stages of ischaemic stroke (e.g. from < 7 hours[104] - 84 days[99] after stroke onset), and used small numbers of patients (e.g. n = 12[104] – 28[100]; Table 2.1).

Table 2.1 Summary of papers measuring reliability of DWI lesion volume measurement. All studies employed a manual outline method of measuring DWI lesions. n = number of patients, MR time = time from stroke onset to MRI, r = Pearson's product moment correlation coefficient.

Study	# scans	n	MR time	Observers	What were the findings?
Baird et al.[100]	44	28	< 53 h	3 observers, twice	Interobserver reliability: r > 0.95; intraobserver variation: < 5%
Barber et al.[99]	52	18	12 h - 84 d	2 neurologists	Interobserver/intraobserver variation: < 5%
Rana et al.[107]	38	15	< 24 h – 14 d	medical physicist and neuroscientist	Interobserver coefficient of variation: 85 ± 130%
Thijs et al.[104]	24	12	< 7 h - 7 d	2 observers	Interobserver reliability: r > 0.95

Others who simply rated the presence or absence of a DWI lesion in the hyperacute (< 6 hours after stroke onset) stages of ischaemic stroke have demonstrated a lower degree of interobserver agreement (Table 2.2)[64,65,67,107,108]. The lesion is likely to be less hyperintense on DWI in the hyperacute stage of ischaemic stroke[59], so manual lesion measurements would most likely also be less reliable on hyperacute scans. Furthermore, imaging studies often fail to list details of the observers[100,104], for instance whether they are neurologists or radiologists, or what experience they have in viewing and assessing DWI scans. Observer experience has been shown to be important; 'expert' observers have been found to have much higher levels of interobserver agreement than 'novice' observers[65]. Factors affecting the variability of manual lesion measurement on acute DWI will be explored further in Chapter 5.

Table 2.2 Summary of papers measuring reliability of the measurement of the presence and subjective extent of DWI lesions. n = number of patients, MR time = time from stroke onset to MRI, κ = Cohen's reliability coefficient.

Study	# scans	n	MR time	Observers	What was measured?	What were the findings?
Fiebach et al.[65]	50	50	< 6 h	1 neurologist, 4 neuroradiologists, 4 residents	Presence of DWI lesion, lesion extent, and lesion type for experts (neurologist and neuroradiologists) vs. novices (residents)	Interobserver agreement: presence of DWI lesion experts κ = 0.84, novices κ = 0.76; lesion extent experts κ = 0.62, novices κ = 0.55; lesion type experts κ = 0.52, novices κ = 0.36
Girot et al.[108]	17	17	< 6 h	3 neuroradiologists, 1 neurologist	Presence of DWI lesion	Interobserver agreement: κ = 0.82; intraobserver agreement: κ > 0.60
Lansberg et al.[64]	19	19	< 7 h	stroke neurologist and neuroradiologist	If DWI lesion > 1/3 MCA territory	Interobserver agreement: κ = 0.63
Saur et al.[67]	46	46	< 6 h	3 neuroradiologists, 3 neurologists	Presence of DWI lesion, if > 1/3 MCA territory, and anatomic region	Interobserver agreement: presence of DWI lesion κ = 0.85 (intraobserver κ = 1); > 1/3 MCA κ = 0.68, anatomic region κ = 0.56 - 0.80 (intraobserver κ = 0.67 - 0.90)

Other lesion measurement methods

Other less common lesion measurement methods include: placement of a region of interest in the visible DWI lesion for extraction of ADC values[60,61,69,70,109]; semiautomated thresholding or contouring from a manually placed region or 'seed' based on local DWI SI[77,81,88,110-115]; and multiparametric iterative 'clustering' analysis (with the use of a κ-means algorithm)[68,116-118].

Extracting DWI and PWI values from a small region of interest placed within a DWI lesion is problematic as DWI lesions are heterogeneous, with widely varying degrees of underlying changes in ADC[68,78,119-121] and perfusion[113] values – changing the placement of the region of interest even slightly could greatly change the extracted ADC[122] and PWI values.

Semiautomated lesion segmentation is appealing as it theoretically eliminates observer variation, however, all studies of these semiautomated lesion segmentation methods mention the need for some degree of manual observer editing (e.g. for exclusion of ventricles and delineation of anatomical boundaries), so observer variability is still an issue. Furthermore, the problems of lesion heterogeneity would also likely affect semiautomated lesion segmentation – regions of less severe degrees of abnormality may be missed depending on where the initial contour or 'seed' is placed.

Multiparametric clustering analysis is a promising method for measurement of regions of ischaemic tissue as it is observer independent, and using a combination of MR parameters (T_2WI and DWI[68] or T_2WI, DWI, and PWI[116-118]) may solve the issues of individual parameter heterogeneity. Tissue identified as 'at risk' by these multiparametric techniques appears to correlate with clinical outcome[117], and more

accurately represent tissue destined for infarction than either DWI or PWI parameters alone[116]. However, there are few studies investigating these segmentation algorithms, and they were developed in small groups of patients (e.g. n = 8[68] - 14[116]), so these methods require much further study and validation to determine their usefulness in the general population of stroke patients.

Problems with DWI lesion measurement

There is a great variability in changes on DWI and ADC images that often goes unmentioned, despite increasing evidence that many patients do not follow the aforementioned 'accepted' patterns of ischaemic changes on MRI. These problems include: ischaemic lesions that are hazy, ill-defined, and 'patchy' on DWI; the contribution of T_2 'shine through' to DWI lesion appearance; the effect of oedematous swelling on lesion measurements; and the variability of ADC values due to age, tissue type, and individual patient differences.

Ill-defined lesions

Although most studies report that lesions on acute DWI are discrete, clearly defined 'bright' regions, the lesion can have regions of subtle, ill-defined hyperintensity (Figure 2.4). Few have acknowledged the existence of this problem, but it has been suggested that the areas of the DWI lesion that appear 'hazy' and ill-defined represent salvageable tissue, i.e. the 'ischaemic penumbra'[123,124]. However, as suggested by Guadagno et al.[125], lesion regions that are obviously hyperintense on DWI may not indicate irreversible tissue damage, while regions of more subtle hyperintensity on DWI may indicate irreversible tissue damage. The presence of these subtle changes on DWI may be a factor in interobserver variability in lesion

measurements[126]; the effects of acute DWI lesion appearance on lesion measurement will be explored further in Chapter 5.

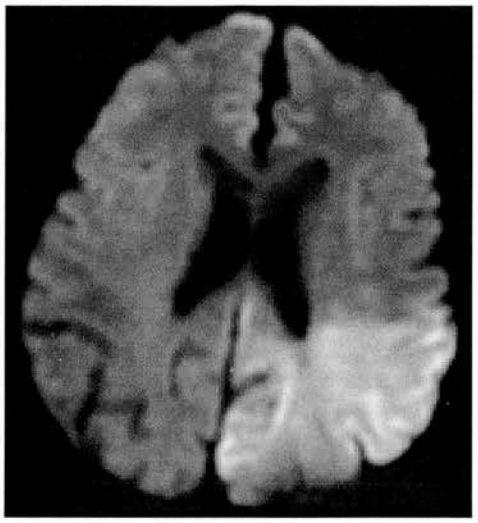

Figure 2.4 DWI from a patient with a left hemisphere ischaemic lesion at 4 hours after stroke onset. Note that the DWI lesion is not uniformly hyperintense, with areas of ill-defined, subtle hyperintensity.

The appearance of subacute and chronic lesions on DWI also present problems for lesion measurement. Not only does the ischaemic lesion become less distinct as it changes from hyperintense to isointense and then hypointense on DWI over time (Figure 2.2), but the appearance of the ischaemic lesion on DWI is also affected by T_2 'shine through' in the later stages of stroke.

T_2 'shine through'

Lesion appearance on DWI has contributions from both the ADC and T_2WI signals, and the relative contribution of each has been shown to change over time[70,79]. Specifically, acute hyperintensity on acute DWI is attributed almost solely to the acute decrease in ADC values, after which hyperintensity on DWI is increasingly attributed to T_2 signal effects until approximately 7 days after stroke onset as ADC

'pseudonormalises' and has less effect on DWI[79]. After 7 days from stroke onset, the effects of increased ADC are cancelled out by an increased T_2WI SI; any remaining hyperintensity on DWI is attributed to this increase in T_2WI SI, or T_2 'shine through'[76,79]. Persistent hyperintensity on DWI has been reported at up to 57 days after stroke onset[74,76], and has been attributed solely to this T_2 'shine through'. However, as previously discussed, ADC values can remain decreased at subacute and chronic time points (e.g. > 7 days after stroke onset[77,78]), so it is entirely possible that persistent hyperintensity on late DWI is still attributable, at least in part, to decreased ADC. What do persistent decreases in ADC on images from late after stroke onset indicate? The evolution of diffusion and perfusion parameters in regions of persistent hyperintensity on late DWI will be explored further in Chapter 7.

Lesion swelling

Another problem affecting lesion volume measurements is oedematous swelling. Oedema of the ischaemic lesion at subacute times, with apparent maximal effect at 1 – 3 days after stroke onset in humans[127], may cause overestimation of the volume of the ischaemic lesion. Studies in rats have indicated that up to 25% of the volume of the visible lesion on T_2WI at 24 hours after stroke onset may be attributable to oedema[128]. Few studies of serial MRI in human ischaemic stroke consider the possibility that differences in lesion volume over time may be the effect of oedematous swelling and possible subsequent tissue atrophy as necrotic tissue is 'reabsorbed' and hydrocephalus *ex vacuo* develops (Figure 2.2). Oedema (whether of mass effect or less severe localised swelling) in the first few days after ischaemic stroke is almost universal[129]: severe oedema causing compression of the lateral ventricles and lateral shift of midline structures was observed in 13% of patients in

one study[59], and it is likely that lesser degrees of oedema that could nonetheless affect lesion volume measurements went unnoticed[129]. Although several studies of human ischaemic stroke patients acknowledge that a decrease in lesion volume between early DWI and late T_2WI may be attributable to oedema that subsequently resolves[77,97,100], only one study attempted to eliminate these effects by measuring lesion volume over time using anatomical landmarks[78]. The effects of lesion swelling will be addressed further in Chapter 11.

Tissue composition

Besides the variability in the evolution of ADC changes following the onset of ischaemia, ADC can also vary with age and tissue type. ADC values in normal white matter have been shown to be significantly higher in older patients, possibly caused by mild structural changes inherent in the ageing brain[130,131]. Furthermore, grey and white matter exhibit different patterns of changes in both appearance on DWI and underlying ADC values after ischaemic stroke. In the acute stages after stroke onset, ischaemic grey matter appears to be more hyperintense on DWI than ischaemic white matter, suggesting that grey matter is more vulnerable to early ischaemic damage[59,132]. However, the underlying ADC of white matter is significantly more decreased than in grey matter[78,133], so white matter may be more susceptible to ischaemic damage than previously thought, and the lack of early visible changes on DWI may cause underestimation of the amount of white matter involved in the ischaemic lesion[132]. Grey and white matter also exhibit different patterns of ADC evolution after stroke onset – the ADC in ischaemic grey matter appears to increase more quickly than in ischaemic white matter in the subacute stages of ischaemic stroke[7,133]. Differences in grey and white matter appearance and evolution on DWI

and ADC images after ischaemic stroke indicate that lesion composition should be taken into account when evaluating acute lesions and could have implications for predicting lesion outcome – these differences will be discussed further in Chapter 7. Despite the problems affecting lesion measurement, what does the current literature say about the ability of acute DWI to predict tissue destined for infarction?

Acute DWI appearance as a predictor of tissue infarction

Acute DWI lesion volume has been shown to be both a good[90,91,99,112,134] and a poor[135,136] clinical outcome predictor. Several studies suggest that a large (e.g. > 14[96] - 22[97] mL) acute DWI lesion indicates a poor clinical outcome[96,97], but others have found no correlation of DWI lesion volume and clinical outcome[77,135] - there is always the danger that a large lesion may be in a relatively clinically 'silent' area of brain, and a small lesion in particular areas of brain (e.g. the internal capsule) could cause severe deficit[137]. However, the volume of abnormality on acute (< 24 hours after stroke onset) DWI correlates well (e.g. Pearson's product moment correlation coefficient r = 0.72[106] - 0.92[138]) with final infarct volume as measured on T_2WI[64,90,97,99-101,106,138,139]. The concept that the acute DWI lesion represents the 'core' of tissue destined for infarction is in increasing dispute[105,113]; although the acute DWI lesion and final T_2WI lesion correlate well, that does not mean they are equal (i.e. the acute DWI lesion could consistently underestimate or overestimate final lesion extent). Several studies measuring lesion volume on DWI in the

hyperacute (< 6 hours after stroke onset) stages of stroke, when the appearance of the lesion on DWI is likely still evolving, have found that early DWI volume tends to underestimate final infarct extent[100,109]. One study found that DWI lesions from > 6 hours after stroke onset more closely matched the final infarct extent compared to DWI lesions from < 6 hours after stroke onset[100], so consideration of time of imaging is vital, as already discussed in relation to lesion oedema. Animal[16,19,140,141] and human studies[105,125,142] have shown that even regions of severe hyperintensity on DWI and decreased ADC have been shown to recover, and tissue appearing normal on DWI or with mild/no acute decrease in ADC have proceeded to infarction. This poor correlation of appearance on DWI and ADC images with recovery or infarction is likely related to the presence or absence and timing of reperfusion, as well as the time of imaging. Does adding information about the haemodynamic state of the lesion help to identify tissue at risk of infarction?

Measuring the 'ischaemic penumbra' on MRI

Currently the most widely studied method to identify the 'ischaemic penumbra'[21], or tissue that is viable but at risk of infarction, is by assessing acute 'DWI/PWI mismatch'.

'DWI/PWI mismatch'

Because of the apparent ability of DWI to predict final infarct extent, the 'DWI/PWI mismatch' model suggests that the acute DWI lesion represents the dead 'core' of an infarct, and, if a larger lesion on PWI is present, the region of 'mismatch' represents the 'ischaemic penumbra', or 'tissue at risk' of infarction that remains salvageable

(Figure 2.5). Several studies have shown that the presence of a 'DWI/PWI mismatch' predicts that the lesion on final T_2WI will be larger than the lesion on baseline DWI (i.e. the lesion will grow)[99-101,138,143,144].

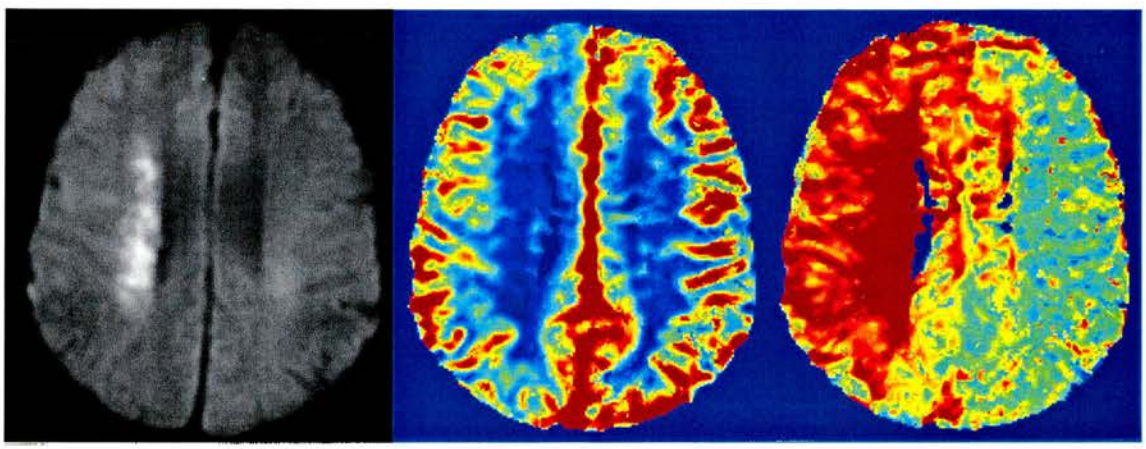

Figure 2.5 DWI, CBF$_i$, and MTT$_i$ images from a patient with a right hemisphere ischaemic lesion at 13 hours after stroke onset. Note the 'DWI/PWI mismatch', i.e. the hyperintense lesion on DWI appears smaller than the visible lesion on the CBF$_i$ and MTT$_i$ images.

However, as previously mentioned, there is some question as to whether the acute DWI lesion accurately identifies the ischaemic 'core', and whether the 'DWI/PWI mismatch' accurately identifies the 'tissue at risk' of infarction[113,145,146]. Furthermore, there is a great disparity in how PWI is measured (as discussed in Chapter 1). Of 10 studies found to investigate acute 'DWI/PWI mismatch' and final (> 30 days after stroke onset) lesion extent, 1/10 used a 'summary' measure of perfusion (TTP)[101], 2/10 used 'index' measures of perfusion (MTT$_i$ and CBV$_i$)[91,102], 5/10 used 'absolute' measures of perfusion (CBF$_a$, CBV$_a$, and MTT$_a$)[106,138,143,144,147], and 2/10 did not adequately describe their methods of perfusion measures (although they probably

measured 'summary' TTP)[99,100]. The great variability of perfusion parameters measured, including TTP, CBV_i, MTT_i, CBF_a, CBV_a, and MTT_a, make it unclear as to what perfusion parameter best represents the ischaemic penumbra[148], although MTT (both MTT_i and MTT_a) appears to overestimate the 'tissue at risk' of infarction[91,99,102,106,144,147].

Various methods of measurement of the 'DWI/PWI mismatch' and final lesion extent on T_2WI were used, including: manual outline of the visible abnormality on DWI, PWI, and T_2WI[91,99-101,106]; use of an MTT_a threshold[143]; thresholds of percentages of contralateral PWI values[147]; lesion edge autosegmentation with manual correction[102,138]; and statistical voxel-by-voxel analysis of ipsilateral vs. contralateral parameter values[144].

The quantification of threshold DWI and PWI values that quickly and reliably identify the 'ischaemic penumbra' would allow clinicians to base treatment decisions on the presence and extent of 'tissue at risk' of infarction.

Thresholds of ischaemic tissue viability

Numerous attempts have been made at obtaining diffusion and perfusion thresholds for identifying tissue destined for infarction, however many of these measure 'outcome' lesion extent on scans from insufficient times after stroke onset (e.g. ≤ 7 days after stroke onset[85,89,104,142]), so do not actually measure final lesion extent. Of six studies found with lesion outcome measures from ≥ 30 days after stroke onset, two suggested a 'relative' (normalised to a normal homologous contralateral region) ADC (ADCr) threshold[119,123] and four suggest perfusion thresholds that predict tissue

infarction[144,147,149,150]. Bykowski et al.[119] and Desmond et al.[123] propose ADCr thresholds of 0.53 and 0.85 respectively, but both warn that there is a large overlap of ADC values between tissue that does and does not proceed to infarction, and that a single MR parameter 'threshold' is unlikely to sufficiently capture the complex ischaemic pathology to allow for clinical decision making.

'Relative' perfusion thresholds for prediction of infarction suggested include: CBFr = 0.59, CBVr = 0.85, and MTTr = 1.63 by Røhl et al.[150], and CBFr = 0.70 (or CBF_a = 33.9 ± 9.7 mL/100g/min) and CBVr = 1.20 (or CBV_a = 4.2 ± 1.9 mL/100g) by Rose et al.[144]. However, both Røhl et al.[150] and Rose et al.[144] caution that a CBV threshold may not be clinically useful due its bimodal behaviour in response to changes in cerebral perfusion pressure, and that the suggested thresholds would need testing on a larger sample of patients. Butcher et al.[149] report a mean MTT_a delay of 8.3 s relative to normal in tissue that proceeds to infarction, but caution that MTT_a and CBF_a values overlap significantly, and that CBV_a values are not significantly different between infarcted and 'salvaged' tissue to distinguish 'tissue at risk' of infarction. Furthermore, Parsons et al.[147] warn against using a single perfusion parameter threshold, as different perfusion parameters provide complementary information about the complex physiology of ischaemic tissue.

The use of a single threshold to predict what tissue will proceed to infarction is clearly problematic; there is a large overlap of ADC and perfusion values in tissue that eventually does and does not become infarcted, and underlying ischaemic physiological processes are complex and variable. Furthermore, the patient sample sizes used in the studies (e.g. n = 11[150] – 35[149]) to identify these ischaemic thresholds have been small and would require testing in much larger patient groups.

Studies using multiparametric predictive models incorporating T_2WI, DWI, and PWI information appear promising, but as aforementioned, have been developed in small samples of patients (e.g. n = 10[117] - 26[151]) and require further investigation and validation to determine their value in predicting what tissue will proceed to infarction[116-118,144,151].

What questions remain unanswered?

Although there have been many studies of DWI and PWI in human ischaemic stroke, it is still unclear what appearance on the different MRI sequences means in terms of the underlying pathology of the ischaemic stroke, and if the acute appearance on MRI informs on the recoverability of the tissue. There is great variability between patients in changes of DWI SI, ADC values, and PWI parameters over time that often goes unmentioned. Thus, to summarise, problems with imaging studies that limit what their results mean and how they can be applied include:

- small numbers of patients studied
- unclear clinical characteristics of patients
- wide range of times of imaging
- wide range of PWI parameters used
- unclear lesion measurement techniques, including lack of observer details and intraobserver and interobserver reliability data
- how to manage the effects of tissue distortion due to oedema
- not accounting for heterogeneity within lesions on DWI and PWI

This thesis will aim to explore these issues in order to help clarify what ischaemic changes on MRI mean in terms of the viability of the underlying tissue and thus perhaps help guide clinical decision making.

3. Systematic review of DWI and PWI in animal models of ischaemic stroke

Introduction

This chapter comprises of a systematic review of the use DWI and PWI in animal models of ischaemic stroke, investigating what particular appearances on DWI mean in terms of the underlying pathophysiology of ischaemic tissue.

What do animal studies tell us about the underlying pathophysiology of ischaemic stroke lesions?

DWI and PWI may distinguish transiently from permanently damaged brain, and lesion appearance on MRI might be a surrogate marker for the effectiveness of new treatments[152]. Although DWI has been available for a decade, the relationship between DWI lesion characteristics and tissue viability remains unclear.

The precise point in the ischaemic cascade where lesions become visible on DWI, and the point of no recoverability, is not known. The 'DWI/PWI mismatch' may represent the 'ischaemic penumbra', or 'tissue at risk' that remains salvageable[153].

Animal studies of focal ischaemia (as a model of human ischaemic stroke) provide an opportunity to investigate the pathological changes underlying lesion appearance on MRI[154]. We aimed to identify information available about the pathophysiological state underlying DWI and/or PWI lesion appearance in animal models of ischaemic stroke, to inform on the interpretation of DWI and PWI lesion appearance and potential for salvage of 'tissue at risk' of infarction in stroke patients.

We therefore performed a systematic review of all experimental studies of DWI and PWI in animal models of focal ischaemic stroke to assess all the available information on the histological correlates of DWI and PWI lesion appearances, and the likelihood of permanent tissue damage or recovery in the presence of particular DWI and/or PWI lesion appearances. Excerpts from this chapter have recently been published in *Cerebrovascular Diseases*[155] (Appendix 2); permission to reproduce the material within this thesis has been obtained by the publisher (S. Karger AG, Basel, Switzerland) and the co-author (JMW).

Systematic review methods

The methodology of this systematic review was adapted from that used in the Cochrane Database of Systematic Reviews[156]. Although developed for systematic reviews of randomised controlled trials, the same principles apply to, and have been successful in, systematic reviews of observational and diagnostic studies.

Search strategy

We searched for published articles of DWI, PWI, or a combination of the two in animal models of ischaemic stroke in the English and non-English language literature on MEDLINE (US National Library of Medicine, National Institutes of Health, Bethesda, MD, USA) and EMBASE (Elsevier Group, Amsterdam, Netherlands) from 1966 - December 31, 2002 (for a complete list of search terms see Appendix 2). To validate the search strategy (in accordance with established systematic review methodology[156]), we also hand searched the last five years (January 1998 - December

2002) of the three journals that contributed the most papers from the literature search (*Brain Research, Journal of Cerebral Blood Flow and Metabolism,* and *Stroke*), and reference lists in all included articles.

Inclusion criteria

We included studies published in full of DWI, PWI, or a combination of the two, in mammalian models of focal ischaemic stroke, with histological analysis performed within a maximum of 24 hours of the last MRI session. One reviewer (the author) identified the abstracts and excluded articles not relevant to this review. Papers were reviewed by the second reviewer (JMW) and final decisions made by discussion.

Exclusion criteria

Studies without DWI or PWI, non-mammalian animal models, non-focal models of stroke, global models of ischaemic insult, non-ischaemic models of brain injury, no histological analysis performed, and histological analysis performed > 24 hours after the last MRI session were excluded (the dynamic nature of ischaemic stroke would prevent histological results being related to imaging appearance after a long time lapse between imaging and histological analysis). Reviews, conference papers, and studies only appearing in abstract form were excluded. Publications which appeared to include data previously published elsewhere were excluded. Where the inclusion of a paper was in question, a consensus was reached between the two reviewers.

Methodological quality scoring

A methodological scoring system was devised to reflect different aspects of animal imaging methodology (Table 3.1). Aspects of the animal model, imaging method, histological procedures and analysis, and blinding of analyses were assessed for all papers. These criteria were drawn up in advance of evaluating the identified papers

as part of the primary methodology of the review in accordance with Cochrane methods[156].

Table 3.1 Methodological quality scoring system.

Question	Issue	1/2 mark	1 mark (in addition to 1/2 mark requirements)
1	Animal ischaemia model reproducible?	method with reference to original procedure	anaesthetic type/dose, surgical procedure, sham/experimental groups described
2	Animal subjects reproducible?	species, strain, sex	source, average weight, housing and feeding details
3	MRI reproducible?	make, model and strength of MR scanner, *b* value	DWI performed in 3 orthogonal directions, method of analysis clearly described
4	Histological procedure reproducible?	fixatives and stains listed without specific values and concentration	concentration of fixatives and stains, size/location brain slices; method of analysis clearly described
5	Histological time	< 24 hours from last imaging session	< 6 hours from last imaging session
6	Blinding of image analysis to histology	implied (e.g. user-independent)	specifically mentioned blinding in text
7	Blinding of histology analysis to imaging	implied (e.g. user-independent)	specifically mentioned blinding in text
8	Imaging/histology comparison	'correlated well' on visual exam	in-depth investigation with methods clearly described
9	Subregion analysis	done on either imaging *or* histology	if performed on both imaging and histological results
10	Aim		clear hypothesis with discussion of how results relate

Data extraction

One reviewer (the author) extracted information on: the study year; number and type of animals used (species, strain, and sex); ischaemia model (method and duration of occlusion, whether transient or permanent); MRI protocol (make, model, strength of scanner, scanning protocol); anaesthetic and animal life support in the MR scanner; time from imaging to histology; histological protocol (details of fixation and analysis of histological slices, including how the histological slices were matched to the MR

slices for analysis), MR image analysis (lesion volume, ADC values, blinding of image and histological analysis and what MRI appearance corresponded to what macroscopic or histological state). Data extraction was verified by the second reviewer (JMW).

Studies explicitly stating that the analysis of the histological lesion was blind to the DWI lesion and *vice versa*, and/or studies achieving a quality score ≥ 6 were examined further to extract specific information about the relationship between DWI appearance and histological damage. We aimed to undertake analyses of how particular DWI and/or PWI appearances were associated with histological features if such information was available.

Results of systematic review

The search yielded 1420 articles on MEDLINE and 1243 article on EMBASE, totalling 2663 papers, 943 of which were repeats, leaving an initial database of 1720 articles. 1579 papers were excluded (reasons given in Table 3.2), mostly because the ischaemia model was not relevant to human ischaemic stroke (e.g. global not focal).

Table 3.2 Reasons for exclusion of papers.

Reason for Exclusion	# of papers	%
Not a stroke model	649	41%
Not an animal study	99	6%
Global ischaemia	162	10%
Inappropriate models (e.g. head trauma or aneurysm)	136	9%
Reviews, letters, abstracts	153	10%
No DWI	297	19%
No histology (includes 11 with histology > 24 hours from last MRI)	83	5%
TOTAL	1579	100%

The remaining 141 studies, concerning the use of DWI and/or PWI were included. The total number of animals in these papers was over 2817 (2/141 studies did not report animal numbers[157,158]), with a mean n = 21 animals per paper (median n = 18).

General details of included studies

Of the 141 included papers, 108/141 (77%, n = 2255, 80% of animals) used rats, 19/141 (14%, n = 315, 11% of animals) used cats, 8/141 (6%, n = 178, 6% of animals) used mice, 3/141 (2%, n = 31, 1% of animals) used pigs, 2/141 (1%, n = 36, 1% of animals) used rabbits, and 1/141 (1%, n = 2, 0.1% of animals) used monkeys (Figure 3.1).

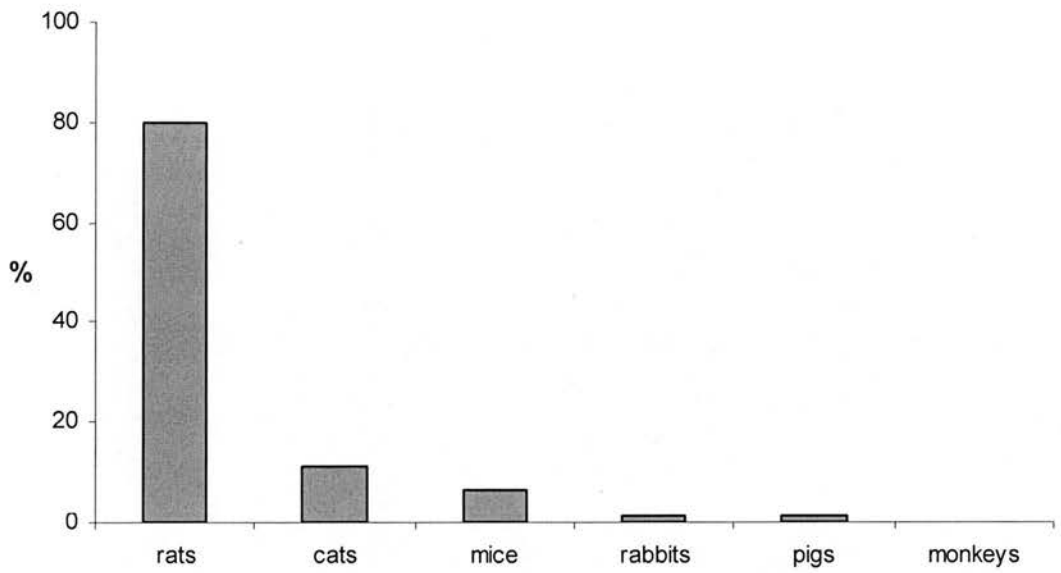

Figure 3.1 Percentage of total animals by species in studies in review. n = number of animal subjects in the studies in the review (mean n = 21, median n = 18, total n > 2500).

A middle cerebral artery occlusion (MCAO) model was used in 130/141 (92%; n = 2641) of the included papers, an internal carotid artery occlusion (ICAO) model in

4/141 (3%; n = 63) papers, a common carotid artery occlusion (CCAO) model in 3/141 (2%; n = 48) papers, the Rose-Bengal cortex lesion model in 3/141 (2%; n = 52) papers, and a combined CCAO & MCAO model in 1/141 (1%; n = 33) paper (Figure 3.2).

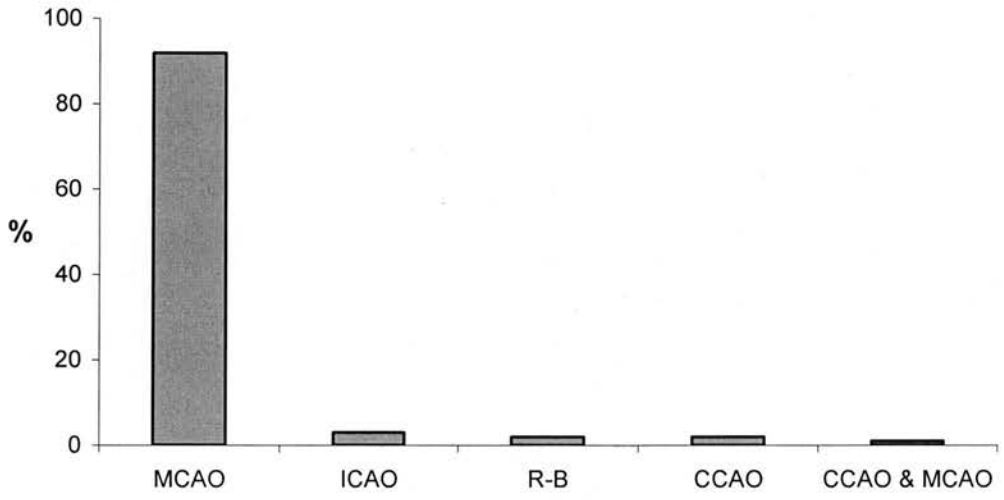

Figure 3.2 Percentage of lesion models in studies in review. R-B = Rose-Bengal cortex lesion.

Methodological quality scores

In general, methods were not reported in detail (Table 3.3, Figure 3.3). The mean total methodological quality score was 5.73/10 (Table 3.3).

Only 13/141 (9%) papers adequately described their animal subjects. Basic differences in animal strain and sex can make a large difference in results (e.g. the apparently neuroprotective effects of oestrogen in a MCAO model of ischaemia in female rats[159]). Only 34/141 (24%) papers adequately described the MR procedures well enough that they might be reproduced. Many papers did not mention

measurement of DWI in three orthogonal directions (necessary to obtain reliable and reproducible quantification of ADC values[32]).

Table 3.3 Average scores on the methodological quality scoring system.

Question	Average Score /1	n scoring 1/1	% scoring 1/1
1	0.92	119	84%
2	0.47	13	9%
3	0.61	34	24%
4	0.85	102	72%
5	0.85	98	70%
6	0.25	9	6%
7	0.09	9	6%
8	0.51	31	22%
9	0.17	18	13%
10	0.88	124	88%
TOTAL	**5.73**	**0 (10/10)**	**0 (10/10)**

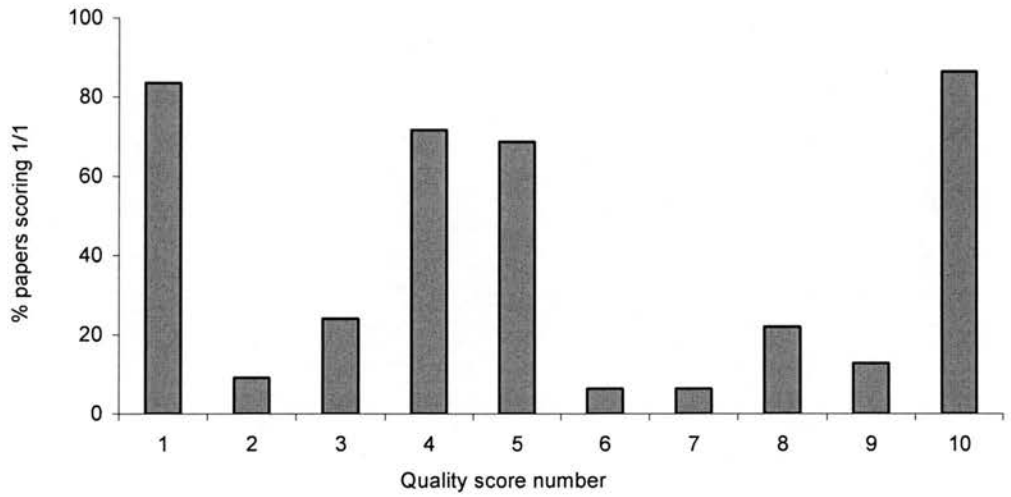

Figure 3.3 Percentage of papers scoring 1/1 on the methodological quality scoring points. See Table 3.1 for the methodological quality scoring criteria.

Few studies mentioned blinding of the image and histological analysis to each other. Failure to employ blinding and randomisation in animal studies of drug effects is known to increase the likelihood of a positive result[160]. Half (71/141, 50%) of the

studies did not mention blinding of any of the analyses at all. Only 3/141 (2%) studies, including 51/2817 (2%) of the total animals used in all included studies, explicitly stated that histological analysis was blind to DWI analysis and *vice versa*[16,161,162], so we can only be sure that data from 2% of the animals was analysed completely free of bias. The way in which the MR images and analyses were compared to histological data generally lacked detail, with only 31/141 (22%) studies comparing DWI and histological slices any further than simply saying they 'correlated well'. However, the precise meaning of a 'good correlation' was not given, and explicit mention of how the histological slices were matched to MR slices for analysis was either lacking, or described only as being 'eyeballed' for a best fit. Only 18/141 (13%) studies examined any subregions of the DWI lesion or histological abnormality.

Perfusion values were obtained and reported in some papers, but in such different ways that it was not possible to extract the information as to the relationship between perfusion parameters, DWI and histological data in ways that allowed data synthesis. We have therefore concentrated on the correlation of DWI and histological data.

Data extracted on DWI and histopathological lesion appearances

Although all 141 papers were examined, papers with a quality score < 6 consistently failed to provide data on the relationship of DWI appearance and histological data, so we focused on papers with a quality score ≥ 6, and papers with explicit mention of blinding of histological and imaging analyses. 51/141 (36%) papers achieved a quality score of ≥ 6, yet only 13/141 (9%) contained information on the relationship of DWI lesion appearance to histological data (Table 3.4), including 3/13 (23%) papers that explicitly mentioned blinding of image to histological analysis[16,161,162].

Only 1/13 (8%) of the papers that compared DWI lesion appearance to histological data explicitly described the method of aligning histological slices to MR slices for analysis[161]; the other 12/13 (92%) papers either did not mention how histological slices were matched to MR slices, or simply used 'eyeballing' to match up the DWI and histological slices. Of the 13 papers that compared DWI lesion appearance to histological data, only 3/13 (23%) papers explicitly mentioned blinding of DWI analysis to histological analysis and *vice versa*[16,161,162]. As these three papers provide the least biased comparison of DWI to histological data, we focused on their results first.

Three papers with explicit blinding of histological to DWI analysis and vice versa

Jacobs et al.[161] used a permanent MCAO model in rats, with an unsupervised, automated tissue segmentation technique (ISODATA) to outline the lesion from a composite of T_2WI and ADC data. The regions obtained with the ISODATA technique were coregistered and compared to manually outlined haematoxylin and eosin (H&E) stained histological slices at acute (4 - 8 hours), subacute (16 - 24 hours), and chronic (48 - 168 hours) times after onset of occlusion. Histological damage, including swollen and shrunken neurons, was seen beyond the edges of the 'bright' DWI lesion at 4 hours after occlusion onset, showing that at acute stages DWI underestimated cortical ischaemia. The ADC image was poorer than the DWI image at assessing the extent of tissue damage in the acute stage, but was better at the subacute and chronic stages after onset of occlusion.

Table 3.4 Details of the histological features in regions of imaging abnormality from the 13 papers scoring > 6 on the methodological quality scoring system and containing information on the relationship of DWI appearance to histology. n = number of animals, min = minutes.

Study	n	Occlusion time	Duration of Reperfusion	Imaging Results	Histological Feature Studied	Histological Results
Detre et al.[163]	6	120 min	0	'centre' ADCr 35% < and 'edge' ADCr 77% < initial	hsp70 expression	hsp70 +ve in 'penumbra' indicating permanent damage
Grohn et al.[164]	12	90 min	24 h	DWI normalises but DWI abnormality recurs @ 24 h	% of neuronal damage	tissue dead despite DWI renormalisation
Jacobs et al.[161]	22	4 - 8 h	0	DWI 14%, ADC 14% volume difference to histology	inspection of H&E stained slices for signs of ischaemic damage	DWI lesion < histological lesion, ADC not significant
		16 - 24 h		DWI 17%, ADC 14% volume difference to histology		ADC and DWI lesions significantly correlated with histology but which was larger (ADC/DWI or histology volume) not specified
		48 - 168 h		DWI 13%, ADC 10% volume difference to histology		
Kokubo et al.[165]	6	60 min	23 h	'caudate' ADCr 65% < initial ADC	hsp70 expression	hsp70 -ve in caudate - 'irreversible damage'
				'cortex' ADCr 80% < initial ADC		hsp70 +ve in cortex - 'reversible damage'
Li et al.[18]	14	30 min	12 h	'caudate' ADC 0.45 x 10^{-3} mm^2/sec	% of neuronal damage	'caudate' > 50% neuronal necrosis
				'cortex' ADC 0.46 – 0.47 x 10^{-3} mm^2/sec		'cortex' < 10% neuronal necrosis
Li et al.[19]	16	10 min	72 h	ADC initial decrease, then complete recovery	% of neuronal damage	17% neuronal necrosis in lesion despite ADC renormalisation
		30 min	72 h	ADC decrease, recovery, secondary decrease @ 12 h, pseudo-normalisation @ 24 - 48 h		95% neuronal necrosis in lesion despite ADC renormalisation
Li et al.[17]	18	30 min	12 h	ADC 25% < normal @ 0-1 h, ADC normalises @ 1.5 h ADC 25% < normal @ 12 h	% of neuronal damage	92% neuronal necrosis, most astrocytes swollen @ 12 h 94% neuronal necrosis, astrocyte disintegration @ > 12 h
Liu et al.[166]	10	90 min	0	ADC contra cortex normal	% of neuronal damage	contra cortex - no neuronal damage
				ADC ipsilateral frontoparietal cortex 25% <initial ADC		ipsilateral frontoparietal cortex - 62% neurons shrunken
				ADC ipsilateral caudoputamen 45% < initial ADC		ipsilateral caudoputamen - 46% neurons shrunken
Muller et al.[153]	8	45 min	70 min	DWI lesion 9.9% of hemispheric area	size unstained H&E lesion	histological lesion < DWI lesion
		120 min	2 h	DWI lesion 29.1% of hemispheric area		histological lesion < DWI lesion
Muller et al.[167]	9	120 min	2 h	15% increase of DWI hyperintensity in 19% of hemi	size unstained H&E lesion	histological lesion (25% of hemi) > DWI lesion (19% of hemi)
Neumann-Haefelin et al.[16]	19	30 min	7 d	DWI lesion disappeared but recurred @ 24 h	size unstained H&E lesion	damage present with no significant difference between groups at 7 d despite different patterns of DWI changes
		60 min		DWI lesion disappeared but recurred @ 24 h		
		150 min		DWI lesion remained without reversal		
Ringer et al.[162]	10	30 min	4.5 h or 7 d	DWI abnormalities reversed @ 3 - 5 h, recurred @ 1 d	MAP2, hsp72, GFAP expression	30% loss of MAP2 reactivity, extensive hsp72 reactivity, 'astrocytes normal' on GFAP
Sutherland et al.[168]	10	90 min	6.5 h	DWI lesion area > T_2 lesion area	size unstained H&E lesion	histological lesion < T_2 lesion < DWI lesion

Neumann-Haefelin et al.[16] compared 30 minutes, 1 hour, or 2.5 hours of transient MCAO in rats with histological analysis at 7 days after onset of occlusion. DWI and ADC abnormalities reversed after 30 minutes and 1 hour (but not after 2.5 hours) of occlusion, but reappeared at 24 hours in all groups. At 24 hours after occlusion onset, the DWI lesion in the 30 minutes and 1 hour occlusion groups was not as extensive as in the 2.5 hours occlusion group. An infarct was seen histologically at 7 days with all three durations of occlusion, and was not significantly different in area between the groups, even in those with complete disappearance of the DWI lesion after reperfusion.

Ringer et al.[162] used a transient 30 minute MCAO model with DWI during, at 3 - 5 hours, 1 day, and 7 days after occlusion onset, and neuronal (microtubule associated protein 2 [MAP-2]), astrocytic (glial fibrillary acidic protein [GFAP]), heat shock protein 72 (hsp72), and cresyl violet stained histological analysis at 5 hours and 7 days after occlusion onset. The DWI abnormalities visible at 30 minutes reversed at 3 - 5 hours, but recurred at 24 hours after reperfusion. When the DWI was normal at 5 hours, there was a significant decrease in MAP-2 immunoreactivity in 30% of the initial DWI lesion, GFAP was normal, hsp72 staining was extensive and, together with cresyl violet staining extent, corresponded to the initial DWI lesion extent. Hence, the 'normalisation' of the DWI abnormality did not indicate that the underlying tissue was normal, as the neurons (MAP-2) showed signs of structural damage and stress. The normal GFAP staining suggested that non-neuronal cell components may be more capable of recovery thereby partially compensating for altered fluid balances and contributing to the apparently 'normal' DWI appearance.

Remaining ten papers with a methodological quality score ≥ 6

Although blinding was not explicitly mentioned in the remaining 10/13 papers that achieved a methodological quality score of ≥ 6, they did achieve high quality scores reflecting good methodological descriptions in other domains. We therefore examined them in detail also. Of these 10 papers, all except one (of cats[168]) used rats. The intraluminal suture method of MCAO was used in 8/10 papers; the remaining two studies by Detre et al.[163] and Sutherland et al.[168] used fibrin-rich emboli to occlude the middle cerebral artery (MCA) and a microaneurysm clip to occlude the MCA respectively. All studies killed the animals immediately after the final MRI except one (who killed animals 2 hours after the start of the final MRI session[168]).

The 13 papers that compared DWI lesion appearance with histological data (Table 3.4) also indicated that histological neuronal damage persisted or progressed despite the apparent waxing and waning of the DWI lesion[16,162,164]. They further support the observation that the resolution of the early DWI lesion after reperfusion, and its reappearance after 24 hours of reperfusion, may be more due to changes in astrocytes and glial cells than a decrease in neuronal damage. A consistent comment in several papers was that astrocytes swelled (presumably restricting the extracellular space and water movement, and thus affecting DWI), while neurons shrank. Neuronal damage appeared to persist once initiated, while astrocytes swelled or shrank, which may explain the apparent 'normalisation' of the DWI lesion[17,162,166]. This suggests that DWI recovery and 'secondary' DWI decline are perhaps not caused by 'secondary injury' to neurons, but occur due to the progression of primary damage of astrocytes (astrocytes swelled and shrank over time)[17,18,162,166]. The DWI lesion signal intensity ('brightness') seemed to reflect the amount of neuronal damage – after 90 minutes of

occlusion and 24 hours of reperfusion, the more intense the DWI signal within the initial DWI lesion, the greater the proportion of dead neurons[164]. Acute ADC values may not be a good determinant for recoverability, one study found that despite great variability in acute ADC values in groups of animals undergoing 30, 60, and 150 minutes of occlusion, all groups showed a similar degree of histological tissue damage at 7 days after occlusion onset[16]. The reduction in ADC at the end of 30 minute occlusion was also similar in areas which, following 24 hours of reperfusion, had only 10% of dead neurons as those which had 50% of dead neurons[18]. However, in another study, the ADC value at the end of vessel occlusion did correspond to the amount of neuronal damage, as larger decreases in the ADC occurring after 90 minutes of occlusion correlated with increasing levels of neuronal damage after 24 hours of reperfusion[164]. It was also clear that even short periods (e.g. 30 minutes) of transient ischaemia in rats caused permanent damage to neurons[16-19]. Differing degrees of damage were also seen in different parts of the brain for a given duration of occlusion - damage to the striatum (particularly the caudoputamen) was worse than damage to the cortex as seen on both DWI and histology[17-19,165].

Discussion

DWI and PWI are frequently used in studies of ischaemic stroke, and are generally thought of as displaying 'neuronal' damage. However, the exact degree of ischaemic damage at the cellular level demonstrated by DWI and PWI, and the likelihood of recovery, has yet to be determined[169]. Although the proportion of studies that we

were able to examine in detail was disappointing (due to missing information), a consistent suggestion emerged - that glial cell ischaemic changes are the main contributors to the both the initial appearance and evolution of the ischaemic lesion on DWI. Thus 'neuroprotection' strategies may not be best monitored with DWI, unless it is likely that the drug in question has actions on non-neuronal cell types. If glial cells are responsible for much of the DWI lesion evolution, then new approaches to avoid adverse events (such as massive infarct swelling) should consider interventions in the glial cell 'ischaemic cascade'.

This review has identified several important correlations between DWI and histological data, but many papers were not informative. It is possible that some studies were not set up specifically to examine the relationship between DWI and histological data, however, the limited description of the animals used, MRI procedures, and histological analysis, combined with absence of blinding of image and histological analyses, uncertainties about how the image data were compared to the histological data, and few subregional analyses, means that there are still many unanswered questions about the relationship of DWI and PWI lesion appearance and the underlying pathophysiological state of the brain tissue. Blinding of image and histological interpretation is vital if biases are to be avoided[160].

We examined all papers, but found that papers scoring < 6 on our quality scoring system did not inform on the relationship between DWI and histological tissue state - frustratingly only 13/51 (26%) of papers scoring ≥ 6/10 had information on the relationship of DWI and histological data.

Amongst the studies scoring ≥ 6 on our quality scoring system (Table 3.4), several potentially important methodological issues became apparent which might explain

some of the differing results. Firstly, several of the studies used repeated or very prolonged periods of anaesthesia with isoflurane[18,19] – either might contribute to cerebral damage in areas of vulnerable ischaemic brain, tipping potentially vulnerable tissue towards permanent damage and making cell damage appear worse for a given ischaemic insult. Secondly, only one study mentioned taking care to perfuse and fix the tissue for histological analysis in a way that should eliminate artefactual 'dark, shrunken' neurons[166]. How much of the neuronal damage seen on histological examination in other studies could be due, even in part, to fixation effects? Perhaps damage inflicted by tissue fixation could account for some of the inconsistency of results, as for example seen in Muller et al.[153] and Muller et al.[167], where the lesion on DWI was larger than the histological lesion in the former, and smaller than the histological lesion in the latter despite using seemingly identical methods in the same research laboratory. When comparing histological slices to MRI slices, it is important to ensure that the same areas of the brain are being compared. It was not clear in the majority of the papers whether, and how, this 'matching' of histological and MR slices was performed, although 'eyeballing' seemed to be the most frequently used method. Thus, it is difficult to be sure that the histological slice represented the same tissue as that of the 'matched' MR image.

Despite this, several consistent patterns emerged (Table 3.4) with implications for studies in human ischaemic stroke patients. Histological damage persists and progresses despite the DWI lesion waxing and waning, i.e. referring to reappearance of the DWI lesion after a period of normalisation as 'secondary injury' in human studies is probably not correct in pathophysiological terms. Acute ADC values are not good predictors of tissue recovery as similar values were obtained from tissue

that subsequently mostly recovered as from other areas which were permanently and severely damaged. However, the intensity ('brightness') of the DWI signal does seem to relate to the proportion of damaged neurons – the more abnormal ('brighter') the DWI signal, the greater the proportion of damaged neurons. The intensity of the DWI signal is the most rapidly and easily interpreted information from DWI in the clinical situation – the observer can assess the lesion 'brightness' immediately, so this is probably one of the more clinically useful results of this work. Changes in astrocytes, rather than neurons, probably account for much of the DWI lesion waxing and waning – the neurons are said to shrink, while the astrocytes are reported to swell. If DWI signal change is at least in part the result of restricted water movement in the extracellular space, then swollen astrocytes rather than shrunken neurons (assuming the 'shrinkage' is not a fixation artefact) could be the major contributor to this appearance. In rats, even 30 minutes of ischaemia is lethal to some neurons, and damage to the caudoputamen (both on DWI and histological slices) was worse for a given degree of ischaemia than damage in the cortex.

Where next? Experimental methodology could be more clearly and consistently described; occlusion methods, animals, and MRI methods should be described in a reproducible way, and blinded methods of image and histological analyses are essential to reduce bias. More information is required on how DWI abnormalities relate to cellular changes – at what degree of 'brightness' on DWI does the tissue pass the point of no recovery, and how does this change with increasing time after stroke onset? The Stroke Therapy Academic Industry Roundtable discussion concluded that little animal research done to date 'has translated into effective treatment modalities for stroke in humans'[170]. Perhaps the focus on neurons, both

experimentally and in imaging studies, has deflected attention from the contribution of other important cell types to the total damage and likelihood of recovery in ischaemic lesions as a whole. Experimental studies may help with translational research to clarify and determine mechanisms for important relationships between MRI appearances found in clinical studies and histopathology. However the methodology should be clearly described, the model should be relevant to stroke patients, and important differences in proportions of cerebral cells (e.g. neurons and glial cells) between animals and humans and their contributions to the ischaemic process should be considered.

4. Patient cohort and basic lesion measurement

Introduction

This chapter presents the methods for the recruitment, imaging, and basic lesion measurement of the large cohort of patients used for the analyses in this thesis. Results of basic manual lesion analysis, including DWI and PWI parameter values from the visible DWI and PWI abnormalities from baseline (< 24 hours after stroke onset) to final outcome (90 days after stroke onset) imaging are presented.

Methods

Patient Recruitment

Patients were recruited prospectively (between June 2000 and June 2004) from the hospital stroke service at Western General Hospital, Edinburgh by stroke physicians. Patients with symptoms of ischaemic stroke of all severities who could be imaged within a maximum of 24 hours of stroke onset (baseline) were eligible for this study. Local ethics approval was obtained from the Lothian Local Research Ethics Committee. All patients were examined by a trained stroke physician on admission and diagnosed as having probable or definite stroke. Baseline clinical assessment and stroke scoring were performed immediately using the National Institutes of Health Stroke Scale (NIHSS)[171] and Oxfordshire Community Stroke Project (OCSP) classifications[13]. Imaging was repeated at approximately 5, 14, 30, and 90 days after stroke onset. Patients were followed up at 90 days after stroke onset to determine their functional status using the modified Rankin Scale (mRS)[172,173]. A final diagnosis (stroke, TIA, or non-stroke) was reached by a panel of experts in stroke

neurology and imaging using all available clinical and imaging information for each patient after the patient was discharged.

Imaging

All MRI data were obtained using a GE Signa LX 1.5 T (General Electric, Milwaukee, WI, USA) clinical scanner (located in the Scottish Higher Education Funding Council [SHEFC] Brain Imaging Research Centre for Scotland [SBIRCS] in the Division of Clinical Neurosciences, Western General Hospital, Edinburgh), equipped with a self-shielding gradient set (22 mT/m maximum gradient strength and 120 T/m/s slew rate) and manufacturer-supplied 'birdcage' quadrature head coil. The MRI examination consisted of standard sequences for stroke diagnosis including a fast SE-T_2W sequence, a gradient echo T_1W sequence, and DWI and PWI as detailed below. The total duration of the MRI examination from the patient entering to leaving the MRI suite was 20 - 40 minutes.

Imaging was repeated where possible at 5, 14, 30, and 90 days after stroke onset. To ensure that the slice locations used in the follow-up scans corresponded as closely as possible to those in the first, the subject's head position and tilt in the first scan were recorded and the patient was repositioned as close as possible to this position in the follow-up scans.

DWI

Diffusion MRI data were acquired using a DT-MRI protocol based on SE-EP imaging. In this protocol, sets of axial DW-EP images (b = 0 and 1000 s/mm^2) were collected with diffusion gradients applied sequentially along six non-collinear directions[174]. Five acquisitions consisting of a baseline T_2W-EP image and 6 DW-EP images (a total of 35 images) were collected per slice position. The acquisition

parameters for the DW-EP imaging sequence were: 15 axial slices of 5 mm thickness and 1 mm slice gap, a field-of-view (FOV) of 240 × 240 mm, an acquisition matrix of 128 × 128 (zero filled to 256 × 256), a TR of 10 s and a TE of 98.8 ms. In a small number of patients who were very ill and judged unlikely to tolerate the entire DT-MRI protocol, a shorter DW-MRI sequence was used. This sequence shared the same acquisition parameters as the DT-MRI protocol, except that only two averages were collected and the diffusion gradients were applied sequentially in three orthogonal directions. Other than not containing diffusion anisotropy data, the DWI maps and underlying ADC values were the same in patients receiving the shorter sequence so for the purposes of this thesis data from these shorter DW-MRI sequences will be considered the same as data from the full DT-MRI sequences.

PWI

Perfusion MRI data were acquired by imaging the dynamic signal change following a bolus injection of a gadolinium-based contrast agent (gadopentetate dimeglumine). Patients were injected with either 1.0 mmol Gadovist® (10 mL @ 5 mL/s; Schering AG, Germany) or 0.5 mmol Omniscan™ (20 mL @ 5 mL/s; Amersham Health AS, Norway) in the antecubital vein. Thirty-four volumes of 15 axial slices of 5 mm thickness and 1 mm slice gap were acquired over a period of 82.5 s using a single-shot T_2*-weighted GRE-EP imaging sequence with a FOV of 240 × 240 mm, an acquisition matrix of 128 × 128 (zero filled to 256 × 256), a TR of 2.5 s and a TE of 30 ms. Four baseline volumes were collected before contrast administration.

Image Processing

The DICOM (Digital Imaging and Communications in Medicine, National Electrical Manufacturers Association, Rosslyn, VA, USA) standard format images were

transferred from the scanner to a Sun Ultra Sparc Station 10 (Sun Microsystems, Mountain View, CA, USA) and converted into Analyze™ (Mayo Foundation, Rochester, MN, USA) format using in house software written in the C programming environment.

Computational image realignment techniques were used to realign the diffusion and perfusion imaging data from the baseline and all subsequent scans to the T_2WI volume from the baseline DT-MRI scan. This realignment minimises any small remaining positioning errors and removes bulk patient motion and eddy current induced artefacts[175].

The set of five component DW-EP images for each gradient direction were averaged to obtain seven high signal-to-noise ratio images for each brain slice. From the signal intensities measured from the DW-EP images, the six elements of the apparent diffusion tensor of water (**D**) and T_2WI SI from each voxel were estimated by multivariate linear regression[176]. After diagonalisation of **D** to yield the magnitude sorted eigenvalues (λ_1, λ_2, λ_3), maps of the T_2WI SI and average ADC, calculated as[176]:

$$\text{ADC} = (\text{Trace } \mathbf{D}) / 3 = (\lambda_1 + \lambda_2 + \lambda_3) / 3$$

were generated on a voxel-by-voxel basis.

For the perfusion data, tracer concentration vs. time curves were produced voxel-by-voxel from the SI vs. time data, and gamma-variate fitting procedures were applied to remove the effects of tracer recirculation[177]. 'Index' perfusion measures were calculated; CBV_i as the area under the voxel concentration vs. time curves, MTT_i as the first moment of the voxel concentration vs. time curves, and CBF_i from the Central Volume Principle[34,35]:

$$CBF = CBV/MTT$$

All perfusion data presented in this thesis (CBF, CBV, and MTT) are 'index' parameters as described in Chapter 1 (and thus can be assumed to be CBF_i, CBV_i, and MTT_i). Note, since 'index' perfusion data is not quantitative, extracted perfusion values are in arbitrary units (AU). Colour perfusion maps were produced by windowing the grey-scale perfusion maps to the MATLAB® (The MathWorks, Natick, MA, USA) 'jet' colour scale (Figure 4.1), which ranges from blue (minimum) to red (maximum).

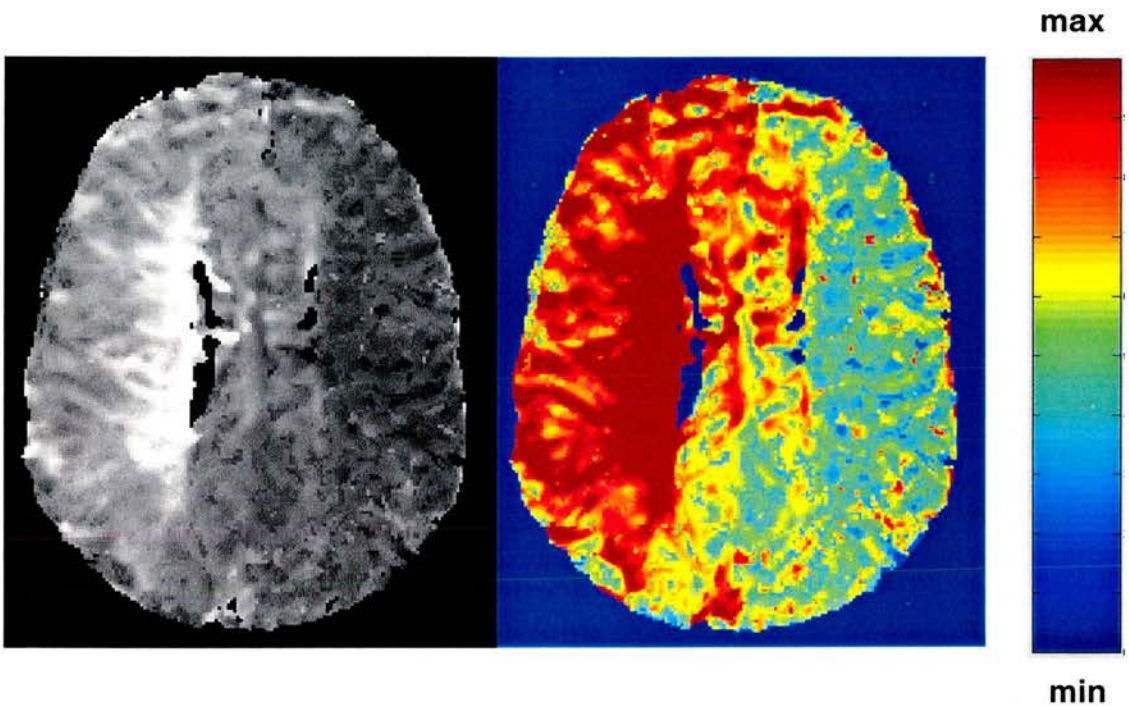

Figure 4.1 Example of a MTT colour map (centre, in a patient with a right hemisphere ischaemic lesion at 13 hours after stroke onset), calculated by windowing the grey-scale signal intensities (left) to the MATLAB® 'jet' colour scale (right).

Basic region of interest analysis

All lesion volume measurements were performed on a Sun Ultra Sparc Station 10 using Analyze™. For each patient, for all scans performed at each MRI time point, the visible abnormalities (if present) on DWI, CBF, and MTT images were measured. DWI SI and colour CBF and MTT maps were printed on paper and a board-certified neuroradiologist with 10 years of DWI lesion interpretation (JMW), blind to clinical and other imaging data, outlined the visible lesion on the paper copy. The author (who had 12 months experience of viewing and measuring acute stroke lesions on DWI at the beginning of the study), blind to baseline clinical and outcome data, used these outlines to trace around the lesions on the Sun workstation, and outlined a homologous contralateral region of interest for each lesion region. Image brightness and contrast were adjusted for maximum contrast between hyperintense tissue and normal appearing brain. ADC, CBF, and MTT values were extracted for the DWI, CBF, and MTT lesion and contralateral regions. Relative ADC, CBF, and MTT (ADCr, CBFr, and MTTr) values were calculated for each patient by dividing the lesion values by the contralateral values to allow for comparison of data between patients and over multiple scan times. Total lesion volumes were obtained by sampling the number of outlined voxels on each slice on which the lesion was visible and multiplying by the slice thickness.

Statistical analyses

General patient demographic data were obtained and compared, including the sex, age (mean and range), initial NIHSS score (mean, median, and range), OCSP classifications, and mRS at 90 days after stroke onset (mean, median, and number of patients dependent [mRS = 3 - 5] and dead [mRS = 6] at 90 days after stroke onset).

Mean (± standard deviation [SD]) time from stroke onset to baseline and subsequent MR scanning are reported.

Mean (± SD) ADCr, CBFr, and MTTr values are reported and compared for all available patient scans at each time point. Baseline ADCr, CBFr, and MTTr were compared to normal (test value = 1, as they are relative values) using standard t-tests. Changes in ADCr, CBFr, and MTTr values over time (from baseline to 90 days after stroke onset) were analysed using general linear model (GLM) repeated measures regression analysis (dependent variables = ADCr, CBFr, and MTTr values). MR parameters were fit to a linear model, except for CBF, which was fit to a quadratic model as the evolution of CBF in ischaemic tissue over time exhibits significant quadratic effects.

All statistical analyses in this thesis were performed in SPSS® 11.0 (SPSS Inc., Chicago, IL, USA). Differences were considered significant at the observed significance level (p) of 0.05 throughout this thesis.

Results

Patient details

A total of 161 patients were recruited, 27 of which were excluded from this analysis for the following reasons: 14 patients had unusable, incomplete scanning (e.g. could not tolerate scanning procedure due to claustrophobia), 11 patients had a haemorrhage, and two patients had a intracerebral tumour.

Of the 134 patients included in the general image analysis, 72/134 (54%) were male, the mean age was 64 (range: 35 - 99 years), and the mean NIHSS score on admission was 9 (median 7, range: 0 - 29). OCSP classifications: 31/134 (23%) patients had a total anterior circulation infarct (TACI), 62/134 (46%) patients had a partial anterior circulation infarct (PACI), 27/134 (20%) patients had a lacunar infarct (LACI), 10/134 (8%) patients had a posterior circulation infarct (POCI), and 4/134 (3%) patients had an uncertain OCSP classification. All patients were treated with aspirin, but none received thrombolysis or any investigational neuroprotective drugs. Mean mRS score at 90 days after stroke onset was 3 (median 2); 46/134 (34%) patients were dependent (mRS = 3 - 5) and 20/134 (15%) patients were dead (mRS = 6). Final diagnoses by expert panel after patient discharge were: 127/134 (95%) patients had a stroke, 5/134 (4%) patients had a TIA, and 3/134 (2%) patients were classified as non-stroke patients. All patients were included in the general analysis in this chapter, as they represented a typical population of patients presenting with stroke-like symptoms, but patients diagnosed as only having had a TIA and non-stroke patients were excluded from further in-depth analyses presented later in this thesis. All patients included in any subsequent analyses in this thesis were selected from this population of patients.

Imaging details

General patient scan characteristics

Mean (± SD) time from stroke onset to baseline MRI was 14 ± 11 hours, with 42/134 (31%) patients imaged within 6 hours, 29/134 (22%) patients between 6 and 12 hours, and 63/134 (47%) patients between 12 and 24 hours after stroke onset (Table 4.1). 60/134 (45%) patients had a scan at 5 days, performed at a mean of 5.4 ± 1.0

days; 52/134 (39%) patients had a scan at 14 days, performed at a mean of 12 ± 2 days; 43/134 (32%) patients had a scan at 30 days, performed at a mean of 31 ± 3 days; 40/134 (30%) patients had a scan at 90 days, performed at a mean of 96 ± 7 days after stroke onset (Table 4.1). Whether PWI was performed (some patients were unable to complete PWI, or had unusable images due to movement artefacts), and the number of patients with visible lesions on DWI, CBF, and MTT images for each scan time can be found in Table 4.1. Six patients had non-sequential multiple scanning: one patient had the baseline and 14 day scans only; two patients had the baseline and 90 day scans only; one patient had the baseline, 5 day, and 90 day scans only; one patient had the baseline, 30 day, and 90 day scans only; and one patient had all but the 14 day scan.

Table 4.1 Mean (± SD) scan times, number of patients (n), whether PWI was performed, and number of patients with a visible DWI, CBF, and MTT lesion at each scan time.

Scan time	Total n	PWI performed		Visible DWI lesion present		Visible CBF lesion present		Visible MTT lesion present	
		n	%	n	%	n	%	n	%
14 ± 11 h	134	123	92%	111	83%	61	50%	66	54%
5 ± 1 d	60	58	97%	58	97%	32	55%	34	59%
12 ± 2 d	52	48	92%	45	87%	21	44%	25	52%
31 ± 3 d	43	42	98%	39	91%	24	57%	23	55%
96 ± 7 d	40	23	58%	28	70%	16	70%	13	57%

MRI characteristics of the regions of interest

All three patients with a final diagnosis of 'non-stroke' had a baseline scan only, on which there were no visible lesions on DWI or PWI.

Table 4.2 Mean (± SD) scan times, number of patients (n), mean (± SD) ADCr, CBFr, and MTTr values, and DWI, CBF, and MTT lesion volumes (mm^3) at each scan time. Lesion values and volumes were obtained by manually outlining the visible abnormality as seen on each scan on the DWI (for measurement of ADC), CBF, and MTT images.

Scan time	n DWI	ADCr	DWI volume (mm^3)	n PWI	CBFr	CBF volume (mm^3)	MTTr	MTT volume (mm^3)
14 ± 11 h	134	0.815 ± 0.162	23671.715	123	0.865 ± 0.194	34858.422	1.170 ± 0.217	70408.635
5 ± 1 d	60	0.799 ± 0.152	56551.782	58	0.945 ± 0.243	38369.865	1.089 ± 0.160	72654.716
12 ± 2 d	52	0.917 ± 0.149	30891.442	48	1.033 ± 0.237	19276.154	1.069 ± 0.115	48054.108
31 ± 3 d	43	1.077 ± 0.150	34177.214	42	0.879 ± 0.251	39090.925	1.069 ± 0.117	53809.256
96 ± 7 d	40	1.185 ± 0.208	20785.824	23	0.758 ± 0.178	64757.239	1.083 ± 0.117	57150.688

A)

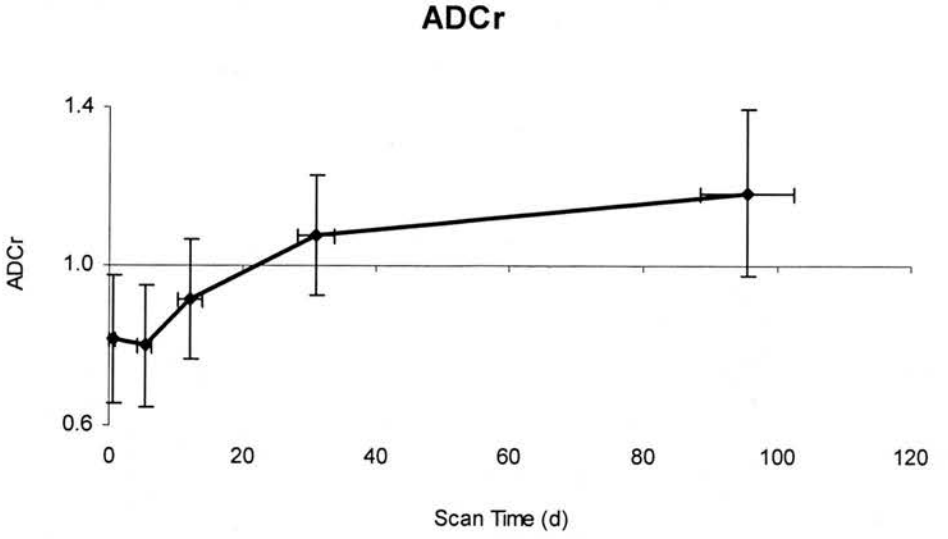

B)

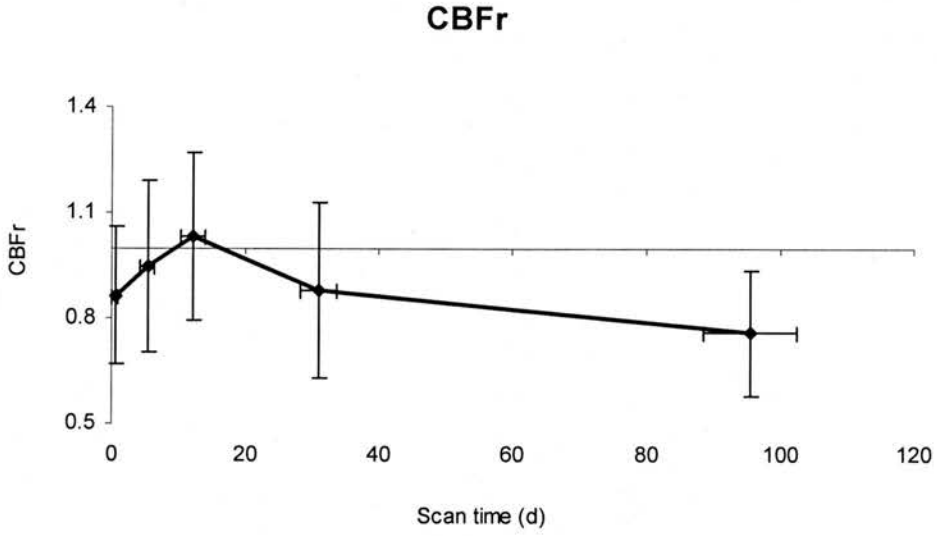

C)

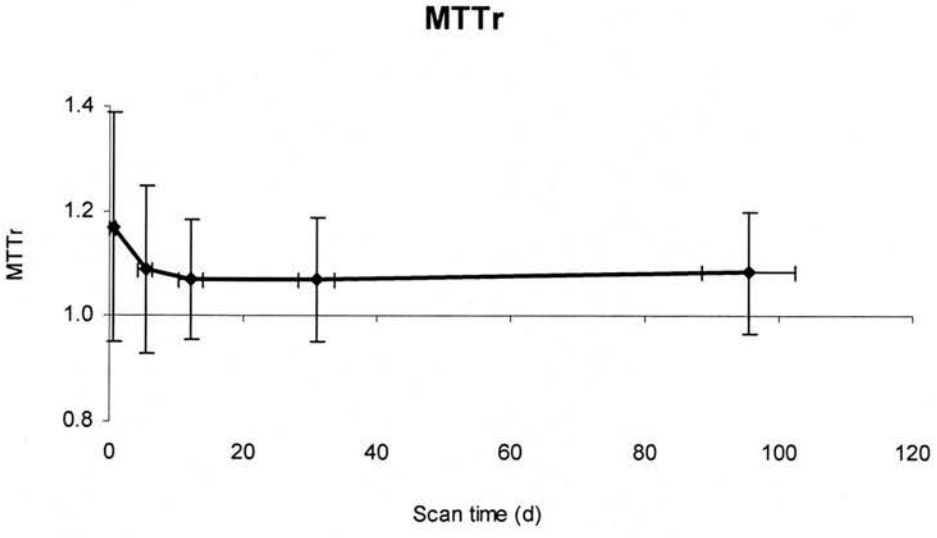

Figure 4.2 Mean A) ADCr, B) CBFr, and C) MTTr values from baseline to 90 days after stroke onset for all patients with any number of scans. See Table 4.2 for patient numbers at each scan time. Values were obtained from the manually-outlined visible abnormality as seen on DWI (for ADCr), CBF, and MTT images at each scan time. Error bars represent ± 1 SD of the mean.

Table 4.2 lists the number of patients with DWI and PWI data at each scanning time point, mean (± SD) ADCr, CBFr, MTTr values, and lesion volumes for the visible abnormality on each scan. Figure 4.2 shows graphs of ADCr, CBFr, and MTTr values from baseline to 90 days after stroke onset.

Baseline ADCr in the lesion was significantly decreased compared to normal (ADCr = 0.815 ± 0.162, n = 134, t-test $p < 0.01$), and increased significantly over time (GLM regression $p < 0.01$; Figure 4.2). ADC appeared to reach a nadir at approximately 5 days after stroke onset (ADCr = 0.799 ± 0.152, n = 60), and appeared to 'pseudonormalise' by approximately 20 days after stroke onset (Table 4.2, Figure 4.2).

Baseline CBFr in the lesion was significantly decreased relative to normal (CBFr = 0.865 ± 0.194, n = 123, t-test $p < 0.01$), and changed significantly over time; appearing to increase to a peak at approximately 14 days after stroke onset and subsequently decrease (GLM regression $p = 0.01$; Table 4.2, Figure 4.2). Baseline MTTr in the lesion was significantly prolonged relative to normal (MTTr = 1.170 ± 0.217, n = 123, t-test $p < 0.01$), and decreased significantly over time (GLM regression $p < 0.05$), appearing to reach a nadir at approximately 14 days after stroke onset (MTTr = 1.069 ± 0.115, n = 48; Table 4.2, Figure 4.2).

Discussion

General patient characteristics

This study represents one of the largest cohorts of ischaemic stroke patients with serial DWI and PWI to date, with all acute and subsequent clinical and imaging assessments and analyses performed blindly and independently of each other. Final diagnosis was determined after patient discharge by a panel of experts using all available clinical and imaging details – this represents the 'gold standard' for stroke diagnosis, but is not often employed. Without this final diagnosis, there is a danger of including patients with TIA and patients that have not had a stroke, which would possibly underestimate or bias the assessment of the usefulness of MRI in stroke, and affect the diffusion and perfusion parameters extracted.

Diffusion and perfusion parameters

Previous studies have reported initial ADCr values of 0.53 - 0.81 sampling regions manually drawn around the acute (< 24 hours after stroke onset) DWI abnormality[70,76,77,97,178] ; the initial ADCr decrease found in this study is at the 'least-decreased' end of this spectrum. However, these previous studies have been in smaller numbers of patients (mean n = 43), and have mainly included only patients with more severe strokes. Other studies report even more severely decreased baseline ADC values (e.g. ADCr = 0.36 – 0.68)[61,72,73,119]. However these studies measured ADC values only from a small region of interest placed in the centre of the visible DWI abnormality. As discussed in Chapter 2, sampling ADC in a small region within a lesion is problematic due to the heterogeneity of ADC values within lesions.

In this study, ADCr values were still decreased relative to normal at 14 days after stroke onset, i.e. ADC values had not yet 'pseudonormalised'. As mentioned in

Chapter 2, previous studies report 'pseudonormalisation' of ADC values within a wide variety of times, from 18 hours - 85 days after stroke onset, with the majority within 4 - 10 days after stroke onset, earlier than found in this study. Again, the small patient numbers (typically n = 20 - 30) and inclusion of only more severe stroke patients in previous studies, compared to the large number of patients and inclusion of patients with all severities of stroke in this study, may explain the differences in the evolution of ADC values reported. Furthermore, this study had serial scanning in a large number of patients at specific time points – the values are not individual 'snapshots' of different patients at widely varying imaging times that were 'stitched' together in an attempt to determine patterns of ADC change. This study also utilised relative ADC values, with each patient acting as their own 'control', thus eliminating the effects of any individual differences in ADC (e.g. differences in age-related ADC changes which were not always accounted for in previous studies).

Few studies have reported the actual perfusion values in the acute visible PWI lesion - most studies of acute PWI have investigated only how the acute PWI lesion volume, or how the presence and degree of 'DWI/PWI mismatch', relates to the final infarct volume. One study measuring acute CBF_a and MTT_a values within the visible acute DWI lesion found both more severely prolonged MTT and lower CBF than in the present study[179]. However, as acute PWI lesions are generally larger than the acute DWI lesions, measuring CBF and MTT values from only the acute DWI lesion will likely represent only the most severely affected tissue - in this study, CBF and MTT values were extracted from the entire visible abnormality on CBF and MTT images, thus likely incorporating regions of less severe deficit (i.e. 'oligaemic' tissue, especially for MTT).

Several studies have attempted to define a MTTr or CBFr 'threshold' that predicts tissue infarction. Suggested MTTr (e.g. 1.28[149] – 1.63[150]) and CBFr (e.g. 0.59[150] – 0.70[144]) thresholds indicate more prolonged MTT and decreased CBF than found in this study, but again it is likely that the initial PWI lesion as measured in this study includes oligaemic tissue that will not infarct. Furthermore, it is still unclear which perfusion measure (e.g. 'index' vs. 'absolute') and parameter (e.g. CBF vs. MTT) most closely identifies 'tissue at risk' of infarction[145]. Extracting baseline CBF and MTT values from a region comprising of tissue that is part of the final (e.g. ≥ 30 days after stroke onset) infarct on T_2WI would be more appropriate for development of a baseline perfusion threshold. The relationship of baseline PWI parameters and the 'DWI/PWI mismatch' to final infarct extent will be explored further in Chapter 6.

5. Factors affecting lesion measurement on acute DWI

Introduction

This chapter assesses factors that affect lesion volume measurement on DWI by examining the differences in measured lesion volumes between two observers, and how the differences relate to lesion morphology and observer experience.

Factors affecting lesion measurement on acute DWI

Acute (< 24 hours after stroke onset) DWI lesion volume may predict clinical outcome[96-98], and patient management and clinical trial design are increasingly influenced by information obtained from DWI[63,64,180]. However, factors influencing DWI lesion measurement have not been widely assessed. Studies which simply assessed observer reliability in detecting the presence and subjective extent (e.g. whether the lesion occupied less than or greater than 1/3 of the MCA territory) of an acute DWI lesion without objectively measuring lesion volume were not considered directly relevant to factors influencing lesion volume measurement (Table 2.2)[64,65,67,108]. Problems with lesion measurement highlighted in Chapter 2 included measurement of DWI lesion volumes at widely varying stages after ischaemic stroke (e.g. from < 7 hours[104] - 84 days[99] after stroke onset), and small numbers of patients (e.g. n = 12[104] - 28[100]; Table 2.1). Some discrepancies between these studies could be due to different methods used to measure ischaemic lesion volumes on DWI, or possibly to inherent features of the lesions which might influence volume measurement. For instance, during the hyperacute (< 6 hours after stroke onset) stages of ischaemic stroke, the lesion on DWI is likely less hyperintense and the

edges less well defined than at later times[59], so acute lesion volume measurements could be less reliable than these studies suggest. Also, previous studies have not explored factors that might affect DWI lesion volume measurement.

Therefore we tested the effect of baseline (< 24 hours after stroke onset) DWI ischaemic lesion appearance on the difference in baseline DWI lesion volume obtained by two typical measurement approaches. To test if the use of an automated ADC threshold (which would reduce observer differences as discussed in Chapter 2) was feasible, we also applied two appropriate ADC thresholds in four exemplar patients.

Methods

The first 83 patients recruited as part of the larger cohort of patients as described in Chapter 4 were included in the present analysis.

Lesion measurement

In addition to the measurement method as described in Chapter 4 (method A, neuroradiologist-guided manual outlining of the visible DWI abnormality), a second method of lesion measurement was employed. This second method (method B) was the same as method A, with the exception that the neuroscientist (the author), blind to baseline clinical and outcome data, independently traced around the hyperintense lesion on the baseline DWI without guidance from the neuroradiologist. Total lesion volumes were obtained by summing the number of outlined voxels on each slice on which the lesion was visible and multiplying by the slice thickness.

Lesion morphology categorisation

Each lesion was scored by the neuroradiologist, blind to all clinical and other imaging data, according to whether it appeared: a) solitary or multi-focal; and b) had well-defined or ill-defined edges on baseline DWI (see examples in Figure 5.1).

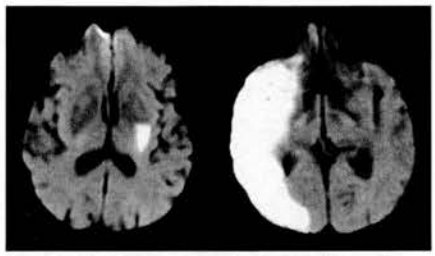

A) Solitary, Well-Defined

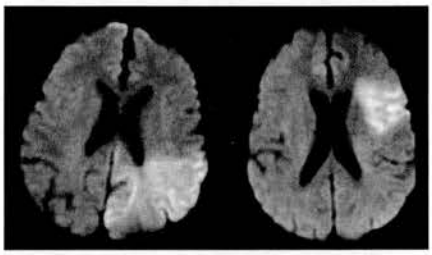

B) Solitary, Ill-Defined

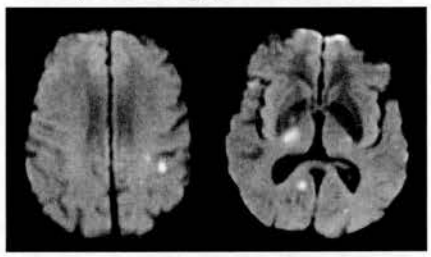

C) Multi-focal, Well-Defined

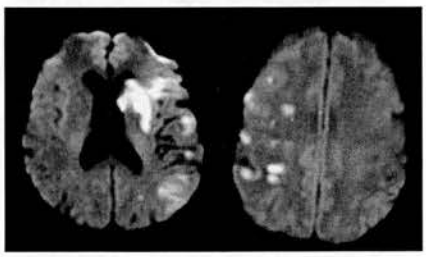

D) Multi-focal, Ill-Defined

Figure 5.1 Examples of ischaemic lesions on DWI at < 24 hours after stroke onset showing the four lesion appearance morphologies. Note the right and left images are from different patients.

We defined a 'solitary' lesion as a single, solitary hyperintense lesion on DWI, and a 'multi-focal' lesion as two or more separate hyperintense lesions on DWI of similar age and within the same arterial territory. We defined a lesion as 'well-defined' if its edges were clear and sharp, and 'ill-defined' if its edges were subtle, not easily distinguished, with less signal intensity difference between the lesion and normal brain.

Lesion measurement by ADC thresholding

To assess the effect of thresholding on an ADC value on lesion volume, we chose four exemplar patients, one from each lesion category (single and well-defined, single and ill-defined, multi-focal and well-defined, and multi-focal and ill-defined), and applied two ADC thresholds commonly mentioned in previous studies and thought to indicate thresholds for ischaemic but viable vs. non-viable brain (0.55 and 0.65×10^{-3} mm^2/s)[61,70,74,79,80,88,117,120,123,132,178,181-185].

Statistical analyses

General patient demographic data were obtained and compared as previously described (Chapter 4).

The DWI lesion volumes measured by methods A and B were not normally-distributed (Kolmogorov-Smirnov test $p < 0.01$), so the range and median lesion volumes are reported, and median lesion volumes were compared using Wilcoxon signed rank sum tests. We calculated the absolute difference of lesion volumes between methods A and B.

To determine if the degree of difference between the two measurement methods was related to the time from stroke onset to MRI, absolute lesion volume difference for

MRI data from < 6 hours, 6 – 12 hours, and > 12 hours after stroke onset were compared with a Kruskal-Wallis test.

To assess any association of degree of difference between the two measurement methods with lesion appearance, absolute lesion volume difference between the different lesion morphologies (solitary and well-defined, solitary and ill-defined, multi-focal and well-defined, and multi-focal and ill-defined) were compared with a Kruskal-Wallis test.

To assess any association of time from stroke onset to MRI and lesion clarity, time from stroke onset to MRI (< 6 hours, 6 – 12 hours, or > 12 hours after stroke onset) and lesion clarity (ill-defined or well-defined) were compared with a Chi-Square (χ^2) test.

To determine if lesion volume was associated with the degree of difference between the two measurement methods, we plotted the difference (method B – method A) vs. the mean of the lesion volume measurements between lesion measurement methods A and B (Bland Altman plots[186]). We also assessed whether larger lesions had a greater degree of observer difference by comparing the absolute lesion volume difference between the two measurement methods and whether the mean lesion volume was < 5000 mm^3 or not using a Mann-Whitney U-test.

In the four exemplar patients we used to test ADC thresholds, we compared the lesion volumes obtained by applying the two ADC thresholds and the two manual lesion measurement methods with a Friedman test.

Results

Patient details

In total, 83 patients were recruited, but 20/83 (24%) patients had no visible lesion on DWI so were excluded from the present analysis. Of the remaining 63 patients: 34/63 (54%) were male, the mean age was 73 years (range: 39 - 95 years), and the mean NIHSS score on admission was 8 (median 6, range: 0 - 28). OCSP classifications: 10/63 (16%) patients had a TACI, 29/63 (46%) patients had a PACI, 20/63 (32%) patients had a LACI, and 4/63 (6%) patients had a POCI. Mean mRS score at 90 days after stroke onset was 3 (median 2); 22/63 (35%) patients were dependent (mRS = 3 - 5) and 8/63 (13%) patients were dead (mRS = 6).

General patient scan characteristics

Mean (± SD) time from stroke onset was 15 ± 14 hours, with 21/63 (33%) patients imaged within 6 hours, 12/63 (19%) patients between 6 and 12 hours, and 30/63 (48%) patients between 12 and 24 hours after stroke onset.

Lesion volume differences

The lesions as measured by method B (neuroscientist alone, median volume = 3498.1 mm^3, range: 74.7 – 269731.9 mm^3; Table 5.1) were significantly smaller than those measured by method A (neuroradiologist-guided, median volume = 4293.5 mm^3, range: 96.7 – 334472.2 mm^3, Wilcoxon test $p < 0.01$; Table 5.1). 51/63 (81%) of the lesion volumes measured were smaller with method B compared to method A. The median absolute volume difference between the two measurement methods was 1516.1 mm^3 (range: 0 – 64740.2 mm^3; Table 5.1).

Table 5.1 Median and range DWI lesion volumes, absolute differences, and lesion morphology for the two lesion measurement methods. n = number of patients.

Lesion edge clarity	Lesion morphology	n	%	Volume method A (mm^3)		Volume method B (mm^3)		Absolute volume difference (mm^3)	
				median	range	median	range	median	range
Well-defined	Solitary	18	29%	1043.7	96.7 - 334472.2	1329.3	118.7 - 269731.9	162.6	0 - 64740.2
Well-defined	Multi-focal	2	3%	681.2	584.5 - 777.8	905.3	413.1 - 1397.5	395.5	171.4 - 619.6
Ill-defined	Solitary	29	46%	4218.8	149.4 - 120972.7	2693.8	74.7 - 92342.9	1520.5	74.7 - 51376.5
Ill-defined	Multi-focal	14	22%	9052.7	1265.6 - 56201.7	5300.5	435.1 - 56000.0	5466.8	663.6 - 24584.8
OVERALL		63	100%	4293.5	96.7 - 334472.2	3498.1	74.7 - 269731.9	1516.1	0 - 64740.2

Differences in lesion volumes between the two measurement methods were significantly associated with time from stroke onset to MRI (Kruskal-Wallis test $p < 0.04$): lesion volume differences were greatest for lesions from < 6 hours after stroke onset (median difference = 4363.8 mm^3), intermediate for lesions from 6 – 12 hours after stroke onset (median difference = 1340.3 mm^3), and smallest for lesions from > 12 hours after stroke onset (median difference = 670.2 mm^3).

Influence of lesion morphology

Of the 63 patients in the present analysis, 18/63 (29%) patients had solitary and well-defined lesions, 29/63 (46%) patients had solitary and ill-defined lesions, 2/63 (3%) patients had multi-focal and well-defined lesions, and 14/63 (22%) had multi-focal and ill-defined lesions (Table 5.1).

Absolute volume differences were significantly different between the different lesion morphologies (Kruskal-Wallis test $p < 0.01$): the greatest degree of difference between the two measurement methods was in multi-focal and ill-defined lesions (median difference = 5466.8 mm^3; Figure 5.2, Table 5.1), followed by solitary and ill-defined lesions (median difference = 1520.5 mm^3; Figure 5.2, Table 5.1), followed by multi-focal and well-defined lesions (median difference = 395.5 mm^3; Figure 5.2, Table 5.1), and lastly, with the least degree of observer difference, solitary and well-defined lesions (median difference = 162.6 mm^3; Figure 5.2, Table 5.1).

Lesion clarity was significantly associated with time from stroke onset to MRI (χ^2 test $p < 0.01$): lesions from < 6 hours after stroke onset were more likely to be ill-defined (observed 20 vs. expected 14) and lesions from > 12 hours after stroke onset were more likely to be well-defined (observed 15 vs. expected 10).

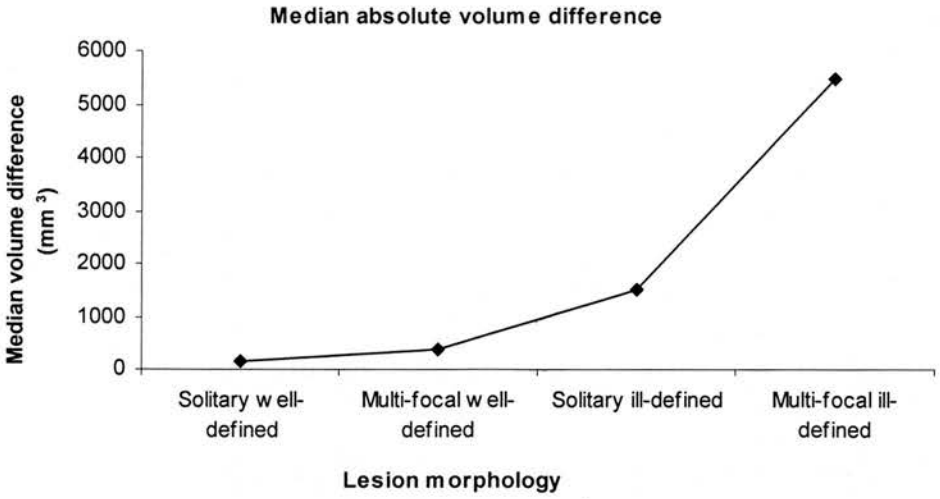

Figure 5.2 Median absolute difference in baseline DWI lesion volume (between lesion measurement methods A and B) by lesion morphology.

Influence of lesion volume

Plots of the difference (method B – A) vs. the mean of the lesion volumes between the two lesion measurement methods are shown in Figure 5.3 (mean ± SD difference = -5373.9 ± 13544.8 mm^3). These plots suggests that larger lesions have greater observer variability than smaller lesions; the difference between methods A and B is nearly zero for lesions less than approximately 5000 mm^3 in volume, but thereafter rapidly increases as lesion volume increases (Figure 5.3).

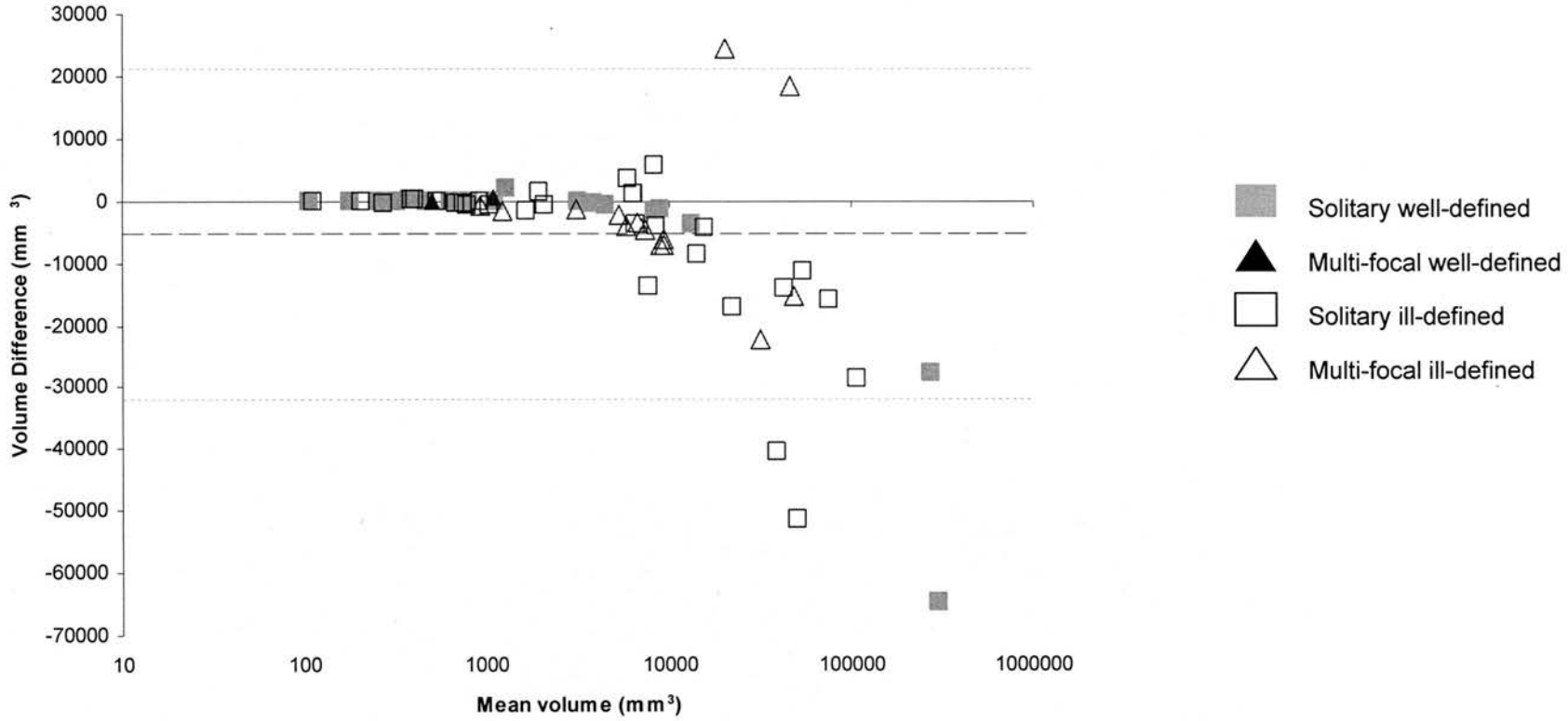

Figure 5.3 The difference (method B – method A) vs. the mean of the two measurement methods by lesion morphology. Note the x-axis is in logarithmic scale. The black dashed line represents the mean volume difference between the two measurement methods (-5373.9 mm^3), the grey dashed lines represent ± 2 SD of the mean difference (95% limits of agreement).

Lesion size was significantly related to the degree of lesion volume difference between the two measurement methods (Mann-Whitney U-test $p < 0.01$): lesions with a mean volume > 5000 mm^3 had larger absolute differences between the two lesion measurement methods (median difference = 7224.6 mm^3) than lesions with a mean volume of < 5000 mm^3 (median difference = 254.9 mm^3).

The influence of lesion volume on the degree of lesion volume difference between the two measurement methods may be confounded by the fact that more larger (> 5000 mm^3) lesions than smaller (< 5000 mm^3) lesions were ill-defined (84% vs. 53% respectively).

Lesion volume measurement by ADC thresholding

In the four exemplar cases, thresholding at an ADC of 0.55×10^{-3} mm^2/s tended to identify a larger volume of tissue than that obtained by the two manual methods of lesion measurement on DWI because of inclusion of tissue apparently normal on DWI remote from the ischaemic region, but also failed to include parts of the actual ischaemic lesion which appeared abnormal on DWI and ADC (Table 5.2, Figure 5.4).

Table 5.2 Volumes (mm^3) of abnormal tissue found for each of the four lesion measurement methods in the four exemplar patients from each lesion morphology category.

Lesion clarity	Lesion morphology	Volume method A (mm^3)	Volume method B (mm^3)	Volume ADC threshold 0.55 $\times 10^{-3}$ mm^2/s (mm^3)	Volume ADC threshold 0.65 $\times 10^{-3}$ mm^2/s (mm^3)
Well-defined	Solitary	288738.3	260916.5	358715.0	395866.4
Well-defined	Multi-focal	584.5	413.1	3053.3	14396.5
Ill-defined	Solitary	76280.3	24903.8	47687.7	104319.1
Ill-defined	Multi-focal	12484.9	6222.7	9703.1	39941.0
OVERALL MEDIAN		44382.6	15563.3	28695.4	72130.1

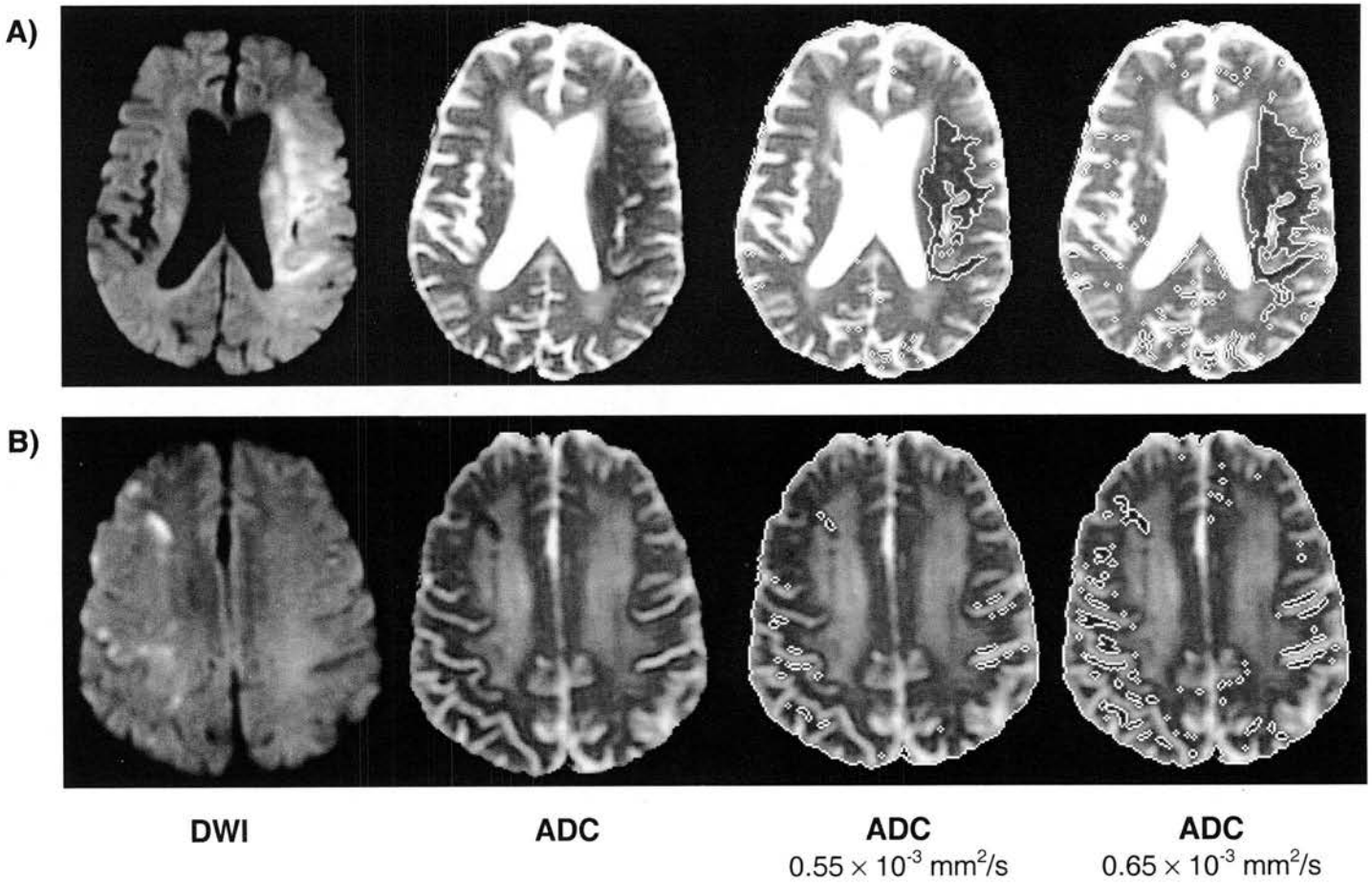

Figure 5.4 Examples of ADC threshold application in two exemplar patients. A) a patient with a left hemisphere ischaemic lesion (solitary and ill-defined on DWI) at 2 hours after stroke onset; B) a patient with a right hemisphere ischaemic lesion (multi-focal and ill-defined on DWI) at 7 hours after stroke onset. Note the ADC thresholds underestimate lesion extent on DWI and ADC, but include several areas of normal brain.

An ADC threshold of 0.65×10^{-3} mm^2/s identified an even larger volume of normal tissue remote from the infarct, both in the ipsilateral and contralateral hemispheres, but still did not include all parts of the visible lesion on DWI and ADC (Figure 5.4).

In the four exemplar cases, lesion volumes obtained from the four lesion measurement methods were significantly different (Friedman test $p < 0.01$): lesion volumes were smallest using measurement method B (median volume = 15563.3 mm^3; Table 5.2), followed by lesion volumes obtained using an ADC threshold of 0.55×10^{-3} mm^2/s (median volume = 28965.4 mm^3; Table 5.2), followed by lesion volumes obtained using measurement method A (median volume = 44382.6 mm^3; Table 5.2), and lastly, measured lesion volumes were largest using an ADC threshold of 0.65×10^{-3} mm^2/s (median volume = 72130.1 mm^3; Table 5.2).

Discussion

The appearance of the acute ischaemic lesion on DWI strongly influences lesion volume measurement. Our patients reflected a range of stroke severity, lesion sizes and appearances typical of many acute stroke patients admitted to hospital and imaged within 24 hours of stroke onset.

DWI lesions that were multi-focal or ill-defined produced the largest differences between all the measurement methods. Hyperacute lesions (i.e. from < 6 hours after stroke onset) were more likely to be ill-defined, and had a greater degree of observer difference than lesions from > 6 hours after stroke onset. Lesion volume was also important; lesions less than approximately 5000 mm^3 in volume produced little

difference between observers, but larger lesions produced substantial differences, possibly because larger lesions tended to be ill-defined.

The less experienced neuroscientist underestimated lesion extent compared with the neuroradiologist. Visual underestimation of DWI lesion extent by less experienced observers was also found by Fiebach et al.[65], who found higher agreement for 'experts' compared to 'novices' in detecting the presence and visually assessing the extent of ischaemic lesions on DWI. Thus, not surprisingly, observer experience is important and should be considered in the study design – despite this many studies do not list observer details[100,104].

Measurement variation for whatever reason may reduce the power of a study, and necessitate an increase in the sample size[187,188]. Having one rater perform all lesion volume measurements, as suggested by Coutts et al.[126], would eliminate interobserver measurement variability, but may not account for differences due to lesion characteristics, is expensive, and is difficult to implement routinely.

ADC thresholds may identify infarcted tissue or 'tissue at risk' of infarction[119,123,178], but we found difficulties with the ADC thresholds because in the four exemplars chosen, neither threshold identified the full extent of the DWI lesion and both detected areas of apparently abnormal tissue quite remote from the infarct that appeared normal on DWI and ADC images. Thus, at the very least, thresholding would require an observer to choose the hemisphere of interest, possibly even the general lesion location, and exclude any tissue erroneously included in the volume, defeating the purpose of applying a threshold to eliminate observer error. Furthermore, white matter ADC values increase with age[130,131], so different thresholds would be needed for patients of different ages, or indeed for patients of

the same chronological ages who might have different levels of age-related background white matter changes[189]. Multiparametric tissue characterisation incorporating ADC values, T_2WI, PWI, or other MRI data[116-118] may avoid this problem, but require further investigation.

DWI is being used increasingly in observational studies and as a 'surrogate outcome predictor' to reduce sample size in clinical trials[190]. It is therefore important that factors which influence lesion volume measurement on DWI are recognised and quantified, and that methods are found to reduce variation. This particularly applies to hyperacute stroke where early lesions are most likely to be ill-defined rather sharply defined. Therefore, studies using DWI in acute stroke should account for the potential factors influencing lesion measurement in sample size calculations, and clearly define their measurement methods.

6. Acute PWI parameters and final infarct extent

Introduction

This chapter explores which baseline PWI parameter, if any, identifies 'tissue at risk' of infarction, and whether the presence of an acute 'DWI/PWI mismatch' as discussed in Chapter 2 is related to lesion growth.

PWI and 'tissue at risk' of infarction

In patients with acute ischaemic stroke, the 'mismatch' between the acute lesion on DWI and PWI may represent the 'ischaemic penumbra'[21] and may provide a target of salvageable tissue both within, and possibly beyond, 6 hours after stroke onset[24]. In several studies, the presence of an acute PWI lesion larger than the DWI lesion at baseline predicted ischaemic lesion growth on final (≥ 30 days after stroke onset) T_2WI[99,101,102,104,147,191]. Some studies also examined ischaemic lesion growth at earlier time points (< 30 days after stroke onset), however the lesion may still be evolving[61], 'fogging' may cause underestimation[93], and oedema may cause overestimation[77,101] of T_2WI infarct extent at these earlier time points. Hence 30 days after stroke onset is the minimum time at which final infarct extent should be assessed.

As discussed in Chapter 1, there are several ways of obtaining perfusion information from DSC PWI, including 'non-quantitative' ('summary' and 'index') and 'quantitative' ('absolute') measures.

'Non-quantitative' perfusion measures

'Summary' estimates of perfusion (e.g. TTP) are easily obtained, and may be a good estimate of MTT[192], but cannot be compared between imaging episodes, and are functions of at least two of the underlying perfusion parameters[33]. 'Index' measures of CBF, CBV, and MTT (CBF_i, CBV_i, and MTT_i) are superior to 'summary' measures as they attempt to model only one of the underlying perfusion parameters, but as discussed in Chapter 1 they are not 'quantitative'.

'Quantitative' perfusion measures

'Quantitative', or 'absolute', perfusion measures require deconvolution of the concentration vs. time curve with an arterial input function[36]. As discussed in Chapter 1, although 'quantitative' perfusion parameters (CBF_a, CBV_a, and MTT_a) have the correct units, they are currently only approximate measures of the true underlying haemodynamics and must be interpreted with caution.

Which perfusion parameter identifies final infarct extent?

CBV is not considered a good predictor of 'tissue at risk' due to its bimodal nature and insensitivity to bolus delay and dispersion[37,150]. Thus, parameters reflecting CBF and MTT have emerged as the most likely candidates for predicting final infarct extent.

Previous studies comparing acute (< 24 hours after stroke onset) PWI data with final lesion extent on T_2WI ≥ 30 days after stroke (Table 6.1) produced rather confusing results. Of the 13 papers found, 2/13 (15%) tested 'summary' measures of perfusion (TTP, total n = 39)[99,101], 2/13 (15%) tested MTT_i (total n = 36)[91,105], 6/13 (46%) tested MTT_a (total n = 146)[138,143,144,149,193,194], and 3/13 (23%) tested CBF_a and MTT_a (total n = 53; Table 6.1)[106,147,150]. None directly compared CBF_i and MTT_i.

TTP correlated strongly with final infarct volume[99,101], MTT_i[91,105] and MTT_a[138,143,144,149,193,194] overestimated final infarct volume, and in the three direct comparisons of CBF_a and MTT_a[106,147,150], two found that CBF_a[106,150] and one that MTT_a[147] related best to final infarct volume (Table 6.1). Some patients also received thrombolysis and/or putative neuroprotective agents, with only 4/13 (31%) studies only including patients treated conservatively[105,144,147,150], and 2/13 (15%) studies were restricted to patients with a 'DWI/PWI mismatch'[147,150], possibly biasing any relationship between baseline PWI and final infarct extent. The small sample sizes (and possible inclusion of the same patients in separate publications), use of different methods for measuring PWI lesions, probable use of inappropriate statistical tests (parametric rather than non-parametric), few comparisons of CBF and MTT, and total absence of data comparing CBF_i and MTT_i (more rapidly calculated in the acute situation than CBF_a and MTT_a), mean that it is unclear which PWI lesion most accurately delineates 'tissue at risk' of infarction.

We aimed to determine whether 'index' CBF_i or MTT_i on baseline (< 24 hours after stroke onset) DSC PWI most closely identified the final (≥ 30 days after stroke onset) infarct extent on T_2WI. We also determined the relationship between 'DWI/PWI mismatch' and 'lesion growth', i.e. how best to identify 'tissue at risk' of infarction in the acute phase of stroke.

Table 6.1 Studies comparing acute PWI lesions with final T_2WI lesion extent. ρ = Spearman's rank, r = Pearson's product moment, correlation coefficient, s = seconds. † likely includes the 18 patients previously reported in Barber et al.[99], ‡ may include 18/38 patients previously reported in Parsons et al.[193]

Paper	n	PWI measure	PWI parameter	Lesion measurement	Statistical analysis of volumes	Results
Baird et al.[91]	18	index	MTT	manual outline	-	MTT volume > final infarct volume in 8/14 patients; MTT may overestimate
Barber et al.[99]	18	summary	TTP (likely)	manual outline	Pearson's r	TTP volume correlated well (ρ = 0.83) with final infarct volume
Barber et al.[143]†	45	absolute	MTT	MTT delay > 4 s threshold	-	tissue with MTT delay > 4 s overestimates final infarct volume
Beaulieu et al.[101]	21	summary	TTP	manual outline	Pearson's r	TTP volume correlates well (r = 0.86) with final infarct volume
Butcher et al.[149]‡	35	absolute	MTT	manual outline of final infarct; MTT delay > 2 s threshold	-	tissue with MTT delay > 2 s overestimates final infarct volume as all patients have areas of 'salvage' (part of acute PWI lesion but not final infarct).
Parsons et al.[193]	38	absolute	MTT	manual outline of final infarct; MTT delay > 4 s and > 6 s thresholds	-	tissue with MTT delay > 4 s appears to overestimate final infarct volume, tissue with MTT delay > 6 s appears to more closely match final infarct volume
Parsons et al.[147]	23	absolute	CBF & MTT	% thresholds of signal intensity on CBF and MTT	Spearman's ρ & Wilcoxon rank sum test	Compared to final infarct volume, tissue with: lowest 30% of CBF signal intensities correlated (ρ = 0.70), and was not significantly different in volume; highest 50% of MTT signal intensities correlated (ρ = 0.77), but was significantly larger; and highest 70% MTT signal intensities correlated (ρ = 0.87), but was significantly smaller.
Røhl et al.[150]	11	absolute	CBF & MTT	autothreshold of DWI, visual assessment of CBF for mismatch with final infarct	-	CBF values distinguish between infarct (part of acute PWI lesion and final infarct) and salvage (part of acute PWI lesion but not final infarct) more sensitively and accurately than MTT values
Røhl et al.[138]	22	absolute	MTT	semi-automated autosegmentation	Spearman's ρ	MTT volume correlates well (ρ = 0.90) with final infarct volume; in 19/21 patients acute MTT lesion volume > final infarct volume
Rose et al.[144]	19	absolute	MTT	'region growing' technique from DWI region seed	? Pearson's r (unspecified)	MTT volume correlates well (r = 0.88) with final infarct volume; 10/12 patients MTT lesion volume > final infarct volume
Rose et al.[106]	19	absolute	CBF & MTT	manual outline	Spearman's ρ	CBF correlates well (ρ = 0.87) with final infarct volume. MTT correlates well (ρ = 0.84) with, but significantly overestimates, final infarct volume. Bolus-delay correction improves correlation
Simonsen et al.[194]	23	absolute	MTT	manual outline	Wilcoxon signed rank test	MTT volume significantly overestimates final infarct volume by 75%
Ueda et al.[105]	18	index	MTT	manual outline	-	MTT overestimates final infarct volume by 282%†

Methods

Patients (as described in Chapter 4) with MRI data at baseline and at ≥ 30 days after stroke onset were included in the present analysis.

Baseline PWI and DWI and final T_2WI lesion volume analysis

A neuroradiologist (JMW), blind to all clinical and other imaging data, guided tracing around the visible lesions on DWI, CBF_i and MTT_i maps as described in Chapter 4. The neuroradiologist also traced around the final T_2WI lesion on the later of the 30 or 90 day scans, (using the same manual outline method as described in Chapter 4). Total lesion volumes were obtained by summing the number of outlined voxels on each slice on which the lesion was visible and multiplying by the slice thickness.

Statistical analyses

General patient demographic data were obtained and compared as previously described (Chapter 4).

The baseline DWI, CBF_i, MTT_i, and final T_2WI volumes were not normally-distributed (Kolmogorov-Smirnov test $p < 0.01$), so median lesion volumes were compared using Wilcoxon signed rank sum tests, and correlations between baseline DWI, CBF_i, and MTT_i volumes with final T_2WI lesion volume were assessed with Spearman's rank correlation coefficients (ρ). We also calculated mean ($\pm$ SD) volumes for comparison with previous studies which reported mean volumes, and Pearson's product moment correlation coefficients (r, appropriate for normally-distributed data) to compare baseline DWI, CBF_i, and MTT_i with final T_2WI lesion volume, to determine whether use of Pearson's r might account for some differences between previous studies.

'Lesion growth' was defined as final T_2WI lesion volume > baseline DWI lesion volume, and 'DWI/PWI mismatch' as baseline PWI lesion volume > baseline DWI lesion volume. Chi-square (χ^2) tests were used to test whether the presence of a DWI/CBF_i or DWI/MTT_i 'mismatch' was related to 'lesion growth'.

Results

Patient details

Forty-six patients were included in the present analysis: 28/46 (61%) were male, the mean age was 72 years (range: 37 - 94 years), and the mean NIHSS score on admission was 8 (median 8, range: 0 - 25). OCSP classifications: 12/46 (26%) patients had a TACI, 29/46 (63%) patients had a PACI, 4/46 (9%) patients had a LACI, and 1/46 (2%) patients had a POCI. Mean mRS score at 90 days after stroke onset was 2 (median 2); 13/46 (28%) patients were dependent (mRS = 3 – 5) and 2/46 (4%) patients were dead (mRS = 6).

General patient scan characteristics

Mean (± SD) time from stroke onset to baseline MRI was 10 ± 7 hours; 18/46 (39%) patients were imaged within 6 hours, 11/46 (24%) patients between 6 and 12 hours, and 17/46 (37%) patients between 12 and 24 hours after stroke onset. Final T_2WI was performed at 30 days after stroke onset (mean 32 ± 4 days) in 6/46 (13%) patients, and at 90 days after stroke onset (mean 96 ± 7 days) in 40/46 (87%) patients.

Baseline PWI and DWI and final T_2WI lesion volumes

Baseline PWI lesion volumes

Baseline median CBF_i and MTT_i lesion volumes were 23737.1 mm^3 and 50603.0 mm^3 respectively (Table 6.2). Baseline CBF_i volumes were significantly smaller than baseline MTT_i volumes (Wilcoxon test $p < 0.01$). There were 11/46 (24%) patients with no visible lesion on baseline CBF_i, and 10/46 (22%) patients with no visible lesion on baseline MTT_i; 6/46 (13%) of these patients had no visible lesion on either baseline CBF_i or MTT_i.

Baseline DWI lesion volumes

All patients had a visible lesion on baseline DWI. The median baseline DWI lesion volume was 13278.1 mm^3 (Table 6.2). Baseline DWI lesion volumes were significantly smaller than baseline CBF_i (Wilcoxon test $p = 0.01$) and MTT_i volumes (Wilcoxon test $p < 0.01$); baseline CBF_i and MTT_i volumes were larger than baseline DWI volumes in 25/46 (54%) and 33/46 (72%) patients respectively.

Final T_2WI lesion volumes

The median final T_2WI lesion volume was 18472.4 mm^3 (Table 6.2). All patients had a visible lesion on final T_2WI corresponding with the lesion indicated on baseline DWI.

Baseline PWI vs. final T_2WI lesion volumes

Baseline CBF_i lesion volumes were not significantly different to final T_2WI volumes (Wilcoxon test p = not significant [NS]; Table 6.2). Baseline MTT_i volumes were significantly larger than final T_2WI volumes (Wilcoxon test $p < 0.01$; Table 6.2). Baseline DWI lesion volumes were not significantly different from final T_2WI lesion volumes (Wilcoxon test p = NS; Table 6.2).

Table 6.2 Mean (± SD) and range baseline DWI, CBF, and MTT lesion volumes compared to final T_2WI volume. p value = exact significance result of Wilcoxon signed rank sum tests between mean baseline DWI, CBF, and MTT lesion volumes and final T_2WI lesion volume; n > T_2WI = the number of DWI/CBF/MTT lesions larger than the final T_2WI volume; ρ = Spearman's rank, r = Pearson's product moment, correlation coefficient (between baseline DWI/CBF/MTT and final T_2WI volumes).

Lesion	Median volume (mm^3)	% of median final T_2WI volume	Minimum volume (mm^3)	Maximum volume (mm^3)	Mean volume (mm^3)	SD (mm^3)	% of mean final T_2W volume	p value	n >T_2WI volume	% >T_2WI volume	ρ	r
Final T_2WI	18472.4		237.3	304804.7	39608.5	57836.9						
Baseline DWI	13278.1	72%	325.2	154489.8	25610.3	32776.9	65%	0.14	20/46	44%	0.68	0.53
Baseline CBF	23737.1	129%	0	287604.5	44135.3	58623.1	111%	0.82	18/46	39%	0.55	0.41
Baseline MTT	50603.0	274%	0	582020.5	96406.3	118159.1	243%	0.00	30/46	65%	0.49	0.66

A)

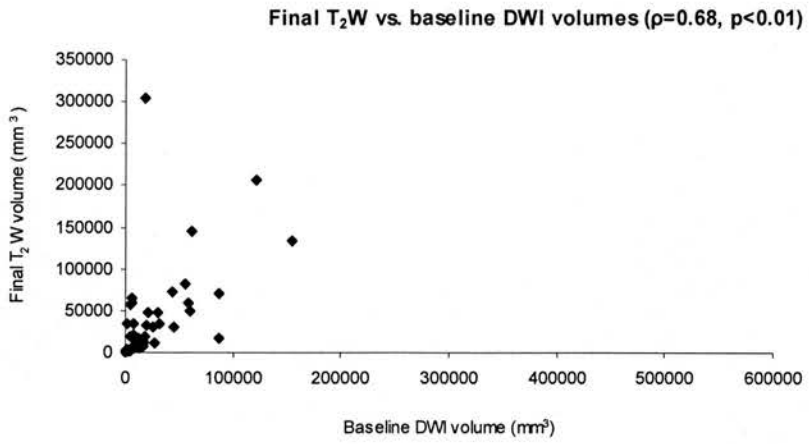

B)

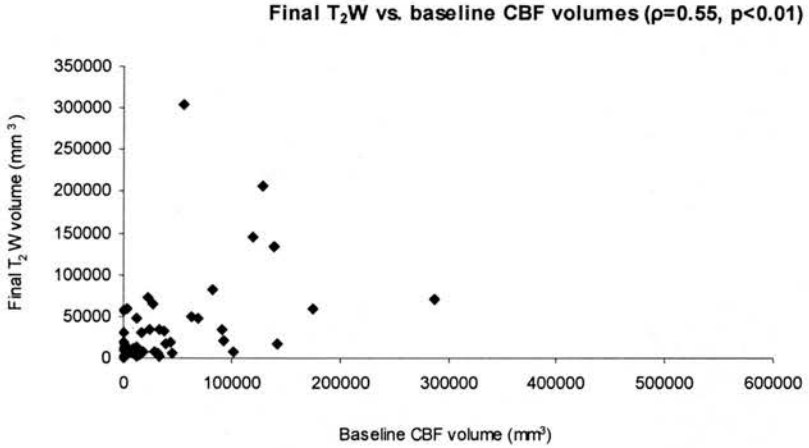

C)

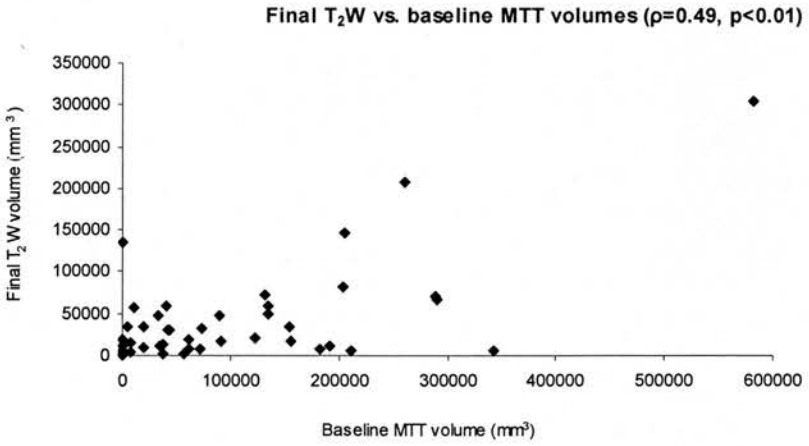

Figure 6.1 Scatter plots of final T_2WI volumes vs. baseline A) DWI, B) CBF, and C) MTT lesion volumes. ρ = Spearman's rank correlation coefficient.

Correlation between baseline DWI, PWI, and final T_2WI lesion volumes

Final T_2WI infarct volume most strongly correlated with baseline DWI lesion volume (Spearman's $\rho = 0.68$, $p < 0.01$), followed by baseline CBF_i lesion volume (Spearman's $\rho = 0.55$, $p < 0.01$), and baseline MTT_i lesion volume (Spearman's $\rho = 0.49$, $p < 0.01$; Figure 6.1, Table 6.2). Using Pearson's r (calculated to see whether use of this less appropriate statistic in previous studies might explain some of the differences in results), final T_2WI lesion volume was most strongly correlated with baseline MTT_i lesion volume (Pearson's $r = 0.66$, $p < 0.01$), followed by baseline DWI lesion volume (Pearson's $r = 0.53$, $p < 0.01$), and baseline CBF_i lesion volume (Pearson's $r = 0.41$, $p < 0.01$; Table 6.2).

'DWI/PWI mismatch' and 'lesion growth'

There was no significant association between 'lesion growth' (final T_2WI lesion volume > baseline DWI lesion volume) and the presence or absence of a 'DWI/PWI mismatch' (baseline CBF_i or MTT_i lesion volume > baseline DWI lesion volume) (Table 6.3). On baseline CBF_i, 15/25 (60%) patients with 'mismatch' had 'lesion growth' and 10/25 (40%) patients did not; 11/21 (52%) without 'mismatch' had 'lesion growth' and 10/21 (48%) did not (χ^2 test p = NS; Table 6.3). On baseline MTT_i, 21/33 (64%) with 'mismatch' had 'lesion growth' and 12/33 (36%) did not; 5/13 (38%) without 'mismatch' had 'lesion growth' and 8/13 (62%) did not (χ^2 test p = NS; Table 6.3). Thus 'DWI/PWI mismatch' was equally common amongst patients whose lesions grew as amongst those whose lesions did not grow between baseline DWI and final T_2WI (Figure 6.2).

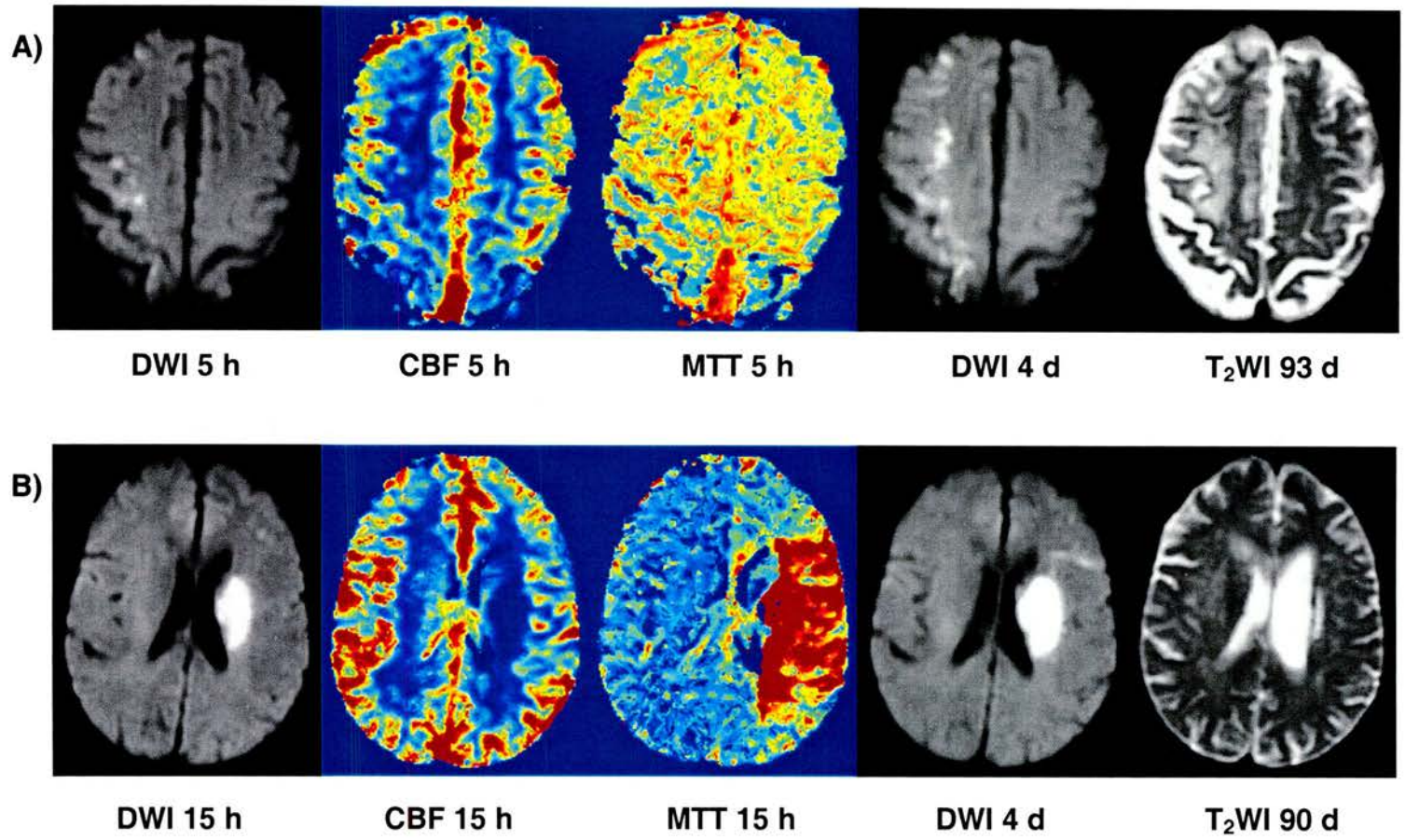

Figure 6.2 Examples of acute 'DWI/PWI mismatch'. A) a patient with a right hemisphere ischaemic lesion with no 'DWI/PWI mismatch' whose lesion grew between baseline DWI and final T_2WI; B) a patient with a left hemisphere ischaemic lesion and acute DWI/CBF and DWI/MTT mismatch, whose lesion did not grow between baseline DWI and final T_2WI. Note how MTT clearly overestimates, while CBF more closely matches, final lesion extent.

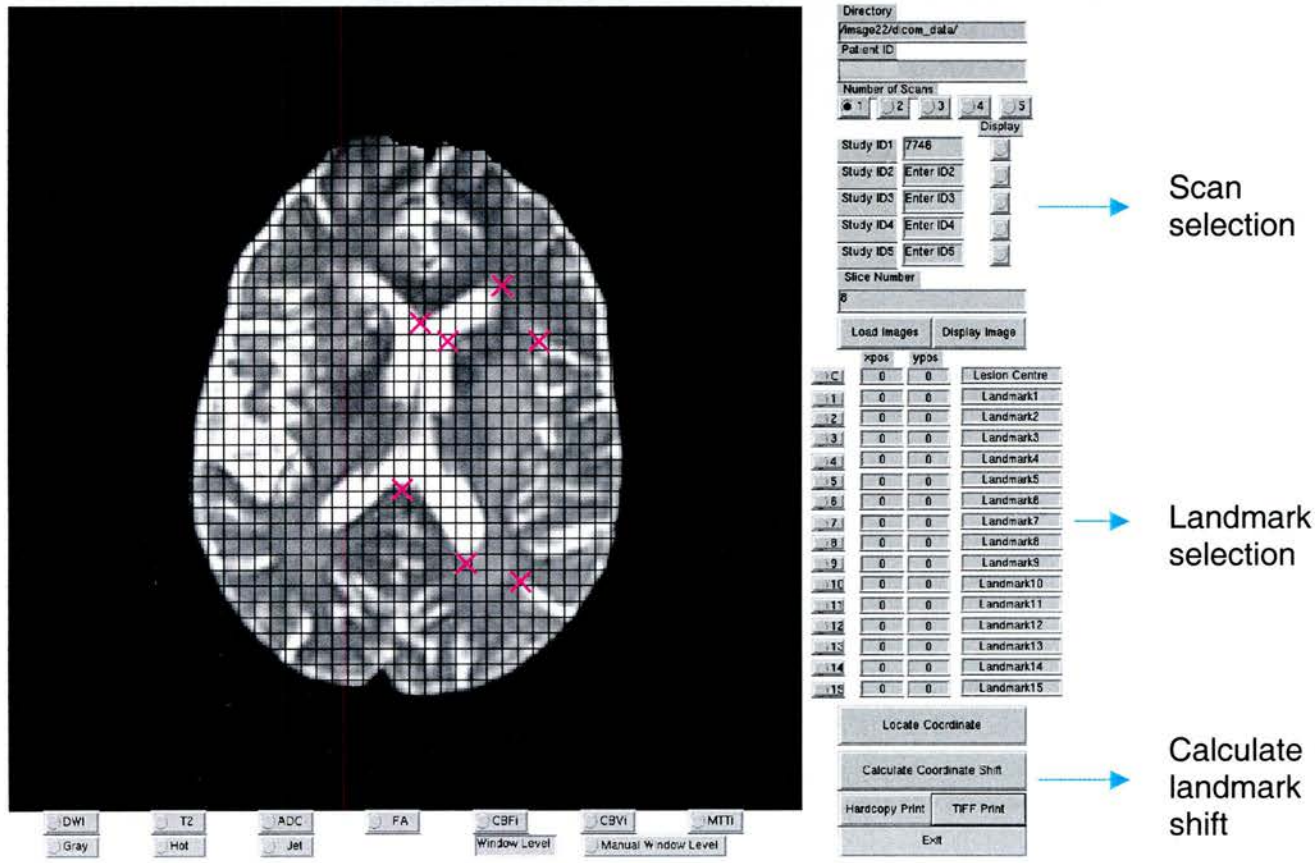

Figure 11.3 The SGAT 'swell tool' program user interface (Patient K with left hemisphere ischaemic lesion on T_2WI at 15 hours after stroke onset). Typical landmarks used in the swelling analyses are marked with ×, and key features of the 'swell tool' are highlighted. SGAT 'swell tool' calculates and records the movement (in mm) of each anatomical landmark scored between each subsequent scan time (i.e. between baseline - 5 days, 5 - 14 days, 14 - 30 days, and 30 - 90 days after stroke onset) and between baseline and 90 days after stroke onset.

Some previous studies found a stronger correlation between acute MTT and final infarct volumes than we did (e.g. Spearman's $\rho = 0.77 - 0.90$[106,138,144,147]), but these studies measured volumes on MTT_a images, were small (mean n = 21, Table 6.1), tested some very restricted perfusion thresholds (e.g. highest 70% of MTT signal intensities[147]), and employed various lesion measurement methods. Furthermore, it is important to distinguish between 'correlation' and 'size equivalence' – a good correlation between baseline MTT volume and final T_2WI lesion volume is compatible with MTT significantly overestimating final infarct volume. Previous studies also support the conclusion that acute MTT (both MTT_i and MTT_a) lesions overestimate final lesion extent[91,105,106,138,143,144,147,149,193,194].

'DWI/PWI mismatch' and 'lesion growth'

We found no significant association between DWI/CBF_i or DWI/MTT_i 'mismatch' and 'lesion growth' (Table 6.3) contrary to some previous studies[99,106,138,143,144,147,150]. By including both patients with and without 'DWI/PWI mismatch' we were able to demonstrate that 'lesion growth' was equally common between patients with and without 'DWI/PWI mismatch'. Half of the patients without 'DWI/PWI mismatch' had 'lesion growth', implying that patients without a 'DWI/PWI mismatch' might benefit from acute stroke treatments and should not be denied this possibility by being excluded from acute stroke treatment trials.

The presence of an acute 'DWI/PWI mismatch' is now being used as a selection criterion for patient inclusion in trials of stroke treatments. Two recent studies used the 'DWI/PWI mismatch' as an inclusion criterion in trials of thrombolysis[195,196], one of which reported a failure to show an association between the volume of 'DWI/PWI mismatch' and lesion expansion[195] (the other did not mention any association of

'DWI/PWI mismatch' with lesion expansion). However, both studies found that reperfusion was inversely associated with 'lesion growth'[195,196]. Many previous studies have shown that reperfusion (whether spontaneous or pharmacologically enhanced) is associated with better clinical outcome[87,101,193,197-199] which has been overlooked in the focus on 'DWI/PWI mismatch' during the last few years.

Should 'index' or 'absolute' perfusion parameters be used?

The superiority of 'absolute' over 'index' measures of perfusion is not yet proven. 'Absolute' measures are still only estimates of the 'true' underlying haemodynamics[37] and require considerably more complex image processing than 'index' measures, so are less appropriate to the acute stroke setting. Newer perfusion measures including flow heterogeneity[194] and bolus-delay corrected maps[106] appear promising in the small groups of patients studied so far (n = 19[106] - 23[194]), but further validation is required to determine their usefulness in the general population of stroke patients.

Limitations and strengths

The strengths of this analysis include the large sample size (although still small considering the heterogeneity of ischaemic stroke), inclusion of patients with and without 'DWI/PWI mismatch', careful clinical characterisation, blinded image analysis and outcome assessment, and careful use of statistics. A possible limitation is our use of manual rather than 'threshold' lesion measurement methods. However, the manual lesion measurement method is currently the most rapid method to apply in the clinical setting. Thresholds might reduce observer variation but problems with 'threshold' lesion measurement (as discussed in Chapters 2 and 5) include: complex and variable haemodynamics underlying ischaemic stroke; great overlap of baseline

perfusion values between tissue that does and does not infarct[147,149]; and the time-dependency of PWI parameter thresholds (i.e. a threshold for ischaemic but viable brain at 3 hours after stroke onset may be very different to that at 6 hours after stroke onset) – to date no studies have been large enough to assess these effects. None of our patients received thrombolysis or any investigational neuroprotective drugs, therefore this series represents a measure of the presence or absence of spontaneous lesion expansion and could be used to estimate sample sizes for future acute stroke treatment trials using acute DWI and PWI features to predict outcome.

In conclusion, acute DWI, CBF_i, and MTT_i lesion volumes all correlated well with final T_2WI lesion volume, but acute MTT_i lesion volume significantly overestimated final infarct volume. Of the two 'index' PWI measures, the acute CBF_i lesion most closely identifies the final T_2WI lesion. There was no clear association between the presence of a 'DWI/PWI mismatch' and lesion expansion – the commonly quoted concept that the 'DWI/PWI mismatch' represents 'tissue at risk' of infarction may be incorrect. About half of all patients without 'DWI/PWI mismatch' have 'lesion growth' so may benefit from acute stroke treatments, and certainly should not be excluded from clinical trials.

7. Persistent hyperintensity on DWI late after ischaemic stroke

Introduction

This chapter investigates ischaemic lesion regions that remain hyperintense on late (≥ 30 days after stroke onset) DWI, and whether these regions are merely the effect of T_2 'shine through' as discussed in Chapter 2, or if they indicate important underlying differences in the pathophysiology of the ischaemic tissue.

Persistent hyperintensity on DWI late after ischaemic stroke

Identifying effective treatments for acute ischaemic stroke requires improved understanding of the mechanisms of development and evolution of the ischaemic lesion. The extreme sensitivity of DWI and PWI to early cerebral ischaemic changes has focused attention on their use as early diagnostic tools to distinguish permanently from transiently damaged brain, and as a surrogate marker for effectiveness of new treatments[152]. However, the evolution of DWI and PWI lesion appearances at later stages after stroke, and the relationship to underlying tissue state, has been less intensively studied.

As discussed in Chapter 2, DWI appearance is influenced by the underlying ADC values and the T_2 relaxation time of the tissue. The ischaemic lesion becomes hyperintense on DWI relative to normal tissue within minutes of injury in animal models of ischaemic stroke[57], and within hours of stroke onset in ischaemic stroke patients[66,69] (Figure 7.1). In the acute stages of ischaemic stroke, hyperintensity on

DWI is mainly caused by a decrease in ADC, while T_2 relaxation time remains relatively normal[79].

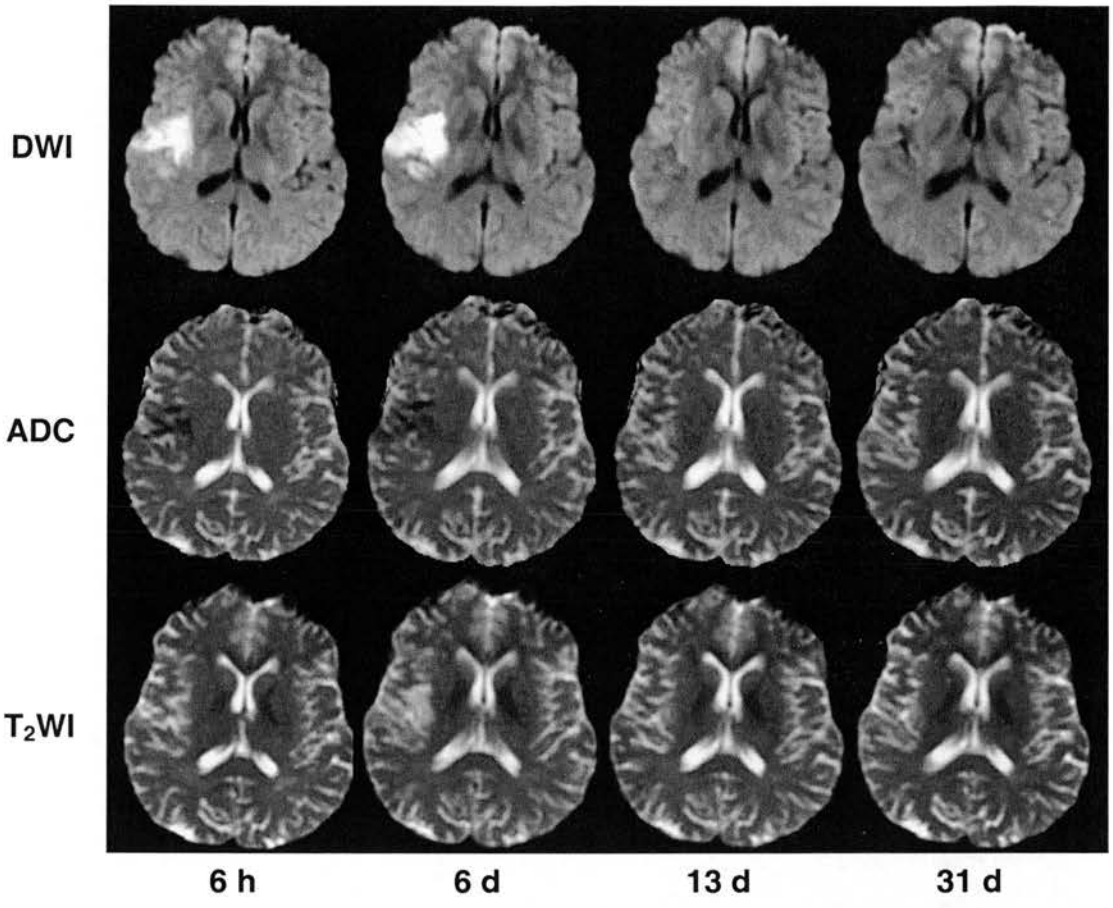

Figure 7.1 DWI, ADC, and T_2WI of a patient with a right hemisphere ischaemic lesion from baseline to 31 days after stroke onset. Note the lesion on DWI is hyperintense compared to normal tissue at 6 hours, and decreases to become isointense or hypointense compared to normal tissue by 13 days after stroke onset.

In the subacute stages of ischaemic stroke, ADC gradually increases to approximately normal values ('pseudonormalisation') at approximately 14 days after stroke onset, after which it becomes increased relative to normal[70]. Thereafter, hyperintensity on DWI has been solely attributed to increases in the T_2 relaxation time of the tissue (T_2 'shine through')[79], thought to reflect increased tissue water

content from vasogenic oedema[61]. The time taken for any hyperintensity on DWI (whether due to ADC or T_2 effects) to become isointense or hypointense relative to normal tissue (Figure 7.1) is reported to occur within 15 - 72 days after stroke onset[61,71,74,76] - any persistent DWI hyperintensity at these late times has been attributed to the T_2 'shine through' effect[58,74,79].

We observed that in some patients, parts of some infarcts remained hyperintense at ≥ 30 days after stroke onset (Figure 7.2), whereas other parts did not, and in some patients all hyperintensity had resolved by 30 days after stroke onset. If persistent hyperintensity at late time points is a T_2 'shine through' effect, why are only some patients affected, and in these patients, why is only part of the infarct hyperintense on DWI?

We hypothesized that regions of infarcts remaining hyperintense late after stroke might have distinct underlying pathophysiology, such as different blood flow patterns, than the infarcts (or parts of infarcts) not remaining hyperintense. Perhaps these regions of late hyperintensity on DWI represent parts of lesions that either: a) became abnormal later than the rest of the infarct but were still following the 'conventional' ischaemic pattern of evolution; b) were progressing through the ischaemic cascade more slowly than the rest of the infarct and thus might represent tissue that remained viable for a longer period; or c) or experienced some other sort of delayed repair process.

We therefore examined the DWI and PWI of a large cohort of patients all imaged from acute (< 24 hours) to late (≥ 30 days) stages after stroke onset to determine if the patterns of DWI and PWI changes were indeed different in the infarct regions

remaining hyperintense compared with those that had become isointense on DWI late after stroke.

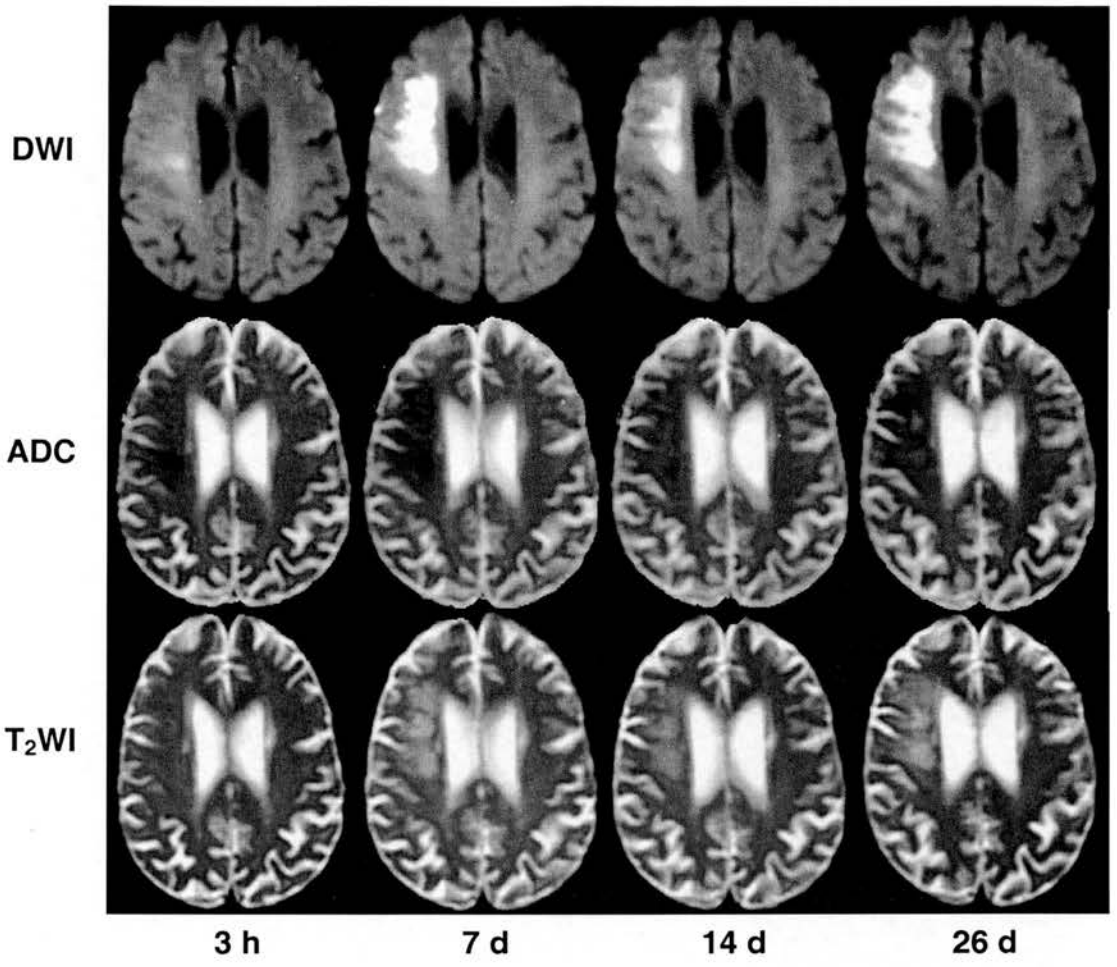

Figure 7.2 DWI, ADC, and T_2WI of a patient with a right hemisphere ischaemic lesion from baseline to 26 days after stroke onset. Note the lesion on DWI has a region of persistent hyperintensity at 26 days after stroke onset, corresponding with a region of hypointensity on the ADC image.

Methods

Patients (as described in Chapter 4) with MRI data at all four MR scanning time points up to 30 days after stroke onset were included in the current analysis. The

visibly abnormal acute lesion on the baseline DWI was manually outlined as described in Chapter 4 (Figure 7.3).

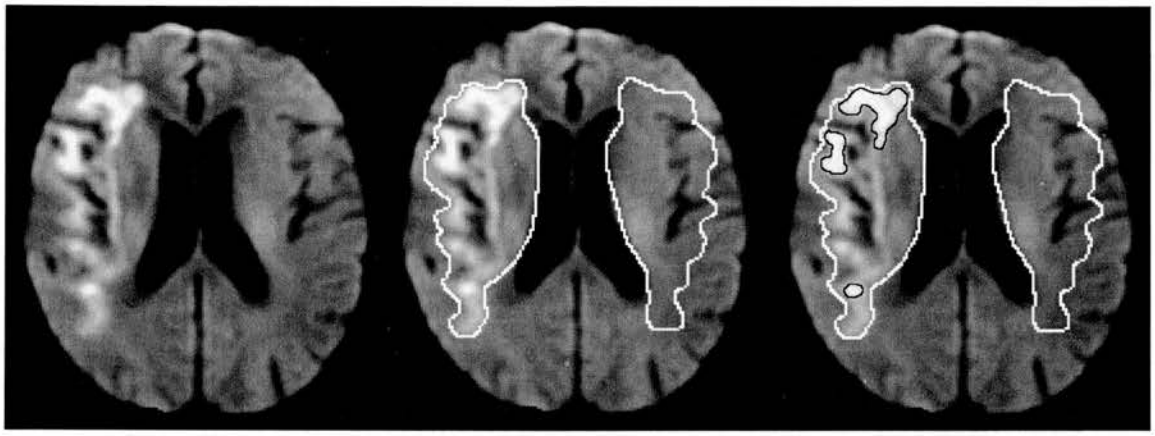

A) B) C)

Figure 7.3 A) DWI of a patient with a right hemisphere ischaemic lesion at 26 days after stroke onset, B) with lesion and homologous contralateral region outlined in white, C) with 'still hyperintense' regions outlined in black.

Measurement of regions 'still hyperintense' on late DWI

The DWI scans from 30 days after stroke onset were assessed for 'still hyperintense' regions, defined as areas of persistent hyperintensity compared to the rest of the visible lesion, by a neuroradiologist (JMW) blind to clinical and other imaging details. Patients with persistent hyperintensity on 30 day DWI were defined as 'still hyperintense', and patients with isointense or hypointense lesions on 30 day DWI were defined as 'isointense'. In patients with still hyperintense infarct regions at 30 days after stroke onset, there were also other areas of the original infarct that were not still hyperintense (i.e. were isointense) – these isointense regions were referred to as 'not still hyperintense'. Areas of persistent hyperintensity on 30 day DWI were separately outlined using the same method as previously described for the acute DWI

lesions (Figure 7.3). Baseline DWI infarct regions and regions appearing 'still hyperintense' on 30 day DWI were applied to the coregistered scans from 5, 14, and 30 days after stroke onset. Patients with no persistent hyperintensity on 30 day DWI had only baseline scan infarct regions applied to the coregistered scans from 5, 14, and 30 days after stroke onset.

ADC, CBF, and MTT values for each scan time were extracted for all areas traced, and relative values (ADCr, CBFr, and MTTr) were calculated as previously described.

All lesions on subsequent scans were checked to ensure they were original lesions and not the result of new ischaemic events.

Lesion composition analysis

A neuroradiologist (JMW), blind to all clinical and other imaging data, scored the lesion on baseline DWI as comprising of grey matter, white matter, or both grey and white matter. If present, the 'still hyperintense' region on the 30 day DWI was also scored as comprising of grey matter, white matter, or both. The scans from 30 days after stroke onset were reviewed blind to the baseline scans. Finally, the 30 day scans were compared with the baseline scan to determine whether the hyperintensity on 30 day DWI had been within the original boundary of the ischaemic lesion at baseline, or whether the hyperintensity at 30 days after stroke onset represented a subsequently developing new area of infarction.

Statistical analyses

General patient demographic data were obtained and compared as previously described (Chapter 4).

Clinical details of 'isointense' and 'still hyperintense' patients were compared: age and time from stroke onset to baseline and subsequent MRI with standard t-tests; baseline NIHSS with a Mann-Whitney U-test; and sex, OCSP classifications, and whether the patients were dead or dependent (mRS = 3 - 6) at 90 days after stroke onset or not with Chi-Square (χ^2) tests.

Mean (± SD) ADCr, CBFr, and MTTr values are reported and compared. To test if persistent hyperintensity reflected an initial difference or prolonged ADC abnormality, standard t-tests (paired for comparing regions within 'still hyperintense' patients, unpaired for the two region types in 'still hyperintense' patients vs. 'isointense' patients) were performed for ADCr values from baseline and 30 days after stroke onset. CBFr and MTTr at baseline and 5 days after stroke onset, and peak CBFr and nadir MTTr values and their timing[200] were also compared with standard t-tests (paired and unpaired as described above for ADCr values) to identify early perfusion differences in tissue destined to be 'isointense' vs. 'still hyperintense'. GLM repeated measures regression analysis was performed to compare changes in ADCr, CBFr, and MTTr values over time (from baseline to 30 days after stroke onset, dependent variables = ADCr, CBFr, and MTTr values; ADCr and MTTr fit to a linear model, CBFr fit to a quadratic model): between patients with 'isointense' infarcts at 30 days after stroke onset and patients with 'still hyperintense' infarcts, both in areas that remained hyperintense and those that became isointense (between subjects factor = 'isointense' vs. 'still hyperintense' and 'isointense' vs. 'not still hyperintense'). As data from lesion areas that remained 'still hyperintense' and 'not still hyperintense' in patients with remaining hyperintensity is paired data, the difference in ADCr, CBFr, and MTTr between the two lesion areas was calculated

and GLM repeated measures regression analysis was performed to analyse any differences between the two areas over time (from baseline to 30 days after stroke onset, dependent variables = difference in ADCr, CBFr, and MTTr values).

Results

Patient details

Forty-two patients with MRI data at all four scanning time points up to 30 days after stroke onset were included in the present analysis: 23/42 (55%) were male, the mean age was 71 years (range: 36 - 93 years), and the mean NIHSS score on admission was 9 (median 8, range: 0 - 25). OCSP classifications: 13/42 (31%) patients had a TACI, 25/42 (60%) patients had a PACI, 3/42 (7%) patients had a LACI, and 1/42 (2%) patients had a POCI. Mean mRS score at 90 days after stroke onset was 2 (median 2); 12/42 (29%) patients were dependent (mRS = 3 – 5) and 2/42 (5%) patients were dead (mRS = 6).

General patient scan characteristics

Mean (± SD) time from stroke onset to baseline MRI was 10 ± 7 hours, with 16/42 (38%) patients imaged within 6 hours, 11/42 (26%) patients between 6 and 12 hours, and 15/42 (37%) patients between 12 and 24 hours after stroke onset. The 5 day scans were performed at a mean of 5 ± 1 days, the 14 day scans at a mean of 12 ± 2 days, and the 30 day scans at a mean of 31 ± 3 days after stroke onset.

MRI characteristics

Table 7.1 lists, and Figure 7.4 shows graphs of the mean (± SD) ADCr, CBFr, and MTTr values for each infarct region from baseline to 30 days after stroke onset.

'Still hyperintense' vs. 'isointense' patients

On 30 day DWI, 27/42 (64%) patients had 'still hyperintense' infarct regions. All regions remaining hyperintense on 30 day DWI were within the baseline lesion (i.e. were not the result of a subsequent ischaemic event).

Patient details

Sex and age did not significantly differ between 'isointense' and 'still hyperintense' patients. Clinically, 'still hyperintense' patients had a higher NIHSS score on admission (mean 10 vs. 6, median 9 vs. 4, Mann-Whitney U-test $p < 0.01$) and were more likely to be dead or dependent (mRS = 3 - 6, χ^2 test $p < 0.05$) compared to 'isointense' patients. It appeared that 'still hyperintense' patients were more likely to have had a TACI than 'isointense' patients (41% vs. 13% respectively), but this was not statistically significant (χ^2 test p = NS).

General patient scan characteristics

'Still hyperintense' patients had their initial MRI scan later after stroke onset than 'isointense' patients (mean 12 hours vs. 7 hours after stroke onset, t-test $p < 0.03$). However, there were no significant differences in the times from stroke onset to subsequent MRI scans between 'still hyperintense' and 'isointense' patients (t-tests all p = NS).

Table 7.1 Mean (± SD) scan times, number of patients (n), and mean (± SD) and range ADCr, CBFr, and MTTr values at each scan time for each region. SH = tissue remaining 'still hyperintense' and NSH = rest of the baseline DWI lesion in 'still hyperintense' patients; ISO = tissue from the baseline DWI lesion in 'isointense' patients, followed through subsequent coregistered scans.

Scan time	Tissue	n	ADCr			CBFr			MTTr		
			mean ± SD	min	max	mean ± SD	min	max	mean ± SD	min	max
10 ± 7 h	SH	27	0.760 ± 0.122	0.569	0.978	0.903 ± 0.458	0.393	2.665	1.510 ± 0.599	0.755	3.465
	NSH	27	0.734 ± 0.110	0.589	1.099	0.823 ± 0.327	0.422	1.537	1.450 ± 0.431	0.945	2.580
	ISO	15	0.850 ± 0.123	0.614	1.138	0.835 ± 0.251	0.475	1.232	1.376 ± 0.347	1.051	2.123
5 ± 1 d	SH	27	0.773 ± 0.165	0.480	1.109	1.130 ± 0.575	0.312	3.387	1.251 ± 0.470	0.830	2.870
	NSH	27	0.766 ± 0.158	0.486	1.170	1.039 ± 0.374	0.364	1.734	1.194 ± 0.436	0.947	2.618
	ISO	14	0.855 ± 0.162	0.518	1.115	1.231 ± 0.252	0.783	1.622	1.035 ± 0.074	0.925	1.155
12 ± 2 d	SH	26	0.915 ± 0.167	0.521	1.149	1.130 ± 0.325	0.322	2.207	1.105 ± 0.218	0.910	2.003
	NSH	26	1.006 ± 0.175	0.536	1.229	1.126 ± 0.229	0.793	1.611	1.070 ± 0.096	0.921	1.283
	ISO	14	1.111 ± 0.167	0.852	1.364	1.145 ± 0.306	0.315	1.589	1.010 ± 0.073	0.903	1.180
31 ± 3 d	SH	27	1.012 ± 0.206	0.506	1.453	0.782 ± 0.162	0.441	1.171	1.064 ± 0.191	0.689	1.579
	NSH	27	1.289 ± 0.229	0.669	1.658	0.829 ± 0.145	0.573	1.124	1.064 ± 0.142	0.927	1.524
	ISO	15	1.209 ± 0.157	0.943	1.516	0.989 ± 0.194	0.716	1.506	1.053 ± 0.071	0.947	1.210

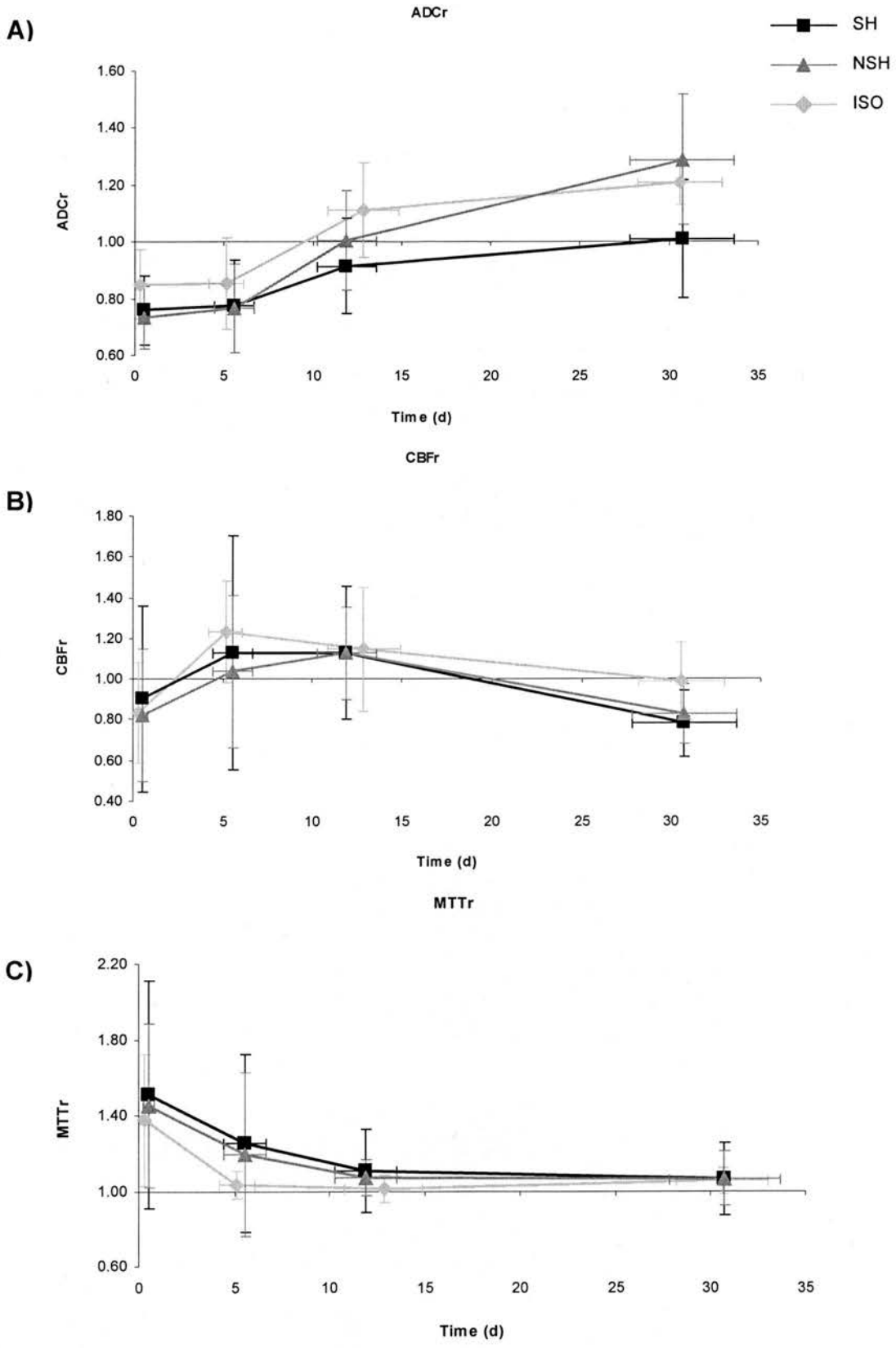

Figure 7.4 Mean A) ADCr, B) CBFr, and C) MTTr values for all patients studied. See Table 7.1 for patient numbers at each scan time. SH = tissue remaining 'still hyperintense' and NSH = rest of the baseline DWI lesion in 'still hyperintense' patients; ISO = tissue from the baseline DWI lesion in 'isointense' patients, followed through subsequent coregistered scans. Error bars represent ± 1 SD of the mean.

ADCr at baseline and 30 days after stroke onset

ADCr at baseline was significantly lower in 'still hyperintense' (ADCr = 0.760 ± 0.122) and 'not still hyperintense' (ADCr = 0.734 ± 0.110) regions in 'still hyperintense' patients compared to the infarct region in 'isointense' patients (ADCr = 0.850 ± 0.123, t-tests $p < 0.05$ and $p < 0.01$ respectively; Table 7.1) suggesting more pronounced ischaemic damage in lesions that would be 'still hyperintense' at 30 days after stroke onset. ADCr values at 30 days after stroke onset were significantly lower in 'still hyperintense' regions (ADCr = 1.012 ± 0.206) compared with both 'not still hyperintense' regions in 'still hyperintense' patients (ADCr = 1.289 ± 0.229, paired t-test $p < 0.01$) and the infarct region in 'isointense' patients (ADCr = 1.209 ± 0.157, t-test $p < 0.01$; Table 7.1).

ADCr evolution

'Still hyperintense' lesion areas had a lower baseline ADCr which remained lower over time compared to lesion areas in 'isointense' patients (GLM regression $p < 0.01$; Figure 7.4). Within patients with 'still hyperintense' lesion areas, ADCr in areas 'not still hyperintense' increased more rapidly than in 'still hyperintense' tissue from 14 days after stroke onset onwards, reaching higher values by 30 days after stroke onset (GLM regression $p < 0.01$; Figure 7.4).

CBFr and MTTr at baseline and 5 days after stroke onset

There was no difference in CBFr or MTTr at baseline between the three groups (t-tests all p = NS). Although the CBFr appeared to be higher in 'isointense' lesions (CBFr = 1.231 ± 0.252) compared with 'still hyperintense' lesions (CBFr = 1.130 ± 0.575) at 5 days after stroke onset, the difference was not statistically significant (t-test p = NS; Table 7.1, Figure 7.4). MTT at 5 days after stroke onset was

significantly prolonged relative to normal in the 'still hyperintense' regions (MTTr = 1.251 ± 0.470) compared with 'isointense' patients (MTTr = 1.035 ± 0.074, t-test $p < 0.05$; Table 7.1, Figure 7.4).

Peak CBFr and nadir MTTr values and their timing

Also, although the peak CBFr and the nadir of the MTTr appeared to occur earlier in 'isointense' than in 'still hyperintense' tissue (mean 6 days vs. 8 days after stroke onset) the difference was not statistically significant. The peak CBFr ('still hyperintense' CBFr = 1.285 ± 0.481 vs. 'isointense' CBFr = 1.319 ± 0.205) and nadir MTTr ('still hyperintense' MTTr = 0.992 ± 0.166 vs. 'isointense' MTTr = 0.991 ± 0.054) values were also not significantly different between 'still hyperintense' and 'isointense' tissue (t-tests all p = NS).

CBFr and MTTr evolution

The evolution of CBFr from baseline to 30 days after stroke onset differed only between 'still hyperintense' and 'not still hyperintense' lesion areas, where the difference in CBF between the two decreased over time (GLM regression $p < 0.05$; Figure 7.4). There was no statistically significant difference in the pattern of change in CBFr over time between 'isointense' and 'still hyperintense' tissue (GLM regression p = NS), despite the CBF in 'isointense' tissue appearing to increase to a higher peak level more quickly within the first 5 days after stroke onset compared to 'still hyperintense' tissue.

Apart from the difference at 5 days after stroke onset mentioned above, there was no significant difference in the pattern of change on MTTr between the three tissue types (GLM regression all p = NS; Figure 7.4).

Lesion composition

Table 7.2 lists the lesion compositions of the different lesion regions. Lesions on the baseline DWI scan were comprised of grey matter in 4/42 (10%) patients, white matter in 5/42 (12%) patients, and both grey and white matter in 33/42 (79%) patients (Table 7.2). Grey matter lesions were all in 'isointense' patients (4/4, 100%), whereas most of the white matter lesions were in 'still hyperintense' patients (4/5, 80%; Table 7.2). Of lesions comprised of both grey and white matter, 23/33 (70%) were in 'still hyperintense' patients (Table 7.2). In 'still hyperintense' patients, the regions of hyperintensity on 30 day DWI were almost exclusively in white matter (25/27, 92%); only 1/27 (4%) were composed of grey matter, and 1/27 (4%) of both grey and white matter (Table 7.2).

Table 7.2 Lesion composition of the baseline DWI lesion and lesion regions 'still hyperintense' on DWI at ≥ 30 days after stroke onset (SH region). Values for 'isointense' patients (ISO), 'still hyperintense' patients (SH), and all patients are reported.

Scan time	Patient/lesion type	Tissue composition					
		Grey matter		White matter		Both	
		n	%	n	%	n	%
Baseline	ISO n = 15	4	27%	1	7%	10	67%
Baseline	SH n = 27	0	0%	4	15%	23	85%
Baseline	all patients n = 42	4	10%	5	12%	33	79%
≥ 30 d	SH region n = 27	1	4%	25	92%	1	4%

Discussion

Persistent hyperintensity on DWI at 30 days after stroke onset has been attributed to T_2 'shine through', but we have found that 'still hyperintense' areas on DWI have significantly different ADCr values than isointense areas, and are therefore not simply caused by T_2 'shine through'. This, combined with the different pattern of perfusion changes observed in 'still hyperintense' areas on late DWI compared with the rest of the infarct, and with infarcts with no areas of persistent hyperintensity, suggest important differences in lesion evolution. 'Still hyperintense' patients were also different in that they had more severe strokes and worse functional outcome at 90 days after stroke onset than 'isointense' patients.

What do these differences in infarct evolution mean? Significantly lower baseline ADCr values in the 'still hyperintense' patients suggest that the tissue was initially more abnormal than in 'isointense' patients. ADCr values recovered less quickly in areas of persistent hyperintensity, perhaps indicating prolonged intracellular oedema or other slower repair processes following the ischaemic insult. Perfusion also recovered more slowly in 'still hyperintense' tissue - MTTr remained prolonged for longer and, although only reaching significance between areas remaining and not remaining hyperintense in patients with 'still hyperintense' lesions, CBFr appeared to recover more slowly. Thus 'still hyperintense' tissue has a slower pattern of recovery of ADC and perfusion parameters. Perhaps 'still hyperintense' tissue experiences a poor reflow phenomenon, or some other factor (e.g. delayed lysis of the thrombus in the major artery supplying the affected area) that contributes to slower recovery of blood flow, possibly prolonging ischaemia and lesion evolution.

We found previously that ADC values evolved differently in grey and white matter from baseline to 14 days after stroke onset[133]. In the current study, the hyperintense regions on 30 day DWI were almost exclusively located in white matter, further supporting evidence for differential evolution of ischaemic damage between grey and white matter.

Several other studies suggest that persistent DWI hyperintensity occurs in patients with specific types and localities of lesions. Geijer et al.[201] suggest that small cortical and lacunar infarcts may remain hyperintense on DWI for longer periods (e.g. 54 - 144 days after stroke onset) than larger infarcts. Schulz et al.[202] found that late (mean of 21 days after stroke onset) DWI hyperintensity was correlated with higher age and acute NIHSS in a group of patients with mild strokes. Both these studies merely drew attention to the existence of late DWI hyperintensity but did not determine the pattern of early infarct evolution.

The possible limitations of the present study include the subjective method of deciding which tissue was 'still hyperintense' on 30 day DWI; a judgement made by visually examining the relative signal hyperintensity of the DWI lesion – if areas clearly stood out from the background by being hyperintense relative to the rest of the infarct or to normal brain, then they were classed as 'still hyperintense'. We did not use a threshold of DWI signal intensity or ADC value specifically to avoid the problem of masking any important tissue differences which might have occurred by imposing a fixed arbitrary parameter value as discussed in Chapters 2 and 5. We used 'index' perfusion parameters which may have masked some subtle between patient differences, however, we calculated and compared relative parameters to limit the impact of any differences between patients and scan times. Although this study is

large compared to other serial studies of DWI and PWI parameters in ischaemic stroke patients, the number of 'isointense' (n = 15) and 'still hyperintense' (n = 27) patients are small. The standard deviations of PWI data are very wide with the current methods of obtaining perfusion information, meaning important differences between patient groups may be missed. There are also several serious statistical issues that impose limitations on the analysis of serial DWI and PWI data. The commonly used conventional statistical models for analysis of repeated measures data, such as GLM regression analysis, require fitting to a linear (or cubic or quadratic) model. However, the complex and variable nature of changes in DWI and PWI parameters after ischaemic stroke make it unclear which fit model is most appropriate. The use of 'summary measures' of serial data[200], such as peak CBFr and nadir MTTr values and their timing as used in this analysis, may eliminate some of the problems related to analysis of repeated measures data, such as complex changes over time that do not fit any existing statistical model and missing data. However, we did not find any significant differences in the 'summary measures' we calculated and compared between lesion types, possibly because of small patient numbers. Matthews et al.[200] also suggest the calculation and comparison of the 'area under the curve' for non-linear (e.g. peaked) repeated measures data, however we did not use this analysis here as the patient groups were small. We do calculate and compare 'area under the curve' data in Chapter 10 with a larger patient group. With use of a larger sample size, improvements in PWI, and development of more appropriate statistical models for serial data the differences in DWI and PWI evolution seen in this analysis would likely be significant.

If persistent DWI hyperintensity indicates slower evolution of ischaemic tissue, then the opportunity might exist to intervene in some way, even late after stroke. Reasons for delayed reperfusion, or the 'poor reflow' phenomenon, are not well understood; perhaps the areas have different inflammatory responses, so treatments such as anti-inflammatory agents or some other method of gentle encouragement of better blood flow (e.g. careful systemic blood pressure regulation) might influence tissue repair at subacute stages after stroke onset.

In summary, tissue remaining hyperintense on late DWI should not just be dismissed as areas of T_2 'shine through'. Further study is required to determine what these 'still hyperintense' lesion areas mean in terms of clinical recovery, and whether any later intervention could improve outcome.

8. Grid-based analysis of ischaemic stroke lesions on baseline DWI

Introduction

This chapter consists of the development of a novel grid-based method to investigate regions of heterogeneity of DWI and PWI parameters within ischaemic lesions. A manual grid-based analysis method is developed and tested in a small group of patients to determine if different degrees of abnormality on baseline DWI indicate different degrees of underlying tissue damage.

Examining lesion heterogeneity with grid-based analysis methods

There is increasing evidence that ischaemic lesions are heterogeneous, with regions of varying appearance on DWI and underlying ADC and perfusion abnormalities[68,78,113,119,120]. However, what these regional differences mean in terms of underlying tissue pathophysiology and viability has not been widely assessed. The most commonly used methods of lesion measurement such as manual tracing or the use of a single parameter 'threshold' as discussed in Chapter 2 do not take account of these underlying subregions of varying abnormality.

To be able to more easily track and analyse the evolution of DWI and PWI parameters in subregions of ischaemic lesions, we developed and tested a grid-based analysis approach. Grid-based analysis allows for classification tissue according to differences in appearance on DWI. We implemented a manual grid-based analysis method in a series of patients to assess if differences in lesion appearance on baseline

DWI indicated differences in the underlying tissue abnormality as determined by ADC values, and how this related to any differences in PWI parameters.

Manual grid analysis

Methods

Eight patients with a representative range of ischaemic lesion appearance on baseline DWI were selected from the larger patient cohort (as described in Chapter 4) for initial development of the grid-based analysis method: 5/8 (62.5%) patients had 'solitary' DWI lesions, 3/8 (37.5%) patients had 'multi-focal' DWI lesions; 2/8 (25%) patients had 'well-defined' DWI lesions, and 6/8 (75%) patients had 'ill-defined' DWI lesions as described in Chapter 5.

For each patient, the axial slice that passed through the centre of the visible ischaemic lesion on baseline DWI was chosen for analysis. A 5 × 5 voxel grid (voxel = 4.39 mm^3, grid box = 109.86 mm^3) was applied over the chosen DWI slice in Analyze™ (Figure 8.1). A 10 × 10 voxel grid (grid box = 439.45 mm^3) was also tested in the development of the manual grid-based analysis, however the 10 × 10 voxel grid was too large to allow for sufficient discrimination between areas of different degrees of abnormality on DWI so the smaller 5 × 5 voxel grid was used. Image brightness and contrast were adjusted for maximum distinction between hyperintense tissue and normal appearing brain.

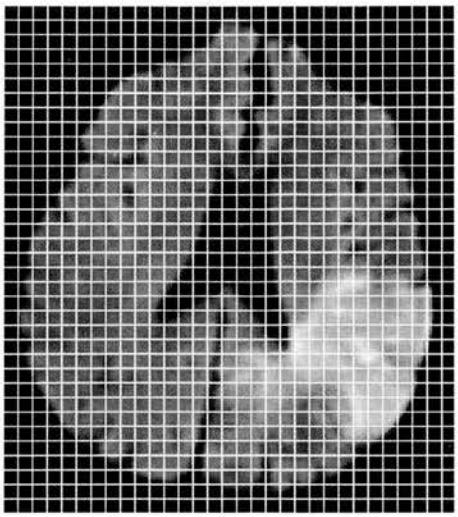

Figure 8.1 Manual grid analysis example image (Patient A, left hemisphere ischaemic lesion on DWI at 4 hours after stroke onset). Each grid box is 4.69 × 4.69 mm.

The images were printed out onto paper, and a neuroradiologist (JMW), blind to clinical and other imaging details, scored each grid box according to the appearance of the tissue inside the grid box on baseline DWI (Figure 8.1). A grid box was excluded from analysis if > 25% of the box was comprised of 'background' (outside of brain) or CSF to avoid skewing results with partial volume effects.

Tissue classification

Grid boxes were scored as follows: 'definitely abnormal', if the whole grid box contained clearly hyperintense tissue; 'possibly abnormal', if > 50% of the box appeared hyperintense relative to normal tissue, or if the hyperintensity was only subtle; 'ipsilateral normal', if the tissue in the grid box appeared normal and was in the hemisphere ipsilateral to the ischaemic lesion; or 'contralateral normal' if the tissue in the grid box appeared normal and was in the hemisphere contralateral to the ischaemic lesion (Figure 8.2).

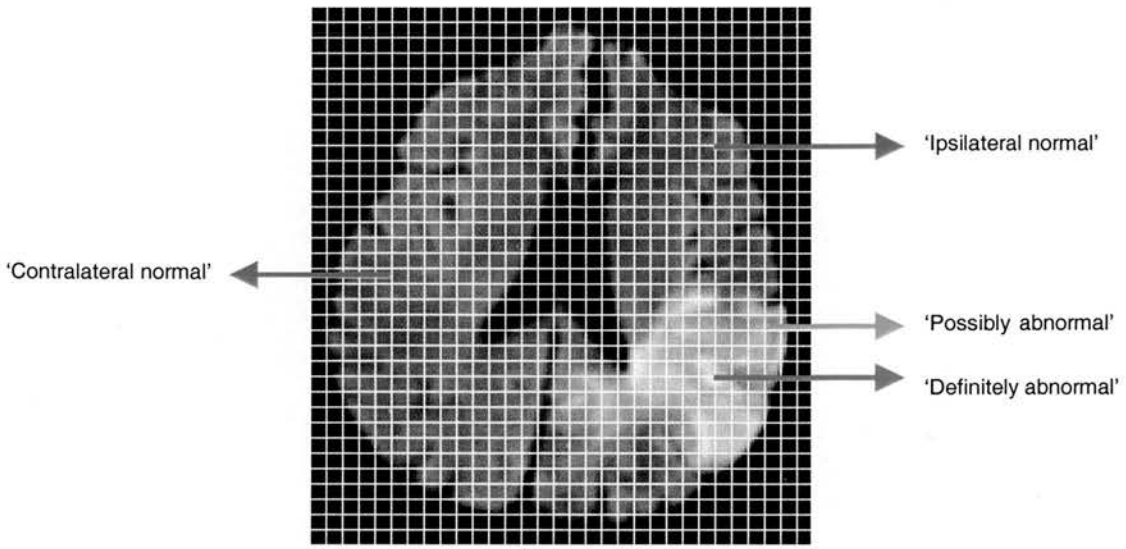

Figure 8.2 Examples of the tissue classifications scored according to baseline DWI appearance as used in the grid-based analysis method (Patient A, left hemisphere ischaemic lesion on DWI at 4 hours after stroke onset).

The grid box classifications from the baseline scan were applied to the subsequent coregistered scans from 5, 14, and 30 days after stroke onset. DWI SI, ADC, CBF, and MTT values for each grid box and mean values for each tissue classification at each scan time were extracted. Relative values (DWIr, ADCr, CBFr, and MTTr) were calculated and compared by dividing the 'definitely abnormal', 'possibly abnormal', and 'ipsilateral normal' values by the 'contralateral normal' values.

Statistical analyses

General patient demographic data were obtained and compared as previously described (Chapter 4).

Mean (± SD) DWIr, ADCr, CBFr, and MTTr values are reported and compared. Baseline DWIr, ADCr, CBFr, and MTTr values for 'definitely abnormal', 'possibly

abnormal', and 'ipsilateral normal' tissue were compared to normal (test value = 1, as they are relative values) using standard t-tests. Baseline ADCr, CBFr, and MTTr in 'definitely abnormal' and 'possibly abnormal' tissues were compared using standard paired t-tests to determine if differences in baseline DWI appearance were indicative of the degree of underlying baseline ADC, CBF, and MTT abnormality. ADCr at 30 days after stroke onset in 'definitely abnormal' and 'possibly abnormal' tissues were also compared using standard paired t-tests to determine if differences in baseline DWI appearance were indicative of the degree of underlying damage as suggested by ADC abnormality at outcome. Changes in ADCr, CBFr, and MTTr values over time (from baseline to 30 days after stroke onset) were analysed using GLM repeated measures regression analysis (dependent variables = ADCr, CBFr, and MTTr values; ADCr and MTTr fit to a linear model, CBFr fit to a quadratic model).

Results

Patient details

Eight patients were included in the present analysis: 7/8 (88%) were male, the mean age was 66 years (range 39 – 80 years), and the mean NIHSS score on admission was 10 (median 8, range: 4 - 25). OCSP classifications: 3/8 (38.5%) patients had a TACI, and 5/8 (62.5%) patients had a PACI. Mean mRS score at 90 days after stroke onset was 3 (median 2); 2/8 (25%) patients were dependent (mRS = 3 – 5) and 1/8 (12.5%) patients were dead (mRS = 6). Individual patient details are listed in Table 8.1.

Table 8.1 Demographics, clinical details, and MR scan times for the patients analysed with the manual grid-based analysis methods (n = 8).

Patient	Sex	Age (y)	Baseline NIHSS	OCSP class	90 d mRS	Time from onset to MRI			
						1 (h)	2 (d)	3 (d)	4 (d)
A	M	78	4	PACI	2	4	4	9	31
B	M	80	7	PACI	1	14	7	13	33
C	M	39	8	TACI	0	5	4	11	27
D	M	78	8	PACI	6	3	6	13	30
E	M	70	25	TACI	5	4	7	13	30
F	F	52	20	TACI	5	5	6	13	31
G	M	67	5	PACI	0	7	6	13	27
H	M	68	6	PACI	1	5	6	10	
Mean		66	10		3	6 h	6 d	12 d	30 d
Median			8		2				

General patient scan characteristics

Mean (± SD) time from stroke onset to baseline imaging was 6 ± 4 hours, with 6/8 (75%) patients imaged within 6 hours, 1/8 (12.5%) patients between 6 and 12 hours, and 1/8 (12.5%) patients between 12 and 24 hours after stroke onset. The 5 day scans were performed at a mean of 6 ± 1 days, the 14 day scans at a mean of 12 ± 2 days, and the 30 day scans at a mean of 30 ± 2 days after stroke onset (Table 8.2). Individual patient scan times are listed in Table 8.1. Note one patient (Patient H) did not have imaging at 30 days after stroke onset.

MRI characteristics

Table 8.2 lists and Figure 8.3 shows graphs of the mean (± SD) DWIr, ADCr, CBFr, and MTTr values for each tissue classification (scored according to baseline DWI appearance and applied to subsequent scans) from baseline to 30 days after stroke onset.

Table 8.2 Mean (± SD) scan times and DWIr, ADCr, CBFr, and MTTr values for the three tissue classifications at each scan time for the patients analysed with the manual grid-based analysis methods (n = 8). Tissue classifications were scored according to baseline DWI appearance, which were applied to subsequent coregistered scans.

Scan time	Tissue classification	DWIr	ADCr	CBFr	MTTr
6 ± 4 h	Definitely abnormal	1.634 ± 0.171	0.712 ± 0.151	0.765 ± 0.484	1.429 ± 0.365
	Possibly abnormal	1.277 ± 0.137	0.817 ± 0.098	0.870 ± 0.442	1.290 ± 0.214
	Ipsilateral normal	0.999 ± 0.022	1.021 ± 0.064	1.032 ± 0.150	1.139 ± 0.142
6 ± 1 d	Definitely abnormal	2.070 ± 0.635	0.668 ± 0.183	1.324 ± 0.310	0.992 ± 0.091
	Possibly abnormal	1.611 ± 0.453	0.748 ± 0.145	1.194 ± 0.256	1.009 ± 0.072
	Ipsilateral normal	1.073 ± 0.120	0.972 ± 0.055	1.065 ± 0.105	1.047 ± 0.084
12 ± 2 d	Definitely abnormal	1.415 ± 0.491	0.912 ± 0.255	1.359 ± 0.429	1.104 ± 0.177
	Possibly abnormal	1.235 ± 0.256	0.879 ± 0.129	1.117 ± 0.298	1.118 ± 0.128
	Ipsilateral normal	1.014 ± 0.044	1.007 ± 0.033	0.992 ± 0.061	1.062 ± 0.083
30 ± 2 d	Definitely abnormal	1.208 ± 0.124	1.124 ± 0.198	0.776 ± 0.220	1.158 ± 0.209
	Possibly abnormal	1.150 ± 0.133	1.009 ± 0.088	0.795 ± 0.132	1.114 ± 0.094
	Ipsilateral normal	0.994 ± 0.044	1.070 ± 0.076	0.940 ± 0.074	1.036 ± 0.047

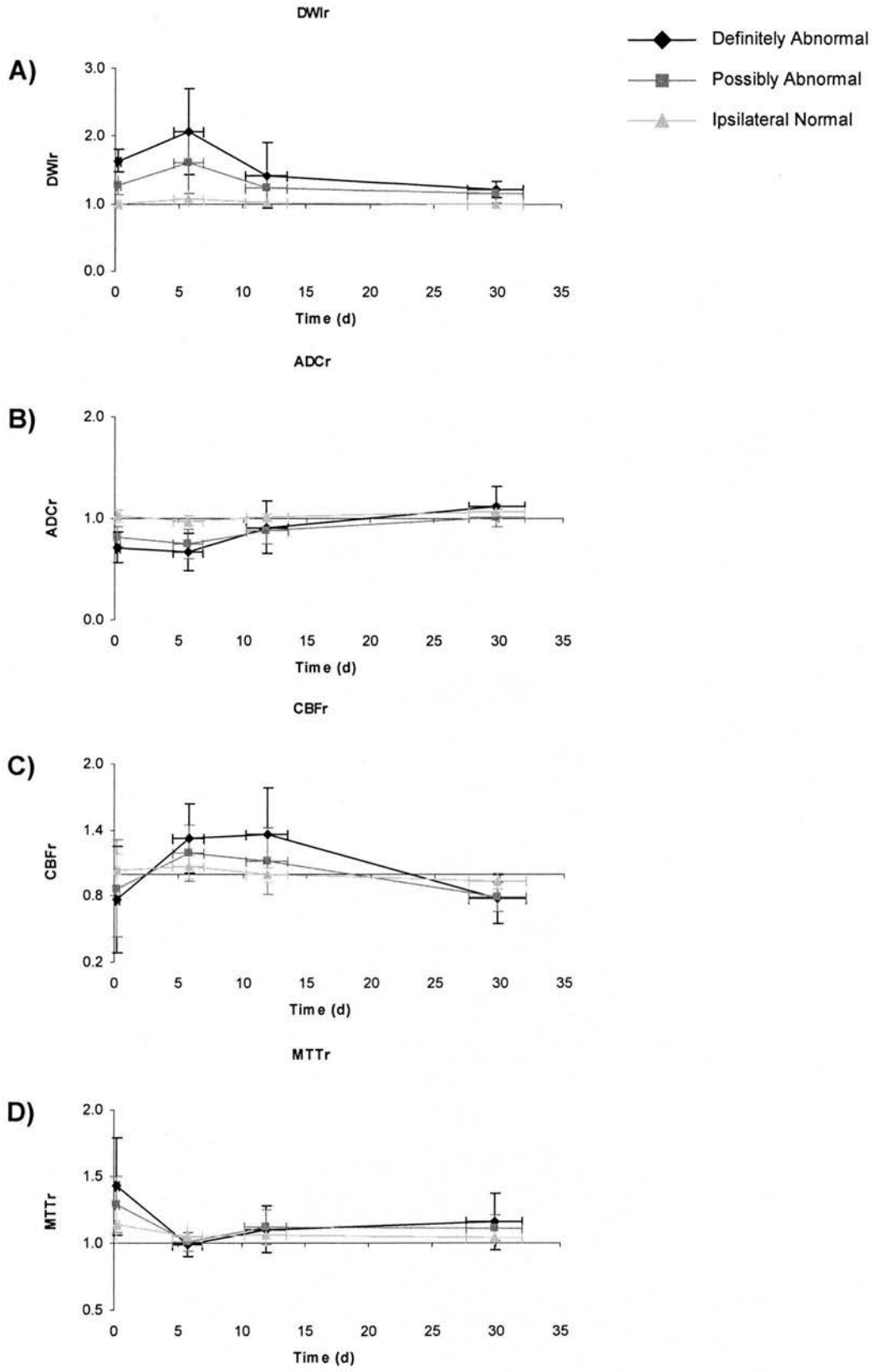

Figure 8.3 Mean A) DWIr, B) ADCr, C) CBFr, and D) MTTr for the patients analysed with the manual grid-based analysis method (n = 8). Tissue classifications were scored according to baseline DWI appearance, which were applied to subsequent coregistered scans. Error bars represent ± 1 SD of the mean.

Tissue classified as 'possibly abnormal' and 'definitely abnormal' had significantly increased baseline DWIr compared to normal ('possibly abnormal' DWIr = 1.634 ± 0.171, 'definitely abnormal' DWIr = 1.277 ± 0.137, t-tests both $p < 0.01$; Table 8.2); 'definitely abnormal' tissue had significantly higher DWI SI at baseline than 'possibly abnormal' tissue (paired t-test $p < 0.01$). The DWIr in both 'definitely abnormal' and 'possibly abnormal' tissue changed significantly over time (GLM regression both $p < 0.01$), with a peak at approximately 5 days after stroke onset, after which it declined to approximately normal at 30 days after stroke onset (Figure 8.3). There were no significant differences in DWIr at baseline or over time in tissue classified as 'ipsilateral normal' (t-tests p = NS, GLM regression p = NS; Figure 8.3).

In terms of underlying ADCr values, both 'possibly abnormal' and 'definitely abnormal' tissue had significantly decreased ADC relative to normal at baseline ('possibly abnormal' ADCr = 0.712 ± 0.151, 'definitely abnormal' ADCr = 0.817 ± 0.098, t-tests both $p < 0.01$; Table 8.2); 'definitely abnormal' tissue had a significantly lower ADC than 'possibly abnormal' tissue (t-test $p = 0.03$). The ADC in both 'definitely abnormal' and 'possibly abnormal' tissue increased significantly over time (GLM regression both $p < 0.01$), appearing to reach a nadir at approximately 5 days after stroke onset, after which it 'pseudonormalised', and became slightly increased relative to normal at approximately 30 days after stroke onset (Figure 8.3). There were no significant differences in ADCr in 'ipsilateral normal' tissue at baseline or over time (t-test p = NS, GLM regression p = NS; Figure 8.3). There was no significant difference in ADC at 30 days after stroke onset between 'definitely abnormal' and 'possibly abnormal' tissue (paired t-test = NS).

Baseline CBF was significantly decreased relative to normal only in 'definitely abnormal' tissue (CBFr = 0.765 ± 0.484, t-test $p < 0.01$; Table 8.2); baseline CBF in 'definitely abnormal' tissue was significantly lower than in 'possibly abnormal' tissue (paired t-test $p < 0.05$). CBF in 'definitely abnormal' tissue also changed significantly over time (GLM regression $p = 0.01$), appearing to increase from an initially decreased relative to normal value between approximately 5 - 14 days after stroke onset, and subsequently appeared to decrease to a below-normal level by 30 days after stroke onset (Figure 8.3). There were no significant changes in CBF over time in 'possibly abnormal' or 'ipsilateral normal' tissue (GLM regression both p = NS), although CBF in 'possibly abnormal' tissue appeared to follow a similar pattern to CBF in 'definitely abnormal' tissue, i.e. increase from an initially decreased relative to normal value between approximately 5 - 14 days after stroke onset, and subsequently appeared to decrease to a below-normal level by 30 days after stroke onset (Figure 8.3).

Baseline MTT was significantly prolonged relative to normal in 'definitely abnormal' (MTTr = 1.429 ± 0.365, t-test $p = 0.01$), 'possibly abnormal' (MTTr = 1.290 ± 0.214, t-test $p < 0.01$), and 'ipsilateral normal' (MTTr = 1.139 ± 0.142, t-test $p = 0.03$) tissues (Table 8.2). There was no significant difference between the baseline MTT in 'definitely abnormal' and 'possibly abnormal' tissue (paired t-test p = NS). Although MTT appeared to decrease over time in all tissue classifications, reaching a nadir at approximately 5 days after stroke onset, these trends were not statistically significant (GLM regression all p = NS; Figure 8.3).

Differences in the evolution of 'possibly abnormal' tissue

When the individual patient data were examined, two patterns of DWIr and ADCr evolution in 'possibly abnormal' tissue emerged. In 4/8 (50%) patients (Patients C, F, G & H), the 'possibly abnormal' tissue appeared to be initially similar, and follow a similar evolution to, 'ipsilateral normal' tissue; in the other 4/8 (50%) patients (Patients A, B, D & E), the 'possibly abnormal' tissue appeared to be initially similar, and follow a similar evolution to, 'definitely abnormal' tissue in terms of DWIr and ADCr values (Figure 8.4).

Methods

Patients were grouped into 'possibly abnormal' like 'normal' tissue (Group 1) and 'possibly abnormal' like 'definitely abnormal' tissue (Group 2).

Statistical analyses

Clinical details of Group 1 and Group 2 patients were compared: age and time from stroke onset to baseline and subsequent MRI with standard t-tests; baseline NIHSS with a Mann-Whitney U-test; and sex, OCSP classifications, and whether the patients were dead or dependent (mRS = 3 - 6) at 90 days after stroke onset or not with Chi-Square (χ^2) tests.

Mean (± SD) DWIr, ADCr, CBFr, and MTTr values are reported and compared. Baseline DWIr, ADCr, CBFr, and MTTr values between Group 1 and Group 2 were compared with standard t-tests. GLM repeated measures regression analysis was performed to compare changes in DWIr, ADCr, CBFr, and MTTr values over time (from baseline to 30 days after stroke onset) between Group 1 and Group 2

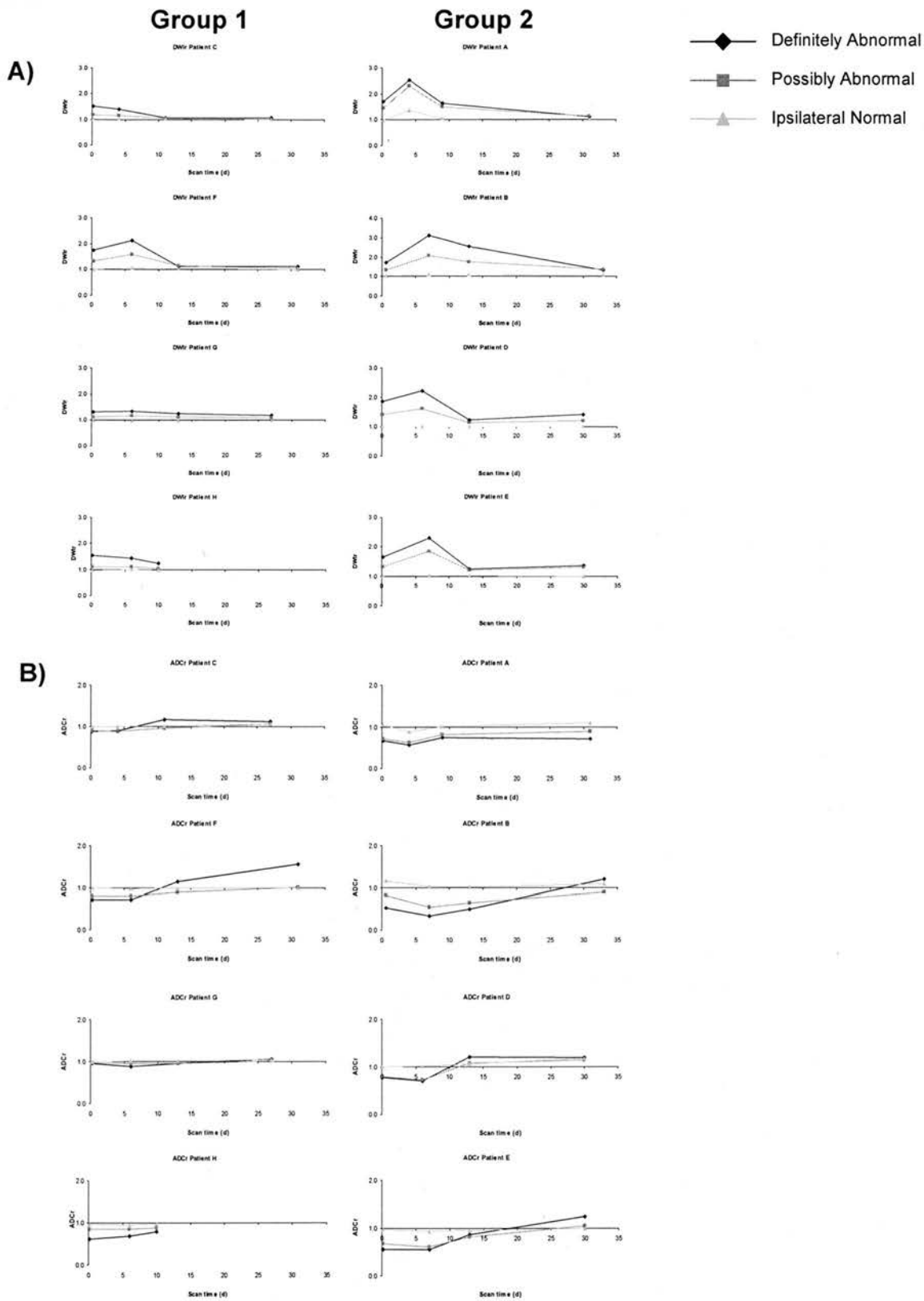

Figure 8.4 Individual mean A) DWIr and B) ADCr values from baseline to 30 days after stroke onset for the patients analysed with the manual grid-based analysis method (n = 8). Note that the 'possibly abnormal' values in the patients in Group 1 (left) appear to follow 'normal' tissue patterns, while in Group 2 (right) they follow 'definitely abnormal' tissue patterns. Tissue classifications were scored according to baseline DWI appearance, which were applied to subsequent coregistered scans. Error bars represent ± 1 SD of the mean.

(dependent variables = DWIr, ADCr, CBFr, and MTTr values; between subjects factor = Group 1 vs. Group 2; ADCr and MTTr fit to a linear model, CBFr fit to a quadratic model).

Results

Patient details

There were no significant differences in the sex, baseline NIHSS, OCSP classifications, or likelihood of being dead or dependent at 90 days after stroke onset between the patients in Groups 1 and 2. However, the patients in Group 2 ('possibly abnormal' like 'definitely abnormal' tissue) were significantly older than the patients in Group 1 ('possibly abnormal' like 'normal' tissue); mean age 76 years vs. 57 years, t-test $p < 0.05$).

General patient scan characteristics

There were no significant differences in time from stroke onset to baseline or any subsequent MRI between the patients in Groups 1 and 2 (t-tests all p = NS).

MRI characteristics of Group 1 vs. Group 2

Table 8.3 lists and Figure 8.5 shows graphs of the mean (± SD) DWIr, ADCr, CBFr, and MTTr values for each tissue classification (scored according to baseline DWI appearance and applied to subsequent scans) for Group 1 and Group 2 from baseline to 30 days after stroke onset.

DWI SI in 'possibly abnormal' tissue was initially significantly more increased relative to normal in Group 2 compared to Group 1 (Group 2 DWIr = 1.383 ± 0.064 vs. Group 1 DWIr = 1.171 ± 0.098, t-test p = 0.01; Table 8.3), and remained more increased relative to normal over time (GLM regression p = 0.02; Figure 8.5).

Table 8.3 Mean (± SD) scan time, DWIr, ADCr, CBFr, and MTTr values for Group 1 ('possibly abnormal' like 'normal' tissue, n = 4) and Group 2 ('possibly abnormal' like 'definitely abnormal' tissue, n = 4) patients at each scan time for all tissue classifications. Tissue classifications were scored according to baseline DWI appearance, which were applied to subsequent coregistered scans.

Scan time	Tissue class	DWIr		ADCr		CBFr		MTTr	
		Group 1	Group 2	Group 1	Group 2	Group 1	Group 2	Group 1	Group 2
6 ± 4 h	Definitely abnormal	1.529 ± 0.175	1.739 ± 0.093	0.791 ± 0.154	0.633 ± 0.115	1.074 ± 0.481	0.456 ± 0.248	1.475 ± 0.533	1.383 ± 0.144
	Possibly abnormal	1.171 ± 0.098	1.383 ± 0.064	0.881 ± 0.075	0.752 ± 0.074	1.123 ± 0.431	0.617 ± 0.315	1.259 ± 0.217	1.320 ± 0.239
	Ipsilateral normal	0.994 ± 0.021	1.004 ± 0.026	0.996 ± 0.013	1.046 ± 0.087	1.066 ± 0.193	0.997 ± 0.112	1.081 ± 0.125	1.197 ± 0.150
6 ± 1 d	Definitely abnormal	1.574 ± 0.375	2.565 ± 0.383	0.797 ± 0.110	0.538 ± 0.146	1.344 ± 0.377	1.297 ± 0.269	1.031 ± 0.083	0.939 ± 0.087
	Possibly abnormal	1.244 ± 0.224	1.977 ± 0.266	0.869 ± 0.064	0.627 ± 0.075	1.141 ± 0.244	1.263 ± 0.307	1.042 ± 0.070	0.965 ± 0.055
	Ipsilateral normal	1.012 ± 0.033	1.135 ± 0.150	0.983 ± 0.029	0.961 ± 0.077	1.023 ± 0.109	1.120 ± 0.085	1.021 ± 0.060	1.081 ± 0.113
12 ± 2 d	Definitely abnormal	1.166 ± 0.083	1.664 ± 0.625	1.016 ± 0.177	0.809 ± 0.303	1.274 ± 0.344	1.422 ± 0.526	1.059 ± 0.087	1.138 ± 0.232
	Possibly abnormal	1.077 ± 0.050	1.394 ± 0.289	0.921 ± 0.039	0.836 ± 0.179	0.938 ± 0.119	1.251 ± 0.336	1.103 ± 0.102	1.130 ± 0.159
	Ipsilateral normal	0.991 ± 0.025	1.037 ± 0.050	1.002 ± 0.018	1.012 ± 0.047	0.968 ± 0.055	1.009 ± 0.067	1.043 ± 0.090	1.076 ± 0.113
30 ± 2 d	Definitely abnormal	1.114 ± 0.056	1.279 ± 0.115	1.169 ± 0.137	1.089 ± 0.249	0.947 ± 0.202	0.648 ± 0.137	1.111 ± 0.142	1.194 ± 0.265
	Possibly abnormal	1.047 ± 0.041	1.227 ± 0.125	1.030 ± 0.030	0.994 ± 0.120	0.899 ± 0.080	0.717 ± 0.109	1.096 ± 0.068	1.128 ± 0.118
	Ipsilateral normal	0.988 ± 0.019	0.998 ± 0.060	1.030 ± 0.038	1.099 ± 0.088	0.970 ± 0.097	0.918 ± 0.055	1.046 ± 0.040	1.028 ± 0.057

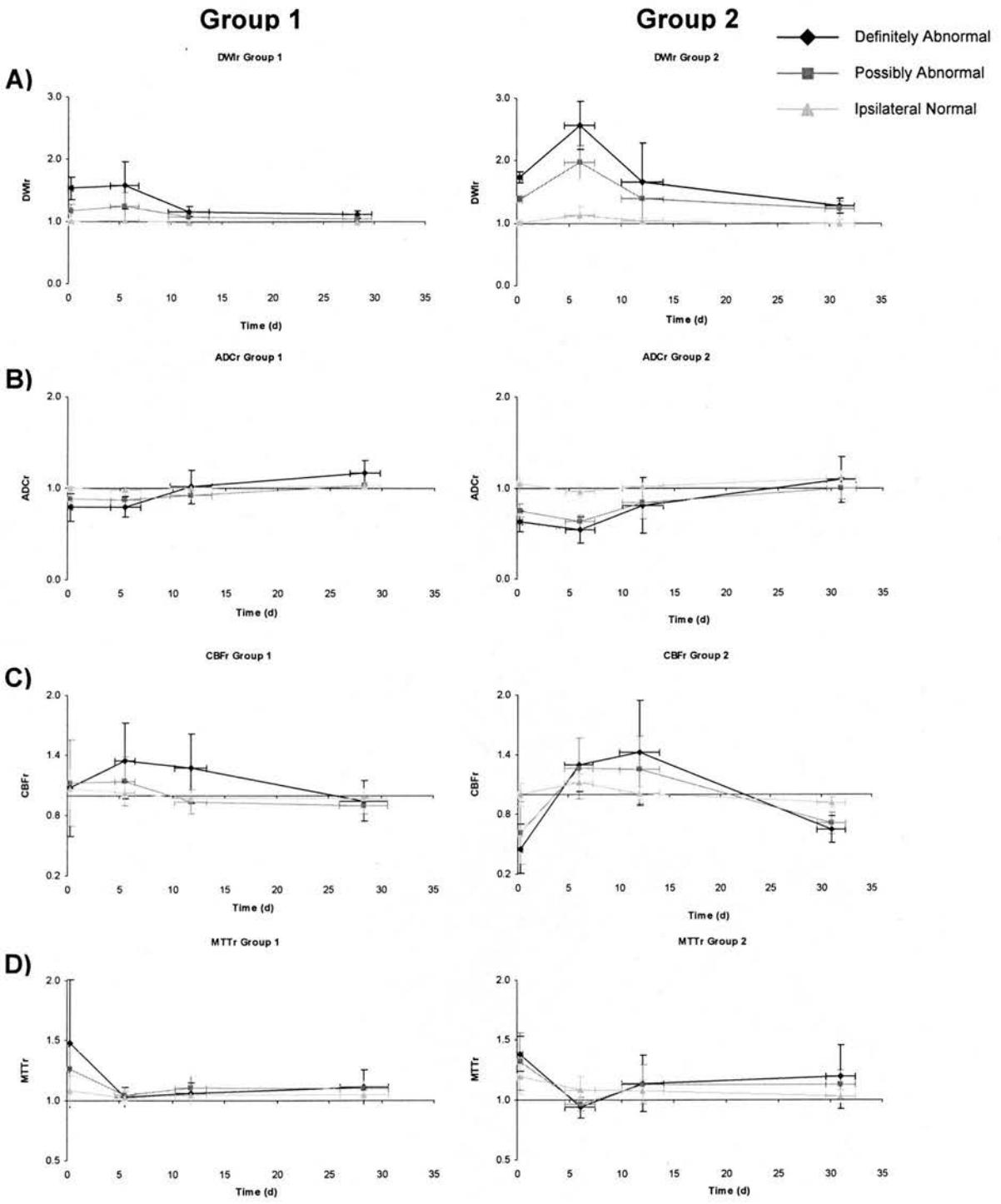

Figure 8.5 Mean A) DWIr, B) ADCr, C) CBFr, and D) MTTr for Group 1 ('possibly abnormal' like 'normal' tissue, n = 4) and Group 2 ('possibly abnormal' like 'definitely abnormal' tissue, n = 4) patients. Error bars represent ± 1 SD of the mean.

Although not significantly different at baseline (t-test p = NS), the DWI SI in 'definitely abnormal' tissue was more increased relative to normal in Group 2 compared with Group 1 over time (GLM regression p = 0.04; Figure 8.5).

Baseline ADC in 'possibly abnormal' tissue was significantly more decreased relative to normal in Group 2 vs. Group 1 (Group 2 ADCr = 0.752 ± 0.074 vs. Group 1 ADCr = 0.881 ± 0.075, t-test p = 0.05; Table 8.3), and although not statistically significant, appeared to remain decreased relative to normal for longer in Group 2 vs. Group 1 (GLM regression p = NS; Figure 8.5). Although not statistically significant, the ADC in 'definitely abnormal' tissue in Group 2 appeared to be more decreased relative to normal at baseline (t-test p = NS), and remain decreased relative to normal for longer than in Group 1 (GLM regression p = NS; Figure 8.5).

Although the baseline CBF of 'possibly abnormal' tissue appeared to be lower in Group 2 compared to Group 1 (Group 2 CBFr = 0.617 ± 0.315 vs. Group 1 CBFr = 1.123 ± 0.431), there was no statistically significant difference between groups (t-test p = NS; Table 8.3). However, there was a significant difference between the evolution of CBF in 'possibly abnormal' tissue between Groups 1 and 2 (GLM regression $p < 0.01$); CBF increased more rapidly between baseline and 5 days after stroke onset, and the peak CBF occurred later in Group 2 than in Group 1 (approximately 12 days vs. 5 days after stroke onset; Figure 8.5). Although the baseline CBF of 'definitely abnormal' tissue appeared to be lower in Group 2 compared to Group 1 (Group 2 CBFr = 0.456 ± 0.248 vs. Group 1 CBFr = 1.074 ± 0.481), there was no statistically significant difference between groups (t-test p = NS; Table 8.3). However, the evolution of CBF in 'definitely abnormal' tissue was significantly different between Groups 1 and 2 (GLM regression p = 0.03); CBF

increased more rapidly between baseline and 5 days after stroke onset, and the peak CBF occurred later in Group 2 than in Group 1 (approximately 12 days vs. 5 days after stroke onset; Figure 8.5).

Baseline MTT of 'possibly abnormal' tissue was not significantly different between Group 1 and Group 2 (t-test p = NS; Table 8.3). Although it appeared that the MTT in 'possibly abnormal' tissue in Group 2 decreased more rapidly between baseline and 5 days after stroke onset relative to Group 1, this pattern was not statistically significant (GLM regression p = NS; Figure 8.5). There were no significant differences in MTT between Groups 1 and 2 in 'definitely abnormal' tissue either at baseline or over time (t-test p = NS, GLM regression p = NS).

There were no significant differences in DWI SI, ADC, CBF, or MTT between Group 1 and Group 2 in 'ipsilateral normal' tissue either at baseline or over time (t-tests all p = NS, GLM regression all p = NS; Table 8.3, Figure 8.5).

Discussion

The manual grid method demonstrated that the subregions of abnormality (degrees of 'brightness') on DWI probably reflect the underlying degree of tissue damage as measured by ADC abnormality. Tissue that appears 'possibly abnormal' on DWI is initially significantly less abnormal in terms of ADC values than tissue that appears 'definitely abnormal'. The fate of the 'possibly abnormal' tissue appears to be related to baseline CBF and MTT values, and the pattern of changes in CBF and MTT from baseline to approximately 5 days after stroke onset. The age of the patient might also

be important – patients whose 'possibly abnormal' tissue became less abnormal were significantly younger than patients whose 'possibly abnormal' tissue became more abnormal, although the small sample size means that this analysis is only exploratory. However, analysis of a larger sample of patients with the manual grid-based analysis is impractical as it is extremely labour intensive and liable to observer error; each grid box must be individually identified, the 'place' in the grid must be manually calculated, and extracted DWI and PWI parameters must be manually assigned to the appropriate tissue classification category.

Exploring these issues in a larger group of patients with a more automated approach would help to elucidate how early diffusion and perfusion changes affect outcome; thus we developed a grid-based program to reduce analysis time and observer error. The development and testing of observer variation of this grid-based program will be discussed in the following chapter.

9. Development and observer variation of a grid-based analysis program

Introduction

This chapter concerns the development of a more efficient grid-based analysis program for analysis of a larger sample of patients. The effect of observer differences on lesion volume and extracted DWI and PWI values from lesion analysis with the grid-based program is assessed.

SGAT grid analysis

After the initial testing of the manual grid-based analysis in Chapter 8, an internally-developed grid-based program, SBIRCS Grid Analysis Tool (SGAT), was developed in MATLAB® by Dr. Paul Armitage to provide a more efficient method of grid-based analysis in a larger group of patients.

Methods

For each patient, the axial slice that passed through the centre of the visible ischaemic lesion on baseline DWI was chosen for analysis. The SGAT program displays an observer-selected image from the DWI sequence, windowed to a standard signal intensity, with a 5 × 5 voxel grid (voxel = 4.39 mm^3, grid box = 109.86 mm^3) laid over the image (Figure 9.1). Grid boxes containing only background or CSF are automatically segmented using FSL software BET[203] and FAST[204] (FMRIB Analysis Group, Oxford, UK) and marked by the program (although these can still be edited by the observer if necessary). The observer first marks a line of voxels separating the right and left hemispheres, and indicates which

hemisphere is ipsilateral to the ischaemic lesion by clicking on it with the mouse. The observer can then classify each grid box (as 'definitely abnormal' or 'possibly abnormal') according to its appearance on baseline DWI by selecting it with the mouse. A coloured '×' appears in each box as it is classified, the colour corresponding to the classification. Once all the 'definitely abnormal' and 'possibly abnormal' tissue is classified, large numbers of grid boxes containing 'normal' tissue can be classified by clicking on the 'fill' option, which scores all unclassified boxes as either 'ipsilateral normal' or 'contralateral normal' in relation to the hemisphere selection as described above. This grid-based analysis is much faster to perform than the manual grid-based analysis and overcomes observer error issues, such as losing one's 'place' in the grid.

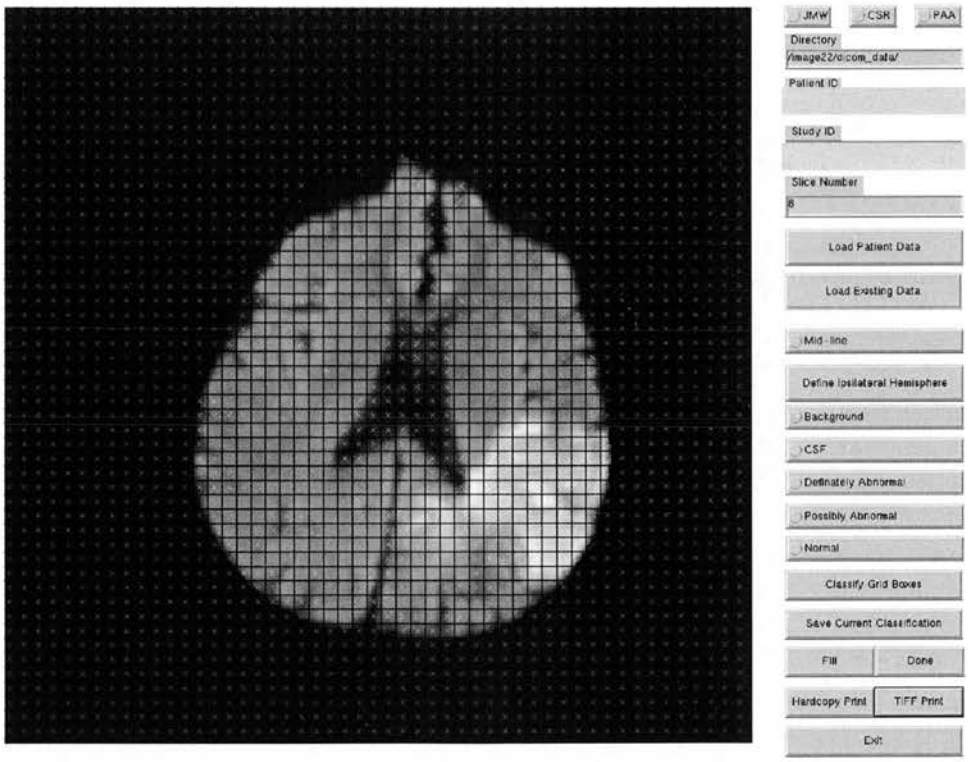

Figure 9.1 The SGAT grid analysis program user interface (Patient A, left hemisphere ischaemic lesion on DWI at 4 hours after stroke onset). Each grid box is 4.69 × 4.69 mm.

Tissue classification

Tissue classifications ('definitely abnormal', 'possibly abnormal', 'ipsilateral normal', and 'contralateral normal') and scoring criteria were the same as previously described in Chapter 8 for the manual grid analysis (Figure 8.2).

Observer variation in SGAT grid analysis

Methods

A group of 50 patients with visible lesions on baseline DWI from the larger cohort of patients as described in Chapter 4 were included in the present analysis. Two observers scored the baseline DWI scans to evaluate the effect of observer differences on the volume of tissue selected as each tissue classification and the effect on measured DWI and PWI parameters between two observers using the SGAT grid-based analysis program. The evolution of diffusion and perfusion parameters in the different tissue classifications will be presented in Chapter 9.

Tissue classification

Grid-scoring was performed by the author (Observer A), and a neuroradiologist (JMW, Observer B), blindly and independently of one another and clinical and other imaging details.

Statistical analyses

General patient demographic data was obtained and compared as previously described (Chapter 4).

We combined 'possibly abnormal' and 'definitely abnormal' tissue (weighted mean of the two) to compare all 'abnormal' tissue as some patients did not have any tissue that was rated as 'definitely abnormal' by one or both of the observers. DWI SI, T_2WI SI, ADC, CBF, CBV, and MTT values for each grid box and mean values for each tissue classification for each observer were extracted. Note that DWI SI, T_2WI SI, CBF, CBV, and MTT values are not quantitative, so are in arbitrary units (AU).

We compared the volume of tissue scored as each tissue classification by each observer. The volume of tissue scored as each tissue classification by each observer was calculated by multiplying the number of boxes scored as each tissue classification by the volume of a grid box (109.86 mm^3). The volume data was not normally-distributed (Kolmogorov-Smirnov test $p < 0.01$), so median volumes of each classification of tissue were compared using Wilcoxon signed rank sum tests and correlations between the volume of tissue scored as each tissue classification by the two observers were assessed with Spearman's rank correlation coefficients (ρ).

Plots of the difference (Observer A – Observer B) vs. the mean DWI SI, T_2WI SI, ADC, CBF, CBV, and MTT values (Bland Altman plots[186]) for each tissue classification between Observers A and B were compared to assess differences in MR parameters when two observers score lesions according to baseline DWI appearance using the SGAT grid analysis program.

In order to compare the magnitude of 'between observer differences' directly across different MR parameters, which have different mean values and ranges of values, we also expressed the 95% limits of agreement (mean difference ± 2 SD) of the 'observer difference' as a percentage of the mean DWI SI, T_2WI SI, ADC, CBF,

CBV, and MTT values between observers (95% limits of agreement between observers divided by the mean between observers, expressed as a percentage).

Results

Patient details

Fifty patients with visible lesions on baseline DWI were included in the present analysis: 31/50 (62%) were male, the mean age was 73 years (range: 37 - 94 years), and the mean NIHSS score on admission was 10 (median 8, range: 0 - 27). OCSP classifications: 16/50 (32%) patients had a TACI, 29/50 (58%) patients had a PACI, 4/50 (8%) patients had a LACI, and 1/50 (2%) patients had a POCI. Mean mRS score at 90 days after stroke onset was 3 (median 2); 14/50 (28%) patients were dependent (mRS = 3 – 5) and 7/50 (14%) patients were dead (mRS = 6).

General patient scan details

Mean (± SD) time from stroke onset to baseline imaging was 9 ± 6 hours, with 25/50 (50%) patients imaged within 6 hours, 10/50 (20%) patients between 6 and 12 hours, and 15/50 (30%) patients between 12 and 24 hours after stroke onset.

Tissue classification

In all 50 patients, both observers scored at least one grid box as 'possibly abnormal'. In 3/50 (6%) patients, neither observer scored any tissue as 'definitely abnormal', and in 7/50 (14%) patients, the less experienced observer (the author) did not score any tissue as 'definitely abnormal' whereas the more experienced observer (JMW) did.

Tissue classification volumes

The volume of tissue scored as 'abnormal' (combined 'definitely abnormal' and 'possibly abnormal') by Observer A was significantly smaller than the volume of tissue scored as 'abnormal' by Observer B (median volume Observer A = 3021.24 mm^3 vs. Observer B = 4174.80 mm^3, Wilcoxon test $p < 0.01$; Table 9.1). There were no significant differences in the volumes of tissue scored as 'ipsilateral normal' (median volume Observer A = 19006.35 mm^3 vs. Observer B = 18072.51 mm^3, Wilcoxon test p = NS) or 'contralateral normal' (median volume Observer A = 21588.14 mm^3 vs. Observer B = 21643.07 mm^3, Wilcoxon test p = NS; Table 9.1).

The volume of tissue scored as 'abnormal', 'ipsilateral normal', and 'contralateral normal' by each observers correlated very highly (Spearman's $\rho = 0.95$, $\rho = 0.94$, and $\rho = 0.79$ respectively, all $p < 0.01$; Table 9.1).

Table 9.1 Median volume of tissue scored as each tissue classification for each observer using the SGAT grid analysis program, Wilcoxon signed rank sum tests and Spearman's rank correlation coefficients (ρ) between observers.

Tissue classification	Median volume (mm^3)		Wilcoxon test	Spearman's ρ
	Observer A	Observer B		
Abnormal	3021.24	4174.80	$p < 0.01$	0.95
Ipsilateral normal	19006.35	18072.51	NS	0.94
Contralateral normal	21588.14	21643.07	NS	0.79

Table 9.2 Mean DWI SI, T_2WI SI, ADC, CBF, and MTT values for each tissue classification for each observer using the SGAT grid analysis program.

Parameter	Observer	Abnormal Tissue	Ipsilateral normal tissue	Contralateral normal tissue
DWI SI (AU)	A	440.19 ± 77.54	293.71 ± 22.74	288.46 ± 24.32
	B	415.56 ± 73.22	286.86 ± 23.68	285.56 ± 25.12
T_2W SI (AU)	A	944.66 ± 134.35	788.58 ± 105.56	783.91 ± 96.96
	B	945.09 ± 136.42	775.48 ± 93.95	770.64 ± 91.22
ADC (10^{-6} mm^2/s)	A	760.62 ± 157.89	963.37 ± 92.06	974.53 ± 89.47
	B	817.77 ± 175.88	971.64 ± 83.63	971.44 ± 89.84
CBF (AU)	A	974.56 ± 451.61	1146.96 ± 347.40	1180.47 ± 350.30
	B	1027.60 ± 438.64	1151.97 ± 340.57	1166.88 ± 340.97
CBV (AU)	A	1138.60 ± 451.55	1191.78 ± 469.03	1132.25 ± 425.90
	B	1187.83 ± 453.11	1192.08 ± 467.48	1127.86 ± 423.51
MTT (AU)	A	1323.97 ± 522.92	1072.63 ± 378.16	977.54 ± 315.30
	B	1295.99 ± 508.89	1058.88 ± 371.74	980.34 ± 316.26

MRI characteristics

Table 9.2 lists the mean (± SD) DWI SI, T_2WI SI, ADC, CBF, CBV, and MTT values for each tissue classification for Observers A and B. Plots of the difference (Observer A – Observer B) vs. the mean DWI SI, T_2WI SI, ADC, CBF, CBV, and MTT values between the two observers for are shown in Figure 9.2 for 'abnormal' tissue, Figure 9.3 for 'ipsilateral normal' tissue, and Figure 9.4 for 'contralateral normal' tissue. Figures 9.2 – 9.4 also include the mean between observers and 95% limits of agreement (mean difference ± 2 SD) for each MR parameter.

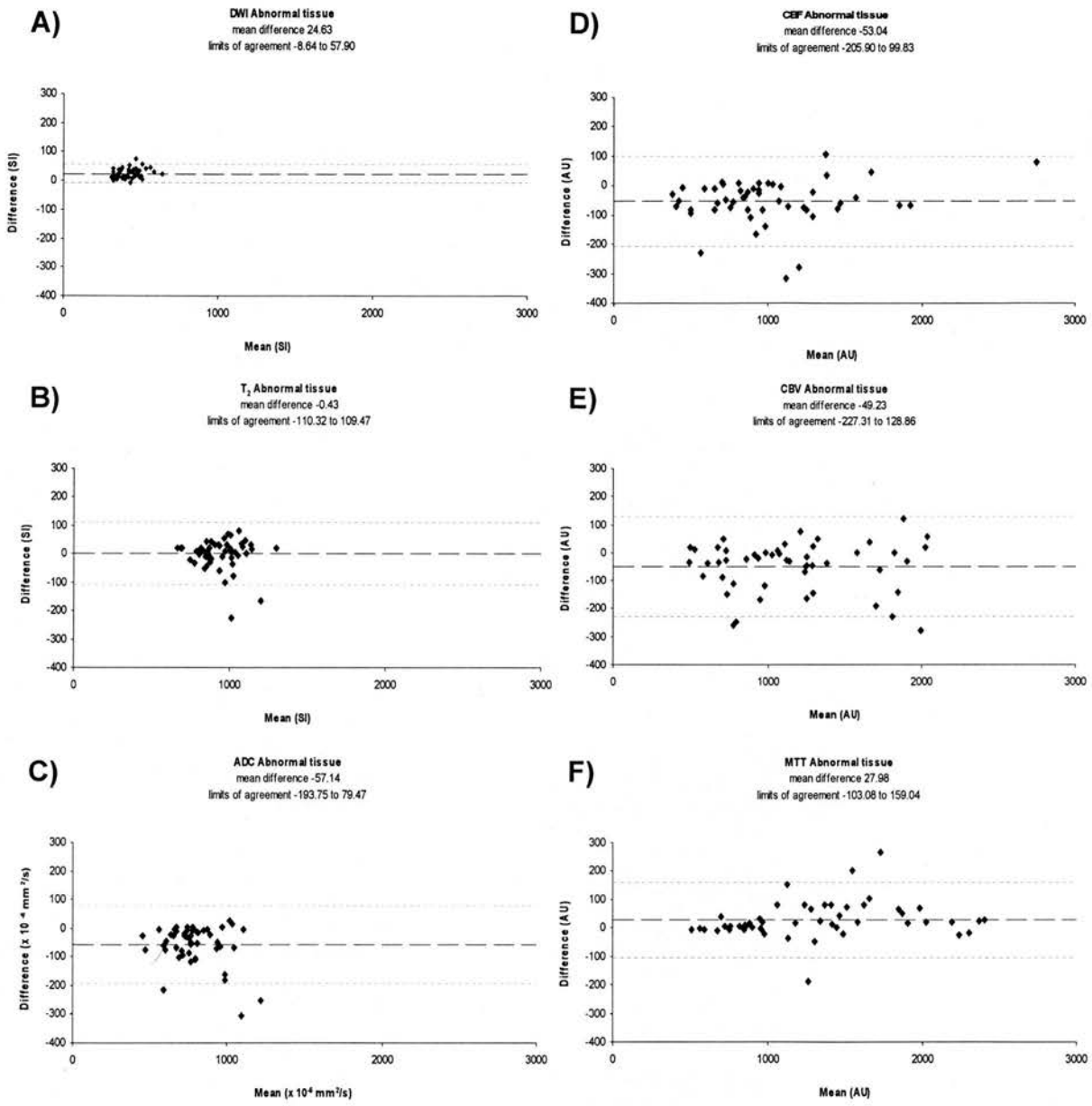

Figure 9.2 Bland Altman plots of A) DWI SI, B) T_2WI SI, C) ADC, D) CBF, E) CBV, and F) MTT values from tissue rated 'abnormal' (combined 'definitely abnormal' and 'possibly abnormal' tissue) by two observers. The black dashed line represents the mean difference, and the grey dashed lines represent ± 2 SD of the mean (95% limits of agreement).

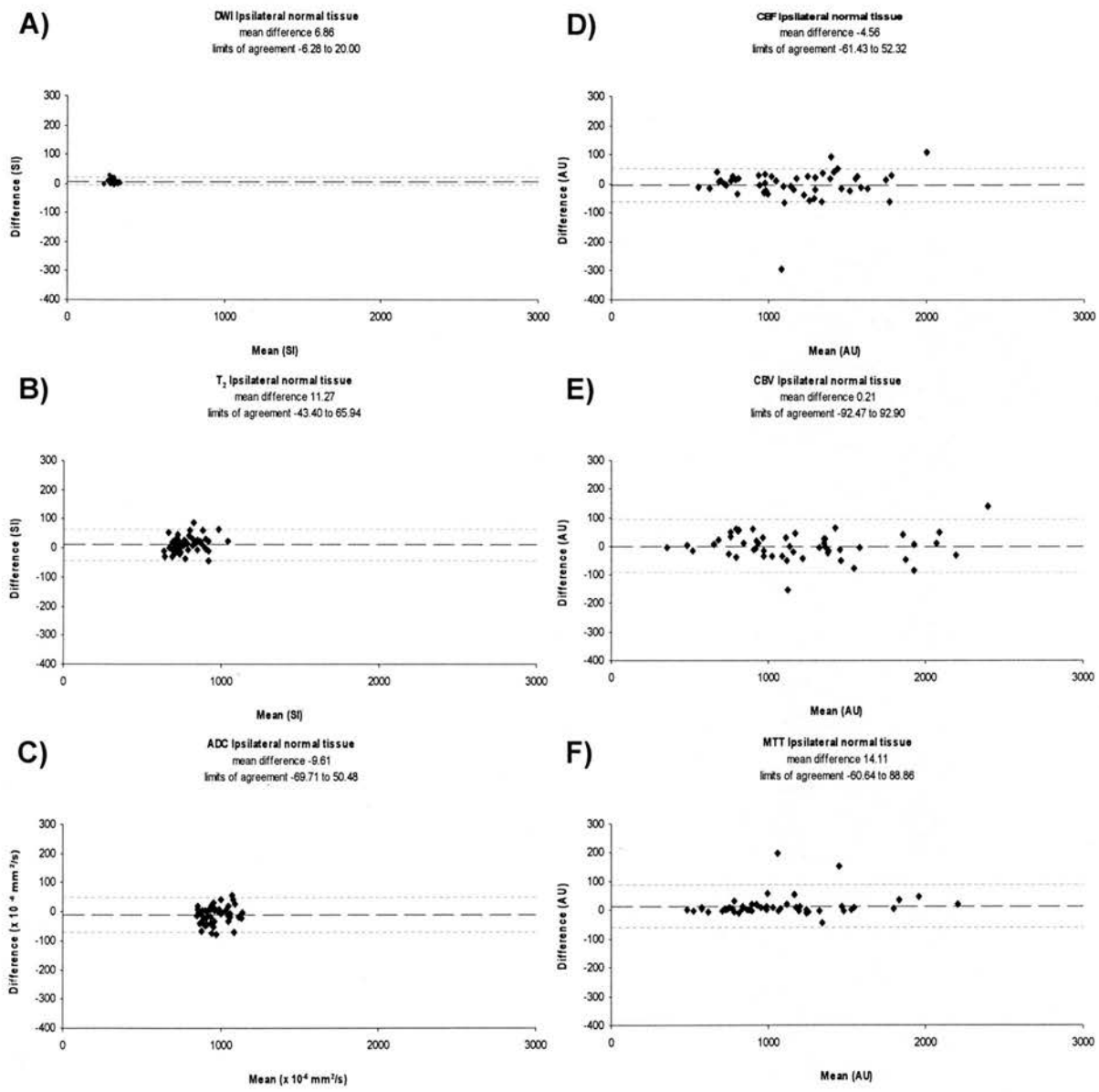

Figure 9.3 Bland Altman plots of A) DWI SI, B) T_2WI SI, C) ADC, D) CBF, E) CBV, and F) MTT values from tissue rated 'ipsilateral normal' by two observers. The black dashed line represents the mean difference, and the grey dashed lines represent ± 2 SD of the mean (95% limits of agreement).

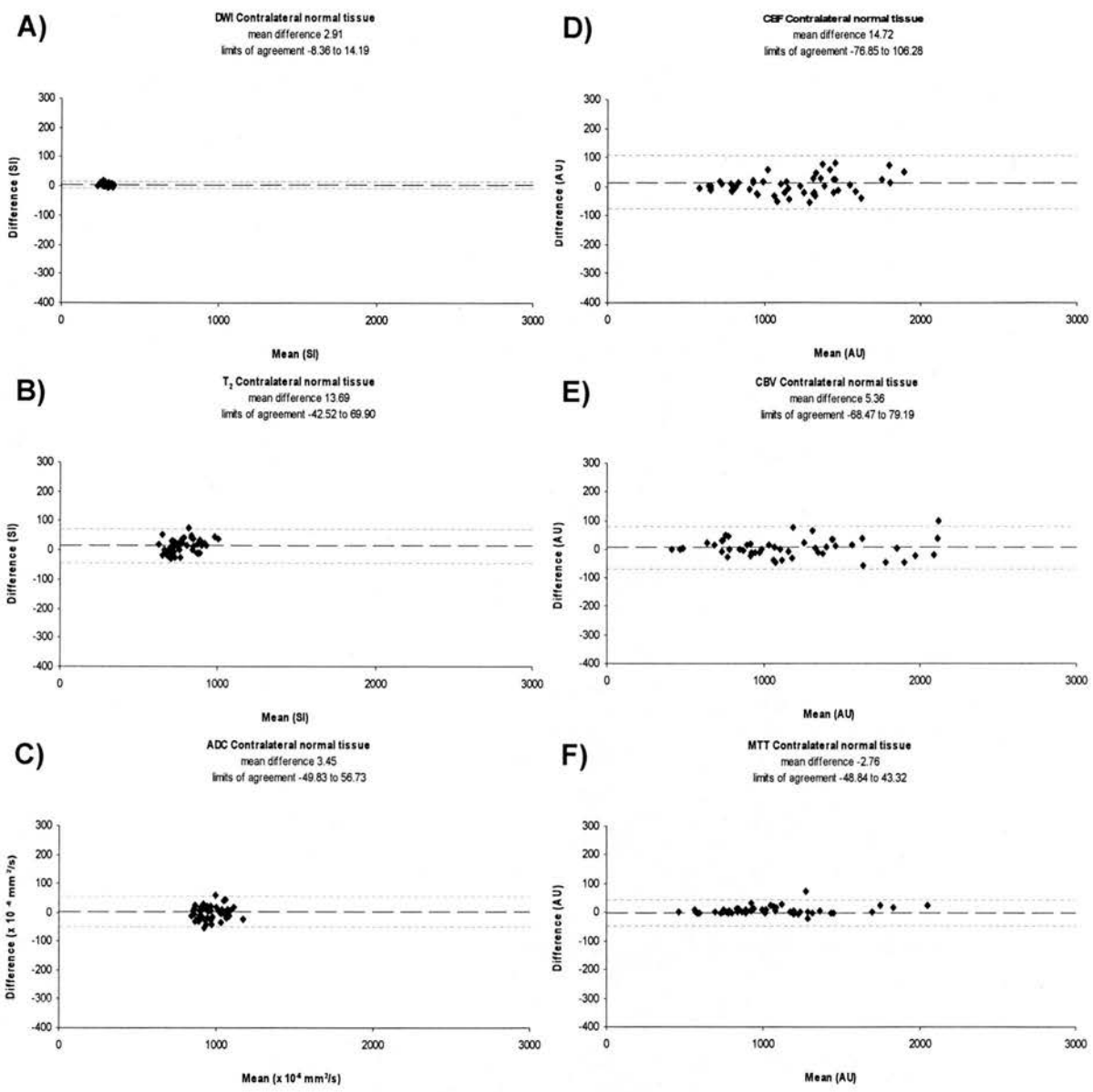

Figure 9.4 Bland Altman plots of A) DWI SI, B) T_2WI SI, C) ADC, D) CBF, E) CBV, and F) MTT values from tissue rated 'contralateral normal' by two observers. The black dashed line represents the mean difference, and the grey dashed lines represent ± 2 SD of the mean (95% limits of agreement).

DWI and observer differences

The mean DWI SI value for 'abnormal' tissue was more abnormal (i.e. 'brighter') for Observer A compared to Observer B (440.19 ± 77.54 vs. 415.56 ± 73.22 AU; mean difference Observer A - Observer B = 24.63 AU; Figure 9.2, Table 9.2). Observer A's more abnormal DWI SI values for 'abnormal' tissue, together with the significantly smaller volume of tissue scored as 'abnormal' by Observer A compared to Observer B, means that Observer A was less perceptive in scoring tissue as appearing 'possibly abnormal' or 'definitely abnormal' on baseline DWI. The 95% limits of agreement for 'abnormal' tissue DWI SI values are narrow (-8.64 – 57.90 AU; Figure 9.2).

There was little difference between Observers A and B in terms of DWI SI values in tissue classified as 'ipsilateral normal' (mean difference Observer A – Observer B = 6.86 AU) and 'contralateral normal' (mean difference Observer A – Observer B = 2.91 AU) tissue classifications (Figure 9.3, Figure 9.4). The 95% limits of agreement for DWI SI values between Observers A and B are narrow for DWI values for 'ipsilateral normal' (-6.26 – 20.00 AU; Figure 9.3) or 'contralateral normal' (-8.36 – 14.19 AU; Figure 9.4) tissue.

ADC and observer differences

When tissue was classified according to baseline DWI appearance, the mean ADC value for 'abnormal' tissue was more abnormal (i.e. lower) for Observer A compared to Observer B (mean ADC Observer A = 760.62 ± 157.89 vs. Observer B = 817.77 ± 175.55 × 10^{-6} mm^2/s; mean difference Observer A - Observer B = -57.14 × 10^{-6} mm^2/s; Figure 9.2, Table 9.2). These ADC values agree with the volume and DWI SI value results that suggest Observer A was more conservative in scoring tissue as

appearing 'abnormal' on baseline DWI. The 95% limits of agreement for 'abnormal' tissue ADC values are much wider than for DWI values (–193.75 – 79.47 × 10^{-6} mm^2/s; Figure 9.2).

There was less difference in ADC values between observers in 'ipsilateral normal' (mean difference Observer A – Observer B = -9.61 × 10^{-6} mm^2/s; Figure 9.3) and 'contralateral normal' (mean difference Observer A – Observer B = 3.45 × 10^{-6} mm^2/s; Figure 9.4) tissue than in 'abnormal' tissue. However, the 95% limits of agreement for ADC values between Observers A and B are still wide in comparison to DWI SI values for 'ipsilateral normal' (–69.71 – 50.48 × 10^{-6} mm^2/s; Figure 9.3) and 'contralateral normal' (–49.83 – 56.73 × 10^{-6} mm^2/s; Figure 9.4) tissue.

PWI and observer differences

When scored according to baseline DWI appearance, PWI values for 'abnormal' tissue between Observers A and B vary widely compared to DWI SI values: 95% limits of agreement are widest for CBV values (–227.31 – 128.86 AU; Figure 9.2), intermediate for CBF values (–205.90 – 99.83 AU; Figure 9.2), and narrowest (though still wide in comparison to DWI) for MTT values (–103.08 – 159.04 AU; Figure 9.2).

PWI values for 'ipsilateral normal' tissue between Observers A and B also vary widely compared to DWI values: the 95% limits of agreement are widest for CBV values (–92.47 – 92.90 AU; Figure 9.3), intermediate for MTT values (–60.64 – 88.86 AU; Figure 9.3), and narrowest for CBF values (–61.43 – 52.32 AU; Figure 9.3). PWI values for 'contralateral normal' tissue between Observers A and B also vary widely compared to DWI SI values: the 95% limits of agreement are widest for CBF values (–76.85 – 106.28 AU; Figure 9.4), intermediate for CBV values (–68.47

– 79.19 AU; Figure 9.4), and narrowest for MTT values (–48.84 – 43.32 AU; Figure 9.4).

T_2WI SI and observer differences

Although there does not appear to be a systematic difference in T_2WI SI values between the 'abnormal' tissue as scored by Observers A and B on baseline DWI (mean difference Observer A – Observer B = -0.43 AU; Figure 9.2), the 95% limits of agreement are wide compared to DWI SI values (–110.32 – 109.47 AU; Figure 9.2). The 95% limits of agreement for T_2WI SI values between Observers A and B are also wide compared to DWI SI values for 'ipsilateral normal' (–43.30 – 65.94 AU; Figure 9.3) and 'contralateral normal' (–42.52 – 69.90 AU; Figure 9.4) tissue.

Differences between observers as a proportion of parameter values

Table 9.3 lists the proportion of DWI SI, T_2WI SI, ADC, CBF, CBV, and MTT values for each tissue classification attributable to differences between Observers A and B. For all tissue classifications, DWI SI values have the least degree of difference between observers. For 'abnormal' tissue, ADC values have the greatest degree of difference between observers (35%), compared to 16% for DWI SI values. For 'ipsilateral normal' tissue, CBV values have the greatest degree of difference between observers (15%), compared to 9% for DWI SI values. For 'contralateral normal' tissue, CBF values have the greatest degree of difference between observers (16%), compared to 8% for DWI SI values.

Table 9.3 Comparison of observer differences in DWI and PWI parameters: proportion of actual values attributable to differences between Observers A and B using the SGAT grid analysis program. Tissue classifications were scored according to baseline DWI appearance, which were applied to subsequent coregistered scans.

Parameter	Abnormal tissue			Ipsilateral normal tissue			Contralateral normal tissue		
	Range of 95% limits of agreement	Mean between observers	Difference between observers	Range of 95% limits of agreement	Mean between observers	Difference between observers	Range of 95% limits of agreement	Mean between observers	Difference between observers
DWI SI (AU)	66.44	427.88	16%	26.28	290.08	9%	22.55	286.77	8%
T_2WI SI (AU)	219.79	944.88	23%	109.34	776.63	14%	112.42	772.41	15%
ADC (10^{-6} mm^2/s)	273.22	789.20	35%	120.19	962.60	12%	106.56	968.45	11%
CBF (AU)	305.73	1001.08	31%	113.75	1152.67	10%	183.13	1172.50	16%
CBV (AU)	356.17	1163.22	31%	185.37	1199.79	15%	147.66	1132.59	13%
MTT (AU)	262.12	1309.98	20%	149.50	1071.21	14%	92.16	982.51	9%

Discussion

As discussed in Chapter 2, there is currently much interest in developing thresholds of baseline MR parameter values to predict what tissue is at risk of infarction. A 'good' parameter for development of a threshold would clearly distinguish between tissue that is already infarcted, tissue that will proceed to infarction, and tissue that will not proceed to infarction, yet would be also robust to measurement differences such as observer variation.

Tissue classification volumes

The less experienced observer (Observer A) scored significantly less tissue as appearing 'abnormal' on baseline DWI compared with the more experienced observer (Observer B) using the SGAT grid analysis. The tissue scored as 'abnormal' by Observer A was also more abnormal in terms of DWI SI and ADC values ('brighter' DWI SI and lower ADC values) than tissue scored as 'abnormal' by Observer B. This agrees with the results of Chapter 5, where, measuring lesions by manually outlining the visible abnormality on baseline DWI, the less experienced observer also measured smaller lesion volumes than the more experienced observer. This reinforces the importance of observer experience on lesion measurement, and how observer details should be listed in studies reporting lesion measurements.

It is interesting that although the volume of tissue scored as 'abnormal' by Observers A and B is significantly different, the volume of tissue scored as 'ipsilateral normal' is not significantly different between observers. However, the volume of tissue scored as 'abnormal' is much smaller than the volume of tissue scored as 'ipsilateral normal', so small differences between the observers in the volume of tissue scored as 'abnormal' are more likely to be significant.

MRI characteristics

When tissue is scored on the appearance of baseline DWI by two observers, the DWI SI values demonstrate little variability between observers for all tissue classifications, whereas other measured MR parameters vary widely in comparison, even for 'contralateral normal' tissue. The 95% limits of agreement for ADC values between Observers A and B cover a range of 273.22×10^{-6} mm^2/s; this range is extremely wide considering that the difference in ADC values between normal tissue and tissue that proceeds to infarction has been reported to be between approximately $160 - 350 \times 10^{-6}$ mm^2/s[119,123]. Developing an ADC threshold to accurately predict tissue infarction is thus unlikely, as even small observer differences cause large degrees of variation in the ADC values measured. Using ADC images to classify tissue abnormality would not be likely to reduce this observer variability in ADC values, and would in fact likely introduce more variability as ischaemic lesions on acute ADC images are harder to distinguish (dark lesions on a dark background) than on acute DWI ('bright' lesions against a dark background) as discussed in Chapter 2. PWI values between the two observers for tissue classified as 'abnormal' on baseline DWI also varied widely in comparison to DWI SI values (Figure 9.2). CBV values appeared to have the largest, CBF values intermediate, and MTT values the smallest degree of variance between observers for 'abnormal' tissue. PWI values for 'ipsilateral normal' (Figure 9.3) and 'contralateral normal' (Figure 9.4) tissue also varied considerably between observers in comparison to DWI SI values, particularly for CBV values. As discussed in Chapter 6, CBV is not considered a good predictor of 'tissue at risk' as it exhibits a bimodal behaviour in response to changes in cerebral perfusion pressure and is insensitive to bolus delay and dispersion[37,150],

possible explanations for why CBV appears to be most prone to small measurement differences. CBF and MTT values are the most likely PWI measures for predicting 'tissue at risk' as discussed in Chapter 6. However, the wide 95% limits of agreement of CBF and MTT values between Observer A and B for 'contralateral normal' tissue, where one would expect little observer variability, suggest that any threshold for predicting infarction from these parameters would likely be unreliable.

The 95% limits of agreement are much narrower for DWI SI values than any other measured MR parameters; which may be explained in part by the tissue being classified according to DWI appearance. However, this would not explain why the 95% limits of agreement for DWI SI values are also much narrower than for other MR parameters in 'contralateral normal' tissue, where one would expect little variability between observers, particularly as there was no significant volume difference between observers, and as most of the 'normal' tissue was automatically classified using the 'fill' function in the SGAT program. This suggests that even very small measurement differences cause large degrees of variability in measured T_2W SI, ADC, CBF, CBV, and MTT values; indicating these values are probably unsuitable for use as thresholds to predict infarction. These differences cannot be explained by the differences in the mean and range of the parameter values – DWI SI values have the least degree of difference between observers when expressed as a proportion of the actual parameter values (i.e. when adjusted for the differences in mean values for each parameter). DWI SI values appear robust between observers across tissue classifications, however, this may mean that it is less sensitive to more subtle degrees of ischaemic abnormality.

The analysis of observer variation in tissue classification using the SGAT analysis program was performed in a large sample of patients with a wide range of severity of stroke and clinical features, and thus is representative of the general population of stroke patients for which attempts at designing thresholds for predicting infarction are aimed. Although only comparing two observers, it is likely that including more observers in this analysis would only increase the degree of variability of measured MR parameters. Furthermore, although only one slice through the centre of the visible lesion on DWI (likely the 'core' of more severely ischaemic tissue) was analysed for each patient – MR parameters are almost surely more variable throughout the entire lesion (including peripheral lesion regions that are likely to be less severely affected).

Use of grid-based analysis methods in ischaemic stroke

The 'DWI/PWI mismatch' model discussed in Chapters 2 and 6 purports that the initial DWI lesion represents the 'core' of irreversibly damaged tissue. However, the manual grid-based analysis indicated that tissue that appears 'possibly abnormal' on baseline DWI might have the potential for recovery depending on how quickly blood flow is restored. Furthermore, the results of the manual grid-based analysis suggests that the severity of the abnormality ('brightness') on baseline DWI relates to the underlying severity of tissue damage as assessed by ADC abnormality. The small sample size limited the ability to generalise these results; analysis of a larger sample of patients was required. The manual grid-based analysis method is time consuming and has potential for considerable observer error, so a novel grid analysis program was developed.

The SGAT program provides a faster method of grid-based analysis, allowing for analysis of a larger sample of patients, and is less prone to observer error. The faster speed of grid-based tissue classification and DWI and PWI parameter extraction allowed for analysis of a large group of patients with a wide variety of demographic details and stroke severities. Analysis using the SGAT program in the future could likely be made even faster, e.g. with the addition of an option to define larger numbers of grid boxes at one time, and could be used for analysis of different diseases.

The analysis of the effect of observer differences affirmed the importance of observer experience, and the great variability in ADC and PWI values suggests that using these values to predict 'tissue at risk' of infarction accurately is unlikely.

Chapter 10 will discuss the evolution of DWI and PWI parameters in ischaemic stroke lesions using the SGAT grid analysis program.

10. Grid-based analysis of ischaemic lesion evolution on DWI and PWI

Introduction

This chapter investigates the evolution of DWI and PWI parameters in ischaemic lesions in a large group of patients, including whether differences in lesion appearance on baseline DWI are associated with differences in underlying DWI and PWI parameter values using the grid-based analysis method as developed and tested in Chapter 9. Differences in DWI and PWI parameter values at baseline and over time between patients whose lesions grow, stay the same size, or shrink between baseline and final imaging are also assessed.

Using SGAT to assess lesion evolution and growth

Heterogeneity of DWI and PWI parameters in ischaemic lesions has not been widely assessed. Using the manual grid-based analysis in Chapter 8, important differences in blood flow and ADC values (indicating differences in underlying damage) were identified between regions of differing degrees of appearance ('brightness') on DWI. Analysis of a larger sample of patients was required, but was not feasible with the manual grid analysis method. The development of the SGAT grid analysis program (Chapter 9) allowed for faster grid-based analysis that is less prone to observer error. The SGAT program was used to study the evolution of DWI and PWI parameters in the lesions of a large group of ischaemic stroke patients. Patients were then classified as to whether their lesions grew, stayed the same size, or shrank between baseline

and final imaging, and DWI and PWI parameters were compared to assess if lesion growth was associated with differences in underlying ADC, CBF, and MTT values.

Lesion evolution analysis methods

Patients with imaging at baseline (< 24 hours after stroke onset) and at 30 and/or 90 days after stroke onset were chosen for analysis from the larger patient cohort as described in Chapter 4. SGAT grid-scoring (as described in Chapter 9) was performed by a neuroradiologist (JMW), blind to clinical and other imaging details. The grid box classifications ('definitely abnormal', 'possibly abnormal', 'ipsilateral normal', and 'contralateral normal' as defined in Chapter 8) from the baseline scan were applied to the subsequent coregistered scans, and ADC, CBF, and MTT values for each grid box and mean values for each tissue classification at each scan time were extracted. ADC, CBF, and MTT values were also calculated for all 'abnormal' tissue, calculated as the weighted mean of the 'definitely abnormal' and 'possibly abnormal' tissue, for comparison with other data. Relative values for each parameter (ADCr, CBFr, and MTTr) were calculated as previously described.

Statistical analyses

General patient demographic data were obtained and compared as previously described (Chapter 4).

Mean (± SD) ADCr, CBFr, and MTTr values are reported and compared. Baseline ADCr, CBFr, and MTTr values were compared to normal (test value = 1, as they are relative values) using standard t-tests. Baseline ADCr, CBFr, and MTTr in 'definitely abnormal' and 'possibly abnormal' tissues were compared using standard paired t-tests to determine if differences in baseline DWI appearance were indicative of the degree of underlying initial ADC, CBF, and MTT abnormalities. ADCr at 30

and 90 days after stroke onset in 'definitely abnormal' and 'possibly abnormal' tissues were also compared using standard paired t-tests to determine if differences in baseline DWI appearance were indicative of the degree of underlying ADC abnormality at outcome. Changes in ADCr, CBFr, and MTTr values over time (from baseline to 30 days after stroke onset) were analysed using GLM repeated measures regression analysis (dependent variables = ADCr, CBFr, and MTTr values; ADCr and MTTr fit to a linear model, CBFr fit to a quadratic model). The data from 90 days after stroke onset was not included in the GLM repeated measures regression analysis as there were small numbers of patients with MRI data at this last MR scanning time point.

Lesion growth analysis methods

The patients included in the lesion evolution analysis were classified by a neuroradiologist (JMW) as to whether their lesions appeared to grow, stay the same size, or shrink between baseline DWI and final (30 or 90 days after stroke onset) T_2WI, blind to clinical and other imaging details. These classifications were made based on a knowledge of patterns of lesion extent and anatomical boundaries to account for possible tissue distortion due to tissue swelling that may have biased the determination of lesion growth[205]. Differences in mean ADCr, CBFr, and MTTr values for each tissue classification at each scan time between each lesion type (grow, stay the same size, or shrink between baseline DWI and final T_2WI) were assessed.

Statistical analyses

Clinical details of the patients whose lesions grew, stayed the same size, or shrank were compared: age and time from stroke onset to baseline and subsequent MRI with

a one way analysis of variance (ANOVA); baseline NIHSS with a Kruskal-Wallis test; and sex, OCSP classifications, and whether the patients were dead or dependent (mRS = 3 - 6) at 90 days after stroke onset or not with Chi-Square (χ^2) tests.

Baseline ADCr, CBFr, and MTTr values were compared between patients whose lesions grew, stayed the same size, or shrank between baseline DWI and final T_2WI with an ANOVA. The evolution of ADCr, CBFr, and MTTr values over time (from baseline to 30 days after stroke onset) between patients whose lesions grew, stayed the same size, and shrank were compared with GLM repeated measures regression analysis (dependent variables = ADCr, CBFr, and MTTr; between subjects factor = whether the patient's lesion grew, stayed the same size, or shrank between baseline DWI and final T_2WI; ADCr and MTTr fit to a linear model, CBFr fit to a quadratic model). Peak CBFr and nadir MTTr values and their timing, and areas under the curves[200] of ADCr, CBFr, and MTTr values from baseline to 30 days after stroke onset for each lesion type were also calculated and compared between patients whose lesions grew, stayed the same size, or shrank with an ANOVA.

Results of lesion evolution analysis

Patient details

Forty-six patients with visible lesions on baseline DWI and imaging at 30 and/or 90 days after stroke onset were included in the present analysis: 28/46 (61%) were male, the mean age was 72 years (range: 37 - 94 years), and the mean NIHSS score on admission was 8 (median 8, range: 0 - 25). OCSP classifications: 12/46 (26%) patients had a TACI, 29/46 (63%) patients had a PACI, 4/46 (9%) patients had a LACI, and 1/46 (2%) patients had a POCI. Mean mRS score at 90 days after stroke

onset was 2 (median 2); 13/46 (28%) patients were dependent (mRS = 3 – 5) and 2/46 (4%) patients were dead (mRS = 6).

General patient scan characteristics

Mean (± SD) time from stroke onset to baseline imaging was 10 ± 7 hours, with 18/46 (39%) patients imaged within 6 hours, 12/46 (26%) patients between 6 and 12 hours, and 16/46 (35%) patients between 12 and 24 hours after stroke onset. The 5 day scans were performed at a mean of 5 ± 1 days, the 14 day scans at a mean of 12 ± 2 days, the 30 day scans at a mean of 31 ± 3 days, and the 90 day scans at a mean of 96 ± 7 days after stroke onset (Table 10.1). The number of patients with scans at each time point, and whether PWI was performed, are listed in Table 10.1. Note, 2/46 (4%) patients did not have any tissue that was scored as 'definitely abnormal'.

Table 10.1 Mean (± SD) scan times, number of patients (n), and mean (± SD) ADCr, CBFr, and MTTr values at each scan time for all tissue classifications for all patients analysed with the SGAT grid analysis program. Tissue classifications were scored according to baseline DWI appearance, which were applied to subsequent coregistered scans.

Scan time	Tissue Classification	n DWI	ADCr	n PWI	CBFr	MTTr
10 ± 7 h	Definitely abnormal	46	0.743 ± 0.248	46	0.776 ± 0.353	1.415 ± 0.502
	Possibly abnormal		0.874 ± 0.153		0.901 ± 0.257	1.324 ± 0.331
	Ipsilateral normal		1.006 ± 0.048		0.995 ± 0.094	1.096 ± 0.125
5 ± 1 d	Definitely abnormal	43	0.779 ± 0.204	42	1.143 ± 0.460	1.078 ± 0.285
	Possibly abnormal		0.835 ± 0.207		1.079 ± 0.307	1.076 ± 0.212
	Ipsilateral normal		0.968 ± 0.082		0.978 ± 0.106	1.057 ± 0.132
12 ± 2 d	Definitely abnormal	41	1.089 ± 0.302	41	1.277 ± 0.486	1.026 ± 0.111
	Possibly abnormal		1.007 ± 0.204		1.076 ± 0.282	1.041 ± 0.114
	Ipsilateral normal		1.000 ± 0.076		0.962 ± 0.099	1.030 ± 0.076
31 ± 3 d	Definitely abnormal	43	1.367 ± 0.371	42	0.873 ± 0.233	1.057 ± 0.151
	Possibly abnormal		1.150 ± 0.202		0.896 ± 0.204	1.067 ± 0.121
	Ipsilateral normal		1.029 ± 0.059		0.950 ± 0.069	1.036 ± 0.073
96 ± 7 d	Definitely abnormal	40	1.681 ± 0.416	23	0.756 ± 0.240	1.087 ± 0.180
	Possibly abnormal		1.358 ± 0.245		0.813 ± 0.186	1.066 ± 0.117
	Ipsilateral normal		1.092 ± 0.107		0.947 ± 0.110	1.027 ± 0.056

MRI characteristics of SGAT grid analysis

Table 10.1 lists and Figure 10.1 shows graphs of the mean (± SD) ADCr, CBFr, and MTTr values for each tissue classification (scored according to baseline DWI appearance and applied to subsequent coregistered scans) from baseline to 90 days after stroke onset.

The baseline ADC in both 'definitely abnormal' and 'possibly abnormal' tissue was significantly decreased relative to normal ('definitely abnormal' ADCr = 0.743 ± 0.248, 'possibly abnormal' ADCr = 0.874 ± 0.153, t-tests both $p < 0.01$; Table 10.1). ADC was significantly more decreased relative to normal in 'definitely abnormal' tissue compared to 'possibly abnormal' tissue (paired t-test $p < 0.01$; Figure 10.1). The ADC in both 'definitely abnormal' and 'possibly abnormal' tissue significantly increased over time (GLM regression both $p < 0.01$), becoming increased relative to normal at ≥ 14 days after stroke onset after appearing to reach a nadir at baseline for 'definitely abnormal' tissue and at approximately 5 days after stroke onset for 'possibly abnormal' tissue (Figure 10.1). The decrease in ADC in 'possibly abnormal' tissue between baseline and 5 days after stroke onset indicates that at least some 'possibly abnormal' tissue became more abnormal in the first 5 days after stroke onset.

In tissue classified as 'ipsilateral normal', baseline ADC was not significantly different from normal (t-test p = NS), but did increase significantly over time despite a slight decrease at 5 days after stroke onset (GLM regression $p < 0.01$; Figure 10.1). The decrease in ADC in 'ipsilateral normal' tissue in the first 5 days after stroke onset could indicate the recruitment of initially normal tissue into the infarct.

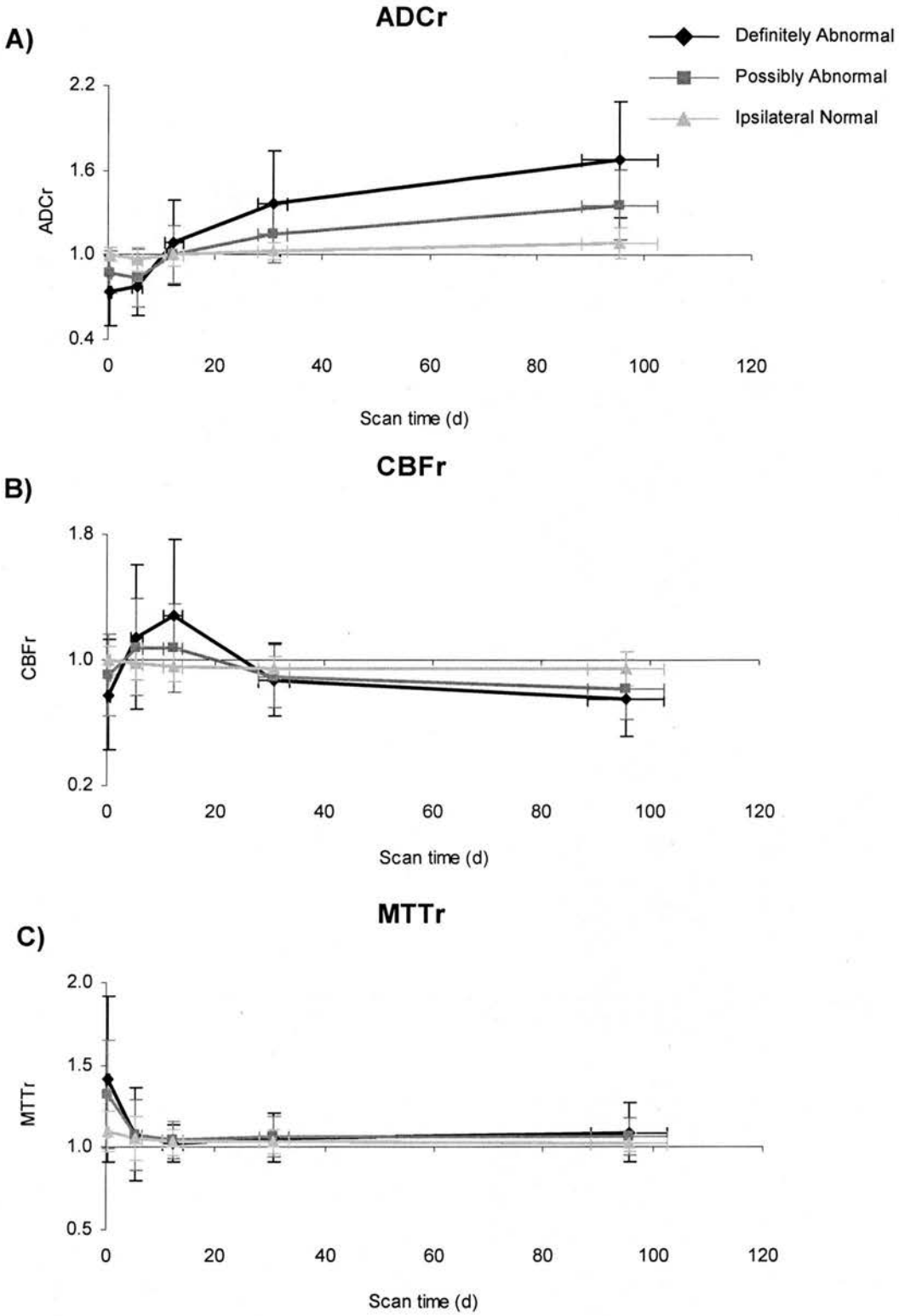

Figure 10.1 Mean A) ADCr, B) CBFr, and C) MTTr values for all tissue classifications for all patients analysed with the SGAT grid analysis program. See Table 10.1 for patient numbers at each scan time. Tissue classifications were scored according to baseline DWI appearance, which were applied to subsequent coregistered scans. Error bars represent ± 1 SD of the mean.

ADC was significantly more increased relative to normal in 'definitely abnormal' tissue compared with 'possibly abnormal' tissue at both 30 days after stroke onset ('definitely abnormal' ADCr = 1.367 ± 0.371 vs. 'possibly abnormal' ADCr = 1.150 ± 0.202, paired t-test $p < 0.01$; Table 10.1) and 90 days after stroke onset ('definitely abnormal' ADCr = 1.681 ± 0.416 vs. 'possibly abnormal' ADCr = 1.358 ± 0.245, paired t-test $p < 0.01$; Table 10.1), indicating that tissue that is more abnormal ('brighter') on baseline DWI is more severely damaged than tissue that appears less abnormal on baseline DWI.

CBF was significantly decreased at baseline in both 'definitely abnormal' and 'possibly abnormal' tissue ('definitely abnormal' CBFr = 0.776 ± 0.353, 'possibly abnormal' CBFr = 0.901 ± 0.257, t-test both $p \leq 0.01$; Table 10.1). Baseline CBF was significantly more decreased relative to normal in 'definitely abnormal' tissue compared to 'possibly abnormal' tissue (paired t-test $p < 0.01$; Figure 10.1). CBF changed significantly over time (GLM regression both $p < 0.01$); CBF in both 'definitely abnormal' and 'possibly abnormal' tissue increased from a below-normal to an above-normal level, peaking at approximately 5 days after stroke onset for 'possibly abnormal' tissue and 14 days after stroke onset for 'definitely abnormal' tissue, and then subsequently decreased to a below-normal level (Figure 10.1).

In tissue classified as 'ipsilateral normal', baseline CBF was not significantly different from normal (t-test p = NS), but did significantly decrease over time (GLM regression $p < 0.01$; Figure 10.1).

MTT in 'definitely abnormal' (MTTr = 1.415 ± 0.502), 'possibly abnormal' (MTTr = 1.324 ± 0.331), and 'ipsilateral normal' (MTTr = 1.096 ± 0.125) tissue was significantly prolonged relative to normal at baseline (t-tests all $p < 0.01$; Table

10.1). There was no significant difference in MTT at baseline between 'definitely abnormal' and 'possibly abnormal' tissue (paired t-test p = NS). MTT decreased significantly over time in all three tissue classifications (GLM regression all $p < 0.01$; Figure 10.1).

Table 10.2 lists and Figure 10.2 shows graphs of ADCr, CBFr, and MTTr values for 'abnormal' tissue (combined 'definitely abnormal' and 'possibly abnormal' tissue) from baseline to 90 days after stroke onset.

Table 10.2 Mean (± SD) scan times, number of patients (n), and mean (± SD) ADCr, CBFr, and MTTr values at each scan time for 'abnormal' tissue for all patients analysed with the SGAT grid analysis program. Tissue classifications were scored according to baseline DWI appearance, which were applied to subsequent coregistered scans.

Scan time	n DWI	ADCr	n PWI	CBFr	MTTr
10 ± 7 h	46	0.825 ± 0.153	46	0.867 ± 0.283	1.360 ± 0.371
5 ± 1 d	43	0.817 ± 0.201	42	1.093 ± 0.347	1.080 ± 0.235
12 ± 2 d	41	1.013 ± 0.196	41	1.116 ± 0.315	1.039 ± 0.109
31 ± 3 d	43	1.223 ± 0.232	42	0.892 ± 0.205	1.061 ± 0.123
96 ± 7 d	40	1.453 ± 0.280	23	0.789 ± 0.188	1.074 ± 0.130

ADC was significantly decreased in 'abnormal' tissue at baseline (ADCr = 0.825 ± 0.153, t-test $p < 0.01$; Table 10.2), appeared to reach a nadir at approximately 5 days after stroke onset, and significantly increased over time (GLM regression $p < 0.01$; Figure 10.2).

CBF was significantly decreased in 'abnormal' tissue at baseline (CBFr = 0.867 ± 0.283, t-test $p < 0.01$; Table 10.2), and changed significantly over time (GLM regression $p < 0.01$), increasing from a below-normal level to an above-normal peak at approximately 14 days after stroke onset and then decreasing (Figure 10.2).

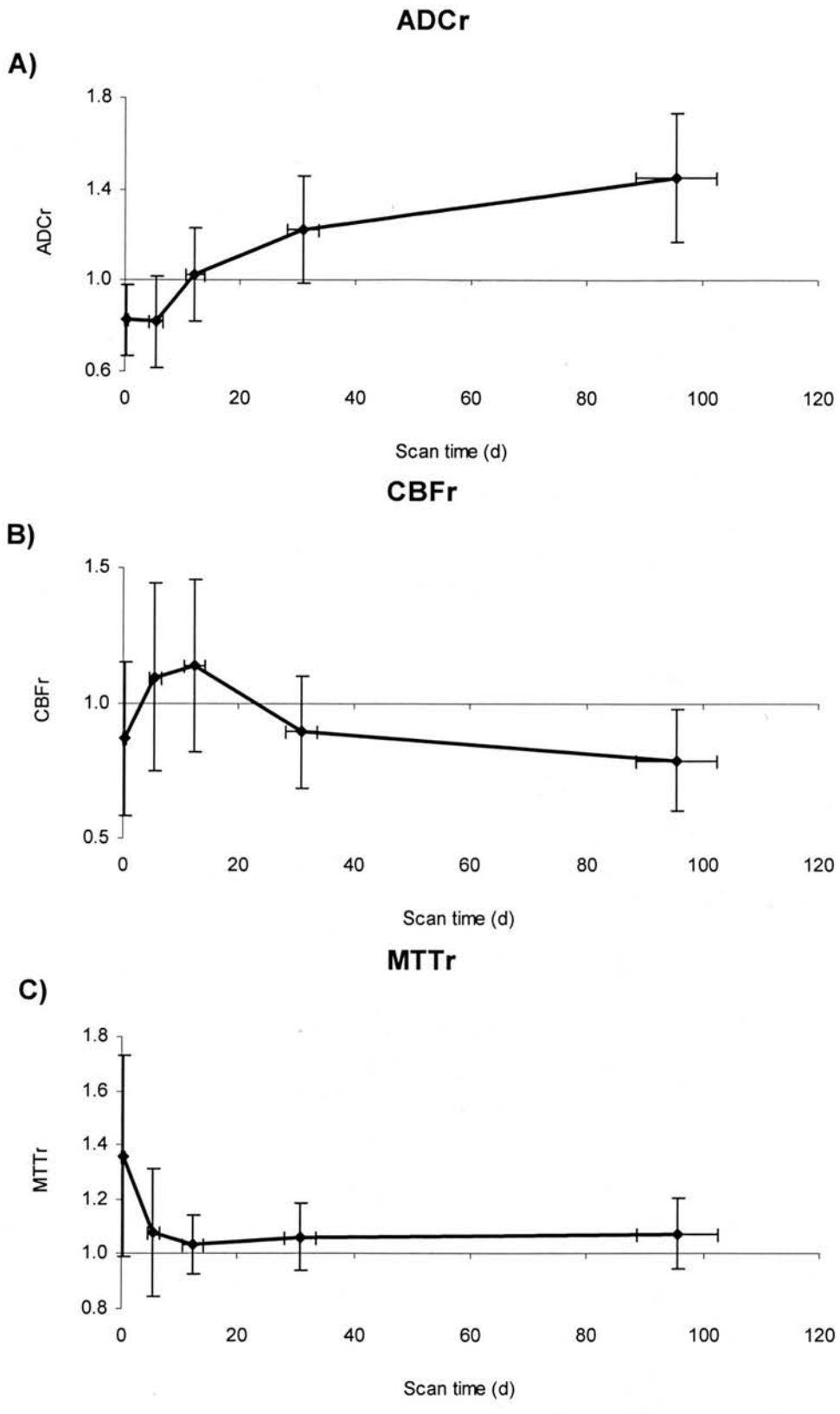

Figure 10.2 Mean A) ADCr, B) CBFr, and C) MTTr values for 'abnormal' (combined 'definitely abnormal' and 'possibly abnormal') tissue for all patients analysed with the SGAT grid analysis program. See Table 10.1 for patient numbers at each scan time. Tissue classifications were scored according to baseline DWI appearance, which were applied to subsequent coregistered scans. Error bars represent ± 1 SD of the mean.

MTT in 'abnormal tissue' was significantly prolonged relative to normal at baseline (MTTr = 1.360 ± 0.371, t-test $p < 0.01$; Table 10.2), and decreased significantly over time (GLM regression $p < 0.01$), reaching a nadir at approximately 14 days after stroke onset (Figure 10.2).

Results of lesion growth analysis

Patient details

Overall patient demographics and clinical details are described earlier in the chapter. There were no significant differences in the baseline NIHSS or OCSP classifications between patients whose lesions grew, stayed the same size, or shrank between baseline DWI and final T_2WI. However, patients whose lesions grew between baseline DWI and final T_2WI were significantly older than patients whose lesions shrank between baseline DWI and final T_2WI (mean age 77 years vs. 64 years, ANOVA $p = 0.01$). There were also significantly more females with lesions that shrank between baseline DWI and final T_2WI than expected (observed 9 vs. expected 5, χ^2 test $p = 0.04$). Patients whose lesions grew between baseline DWI and final T_2WI were more likely to be dead or dependent (mRS = 3 - 6) at 90 days after stroke onset (observed 9 vs. expected 5, χ^2 test $p = 0.02$) than patients whose lesions stayed the same size or shrank between baseline DWI and final T_2WI.

General patient scan characteristics

Overall patient scan characteristics are described earlier in the chapter. Mean (± SD) times from stroke onset to each scan, and the number of patients with DWI and PWI data at each scanning time point for each lesion type are listed in Table 10.3. There were no significant differences in the time from stroke onset to baseline or

subsequent MRI between patients whose lesions grew, stayed the same size, or shrank between baseline DWI and final T_2WI (ANOVA all p = NS).

Table 10.3 lists and Figure 10.3 shows graphs of the mean (± SD) ADCr, CBFr, and MTTr values for 'abnormal' and 'ipsilateral normal' tissue (scored according to baseline DWI appearance and applied to subsequent coregistered scans) for each lesion type from baseline to 90 days after stroke onset.

MR characteristics of 'abnormal' tissue and lesion growth

Baseline ADCr in 'abnormal' tissue was not significantly different between lesions that grew, stayed the same size, or shrank between baseline and final scans (ANOVA p = NS; Table 10.3). There were significant differences in the evolution of ADC in 'abnormal' tissue between the groups: in lesions that either grew or stayed the same size, ADC decreased to a nadir at approximately 5 days after stroke onset, and then subsequently increased, whereas in patients whose lesions shrank, ADC was lowest at baseline and increased more quickly (GLM regression $p < 0.02$; Figure 10.3).

Although baseline CBFr in 'abnormal' tissue appeared lower relative to normal in patients whose lesions grew compared with patients whose lesions either stayed the same size or shrank ('grow' CBFr = 0.739 ± 0.219, 'stay' CBFr = 0.940 ± 0.330, 'shrink' CBFr = 0.929 ± 0.247; Table 10.3), there were no significant differences between the groups (ANOVA p = NS).

Table 10.3 Mean (± SD) scan times, number of patients (n), and mean (± SD) DWIr, ADCr, CBFr, and MTTr values for 'abnormal' (combined 'possibly abnormal' and 'definitely abnormal') and 'ipsilateral normal' tissue at each scan time for each lesion type in the SGAT grid analysis. Tissue classifications were scored according to baseline DWI appearance, which were applied to subsequent coregistered scans.

Scan time	Lesion type	n DWI	ADCr		n PWI	CBFr		MTTr	
			Abnormal	Ipsilateral normal		Abnormal	Ipsilateral normal	Abnormal	Ipsilateral normal
10 ± 5 h	Grow	16	0.787 ± 0.136	1.014 ± 0.058	16	0.739 ± 0.219	0.955 ± 0.085	1.460 ± 0.346	1.103 ± 0.129
12 ± 8 h	Stay	17	0.809 ± 0.152	0.993 ± 0.043	17	0.940 ± 0.330	1.012 ± 0.092	1.307 ± 0.335	1.120 ± 0.153
9 ± 7 h	Shrink	13	0.892 ± 0.164	1.013 ± 0.041	13	0.929 ± 0.247	1.020 ± 0.097	1.306 ± 0.445	1.054 ± 0.058
5 ± 1 d	Grow	15	0.742 ± 0.197	0.936 ± 0.124	15	0.940 ± 0.327	0.932 ± 0.149	1.143 ± 0.227	1.099 ± 0.194
5 ± 1 d	Stay	17	0.796 ± 0.168	0.977 ± 0.042	16	1.145 ± 0.342	1.145 ± 0.342	1.052 ± 0.300	1.026 ± 0.093
5 ± 1 d	Shrink	11	0.953 ± 0.200	0.997 ± 0.039	11	1.225 ± 0.333	1.002 ± 0.065	1.036 ± 0.103	1.045 ± 0.037
12 ± 2 d	Grow	13	0.932 ± 0.206	0.983 ± 0.125	13	1.049 ± 0.359	0.916 ± 0.135	1.066 ± 0.097	1.035 ± 0.108
12 ± 2 d	Stay	17	0.982 ± 0.188	1.004 ± 0.041	17	1.101 ± 0.244	1.101 ± 0.244	1.028 ± 0.120	1.025 ± 0.063
13 ± 2 d	Shrink	11	1.159 ± 0.117	1.012 ± 0.030	11	1.220 ± 0.359	0.980 ± 0.085	1.026 ± 0.109	1.033 ± 0.054
31 ± 3 d	Grow	14	1.239 ± 0.352	1.027 ± 0.078	13	0.811 ± 0.223	0.897 ± 0.068	1.081 ± 0.181	1.047 ± 0.106
30 ± 2 d	Stay	17	1.207 ± 0.139	1.029 ± 0.057	17	0.886 ± 0.200	0.886 ± 0.200	1.052 ± 0.102	1.033 ± 0.066
31 ± 3 d	Shrink	12	1.229 ± 0.177	1.033 ± 0.035	12	0.989 ± 0.161	0.993 ± 0.042	1.053 ± 0.073	1.028 ± 0.036
95 ± 3 d	Grow	12	1.580 ± 0.361	1.124 ± 0.107	7	0.744 ± 0.273	0.888 ± 0.169	1.055 ± 0.208	1.028 ± 0.065
94 ± 6 d	Stay	16	1.443 ± 0.175	1.066 ± 0.062	12	0.781 ± 0.152	0.781 ± 0.152	1.075 ± 0.087	1.032 ± 0.059
99 ± 10 d	Shrink	12	1.341 ± 0.273	1.096 ± 0.146	4	0.893 ± 0.073	1.009 ± 0.055	1.101 ± 0.088	1.009 ± 0.035

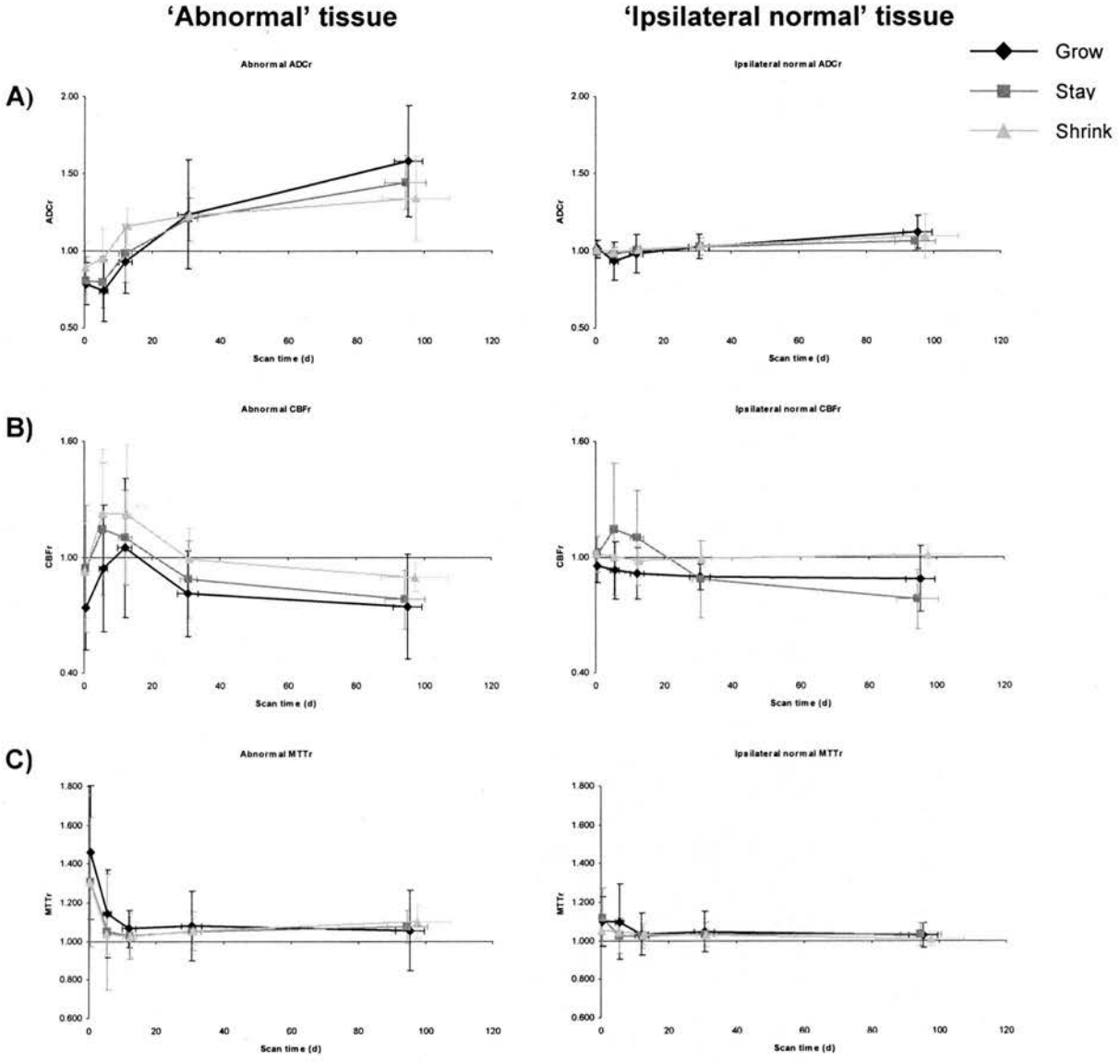

Figure 10.3 Mean A) ADCr, B) CBFr, and C) MTTr values for 'abnormal' tissue (left, combined 'definitely abnormal' and 'possibly abnormal' tissue) and 'ipsilateral normal' tissue (right) by lesion type (grow, stay the same size, or shrink between baseline and final imaging) for all patients in the SGAT grid analysis. See Table 10.3 for patient numbers at each scan time. Tissue classifications were scored according to baseline DWI appearance, which were applied to subsequent coregistered scans. Error bars represent ± 1 SD of the mean.

There were significant differences in the evolution of CBFr in 'abnormal' tissue between lesion types: in patients whose lesions grew, CBFr peaked later and at a lower value than in patients whose lesions stayed the same size or shrank; in patients whose lesions shrank, CBFr peaked earlier and at a higher value, and remained higher relative to normal brain for a longer period of time than in patients whose lesions stayed the same size or grew (GLM regression $p < 0.05$; Figure 10.3).

Despite baseline MTTr in 'abnormal' tissue appearing more prolonged relative to normal in patients whose lesions grew compared to patients whose lesions stayed the same size or shrank ('grow' MTTr = 1.460 ± 0.346, 'stay' MTTr = 1.307 ± 0.335, 'shrink' MTTr = 1.306 ± 0.445; Table 10.3), there were no significant differences between the groups (ANOVA p = NS). There were no differences in the evolution of MTTr in 'abnormal' tissue over time between lesion types (GLM regression p = NS), despite the 'abnormal' tissue MTT of patients whose lesions grew appearing to remain more prolonged relative to normal for a longer period of time (Figure 10.3).

Comparison of the peak CBFr and nadir MTTr values and their timing in 'abnormal' tissue revealed no significant differences between patients whose lesions grew, stayed the same size, or shrank (ANOVA p = NS) despite the apparent differences as discussed above. Comparison of the area under the curve of ADCr and MTTr values for 'abnormal' tissue from baseline to 30 days after stroke onset revealed no significant difference between patients whose lesions grew, stayed the same, or shrank (ANOVA both p = NS; Figure 10.4). However, the area under the curve of CBFr values for 'abnormal' tissue from baseline to 30 days after stroke onset revealed a significant difference between groups: patients whose lesions shrank had

the largest area under the curve, and patients whose lesions grew the smallest area under the curve (ANOVA p = 0.03, Figure 10.4).

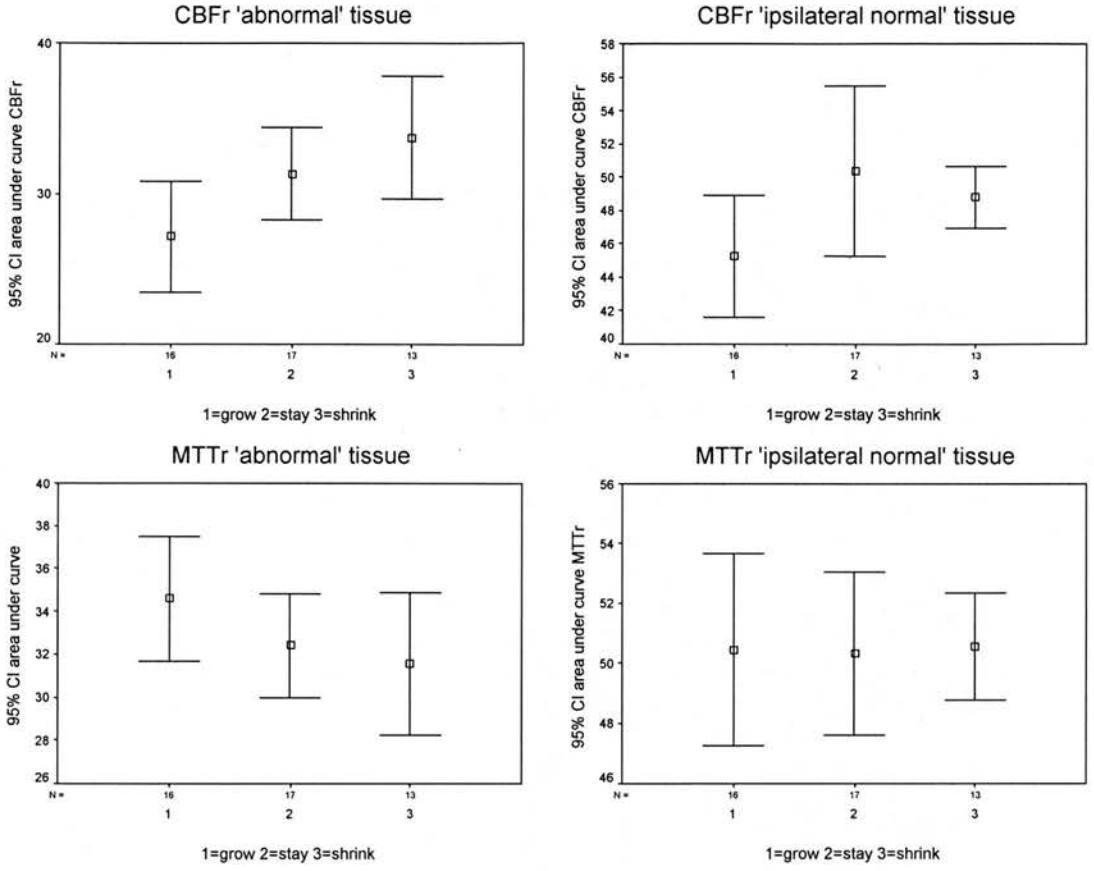

Figure 10.4 95% confidence intervals for the area under the curve of CBFr and MTTr values for 'abnormal' (left) and 'ipsilateral normal' (right) tissue from baseline to 30 days after stroke onset between patients whose lesions grew, stayed the same size, or shrank between baseline DWI and final T_2WI.

MR characteristics of 'ipsilateral normal' tissue and lesion growth

Baseline ADCr in 'ipsilateral normal' tissue was not significantly different between lesion types (ANOVA p = NS; Table 10.3). Despite the apparent fall in ADC in 'ipsilateral normal' tissue in patients whose lesions grew, there were no significant

differences in the evolution of ADCr in 'ipsilateral normal' tissue between lesion types (GLM regression p = NS; Figure 10.3).

Baseline CBFr in 'ipsilateral normal' tissue was not significantly different between lesion types (ANOVA p = NS; Table 10.3). There were significant differences in the evolution of CBFr in 'ipsilateral normal' tissue between lesion types (GLM regression $p < 0.04$): in patients whose lesions grew, CBFr was initially reduced and steadily decreased further over time; in patients whose lesions shrank, CBFr stayed relatively normal; and in patients whose lesions stayed the same size, CBFr appeared to increase until approximately 5 days after stroke onset, then decreased rapidly until approximately 30 days after stroke onset, after which it decreased more slowly (Figure 10.3).

Despite it appearing that baseline MTT in 'ipsilateral normal' tissue in patients whose lesions shrank was more normal than in patients whose lesions stayed the same size or grew, there were no significant differences between the groups (ANOVA p = NS; Table 10.3). There were no significant differences in the evolution of MTTr in 'ipsilateral normal' tissue over time between lesion types (GLM regression p = NS; Figure 10.3). Although not reaching statistical significance (GLM regression p = NS), it appeared that the MTT in 'ipsilateral normal' tissue in patients whose lesions shrank was initially more normal and stayed normal over time, whereas in patients whose lesions stayed the same size or grew, MTT in 'ipsilateral normal' tissue appeared to be prolonged relative to normal initially and subsequently decrease, reaching a nadir more quickly in patients whose lesions stayed the same size than in patients whose lesions grew (approximately 5 days vs. 14 days after stroke onset; Figure 10.3).

The peak CBFr of 'ipsilateral normal' tissue was significantly different between groups (ANOVA $p < 0.01$): peak CBFr was highest in patients whose lesions stayed the same size, and lowest in patients whose lesions grew (Figure 10.3). The timing of the peak CBFr was not significantly different between groups (ANOVA p = NS). Comparison of the nadir MTTr values for 'ipsilateral normal' tissue and their timing for each lesion type revealed no significant differences between patients whose lesions grew, stayed the same size, or shrank (ANOVA p = NS) despite the apparent differences as discussed above. Comparison of the area under the curve of ADCr, CBFr, and MTTr values for 'ipsilateral normal' from baseline to 30 days after stroke onset revealed no significant difference between patients whose lesions grew, stayed the same, or shrank (ANOVA both p = NS; Figure 10.4).

Discussion

The degree of DWI abnormality indicates the severity of underlying damage – 'definitely abnormal' tissue that appears more abnormal ('brighter') on baseline DWI has significantly more decreased ADC values compared to normal at baseline, and significantly more increased ADC values compared to normal at 30 and 90 days after stroke onset, compared to 'possibly abnormal' tissue that appears only moderately abnormal on baseline DWI. As discussed in Chapter 3, animal studies have also found that regions of more severe abnormality ('brighter') on acute DWI were in fact more severely damaged (i.e. higher proportion of dead neurons) compared to regions of less severe abnormality on acute DWI.

However, there are several studies in humans that do not support the link of the severity of abnormality on DWI and the severity of underlying tissue damage. Guadagno et al.[125] found no relation between the severity of DWI abnormality and

permanent tissue damage; however, this was a case study (i.e. n = 1), and DWI regions were defined using a semiautomated contouring method - both problematic issues due to lesion heterogeneity as discussed in Chapter 2. Furthermore, Guadagno et al.[125] do not actually compare DWI appearance to an outcome scan, rather they define 'outcome' tissue damage by applying probabilistic thresholds of *acute* positron emission tomography values. Fiehler et al.[142] report that even severe acute ADC decreases in human ischaemic stroke patients did not predict tissue infarction. However, Fiehler et al.[142] measured tissue 'outcome' at 7 days after stroke onset, when 'fogging' may cause underestimation of lesion extent and lesions are likely still evolving as discussed in Chapter 2. Thus, it is likely that the severity of abnormality as seen on acute DWI does indicate something about the underlying severity of tissue damage.

The severity of abnormality on baseline DWI also relates to the underlying blood flow to the tissue. Tissue appearing abnormal on baseline DWI had significantly decreased CBF, and tissue that appears more abnormal ('brighter') on baseline DWI followed a different pattern of blood flow recovery, seeming to reach a higher peak CBF at a later time after stroke onset, than tissue that appeared only moderately abnormal on baseline DWI. The results of the manual grid analysis (Chapter 8) also indicated that the perfusion changes in the first 5 days after stroke onset might be important in determining tissue fate – perhaps these differences explain why 'definitely abnormal' tissue is significantly more abnormal than 'possibly abnormal' tissue in terms of ADC at outcome.

Tissue appearing abnormal on baseline DWI also had significantly prolonged MTT, however, there did not appear to be any differences between the evolution of MTT in

'definitely abnormal' and 'possibly abnormal' tissue. As previously discussed, MTT abnormalities are generally much larger than DWI and CBF abnormalities (apparent as significantly prolonged baseline MTT in 'ipsilateral normal' tissue), and thus may be insensitive to regional differences in the baseline DWI lesion.

The diffusion and perfusion changes in the 'ipsilateral normal' tissue are of interest. Although not significantly abnormal at baseline, the ADC of 'ipsilateral normal' tissue increases over time, perhaps indicating recruitment of initially normal tissue into the lesion. Although CBF in 'ipsilateral normal' tissue was not significantly abnormal at baseline, there was a significant decrease in CBF in 'ipsilateral normal' tissue over time; perhaps this is also due to recruitment of initially normal tissue into the lesion. MTT was significantly prolonged and decreased over time in 'ipsilateral normal' tissue; baseline MTT lesions have been previously shown to be larger than baseline DWI lesions, so these changes may be indicative of a large initial region of oligaemia (as discussed above) that subsequently recovers.

How do lesion DWI and PWI parameters obtained by analysis of the baseline DWI lesion with the SGAT grid-based program relate to the values obtained by manual outlining of the baseline DWI lesion as described in Chapter 4? The ADCr values for tissue classified as 'abnormal' with the SGAT analysis are very similar to the ADCr values obtained from the manual region of interest analysis in Chapter 4 ('SGAT' ADCr = 0.825 ± 0.153, 'manual region' ADCr = 0.815 ± 0.162; Table 10.2, Table 4.2). The similarity in ADCr values is to be expected as both analysis methods used baseline DWI appearance to classify the abnormal tissue. Interestingly, CBFr values also compare well between the two analysis methods ('SGAT' CBFr = 0.867 ± 0.283, 'manual region' CBFr = 0.865 ± 0.194; Table 10.2, Table 4.2), despite the

SGAT grid analysis using the visible baseline DWI abnormality, and the manual region analysis using the visible baseline CBF abnormality to obtain the CBFr values. There appeared to be a difference in MTTr values between the two methods, with the MTT of 'abnormal' tissue obtained in the SGAT analysis appearing more prolonged than the MTT of the manually outlined baseline MTT abnormality ('SGAT' MTTr = 1.360 ± 0.371, 'manual region' MTTr = 1.170 ± 0.217; Table 10.2, Table 4.2). This difference in MTT values is not surprising, as the SGAT analysis measurements (using the visible baseline DWI abnormality) likely only represent the more severely hypoperfused tissue, whereas the manual region analysis (using the visible baseline MTT abnormality) likely includes a much larger amount of tissue with areas of oligaemia. As discussed in Chapter 6, CBF lesions are generally smaller than MTT lesions, so it is also unsurprising that the CBF values appear to correlate better between the two analysis methods than the MTT values.

How do these diffusion and perfusion changes relate to lesion growth between baseline and final imaging?

Patients whose lesions grew between baseline DWI and final T_2WI were older than patients whose lesions shrank, agreeing with the pilot results of Chapter 8, where age seemed to relate to whether 'possibly abnormal' tissue behaved more like 'normal' or 'definitely abnormal' tissue. Lesion growth was also related to clinical outcome; patients whose lesions grew were more likely to be dead or dependent (mRS = 3 – 6) at 90 days after stroke onset than patients whose lesions stayed the same size or shrank.

There are important differences in early diffusion and perfusion changes that may influence lesion growth. In patients whose lesions shrank, ADC appeared to have

already reached a nadir at baseline, whereas in patients whose lesions stayed the same size or grew, ADC did not reach a nadir until approximately 5 days after stroke onset. Furthermore, ADC increased more rapidly in patients whose lesions shrank compared to patients whose lesions stayed the same size or grew. CBF in patients whose lesions shrank appeared to be less abnormal initially, to increase more rapidly within the first 5 days after stroke onset, and to remain increased for a longer period of time ('prolonged hyperaemia') than in patients whose lesions grew. Patients whose lesion stayed the same size appeared to have rapid increase of CBF within 5 days of stroke onset, but this increase did not seem to last as long as in patients whose lesions shrank. Significant differences in the area under the curve of CBFr values from baseline to 30 days also confirmed that there were important differences in blood flow that were related to lesion growth – patients whose lesions shrank had much better blood flow to the lesion compared to patients whose lesions grew. There were no significant differences in MTT between patients, although it appeared that MTT in both patients whose lesions stayed the same size or shrank between baseline and final T_2WI appeared to be less prolonged initially, and more rapidly returned to normal within approximately 5 days of stroke onset compared to patients whose lesions grew. As discussed earlier in the chapter, MTT is likely to be less sensitive to differences between patients as decreases in MTT tend to be generalised in the hemisphere ipsilateral to the ischaemic lesion.

When examining patients whose lesions grow or shrink between baseline DWI and final T_2WI, the behaviour of the diffusion and perfusion parameters in the 'ipsilateral normal' tissue are of interest. Some tissue that is initially 'ipsilateral normal' in patients whose lesions grow could be expected to become 'abnormal'; indeed it

appears that the CBF in the 'ipsilateral normal' is initially decreased, and becomes more decreased relative to normal over time, and that the MTT remains prolonged relative to normal for a longer period of time in patients whose lesions grow compared with patients whose lesions stay the same size or shrink. Furthermore, there are clear significant differences in CBF in the 'ipsilateral normal' tissue - in patients whose lesions stayed the same size, CBF increases within the first 5 – 10 days after stroke onset, perhaps indicating the presence of 'tissue at risk' that was 'salvaged' due to this early increase in CBF.

It is important to note that, although one of the largest serial studies of DWI and PWI in ischaemic stroke patients, the number of patients whose lesions grew (n = 16), stayed the same size (n = 17) and shrank (n = 13) between baseline DWI and final T_2WI are small. Furthermore, the commonly used conventional statistical models for analysis of serial data, such as GLM repeated measures regression analysis, impose limitations for analysis of DWI and PWI data as the models requires fitting to a particular line shape. However, the evolution of DWI and PWI parameters are complex and variable - attempting to find significant differences in these parameters using the existing analysis methods is not ideal and likely overlooks important differences between groups of patients. The analysis of 'summary measures' such as peak CBFr and area under the curve values[200] as discussed in Chapter 7 may be more appropriate, however the comparison of these measures in the current analysis did not reveal any more differences between the patient groups than the GLM repeated measures regression analysis.

In the current analysis we analysed changes from baseline until 30 days after stroke onset although there were data from 90 days after stroke onset. Using 90 days after

stroke onset as an 'outcome' measure is ideal, however, there were much fewer MRI data at this late time point, and data from 90 days after stroke onset may be biased - patients with more severe strokes may have died and patients making a good recovery may have been unwilling to return for imaging. With use of a larger sample size, and perhaps the future development of more appropriate statistical models, further differences in DWI and PWI parameters in this analysis (and other analyses in this thesis) would likely be found.

11. Tissue distortion caused by swelling after ischaemic stroke

Introduction

This chapter investigates both general and localised tissue distortion due to swelling and tissue cavitation after ischaemic stroke. A novel swelling analysis tool is developed and tested to quantify tissue distortion at key stages after the onset of ischaemic stroke.

The effects of swelling in ischaemic stroke

In the acute stages of ischaemic stroke, the failure of cellular ion pumps causes cytotoxic oedema, or the influx of water from the extracellular space into the intracellular space[3,9]. In later stages after stroke onset, failure of the cellular membrane causes vasogenic oedema, or the leakage of plasma constituents into the extracellular space[9]. Brain tissue may be distorted by oedema, for instance cytotoxic oedema can cause swelling, and cell death and loss of tissue can result in tissue cavitation. As discussed in Chapter 2, swelling may cause overestimation of the volume of the ischaemic lesion, which might be misconstrued as incorporation of new tissue into the lesion (i.e. 'lesion growth'), and tissue cavitation could cause underestimation of lesion extent in the later stages of ischaemic stroke.

During the analyses in this thesis, we noted a considerable number of patients had visible tissue distortion caused by swelling in the acute phase and subsequent tissue cavitation in the late phase of ischaemic stroke. Assessment of this tissue distortion is important because an increase in lesion extent in the acute phase of ischaemic stroke

could represent either a true increase in lesion extent, or could be due to swelling of the affected tissue. Any attempt to measure the effectiveness of a new therapy for ischaemic stroke patients (e.g. measuring the effect of rtPA on lesion growth) that does not recognise these two distinct possibilities could cause biased estimates of the effectiveness of the therapy.

There are a handful of non-linear image registration algorithms that may correct for generalised tissue distortion[206]. We explored a number of non-rigid image registration algorithms said to account for local tissue distortion in the initial planning stages of this stroke study which led to funding for the study from the Chief Scientist Office. None of these algorithms were found to be suitable for distinguishing between a true increase in lesion extent, and an apparent increase in lesion extent due to swelling. Furthermore, only one infarct coding system has ever been described that deliberately distinguishes between a true increase in infarct extent and an increase in lesion extent due to tissue swelling[205], something which simple lesion volume measurement alone can never do. Animal and human studies have largely failed to recognise this important distinction, let alone address it (Chapters 2 and 3). Therefore, we aimed to quantify tissue distortion in a small sample of patients as an exploratory assessment to illustrate the effects of swelling and subsequent tissue cavitation at key stages after the onset of ischaemic stroke. A longer term aim was to obtain information to enable development of better image processing algorithms and lesion measurement methods that could account for local tissue distortion after ischaemic stroke.

To do this, the grid-based analyses as described in Chapters 8 and 9 were used to assess the effects of tissue distortion due to lesion swelling. Firstly, we used the

manual grid-based analysis method to assess the general effect of tissue distortion due to acute swelling and subsequent tissue cavitation by measuring the total volume of brain tissue (excluding CSF-containing spaces) in the hemisphere ipsilateral to the ischaemic lesion from baseline to 30 days after stroke onset. We then investigated the effect of local tissue distortion within the affected hemisphere by investigating the movement of 59 anatomical landmarks in and around the ischaemic lesion in one exemplar between baseline and 4 days after stroke onset.

We then used this information to justify the development of a tool to measure tissue distortion using the SGAT grid-based analysis method (as described in Chapters 9 and 10). We then tested this faster method of measuring tissue distortion in a group of 10 representative patients.

Assessing swelling with manual grid analysis

Methods

We assessed the general effects of swelling in the 8 patients analysed with the manual grid analysis method (Chapter 8), who had a representative range of lesion morphology and appearance on baseline DWI. For each patient, the axial slice that passed through the centre of the visible ischaemic lesion on baseline DWI was chosen for analysis.

Ipsilateral hemisphere volume measurement

The volume of brain tissue of the hemisphere ipsilateral to the ischaemic lesion on the chosen brain slice was identified by marking each grid box that fell on brain

tissue (excluding CSF-containing spaces) in the affected hemisphere on the baseline scan and each subsequent coregistered scan from 5, 14, and 30 days after stroke onset. The volume of the affected hemisphere for the chosen slice for each patient at each time point was calculated and compared to assess the effects of tissue distortion at key stages in the ischaemic process.

Statistical analyses

General patient demographic data were obtained and compared as previously described (Chapter 4).

The volume of the hemisphere ipsilateral to the ischaemic lesion for the chosen slice for each patient was calculated by summing the number of grid boxes classified as brain tissue (i.e. were classified as 'definitely abnormal', 'possibly abnormal', or 'ipsilateral normal' as described in Chapter 8) at each time point and multiplying by the volume of each grid box (109.86 mm^3). The volumes were normally-distributed (Kolmogorov-Smirnov test p = NS) so mean (± SD) volumes are reported and compared. GLM repeated measures regression analysis was performed to assess the change in the volume of brain tissue of the hemisphere ipsilateral to the ischaemic lesion over time (from baseline to 30 days after stroke onset, dependent variable = volume of hemisphere ipsilateral to ischaemic lesion; fit to a linear model).

Results

Patient details

General patient demographic data, scanning details, and MR characteristics for the patients in the current analysis have been reported previously in Chapter 8 (Table 8.1, Table 8.2, Figure 8.3, Figure 8.4).

Changes in ipsilateral hemisphere volume

Table 11.1 lists, and Figure 11.1 shows a graph of the volume of the hemisphere ipsilateral to the lesion, from baseline to 30 days after stroke onset. Mean (± SD) baseline ipsilateral hemisphere volume was 661926.3 ± 114220.5 mm^3 (Table 11.1). The volume of the ipsilateral hemisphere significantly increased over time (GLM regression, $p < 0.01$; Figure 11.1). Only 1/8 (12.5%) patient (Patient F) did not have an increase in the volume of the hemisphere ipsilateral to their ischaemic lesion (Table 11.1). The only apparent significant difference between Patient F and the rest of the patient group is that Patient F is the only female in the group (Table 8.1).

Table 11.1 Volume (mm^3) of the hemisphere ipsilateral to the ischaemic lesion (and % of baseline volume) at each scan time (mean ± SD) for the patients analysed with the manual grid-based analysis method (n = 8).

Patient	Scan time						
	6 ± 4 h	6 ± 1 d		12 ± 2 d		30 ± 2 d	
	Volume (mm^3)	Volume (mm^3)	% of baseline	Volume (mm^3)	% of baseline	Volume (mm^3)	% of baseline
A	585022.0	903625.5	154%	782775.9	134%	700378.4	120%
B	664672.9	694885.3	105%	681152.3	102%	711364.7	107%
C	832214.4	892639.2	107%	876159.7	105%	851440.4	102%
D	475158.7	639953.6	135%	560302.7	118%	585022.0	123%
E	637207.0	758056.6	119%	705871.6	111%	722351.1	113%
F	793762.2	780029.3	98%	763549.8	96%	766296.4	97%
G	694885.3	766296.4	110%	785522.5	113%	771789.6	111%
H	612487.8	648193.4	106%	661926.3	108%		
Mean	661926.3	760459.9	117%	727157.6	111%	729806.1	110%
SD	114220.5	99868.6		96133.2		81765.1	

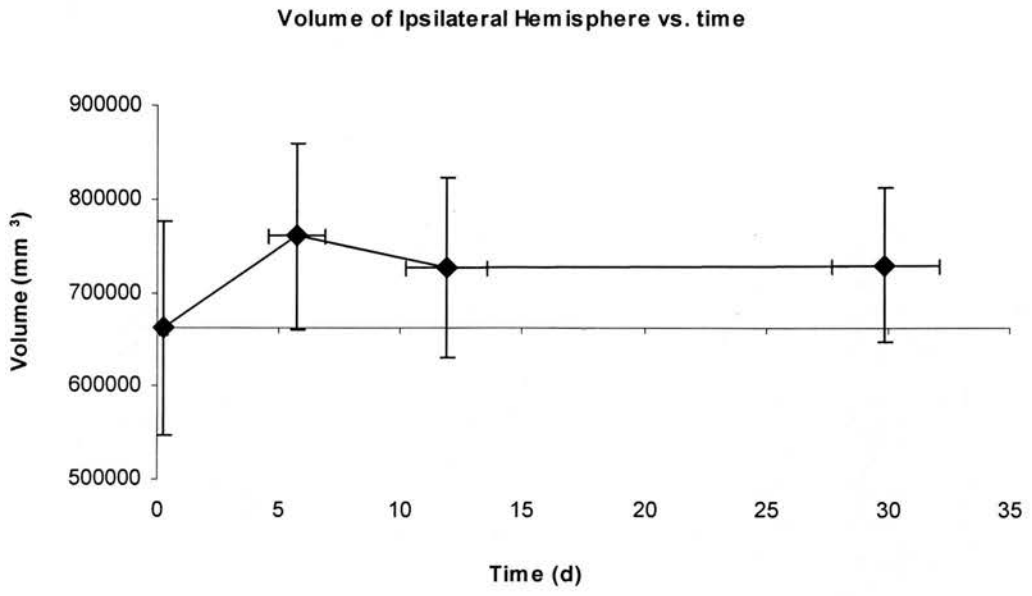

Figure 11.1 Volume (mm^3) of the hemisphere ipsilateral to the ischaemic lesion from baseline to 30 days after stroke onset for the patients analysed with the manual grid-based analysis method (n = 8). Note the x-axis crosses the y-axis at the mean baseline volume. Error bars represent ± 1 SD of the mean.

In depth case study of tissue distortion

One patient (Patient A) from the manual grid analysis with evidence of lesion swelling (Figure 11.2) was chosen to perform a more detailed analysis of localised tissue distortion due to acute lesion swelling using the manual grid-based analysis method.

Methods

A neuroradiologist (JMW), blind to clinical and other imaging details, examined a printout of the axial slice passing through the centre of the visible lesion on DWI at baseline and 4 days after stroke onset and marked 59 standard anatomical landmarks

appropriate to the stroke lesion and location in the brain. These landmarks included the anterior and posterior horns of the lateral ventricles, the genu and splenium of the corpus callosum, the lateral and medial aspects of the Sylvian fissure, and the anteriomedial aspect of the thalamus. The 59 landmarks were then marked on a printout of the patient's scan from 4 days after stroke onset (Figure 11.2). Differences in the location of the landmarks between the baseline and 4 day scans were calculated to assess tissue distortion.

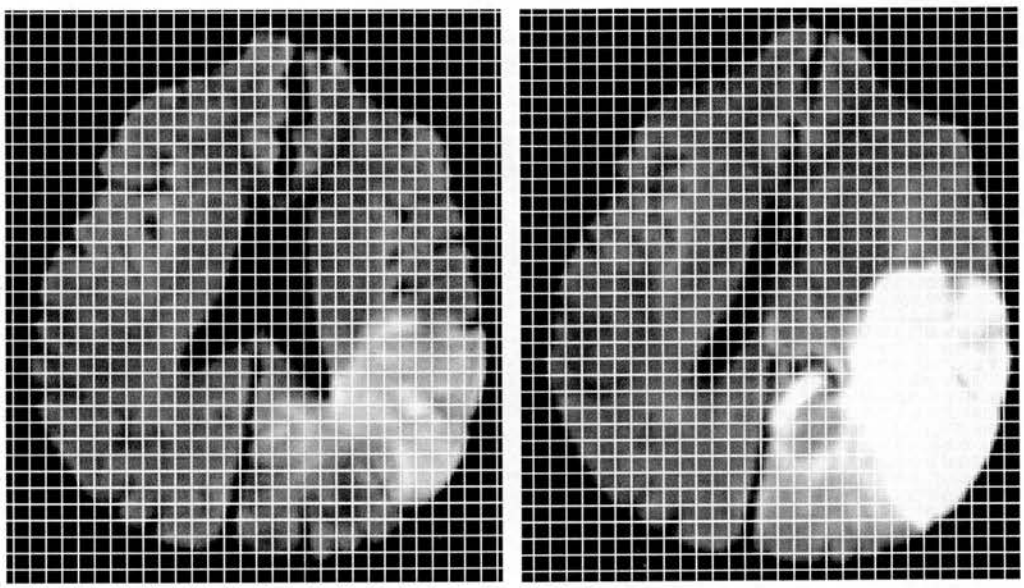

Figure 11.2 DWI at 4 hours and 4 days after stroke onset (in Patient A, with a left hemisphere ischaemic lesion) with overlaid grid as used to score the movement of the 59 anatomical landmarks. Note the swelling at 4 days with the pronounced midline shift and compression of the left lateral ventricle.

Statistical analyses

Movement was quantified by the direction of movement and the number of grid boxes moved, using the centre of the grid boxes as a reference point (grid box = 4.69

mm × 4.69 mm). For example, if the landmark moved one square vertically or laterally, the point was recorded as having moved by 4.69 mm, and a landmark moving both one grid box vertically and one grid box laterally was recorded as having moved by 6.63 mm (= hypotenuse of a right angle triangle where both of the other sides = 4.69 mm), etc. The landmark movements were not normally-distributed (Kolmogorov-Smirnov test $p < 0.01$) so median (and range) landmark movements are reported, however, overall mean (± SD) landmark movements are also reported for comparison with other data.

Results

Patient A's clinical details are listed in Table 8.1. Figure 11.2 shows Patient A's DWI from baseline and 4 days after stroke onset as used for landmark scoring.

Out of the 59 landmarks scored, 53/59 (90%) moved between the baseline and 4 day scan (Table 11.2). The median movement of the 59 landmarks was 9.38 mm (mean ± SD = 8.07 ± 3.95 mm), and the range of landmark movement was 0 – 14.82 mm (Table 11.2).

Table 11.2 Number and % of landmarks by amount of movement (mm) of the 59 landmarks analysed between 4 hours and 4 days after stroke onset in the in-depth study of tissue distortion (Patient A).

Landmark movement (mm)	Number of landmarks	% of landmarks
0	6	10%
4.69	5	9%
6.63	18	31%
9.38	13	22%
10.48	9	15%
14.06	2	3%
14.82	6	10%
Median 9.38	59	100%
Mean 8.07		
SD 3.95		

In Figure 11.2, there is clear evidence of tissue swelling at 4 days after stroke onset, including effacement of the left lateral ventricle and a mild midline shift. Lesion volume measured from this scan could thus misleadingly imply a large increase in lesion extent - the true extent of the lesion in relation to anatomical boundaries does not appear to have greatly increased, rather the apparent increase in lesion extent is likely mostly attributable to tissue swelling (Figure 11.2).

Discussion

The assessment of swelling in ischaemic stroke patients using the manual grid analysis revealed significant tissue distortion between acute and subacute times after stroke onset, and persistence of tissue distortion even in the late stages of ischaemic stroke. Analysis of tissue distortion in a larger group of patients would help to elucidate the effect of swelling and subsequent cavitation on lesion measurement in ischaemic stroke patients at different key stages after stroke onset. However, as discussed in Chapter 8, the manual grid analysis method is time-consuming and prone to observer error, making it impractical for analysis of larger sample sizes. By modifying the SGAT analysis program as discussed in Chapter 9, we developed a 'swell tool' to allow for more efficient analysis of tissue distortion.

Assessing swelling with SGAT 'swell tool'

Methods

A swelling analysis tool ('swell tool') was developed by Dr. P. Armitage as a modification of the SGAT grid analysis program to provide a more efficient method

of measuring the effect of tissue distortion over time caused by swelling and subsequent cavitation after ischaemic stroke. The 'swell tool' (Figure 11.3) allows the user to select and record the location of an anatomical landmark by clicking on it with the mouse. Landmarks can be chosen as appropriate to the individual analysed, i.e. they are not predetermined by the program.

Landmark scoring

Of the 25 patients from the larger cohort of stroke patients as described in Chapter 4 who had MRI data at all five MR scanning time points from baseline to 90 days after stroke onset (and who had not already been analysed with the manual grid-based analysis of tissue distortion), 10 patients were randomly selected for analysis with 'swell tool'.

The axial slice that passed through the centre of each patient's visible lesion on baseline DWI was selected for analysis. Landmarks were scored on the coregistered T_2WI slice on each coregistered scan by a neuroscientist, blind to the clinical and other imaging details. Landmark scoring was performed on T_2WI as it provides better anatomical detail than DWI (Figure 11.3). For each patient, 10 standard anatomical landmarks (midline or ipsilateral to the lesion) were chosen for scoring. These landmarks were distributed throughout the affected hemisphere in order to measure distortion independent of lesion location and extent, and were standard between patients, unless a landmark was not visible on the slice chosen for analysis, in which case another appropriate landmark was chosen. Landmarks included the anterior and posterior horns of the lateral ventricles, the genu and splenium of the corpus callosum, the lateral and medial aspects of the Sylvian fissure, and the anteriomedial aspect of the thalamus (see examples in Figure 11.3).

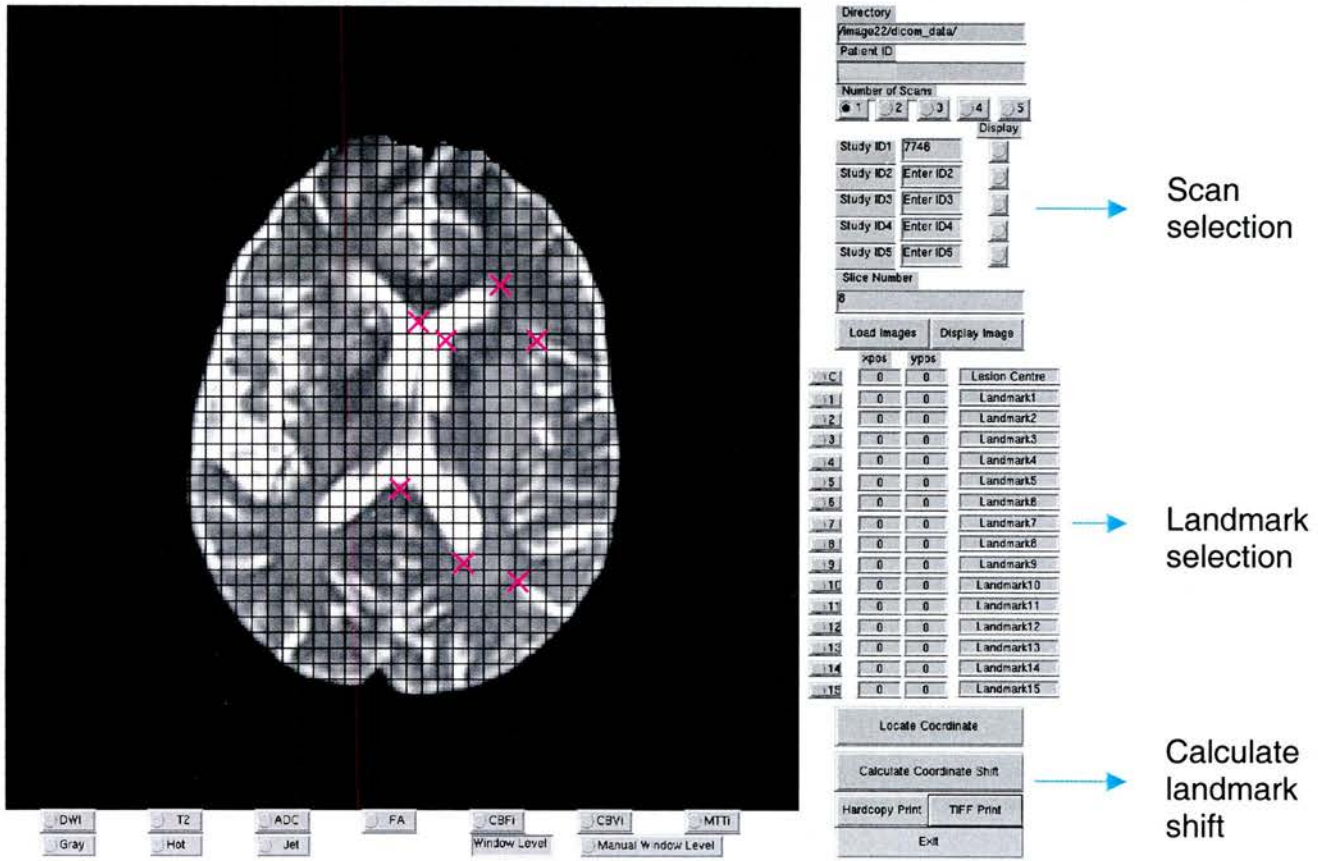

Figure 11.3 The SGAT 'swell tool' program user interface (Patient K with left hemisphere ischaemic lesion on T_2WI at 15 hours after stroke onset). Typical landmarks used in the swelling analyses are marked with ×, and key features of the 'swell tool' are highlighted. SGAT 'swell tool' calculates and records the movement (in mm) of each anatomical landmark scored between each subsequent scan time (i.e. between baseline - 5 days, 5 - 14 days, 14 - 30 days, and 30 - 90 days after stroke onset) and between baseline and 90 days after stroke onset.

Statistical analyses

General patient demographic data were obtained and compared as previously described (Chapter 4).

Landmark movement (in mm, as automatically calculated and recorded by the SGAT 'swell tool') was assessed between each subsequent scan and between baseline and 90 days after stroke onset. The landmark movements were not normally-distributed (Kolmogorov-Smirnov test $p < 0.01$) so median (and range) landmark movements are reported, however, overall mean (± SD) landmark movements are also reported for comparison with other data.

Clinical details were compared between the five patients with the least and greatest degree of landmark movement: age and time from stroke onset to baseline and subsequent MRI with standard t-tests; baseline NIHSS with a Mann-Whitney U-test; and sex, OCSP classifications, and whether the patients were dead or dependent (mRS = 3 – 6) at 90 days after stroke onset or not with Chi-Square (χ^2) tests.

Results

Patient details

Of the 10 patients analysed with 'swell tool': 4/10 (40%) were male, the mean age was 72 years (range: 36 - 91 years), and the mean NIHSS score on admission was 12 (median 10, range: 5 - 23). OCSP classifications: 6/10 (60%) patients had a TACI, and 4/10 (%) patients had a PACI. Mean mRS score at 90 days after stroke onset was 3 (median 3); 6/10 (60%) patients were dependent (mRS = 3 – 5) and 0/10 (0%) patients were dead (mRS = 6). Individual patient details are listed in Table 11.3.

There were no significant demographic or clinical differences between the patients with the least (Patients I, K, N, O and Q) and greatest (Patients J, L, M, P, and R) degree of landmark movement.

Table 11.3 Demographics, clinical details, baseline DWI lesion volume, and MR scan times for the patients analysed with the SGAT 'swell tool' program (n = 10).

Patient	Sex	Age (y)	Baseline NIHSS	OCSP class	Baseline DWI lesion volume (mm^3)	90 d mRS	Time from onset to MRI				
							1 (h)	2 (d)	3 (d)	4 (d)	5 (d)
I	F	91	10	TACI	11118.2	4	11	7	15	30	92
J	F	73	10	TACI	154489.8	3	23	4	14	30	95
K	F	76	11	PACI	13548.3	3	15	4	10	31	90
L	M	64	5	PACI	44701.2	0	21	5	12	33	97
M	F	75	7	PACI	11496.1	0	6	6	13	30	98
N	F	76	12	TACI	27000.0	2	23	5	12	35	91
O	M	83	9	TACI	87077.6	4	7	5	12	35	105
P	M	79	20	TACI	44213.4	5	26	6	10	28	92
Q	F	36	9	PACI	8125.5	2	9	5	12	28	90
R	M	66	23	TACI	86941.4	4	13	6	13	32	94
Mean		72	12		48871.1	3	15 h	5 d	12 d	31 d	94 d
Median			10		35606.7	3					

General patient scan characteristics

Mean (± SD) time from stroke onset to baseline imaging was 15 ± 7 hours, with 1/10 (10%) patients imaged within 6 hours, 3/10 (30%) patients between 6 and 12 hours, and 6/10 (60%) patients between 12 and 24 hours after stroke onset. The 5 day scans were performed at a mean of 5 ± 1 days, the 14 day scans at a mean of 12 ± 2 days, the 30 day scans at a mean of 31 ± 3 days after stroke onset, and the 90 day scans at a mean of 94 ± 5 days after stroke onset.

There were no significant differences in the times from stroke onset to baseline or subsequent MRI between the patients with the least and greatest degree of landmark movement (t-tests all p = NS).

Landmark movement

The median movement of all landmarks in all 10 patients between each of the sequential scan times was 1.88 mm (range: 0 – 22.50 mm; Table 11.4). The maximal median landmark movement between scan times for all 10 patients was 1.88 mm and occurred between three of the analysed time periods; between baseline and 5 days (range: 0 – 10.31 mm), 5 and 14 days (range: 0 – 10.31 mm), and baseline and 90 days after stroke onset (range: 0 – 15.94 mm; Table 11.4). Individual landmark movement was maximal in 3/10 (30%) patients between baseline and 5 days, in 3/10 (30%) patients between 5 and 14 days, and in 1/10 patients between 30 and 90 days after stroke onset (Table 11.4). Note, in 3/10 (30%) patients (Patients I, N, and O), there was an equivalent maximal landmark movement between multiple time points (Table 11.4). The median landmark movement between just baseline and 90 days after stroke onset was 1.88 mm (range: 0 – 15.94 mm; Table 11.4). Although the median movements of landmarks are small, some landmarks move by large degrees (e.g. 22.50 mm), as shown by the range of landmark movements (Table 11.4). As landmarks were specifically not chosen in relation to each lesion to avoid biasing measurement of the effects of tissue distortion, some landmarks were inevitably remote from the individual lesions and thus would experience minimal, if any, degree of movement.

Table 11.4 Median and range of landmark movement (mm) between subsequent scans and between baseline and 90 days after stroke onset for the patients analysed with the SGAT 'swell tool' program (n = 10).

Patient	Mean landmark movement (mm) between scans										Overall median movement between each time point (mm)	
	< 24 h - 5 d		5 - 14 d		14 - 30 d		30 – 90 d		< 24 h – 90 d only			
	median	range	median	range	median	range	median	range	median	range	median	range
I	0.94	0.00 - 3.75	0.94	0.00 - 3.75	0.94	0.00 - 4.69	0.94	0.00 - 3.75	0.94	0.00 - 3.75	1.22	0.00 - 4.69
J	0.94	0.00 - 8.44	3.75	0.94 - 10.31	1.41	0.00 - 13.13	1.41	0.00 - 4.69	3.75	0.00 - 15.94	2.77	0.00 - 13.13
K	0.94	0.00 - 1.88	1.41	0.00 - 7.50	0.94	0.00 - 3.75	0.94	0.00 - 1.88	0.94	0.00 - 7.50	1.36	0.00 - 7.50
L	2.81	0.94 - 7.50	2.34	0.00 - 5.63	1.88	0.00 - 6.56	1.41	0.00 - 9.38	2.34	0.00 - 3.75	2.34	0.00 - 9.38
M	2.34	1.88 - 10.31	2.81	0.94 - 8.44	0.94	0.94 - 2.81	0.94	0.00 - 2.81	1.41	0.94 - 5.63	2.58	0.00 - 10.31
N	1.88	0.94 - 3.75	1.88	0.00 - 3.75	0.94	0.00 - 1.88	1.41	0.94 - 6.56	2.81	0.94 - 6.56	1.83	0.00 - 6.56
O	1.41	0.94 - 4.69	0.94	0.94 - 5.63	1.41	0.94 - 5.63	0.94	0.00 - 3.75	2.34	0.00 - 9.34	1.78	0.00 - 5.63
P	1.41	0.00 - 4.69	1.41	0.00 - 6.56	1.41	0.00 - 5.63	1.88	0.94 - 3.75	1.88	0.00 – 6.56	1.83	0.00 - 6.56
Q	1.88	0.00 - 7.50	0.94	0.00 - 2.81	0.94	0.00 - 2.81	0.94	0.00 - 5.63	1.41	0.00 – 8.44	1.45	0.00 – 7.50
R	6.56	2.81 - 10.31	3.75	0.94 - 7.50	2.81	0.94 - 8.44	1.88	0.94 - 8.44	4.22	0.94 – 14.06	4.17	0.94 - 22.50
Median	1.88	0.00 - 10.31	1.88	0.00 - 10.31	1.69	0.00 - 13.13	0.94	0.00 - 9.38	1.88	0.00 - 15.94	1.88	0.00 - 22.50
Mean	2.66		2.49		1.92		1.81		2.87		2.22	
SD	2.56		2.19		1.99		2.62		2.84		2.34	

Figure 11.4 shows DWI and T_2WI for a patient with mild degrees of landmark movement (Patient N) and a patient with more severe degrees of landmark movement (Patient R). Note the obvious swelling and midline shift of the left lateral ventricle in Patient R at 6 days after stroke onset, and subsequent cavitation at 94 days after stroke onset.

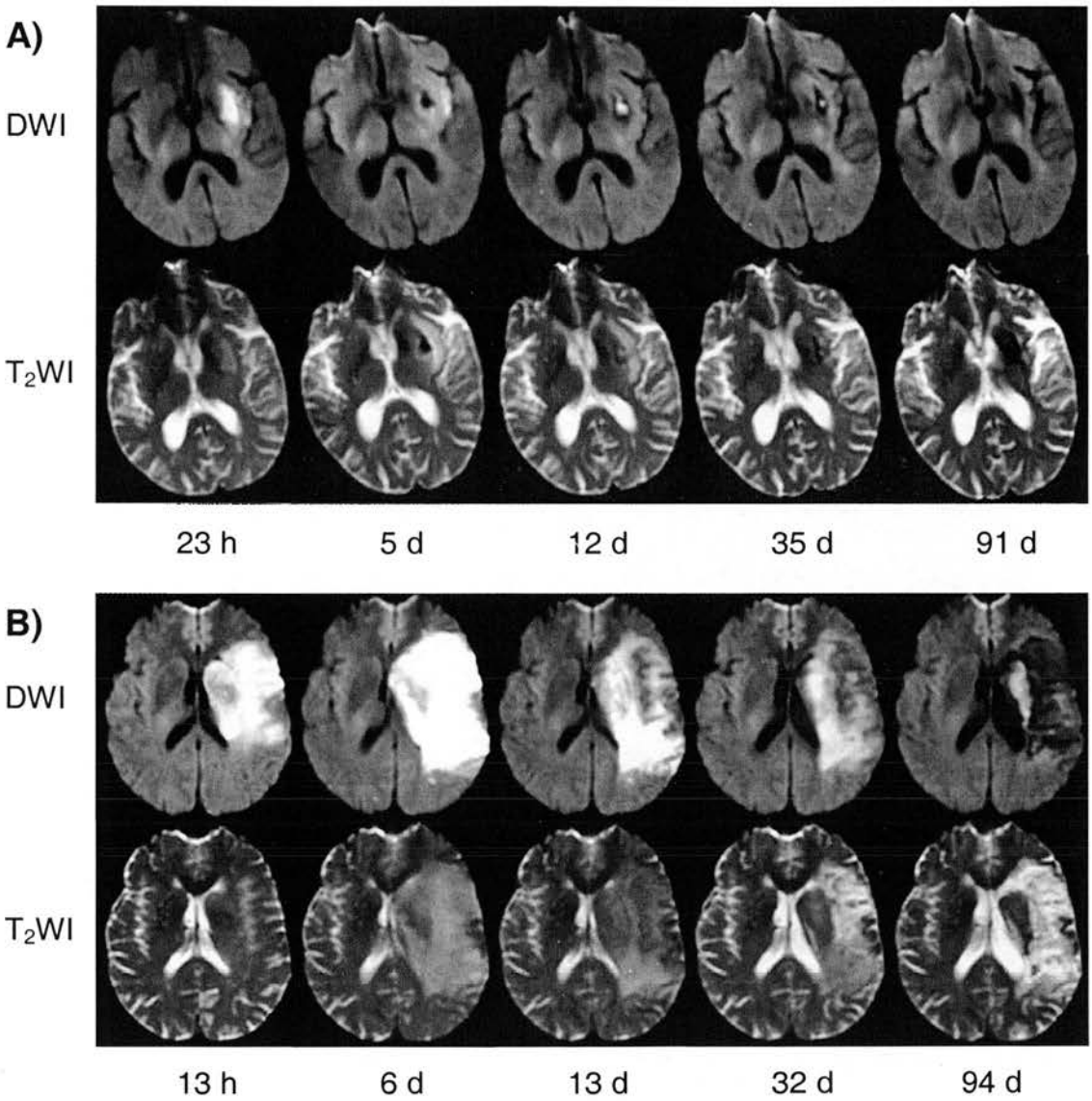

Figure 11.4 DWI and T_2WI from baseline to 90 days after stroke onset for two patients analysed with the SGAT 'swell tool' program. A) Patient N (with left hemisphere ischaemic lesion), with minimal tissue distortion due to swelling; B) Patient R (with left hemisphere ischaemic lesion). with more extensive tissue distortion due to swelling (particularly at 6 days after stroke onset), and *ex vacuo* effect at 94 days after stroke onset.

Discussion

Swelling and subsequent cavitation after ischaemic stroke cause tissue distortion that persists well beyond the acute stages of stroke. This tissue distortion could cause error in lesion volume measurements; swelling could lead to the false conclusion that a lesion had 'grown' (i.e. new tissue had been incorporated into the lesion), and subsequent cavitation could lead to the false conclusion that the lesion had 'shrunk'.

This aim of this analysis was not to determine the time course of swelling and tissue distortion following ischaemic stroke, but rather to highlight the effect of swelling and subsequent tissue cavitation at various key stages after stroke onset when MR data are often collected and lesion volumes are often measured. Tissue distortion was observed between all investigated time points, indicating that the effects of distortion should be considered at all stages of ischaemic stroke.

Although the analyses in this chapter only investigated the effects of tissue distortion on one slice of the brain in each patient, the amount of tissue distortion would likely be greater if assessed on all brain slices and in three dimensions. The SGAT 'swell tool' provided a more efficient method of analysing the movement of landmarks, and could be used in the future to assess the effects of swelling in a larger sample of patients, and could be used to investigate the effects of tissue distortion in other diseases.

What can be done to avoid overestimating lesion extent due to swelling or underestimating lesion extent due tissue cavitation after ischaemic stroke when trying to measure lesion volume? There is one coding system that allows distinction between a true increase in lesion extent and an increase in lesion extent due to swelling[205], however, while this coding system allows an estimation of lesion size, it

does not allow for precise quantification of lesion volume. Measuring lesion extent serially by scoring the presence of ischaemic tissue within a range of pre-defined regions based on anatomical landmarks, as suggested by Yang et al.[78], might minimise the effects of tissue distortion on lesion measurement, however this method is not truly quantitative, has not been validated, is time consuming, and is difficult to implement for smaller lesions and with certain MR sequences. Further modification of the SGAT 'swell tool' might provide a more efficient method of measuring lesions serially with respect to anatomical boundaries that would help to avoid lesion overestimation caused by tissue swelling or underestimation caused by tissue cavitation.

Although it was beyond the scope of this thesis to develop an image processing algorithm that would solve the problem of distinguishing between changes in lesion size due to true changes in lesion extent and changes due to tissue distortion, we have obtained important information about the effects of tissue distortion after ischaemic stroke. This information may help in the future challenge of development of effective image registration algorithms and lesion measurement methods that account for tissue distortion after ischaemic stroke.

12. Summary and conclusions

Summary and final conclusions

The aim of this thesis was to explore the evolution, and issues affecting the analysis of, ischaemic lesions on DWI and PWI from acute to late times after stroke onset, using a large cohort of patients with serial DWI and PWI scanning data. In Chapter 2, we asked:

- what does appearance on DWI mean in terms of underlying tissue state?
- what are the problems with measuring lesions on DWI?
- how do we identify 'tissue at risk' of infarction with MRI?
- are 'thresholds' to predict infarction possible?

What are the strengths and limitations of the analyses in this thesis, what were the results of the analyses of this large patient cohort, and what questions still remain to be answered?

Methodology – strengths and limitations

Patient cohort

This study is one of the largest of serial DWI and PWI in the same patients within discreet MR scanning time points. Despite this, the number of patients available for subgroup analyses in this thesis are lower (e.g. n = 13 – 17 in the analysis of patients whose lesions grew, stayed the same size, or shrank in Chapter 10), reducing the power of the analyses. Patients with all severities of stroke were included, providing a representation of the population of hospital-admitted stroke patients. The patients were recruited prospectively according to standardised criteria and consent was

obtained whenever possible. No patients included in the analyses in this thesis were treated with thrombolysis or any experimental neuroprotective drugs that may have biased the relationship between baseline MR parameters and final infarct extent.

Imaging

The patient cohort were imaged serially, within discreet time points, allowing a more accurate assessment of the temporal evolution of MR parameters in ischaemic stroke patients than past composites of 'snapshot' images from single scans at widely varying times after stroke onset. We also used a measure of outcome (≥ 30 days after stroke onset) that is adequate in terms of lesion evolution, and avoids the problem of 'fogging' as discussed in Chapter 2. Although we aimed to image patients at 90 days after stroke onset, an ideal outcome time, fewer patients were imaged at this late time point. Furthermore, data from 90 days after stroke onset is likely biased by the loss of patients both with more severe strokes who may have died, and patients with less severe strokes who may have made a full recovery and been unwilling to return for this final MR scan. These issues reflect fundamental aspects of the disease of ischaemic stroke – it is simply not possible to image all patients at all time points.

Lesion measurement

We employed a manual method of lesion measurement based on visual estimation of the lesion edge, which most closely represents what is practical in the clinical setting, rather than using a MR parameter (e.g. ADC value) threshold which might reduce observer error. Lesion measurement with thresholds would still require some degree of observer input as discussed in Chapter 2 and as demonstrated for two commonly quoted ADC thresholds in Chapter 5. The heterogeneity of ischaemic lesions is problematic, and the analyses in this thesis suggest that identification of accurate

threshold values to predict lesion infarction would not be possible – ADC, CBF, and MTT values vary too widely to reliably discriminate ischaemic from normal tissue (Chapter 9).

The differentiation of 'definitely abnormal' and 'possibly abnormal' tissue was subjective, however this classification method successfully differentiated tissue with significantly different degrees of underlying damage as identified by ADC and PWI values (Chapters 8 and 10).

The 'index' measures of PWI parameters used in this thesis are not quantitative, however current 'quantitative' measures of PWI parameters are still only estimates that have not been proven superior to 'index' measures.

'Relative' values of DWI and PWI parameters were calculated and compared, making each patient their own 'control' to correct for individual differences and allow for comparison between patients, and between imaging time points.

Analysis of repeated measures data is complex. The statistics used for analysis of the serial data in this thesis are conventional for the analysis of repeated measures data, and despite their drawbacks these methods identified important differences in DWI and PWI parameters between different lesion regions and patient groups; we consider the these findings to be robust.

Development of a novel grid-based lesion analysis method

We developed a novel grid-based lesion analysis method in order to analyse subregions of heterogeneity within ischaemic lesions. The grid-based analysis program allowed rapid and accurate differentiation of regions of heterogeneity on DWI, and underlying differences in ADC, CBF, and MTT values. From these analyses, the DWI signal intensity, the most obvious visible MRI feature in the

clinical setting, closely related to different degrees of pathology, and was least susceptible to observer variation.

What does appearance on DWI mean in terms of underlying tissue state?

The results of the systematic review of DWI and PWI in animal models of ischaemic stroke (Chapter 3) indicated that DWI appearance is linked to underlying tissue state; tissue that is more abnormal ('brighter') on DWI has a greater proportion of dead neurons on histological analysis than tissue that appears less abnormal on DWI. However, the review also highlighted that changes on DWI, for example 'secondary decline', may be caused by glial cells changes rather than being indicative of worsening or resolution of neuronal damage.

The various analyses of the large patient cohort in this thesis also demonstrated that appearance on DWI is indicative of underlying tissue state. The manual grid-based analysis in Chapter 8 and SGAT grid-based analysis in Chapter 10 showed that tissue that appears more abnormal ('brighter') on baseline DWI ('definitely abnormal' tissue) was more abnormal in terms of underlying baseline ADC and PWI values than tissue that appeared less abnormal on baseline DWI ('possibly abnormal' tissue). Furthermore, the degree of abnormality on baseline DWI was related to the degree of late tissue damage as indicated by ADC values from 30 and 90 days after stroke onset. As discussed in Chapter 8, the fate of ischaemic tissue is related to tissue haemodynamics within the first 5 days after stroke onset. Patient age might

also be important; 'possibly abnormal' tissue may be more likely to become more abnormal in older patients, although this may be an artefact of the case mix and small sample size.

What are the problems with measuring lesions on DWI?

Manual lesion measurement has been the most common method of lesion measurement in studies of MRI in ischaemic stroke, and, as discussed in Chapter 2, avoids the problems of lesion heterogeneity and unproven assumptions that are inherent in other less common methods of lesion measurement such as using thresholds of MR parameter values.

Manual lesion measurement

In Chapter 5 we evaluated factors that may affect lesion volume measurement on DWI. Lesion morphology, lesion volume, and observer experience were important factors in lesion measurement: lesions that were ill-defined and > 5000 mm^3 in volume had the greatest degree of volume difference between the two observers. The less experienced observer was more conservative in outlining baseline DWI abnormality, obtaining lesion volumes that were significantly smaller than the more experienced observer.

T_2 'shine through'

Hyperintensity on DWI late after stroke onset has in the past been dismissed as T_2 'shine through'. However, in Chapter 7, we demonstrated that tissue that remains

hyperintense on late DWI was more abnormal in terms of underlying ADC values at ≥ 30 days after stroke onset compared to tissue that is isointense or hypointense, invalidating the common assumption that hyperintensity on late DWI is merely T_2 'shine through' without any underlying pathological basis. The ADC of tissue remaining hyperintense on late DWI was also significantly more decreased relative to normal at baseline, and increased more slowly over time compared to tissue that did not remain hyperintense. There also appeared to be differences in blood flow within the first 5 days after stroke onset between regions that did and did not remain hyperintense on late DWI – peak CBF and nadir MTT values seemed to occur later in regions remaining hyperintense. These differences in ADC, CBF, and MTT values suggest that tissue that remains hyperintense on late DWI experiences a delayed, slower progression through the 'ischaemic cascade'; perhaps this tissue remains viable for longer periods of time, or experiences progressive tissue damage, providing the opportunity to intervene at later stages after stroke onset. Until intervention is attempted, it is difficult to know whether these late differences represent reversible changes or not.

Tissue composition

Tissue that remained hyperintense on late DWI was almost exclusively white matter. As discussed in Chapter 2, there is evidence that grey and white matter may be different in terms of vulnerability to ischaemia, appearance on DWI, and evolution after stroke onset. The results of Chapter 7 imply that there are important differences in the evolution of tissue damage in grey and white matter, and that white matter may be more vulnerable to ischaemia than previously thought.

Lesion swelling

Using the grid-based analysis method, we quantified the effect of tissue distortion caused by swelling and tissue cavitation after ischaemic stroke (Chapter 11). There was significant tissue distortion at key stages in the ischaemic process, from acute to late stages after stroke onset. Swelling may cause lesion overestimation, which may erroneously suggest 'lesion growth', and tissue cavitation may erroneously suggest lesion resolution.

How do we identify 'tissue at risk' of infarction with MRI?

Identifying the 'ischaemic penumbra', or 'tissue at risk' of infarction may provide a target of salvageable tissue in the acute stages of stroke. The 'DWI/PWI mismatch' model is generally considered to represent the 'ischaemic penumbra', and is in fact being used as a selection criterion for trials of thrombolysis. However it is unclear what PWI parameter, if any, best identifies 'tissue at risk' of infarction.

'DWI/PWI mismatch'

In Chapter 6 we demonstrated that neither an acute DWI/CBF or DWI/MTT 'mismatch' correlated with 'lesion growth'. Approximately half of the patients that had 'lesion growth' did not have a 'DWI/PWI mismatch', meaning that patients with potentially salvageable tissue may have been excluded from trials of therapies from which they might have benefited. The presence and timing of reperfusion is more

likely to be correlated with 'lesion growth', however, this has been largely ignored in the focus on the 'DWI/PWI mismatch' in the past few years.

Can we develop thresholds to predict tissue infarction?

Developing thresholds of baseline MR parameter values that predict tissue infarction could reduce observer variation and allow for rapid estimation of the extent of permanently damaged or potentially salvageable ischaemic tissue. However, the underlying heterogeneity of ischaemic lesions means regions of different degrees of tissue damage or vulnerability to ischaemia may be overlooked.

ADC thresholds

Although thresholds of baseline ADC values are frequently used to measure ischaemic lesions, the results of several analyses in this thesis suggest that baseline ADC values are poor discriminators of infarcted tissue, 'tissue at risk' of infarction, and normal tissue. Firstly, animal studies from the systematic review in Chapter 3 demonstrated that initial decreases in ADC are not significantly different between areas of tissue that have almost no neuronal damage and areas that have almost complete neuronal death. Secondly, analysis of interobserver variability of MR parameters in the SGAT grid-based analysis of Chapter 9 showed that ADC values are widely variable – even in the 'contralateral normal' hemisphere where there was little, if any, observer input. Lastly, the results of Chapter 10 demonstrated that baseline ADC values were not significantly different between lesions that grew,

stayed the same size, or shrank between baseline and final imaging. Thus it appears likely that baseline ADC values are too variable and overlap too much between infarcted tissue, 'tissue at risk' of infarction, and normal tissue to provide a clinically useful threshold.

PWI thresholds

Several studies suggest PWI thresholds that might identify tissue infarction and 'tissue at risk' of infarction. Which, if any, PWI parameter best identifies 'tissue at risk' of infarction?

CBF information appears to be most useful in the analysis of ischaemic lesions: the visible baseline CBF abnormality appeared to identify the final lesion (Chapter 6); there were significant differences in baseline CBF values and in the evolution of CBF values over time in tissue with different degrees of tissue damage indicated by underlying ADC values (Chapter 8); and, despite no difference in baseline CBF values, there were significant differences in the subsequent evolution of CBF values between patients whose lesions grew, stayed the same size, or shrank between baseline to final imaging (Chapter 10). In other words, no baseline CBF value identifies whether the lesion will grow or not, but early and pronounced improvement in CBF after baseline is associated with tissue salvage. Furthermore, the analysis of interobserver variation in the SGAT grid-based analysis (Chapter 9) demonstrated that CBF values are widely variable, even in normal tissue.

It is unlikely that MTT values can identify 'tissue at risk' of infarction: visible baseline MTT lesions significantly overestimated the final lesion (Chapter 6);

there were no significant differences in MTT values between regions of different degrees of tissue damage on DWI, or indeed between abnormal and normal tissue

(Chapter 8); there were no significant differences in MTT values between patients whose lesions grew, stayed the same size, or shrank between baseline and final imaging (Chapter 10); and MTT values are widely variable, even in normal tissue (Chapter 9).

The analyses in this thesis suggest that a single threshold of any PWI parameter value would not be able to distinguish between tissue that is infarcted tissue, 'tissue at risk' of infarction, and normal tissue. Outcome is highly dependent on the timing and presence of reperfusion: thresholds of PWI values would be highly time dependent, and would also likely be highly patient dependent.

The future of DWI and PWI in the study of ischaemic stroke

Future studies of MRI in ischaemic stroke, or indeed any imaging study in any disease, should both consider and report observer details, such as observer experience, that might effect lesion measurement. Studies should also use appropriate final time points, allowing for completion of lesion evolution before making 'outcome' measurements.

The conventional statistics for analysis of repeated measures data are not ideal, particularly for MR parameters that exhibit complex and variable evolution over time after stroke onset. Development of more complex statistical models for these serial data could elucidate further important differences between lesion regions and patients.

Although PWI parameters are being used as selection criteria in large clinical trials, there is no consensus on what method of obtaining PWI information and what PWI parameter is best, indeed there are few study groups using similar methods so it will be hard to validate the results of any one group. Discussion of the problems with current PWI methods and development of a standardised approach would clarify the complex changes in PWI parameters after ischaemic stroke.

Future analysis of a larger patient cohort with the grid-based analysis method developed in this thesis would clarify the evolution of DWI and PWI parameters after ischaemic stroke onset, and would elucidate any differences in MR parameters between patients whose lesions grow and do not grow between baseline and final imaging, as well as relationships to other factors such as stroke severity, reperfusion, and other demographic and clinical data. A multiparametric model for identifying 'tissue at risk' could be developed and tested in a large patient cohort. The grid-based analysis method developed in this thesis could also be implemented in the study of other diseases.

The effect of tissue distortion after ischaemic stroke on lesion measurement needs to be addressed, perhaps with use of an automated non-rigid image registration method if one could be developed with the necessary reliability. A method of lesion measurement that avoids lesion overestimation due to swelling and lesion underestimation due to tissue cavitation needs to be developed, perhaps with the use of the grid-based analysis method.

Late hyperintensity on DWI may indicate delayed lesion evolution, meaning there is potentially the opportunity for intervention at later times after stroke onset – this

should be examined further in a larger patient cohort to elucidate underlying pathology and perhaps point to suitable interventions.

The use of the 'DWI/PWI mismatch' as a selection criterion in clinical trials of thrombolysis means about half of patients with potentially salvageable tissue are missing out on potentially beneficial treatments, and this popular approach should thus be reconsidered.

13. References

1. The New Shorter Oxford English Dictionary on Historical Principles. 1993. Clarendon Press, Oxford, U.K.

2. Hankey GJ. Stroke. Your Questions Answered. 2002. Churchill Livingstone, Edinburgh, U.K.

3. Warlow CP, Dennis MS, van Gijn J, Hankey GJ, Sandercock PAG, Bamford JM, Wardlaw JM. Stroke. A practical guide to management. 2nd edition. 2001. Blackwell Science Ltd., Oxford, U.K.

4. Schiller F. Concepts of stroke before and after Virchow. *Medical History*. 1970; 14(2):115-131.

5. Fields WS, Lemak NA. A History of Stroke. Its Recognition and Treatment. 1989. Oxford University Press, New York, U.S.A.

6. Mackay J, Mensah GA. The Atlas of Heart Disease and Stroke. 2004. World Health Organization, Geneva, Switzerland.

7. Astrup J, Symon L, Branston NM, Lassen NA. Cortical evoked potential and extracellular K+ and H+ at critical levels of brain ischemia. *Stroke*. 1977; 8(1):51-57.

8. Hatano S. Experience from a multicentre stroke register: a preliminary report. *Bulletin of the World Health Organisation*. 1976; 54(5):541-553.

9. Hacke W, Hennerici M, Gelmers HJ, Krämer G. Cerebral Ischemia. 1991. Springer-Verlag, Berlin, Germany.

10. WHO MONICA Project. Part IV. Event Registration. MONICA Manual. 1990. World Health Organization, Geneva, Switzerland.

11. Bamford J, Sandercock P, Dennis M, Warlow C, Jones L, McPherson K. A prospective study of acute cerebrovascular disease in the community: the Oxfordshire Community Stroke Project 1981-86. 1. Methodology, demography and incident cases of first-ever stroke. *Journal of Neurology, Neurosurgery, and Psychiatry*. 1988; 51(11):1373-1380.

12. Sudlow CLM, Warlow CP. Comparable studies of the incidence of stroke and its pathological types. Results from an international collaboration. *Stroke*. 1997; 28(3):491-499.

13. Bamford J, Sandercock P, Dennis M, Burn J, Warlow C. Classification and natural history of clinically identifiable subtypes of cerebral infarction. *Lancet*. 1991; 337(8756):1521-1526.

14. Hossman KA. Pathophysiology of cerebral infarction. 107-139. In: Vinken PJ, Bruyn GW, Klawans HL, Toole JF, editors. Vascular Diseases Part 1. 1988. Elsevier Science Publishers, Amsterdam, Netherlands.

15. Fieschi C, Di Piero V, Lenzi GL, Pantano P, Giubilei F, Buttinelli C, Carolei A. Pathophysiology of ischemic brain disease. *Stroke*. 1990; 21(Suppl IV):IV-9-IV-11.

16. Neumann-Haefelin T, Kastrup A, de Crespigny A, Yenari MA, Ringer T, Sun GH, Moseley ME. Serial MRI after transient focal cerebral ischemia in rats: dynamics of tissue injury, blood-brain barrier damage, and edema formation. *Stroke*. 2000; 31(8):1965-1972.

17. Li F, Liu KF, Silva MD, Meng X, Gerriets T, Helmer KG, Fenstermacher JD, Sotak CH, Fisher M. Acute postischemic renormalization of the apparent diffusion coefficient of water is not associated with reversal of astrocytic swelling and neuronal shrinkage in rats. *American Journal of Neuroradiology*. 2002; 23(2):180-188.

18. Li F, Silva MD, Liu KF, Helmer KG, Omae T, Fenstermacher JD, Sotak CH, Fisher M. Secondary decline in apparent diffusion coefficient and neurological outcomes after a short period of focal brain ischemia in rats. *Annals of Neurology*. 2000; 48(2):236-244.

19. Li F, Liu KF, Silva MD, Omae T, Sotak CH, Fenstermacher JD, Fisher M, Hsu CY, Lin W. Transient and permanent resolution of ischemic lesions on diffusion-weighted imaging after brief periods of focal ischemia in rats: correlation with histopathology. *Stroke*. 2000; 31(4):946-954.

20. Pulsinelli W. Pathophysiology of acute ischaemic stroke. *Lancet*. 1992; 339(8792):533-536.

21. Astrup J, Siesjo BK, Symon L. Thresholds in cerebral ischemia - the ischemic penumbra. *Stroke*. 1981; 12(6):723-725.

22. Sandercock P, Willems H. Medical treatment of acute ischaemic stroke. *Lancet*. 1992; 339(8792):537-539.

23. Wardlaw JM, Zoppo G, Yamaguchi T, Berge E. Thrombolysis for acute ischaemic stroke. *The Cochrane Database of Systematic Reviews*. 2003; 3:CD000213.

24. Ribo M, Molina CA, Rovira A, Quintana M, Delgado P, Montaner J, Grive E, Arenillas JF, Alvarez-Sabin J. Safety and Efficacy of Intravenous Tissue Plasminogen Activator Stroke Treatment in the 3- to 6-Hour Window Using

Multimodal Transcranial Doppler/MRI Selection Protocol. *Stroke*. 2005; 36(3):602-606.

25. Liberatore GT, Samson A, Bladin C, Schleuning WD, Medcalf RL. Vampire bat salivary plasminogen activator (desmoteplase): a unique fibrinolytic enzyme that does not promote neurodegeneration. *Stroke*. 2003; 34(2):537-543.

26. Kertesz A, Black SE, Nicholson L, Carr T. The sensitivity and specificity of MRI in stroke. *Neurology*. 1987; 37(10):1580-1585.

27. Fisher M, Sotak CH. Diffusion-weighted MR imaging and ischemic stroke. *American Journal of Neuroradiology*. 1992; 13(4):1103-1105.

28. Moseley ME, Cohen Y, Mintorovitch J, Chileuitt L, Shimizu H, Kucharczyk J, Wendland MF, Weinstein PR. Early detection of regional cerebral ischemia in cats: comparison of diffusion- and T2-weighted MRI and spectroscopy. *Magnetic Resonance in Medicine*. 1990; 14(2):330-346.

29. Gadian DG. NMR and its applications to living systems. 2nd edition. 1995. Oxford University Press, Oxford, U.K.

30. Elster AD, Burdette JH. Questions & Answers in Magnetic Resonance Imaging. 2nd edition. 2001. Mosby, St. Louis, U.S.A.

31. Stejskal EO, Tanner JE. Spin Diffusion Measurements: Spin Echoes in the Presence of a Time-Dependent Field Gradient. *The Journal of Chemical Physics*. 1965; 42(1):288-292.

32. Ulug AM, Beauchamp N, Jr., Bryan RN, van Zijl PC. Absolute quantitation of diffusion constants in human stroke. *Stroke*. 1997; 28(3):483-490.

33. Calamante F, Thomas DL, Pell GS, Wiersma J, Turner R. Measuring cerebral blood flow using magnetic resonance imaging techniques. *Journal of Cerebral Blood Flow & Metabolism*. 1999; 19(7):701-735.

34. Meier P, Zierler KL. On the theory of the indicator-diluted method for measurement of blood flow and volume. *Journal of Applied Physiology*. 1954; 6(12):731-744.

35. Zierler KL. Equations for measuring blood flow by external monitoring of radioisotopes. *Circulation Research*. 1965; 16(4):309-321.

36. Ostergaard L, Weisskoff RM, Chesler DA, Gyldensted C, Rosen BR. High resolution measurement of cerebral blood flow using intravascular tracer bolus

passages. Part I: Mathematical approach and statistical analysis. *Magnetic Resonance in Medicine*. 1996; 36(5):715-725.

37. Calamante F, Gadian DG, Connelly A. Quantification of perfusion using bolus tracking magnetic resonance imaging in stroke: assumptions, limitations, and potential implications for clinical use. *Stroke*. 2002; 33(4):1146-1151.

38. Singer OC, Sitzer M, du Mesnil de Rochemont R, Neumann-Haefelin T. Practical limitations of acute stroke MRI due to patient-related problems. *Neurology*. 2004; 62(10):1848-1849.

39. Hand PJ, Wardlaw JM, Rowat AM, Haisma JA, Lindley RI, Dennis MS. MR brain imaging in patients with acute stroke - feasibility and patient-related difficulties. *Journal of Neurology, Neurosurgery, and Psychiatry*. 2005; 76(11):1525-1527.

40. Fiebach JB, Schellinger PD, Gass A, Kucinski T, Siebler M, Villringer A, Olkers P, Hirsch JG, Heiland S, Wilde P, Jansen O, Rother J, Hacke W, Sartor K (for the Kompetenznetzwerk Schlaganfall B5). Stroke magnetic resonance imaging is accurate in hyperacute intracerebral hemorrhage. A multicenter study on the validity of stroke imaging. *Stroke*. 2004; 35(2):502-507.

41. von Kummer R. MRI: the new gold standard for detecting brain hemorrhage? *Stroke*. 2002; 33(7):1748-1749.

42. Hacke W, Kaste M, Fieschi C, von Kummer R, Davalos A, Meier D, Larrue V, Bluhmki E, Davis S, Donnan G, Schneider D, Diez-Tejedor E, Trouillas P. Randomised double-blind placebo-controlled trial of thrombolytic therapy with intravenous alteplase in acute ischaemic stroke (ECASS II). Second European-Australasian Acute Stroke Study Investigators. *Lancet*. 1998; 352(9136):1245-1251.

43. The National Institute of Neurological Disorders and Stroke rt-PA Stroke Study Group. Tissue plasminogen activator for acute ischemic stroke. *New England Journal of Medicine*. 1995; 333(24):1581-1587.

44. Arnould MC, Grandin CB, Peeters A, Cosnard G, Duprez TP. Comparison of CT and three MR sequences for detecting and categorizing early (48 hours) hemorrhagic transformation in hyperacute ischemic stroke. *American Journal of Neuroradiology*. 2004; 25(6):939-944.

45. Bradley WG, Jr. MR appearance of hemorrhage in the brain. *Radiology*. 1993; 189(1):15-26.

46. Kidwell CS, Chalela JA, Saver JL, Starkman S, Hill MD, Demchuk AM, Butman JA, Patronas N, Alger JR, Latour LL, Luby ML, Baird AE, Leary MC,

Tremwel M, Ovbiagele B, Fredieu A, Suzuki S, Villablanca JP, Davis S, Dunn B, Todd JW, Ezzeddine MA, Haymore J, Lynch JK, Davis L, Warach S. Comparison of MRI and CT for detection of acute intracerebral hemorrhage. *Journal of the American Medical Association*. 2004; 292(15):1823-1830.

47. Patel MR, Edelman RR, Warach S. Detection of hyperacute primary intraparenchymal hemorrhage by magnetic resonance imaging. *Stroke*. 1996; 27(12):2321-2324.

48. Schellinger PD, Jansen O, Fiebach JB, Hacke W, Sartor K. A standardized MRI stroke protocol: comparison with CT in hyperacute intracerebral hemorrhage. *Stroke*. 1999; 30(4):765-768.

49. Yuh WTC, Crain MR, Loes DJ, Greene GM, Ryals TJ, Sato Y. MR imaging of cerebral ischaemia: findings in the first 24 hours. *American Journal of Neuroradiology*. 1991; 12(4):621-629.

50. Bryan RN, Willcott MR, Schneiders NJ. Nuclear magnetic resonance evaluation of stroke. A preliminary report. *Radiology*. 1983; 149(1):189-192.

51. Bryan RN, Levy LM, Whitlow WD, Killian JM, Preziosi TJ, Rosario JA. Diagnosis of acute cerebral infarction: comparison of CT and MR imaging. *American Journal of Neuroradiology*. 1991; 12(4):611-620.

52. Gonzalez RG, Schaefer PW, Buonanno FS, Schwamm LH, Budzik RF, Rordorf G, Wang B, Sorensen AG, Koroshetz WJ. Diffusion-weighted MR imaging: diagnostic accuracy in patients imaged within 6 hours of stroke symptom onset. *Radiology*. 1999; 210(1):155-162.

53. Le Bihan D, Breton D, Lallemand D, Grenier P, Cabanis E, Laval-Jeantet M. MR imaging of intravoxel incoherent motions: application to diffusion and perfusion in neurological disorders. *Radiology*. 1986; 161(2):401-407.

54. Chien D, Buxton RB, Kwong KK, Brady TJ, Rosen BR. MR diffusion imaging of the human brain. *Journal of Computer Assisted Tomography*. 1990; 14(4):514-520.

55. Mintorovitch J, Moseley ME, Chileuitt L, Shimizu H, Cohen Y, Weinstein PR. Comparison of diffusion- and T2-weighted MRI for the early detection of cerebral ischemia and reperfusion in rats. *Magnetic Resonance in Medicine*. 1991; 18(1):39-50.

56. Minematsu K, Li L, Fisher M, Sotak CH, Davis MA, Fiandaca MS. Diffusion-weighted magnetic resonance imaging: rapid and quantitative detection of focal brain ischemia. *Neurology*. 1992; 42(1):235-240.

57. Moseley ME, Kucharczyk J, Mintorovitch J, Cohen Y, Kurhanewicz J, Derugin N, Asgari H, Norman D. Diffusion-weighted MR imaging of acute stroke: correlation with T2-weighted and magnetic susceptibility-enhanced MR imaging in cats. *American Journal of Neuroradiology*. 1990; 11(3):423-429.

58. Moseley ME, Butts K, Yenari MA, Marks M, de Crespigny A. Clinical aspects of DWI. *NMR in Biomedicine*. 1995; 8(7-8):387-396.

59. Warach S, Chien D, Li W, Ronthal M, Edelman RR. Fast magnetic resonance diffusion-weighted imaging of acute human stroke. *Neurology*. 1992; 42(9):1717-1723.

60. Lutsep HL, Albers GW, DeCrespigny A, Kamat GN, Marks MP, Moseley ME. Clinical utility of diffusion-weighted magnetic resonance imaging in the assessment of ischemic stroke. *Annals of Neurology*. 1997; 41(5):574-580.

61. Warach S, Gaa J, Siewert B, Wielopolski P, Edelman RR. Acute human stroke studied by whole brain echo planar diffusion-weighted magnetic resonance imaging. *Annals of Neurology*. 1995; 37(2):231-241.

62. Marks MP, de Crespigny A, Lentz D, Enzmann DR, Albers GW, Moseley ME. Acute and chronic stroke: navigated spin-echo diffusion-weighted MR imaging. *Radiology*. 1996; 199(2):403-408.

63. Albers GW, Lansberg MG, Norbash AM, Tong DC, O'Brien MW, Woolfenden AR, Marks MP, Moseley ME. Yield of diffusion-weighted MRI for detection of potentially relevant findings in stroke patients. *Neurology*. 2000; 54(8):1562-1567.

64. Lansberg MG, Albers GW, Beaulieu C, Marks MP. Comparison of diffusion-weighted MRI and CT in acute stroke. *Neurology*. 2000; 54(8):1557-1561.

65. Fiebach JB, Schellinger PD, Jansen O, Meyer M, Wilde P, Bender J, Schramm P, Juttler E, Oehler J, Hartmann M, Hahnel S, Knauth M, Hacke W, Sartor K. CT and diffusion-weighted MR imaging in randomized order: diffusion- weighted imaging results in higher accuracy and lower interrater variability in the diagnosis of hyperacute ischemic stroke. *Stroke*. 2002; 33(9):2206-2210.

66. Barber PA, Darby DG, Desmond PM, Gerraty RP, Yang Q, Li T, Jolley D, Donnan GA, Tress BM, Davis SM. Identification of major ischemic change: Diffusion-weighted imaging versus computed tomography. *Stroke*. 1999; 30(10):2059-2065.

67. Saur D, Kucinski T, Grzyska U, Eckert B, Eggers C, Niesen W, Schoder V, Zeumer H, Weiller C, Rother J. Sensitivity and interrater agreement of CT and

diffusion-weighted MR imaging in hyperacute stroke. *American Journal of Neuroradiology*. 2003; 24(5):878-885.

68. Welch KM, Windham J, Knight RA, Nagesh V, Hugg JW, Jacobs M, Peck D, Booker P, Dereski MO, Levine SR. A model to predict the histopathology of human stroke using diffusion and T2-weighted magnetic resonance imaging. *Stroke*. 1995; 26(11):1983-1989.

69. Chien D, Kwong KK, Gress DR, Buonanno FS, Buxton RB, Rosen BR. MR diffusion imaging of cerebral infarction in humans. *American Journal of Neuroradiology*. 1992; 13(4):1097-1102.

70. Schlaug G, Siewert B, Benfield A, Edelman RR, Warach S. Time course of the apparent diffusion coefficient (ADC) abnormality in human stroke. *Neurology*. 1997; 49(1):113-119.

71. Burdette JH, Ricci PE, Petitti N, Elster AD. Cerebral infarction: time course of signal intensity changes on diffusion-weighted MR images. *American Journal of Roentgenology*. 1998; 171(3):791-795.

72. Ahlhelm F, Schneider G, Backens M, Reith W, Hagen T. Time course of the apparent diffusion coefficient after cerebral infarction. *European Radiology*. 2002; 12(9):2322-2329.

73. Copen WA, Schwamm LH, Gonzalez RG, Wu O, Harmath CB, Schaefer PW, Koroshetz WJ, Sorensen AG. Ischemic stroke: Effects of etiology and patient age on the time course of the core apparent diffusion coefficient. *Radiology*. 2001; 221(1):27-34.

74. Eastwood JD, Engelter ST, MacFall JF, DeLong DM, Provenzale JM. Quantitative assessment of the time course of infarct signal intensity on diffusion-weighted images. *American Journal of Neuroradiology*. 2003; 24(4):680-687.

75. Helenius J, Soinne L, Salonen O, Kaste M, Tatlisumak T. Leukoaraiosis, ischemic stroke, and normal white matter on diffusion- weighted MRI. *Stroke*. 2002; 33(1):45-50.

76. Lansberg MG, Thijs VN, O'Brien MW, Ali JO, de Crespigny AJ, Tong DC, Moseley ME, Albers GW. Evolution of apparent diffusion coefficient diffusion-weighted, and T2-weighted signal intensity of acute stroke. *American Journal of Neuroradiology*. 2001; 22(4):637-644.

77. Schwamm LH, Koroshetz WJ, Sorensen G, Wang B, Copen WA. Time course of lesion development in patients with acute stroke. Serial diffusion- and

hemodynamic-weighted magnetic resonance imaging. *Stroke*. 1998; 29(11):2268-2276.

78. Yang Q, Tress BM, Barber PA, Desmond PM, Darby DG, Gerraty RP, Li T, Davis SM. Serial study of apparent diffusion coefficient and anisotropy in patients with acute stroke. *Stroke*. 1999; 30(11):2382-2390.

79. Burdette JH, Elster AD, Ricci PE. Acute cerebral infarction: Quantification of spin-density and T2 shine-through phenomena on diffusion-weighted MR images. *Radiology*. 1999; 212(2):333-339.

80. Fiehler J, Knab R, Reichenbach JR, Fitzek C, Weiller C, Rother J. Apparent diffusion coefficient decreases and magnetic resonance imaging perfusion parameters are associated in ischemic tissue of acute stroke patients. *Journal of Cerebral Blood Flow & Metabolism*. 2004; 21(5):577-584.

81. Grandin CB, Duprez TP, Smith AM, Mataigne F, Peeters A, Oppenheim C, Cosnard G. Usefulness of magnetic resonance-derived quantitative measurements of cerebral blood flow and volume in prediction of infarct growth in hyperacute stroke. *Stroke*. 2001; 32(5):1147-1153.

82. Heiss WD, Sobesky J, Hesselmann V. Identifying thresholds for penumbra and irreversible tissue damage. *Stroke*. 2004; 35(11 Suppl 1):2671-2674.

83. Karonen JO, Vanninen RL, Liu Y, Ostergaard L, Kuikka JT. Combined diffusion and perfusion MRI with correlation to single-photon emission CT in acute ischaemic stroke. *Stroke*. 1999; 30(8):1583-1590.

84. Liu Y, Karonen JO, Vanninen RL, Ostergaard L, Roivainen R, Nuutinen J, Perkio J, Kononen M, Hamalainen A, Vanninen EJ, Soimakallio S, Kuikka JT, Aronen HJ. Cerebral hemodynamics in human acute ischemic stroke: a study with diffusion- and perfusion-weighted magnetic resonance imaging and SPECT. *Journal of Cerebral Blood Flow & Metabolism*. 2000; 20(6):910-920.

85. Neumann-Haefelin T, Wittsack H-J, Wenserski F, Siebler M, Seitz RJ. Diffusion- and perfusion-weighted MRI. The DWI/PWI mismatch region in acute stroke. *Stroke*. 1999; 30(8):1591-1597.

86. Perkio J, Soinne L, Ostergaard L, Helenius J, Kangasmaki A, Martinkauppi S, Salonen O, Savolainen S, Kaste M, Tatlisumak T, Aronen HJ. Abnormal Intravoxel Cerebral Blood Flow Heterogeneity in Human Ischemic Stroke Determined by Dynamic Susceptibility Contrast Magnetic Resonance Imaging. *Stroke*. 2004; 36(1):44-49.

87. Rordorf G, Koroshetz WJ, Copen WA, Cramer SC, Schaefer PW, Budzik RF. Regional ischaemia and ischemic injury in patients with acute middle cerebral artery stroke as defined by early diffusion-weighted and perfusion-weighted imaging. *Stroke*. 1998; 29(5):939-943.

88. Schaefer PW, Ozsunar Y, He J, Hamberg LM, Hunter GJ, Sorensen AG, Koroshetz WJ, Gonzalez RG. Assessing Tissue Viability with MR Diffusion and Perfusion Imaging. *American Journal of Neuroradiology*. 2003; 24(3):436-443.

89. Schlaug G, Benfield A, Baird AE, Siewert B, Lovblad KO, Parker RA, Edelman RR, Warach S. The ischemic penumbra: operationally defined by diffusion and perfusion MRI. *Neurology*. 1999; 53(7):1528-1537.

90. Lovblad KO, Baird AE, Schlaug G, Benfield A, Siewert B, Voetsch B, Connor A, Burzynski C, Edelman RR, Warach S. Ischemic lesion volumes in acute stroke by diffusion-weighted magnetic resonance imaging correlate with clinical outcome. *Annals of Neurology*. 1997; 42(2):164-170.

91. Baird AE, Lovblad KO, Dashe JF, Connor A, Burzynski C, Schlaug GS, Staroselskaya I, Edelman RR, Warach S. Clinical correlations of diffusion and perfusion lesion volumes in acute ischemic stroke. *Cerebrovascular Diseases*. 2000; 10(6):441-448.

92. Pereira AC, Doyle VL, Clifton A, Howe FA, Griffiths JR, Brown MM. The transient disappearance of cerebral infarction on T2 weighted MRI. *Clinical Radiology*. 2000; 55(9):725-727.

93. O'Brien P, Sellar RJ, Wardlaw JM. Fogging on T2-weighted MR after acute ischaemic stroke: how often might this occur and what are the implications? *Neuroradiology*. 2004; 46(8):635-641.

94. Kelly PJ, Hedley-Whyte ET, Primavera J, He J, Gonzalez RG. Diffusion MRI in ischemic stroke compared to pathologically verified infarction. *Neurology*. 2001; 56(7):914-920.

95. Knight RA, Dereski MO, Helpern JA, Ordidge RJ, Chopp M. Magnetic resonance imaging assessment of evolving focal cerebral ischemia. Comparison with histopathology in rats. *Stroke*. 1994; 25(6):1252-1261.

96. Baird AE, Dambrosia J, Janket S, Eichbaum Q, Chaves C, Silver B, Barber PA, Parsons M, Darby D, Davis S, Caplan LR, Edelman RE, Warach S. A three-item scale for the early prediction of stroke recovery. *Lancet*. 2001; 357(9274):2095-2099.

97. van Everdingen KJ, van der Grond J, Kappelle LJ, Ramos LM, Mali WP. Diffusion-weighted magnetic resonance imaging in acute stroke. *Stroke*. 1998; 29(9):1783-1790.

98. Warach S. Use of diffusion and perfusion magnetic resonance imaging as a tool in acute stroke clinical trials. *Current Controlled Trials in Cardiovascular Medicine*. 2001; 2(1):38-44.

99. Barber PA, Darby DG, Desmond PM, Yang Q, Gerraty RP, Jolley D. Prediction of stroke outcome with echoplanar perfusion- and diffusion-weighted MRI. *Neurology*. 1998; 51(2):418-426.

100. Baird AE, Benfield A, Schlaug G, Siewert B, Lovblad KO, Edelman RR. Enlargement of human cerebral ischemic lesion volumes measured by diffusion-weighted magnetic resonance imaging. *Annals of Neurology*. 1997; 41(5):581-589.

101. Beaulieu C, de Crespigny A, Tong DC, Moseley ME, Albers GW, Marks MP. Longitudinal magnetic resonance imaging study of perfusion and diffusion in stroke: Evolution of lesion volume and correlation with clinical outcome. *Annals of Neurology*. 1999; 46(4):568-578.

102. Kluytmans M, van Everdingen KJ, Kappelle LJ, Ramos LM, Viergever MA, van der Grond J. Prognostic value of perfusion- and diffusion-weighted MR imaging in first 3 days of stroke. *European Radiology*. 2000; 10(9):1434-1441.

103. Wintermark M, Reichhart M, Cuisenaire O, Maeder P, Thiran JP, Schnyder P, Bogousslavsky J, Meuli R. Comparison of admission perfusion computed tomography and qualitative diffusion- and perfusion-weighted magnetic resonance imaging in acute stroke patients. *Stroke*. 2002; 33(8):2025-2031.

104. Thijs VN, Adami A, Neumann-Haefelin T, Moseley ME, Marks MP, Albers GW. Relationship between severity of MR perfusion deficit and DWI lesion evolution. *Neurology*. 2001; 57(7):1205-1211.

105. Ueda T, Yuh WT, Maley JE, Quets JP, Hahn PY, Magnotta VA. Outcome of acute ischemic lesions evaluated by diffusion and perfusion MR imaging. *American Journal of Neuroradiology*. 1999; 20(6):983-989.

106. Rose SE, Janke AL, Griffin M, Finnigan S, Chalk JB. Improved prediction of final infarct volume using bolus delay-corrected perfusion-weighted MRI: implications for the ischemic penumbra. *Stroke*. 2004; 35(11):2466-2471.

107. Rana AK, Wardlaw JM, Armitage PA, Bastin ME. Apparent diffusion coefficient (ADC) measurements may be more reliable and reproducible than lesion

volume on diffusion-weighted images from patients with acute ischaemic stroke - implications for study design. *Magnetic Resonance Imaging*. 2003; 21(6):617-624.

108. Girot M, Leclerc X, Gauvrit JY, Verdelho A, Pruvo JP, Leys D. Cerebral magnetic resonance imaging within 6 hours of stroke onset: inter- and intra-observer reproducibility. *Cerebrovascular Diseases*. 2003; 16(2):122-127.

109. Sorensen AG, Buonanno FS, Gonzalez RG, Schwamm LH, Lev MH, Huang-Hellinger FR. Hyperacute stroke: evaluation with combined multisection diffusion-weighted and hemodynamically weighted echo-planar MR imaging. *Radiology*. 1996; 199(2):391-401.

110. Neumann-Haefelin T, Wittsack HJ, Fink GR, Wenserski F, Li TQ, Seitz RJ, Siebler RJ, Modder U, Freund HJ. Diffusion- and perfusion-weighted MRI: influence of severe carotid artery stenosis on the DWI/PWI mismatch in acute stroke. *Stroke*. 2000; 31(6):1311-1317.

111. Wittsack HJ, Ritzl A, Fink GR, Wenserski F, Siebler M, Seitz RJ, Modder U, Freund HJ. MR imaging in acute stroke: diffusion-weighted and perfusion imaging parameters for predicting infarct size. *Radiology*. 2002; 222(2):397-403.

112. Tong DC, Yenari MA, Albers GW, O'Brien M, Marks MP, Moseley ME. Correlation of perfusion- and diffusion-weighted MRI with NIHSS score in acute (<6.5 hour) ischemic stroke. *Neurology*. 1998; 50(4):864-870.

113. Guadagno JV, Warburton EA, Jones PS, Fryer TD, Day DJ, Gillard JH, Carpenter TA, Aigbirhio FI, Price CJ, Baron JC. The Diffusion-Weighted Lesion in Acute Stroke: Heterogeneous Patterns of Flow/Metabolism Uncoupling as Assessed by Quantitative Positron Emission Tomography. *Cerebrovascular Diseases*. 2005; 19(4):239-246.

114. Perkins CJ, Kahya E, Roque CT, Roche PE, Newman GC. Fluid-attenuated inversion recovery and diffusion- and perfusion-weighted MRI abnormalities in 117 consecutive patients with stroke symptoms. *Stroke*. 2001; 32(12):2774-2781.

115. Sorensen AG, Copen WA, Ostergaard L, Buonanno FS, Gonzalez RG, Rordorf G, Rosen BR, Schwamm LH, Weisskoff RM, Koroshetz WJ. Hyperacute stroke: simultaneous measurement of relative cerebral blood volume, relative cerebral blood flow, and mean tissue transit time. *Radiology*. 1999; 210(2):519-527.

116. Wu O, Koroshetz WJ, Ostergaard L, Buonanno FS, Copen WA, Gonzalez RG, Rordorf G, Rosen BR, Schwamm LH, Weisskoff RM, Sorensen AG. Predicting tissue outcome in acute human cerebral ischemia using combined diffusion- and perfusion-weighted MR imaging. *Stroke*. 2001; 32(4):933-942.

117. Jacobs MA, Mitsias P, Soltanian-Zadeh H, Santhakumar S, Ghanei A, Hammond R, Peck DJ, Chopp M, Patel S. Multiparametric MRI tissue characterization in clinical stroke with correlation to clinical outcome: part 2. *Stroke*. 2001; 32(4):950-957.

118. Mitsias PD, Jacobs MA, Hammoud R, Pasnoor M, Santhakumar S, Papamitsakis NIH, Soltanian-Zadeh H, Lu M, Chopp M, Patel SC. Multiparametric MRI ISODATA ischemic lesion analysis. Correlation with the clinical neurological deficit and single-parameter MRI techniques. *Stroke*. 2002; 33(12):2839-2844.

119. Bykowski JL, Latour LL, Warach S. More accurate identification of reversible ischemic injury in human stroke by cerebrospinal fluid suppressed diffusion-weighted imaging. *Stroke*. 2004; 35(5):1100-1106.

120. Nagesh V, Welch KM, Windham JP, Patel S, Levine SR, Hearshen D, Peck D, Robbins K, D'Olhaberriague L, Soltanian-Zadeh H, Boska MD. Time course of ADCw changes in ischemic stroke: beyond the human eye! *Stroke*. 1998; 29(9):1778-1782.

121. Marks MP, Tong DC, Beaulieu C, Albers GW, de Crespigny A, Moseley ME. Evaluation of early reperfusion and IV tPA therapy using diffusion- and perfusion-weighted MRI. *Neurology*. 1999; 52(9):1792-1798.

122. Bilgili Y, Unal B. Effect of region of interest on interobserver variance in apparent diffusion coefficient measures. *American Journal of Neuroradiology*. 2004; 25(1):108-111.

123. Desmond PM, Lovell AC, Rawlinson AA, Parsons MW, Barber PA, Yang Q, Li T, Darby DG, Gerraty RP, Davis SM, Tress BM. The value of apparent diffusion coefficient maps in early cerebral ischemia. *American Journal of Neuroradiology*. 2001; 22(7):1260-1267.

124. Koroshetz WJ, Gonzales RG. Imaging stroke in progress: magnetic resonance advances but computed tomography is poised for counterattack. *Annals of Neurology*. 1999; 46(4):556-558.

125. Guadagno JV, Warburton EA, Aigbirhio FI, Smielewski P, Fryer TD, Harding S, Price CJ, Gillard JH, Carpenter TA, Baron JC. Does the acute diffusion-weighted imaging lesion represent penumbra as well as core? A combined quantitative PET/MRI voxel-based study. *Journal of Cerebral Blood Flow & Metabolism*. 2004; 24(11):1249-1254.

126. Coutts SB, Simon JE, Tomanek AI, Barber PA, Chan J, Hudon ME, Mitchell R, Frayne R, Eliasziw M, Buchan AM, Demchuk AM. Reliability of assessing percentage of diffusion-perfusion mismatch. *Stroke*. 2003; 34(7):1681-1685.

127. O'Brien MD. Ischemic cerebral edema. A review. *Stroke*. 1979; 10(6):623-628.

128. Loubinoux I, Volk A, Borredon J, Guirimand S, Tiffon B, Seylaz J, Meric P. Spreading of vasogenic edema and cytotoxic edema assessed by quantitative diffusion and T2 magnetic resonance imaging. *Stroke*. 1997; 28(2):419-426.

129. Wardlaw JM, Dennis MS, Lindley RI, Warlow CP, Sandercock PAG, Sellar R. Does early reperfusion of a cerebral infarct influence cerebral infarct swelling in the acute stage or the final clinical outcome? *Cerebrovascular Diseases*. 1993; 3(2):86-93.

130. Engelter ST, Provenzale JM, Petrella JR, DeLong DM, MacFall JR. The effect of aging on the apparent diffusion coefficient of normal-appearing white matter. *American Journal of Roentgenology*. 2000; 175(2):425-430.

131. Gideon P, Thomsen C, Henriksen O. Increased self-diffusion of brain water in normal aging. *Journal of Magnetic Resonance Imaging*. 1994; 4(2):185-188.

132. Mukherjee P, Bahn MM, McKinstry RC, Shimony JS, Cull TS, Akbudak E, Snyder AZ, Conturo TE. Differences between gray matter and white matter water diffusion in stroke: Diffusion-tensor MR imaging in 12 patients. *Radiology*. 2000; 215(1):211-220.

133. Muñoz-Maniega S, Bastin ME, Armitage PA, Farrall AJ, Hand PJ, Rivers CS, Wardlaw JM. Temporal evolution of water diffusion parameters is different in grey and white matter in human ischaemic stroke. *Journal of Neurology, Neurosurgery, and Psychiatry*. 2004; 75(12):1714-1718.

134. Warach S, Dashe JF, Edelman RR. Clinical outcome in ischaemic stroke predicted by early diffusion-weighted and perfusion magnetic resonance imaging: a preliminary analysis. *Journal of Cerebral Blood Flow & Metabolism*. 1996; 16(1):53-59.

135. Schellinger PD, Fiebach JB, Jansen O, Ringleb PA, Mohr A, Steiner T, Heiland S, Schwab S, Pohlers O, Ryssel H, Orakcioglu B, Sartor K, Hacke W. Stroke magnetic resonance imaging within 6 hours after onset of hyperacute cerebral ischemia. *Annals of Neurology*. 2001; 49(4):460-469.

136. Wardlaw JM, Keir SL, Bastin ME, Armitage PA, Rana AK. Is diffusion imaging appearance an independent predictor of outcome after ischaemic stroke? *Neurology*. 2002; 59(9):1381-1387.

137. Zivin JA. Perfusion-Weighted Imaging/Diffusion-Weighted Imaging Mismatch on MRI Can Now Be Used to Select Patients for Recombinant Tissue Plasminogen Activator Beyond 3 Hours. Con. *Stroke*. 2005; 36(5):1099-1100.

138. Rohl L, Geday J, Ostergaard L, Simonsen CZ, Vestergaard-Poulsen P, Andersen G, Le Bihan D, Gyldensted C. Correlation between diffusion- and perfusion-weighted MRI and neurological deficit measured by the Scandinavian Stroke Scale and Barthel Index in hyperacute subcortical stroke (< or = 6 hours). *Cerebrovascular Diseases*. 2001; 12(3):203-213.

139. Weber J, Mattle HP, Heid O, Remonda L, Schroth G. Diffusion-weighted imaging in ischaemic stroke: a follow-up study. *Neuroradiology*. 2000; 42(3):184-191.

140. Mancuso A, Nimura T, Weinstein PR. Prediction of delayed ischemic injury with diffusion-weighted MRI following temporary middle cerebral artery occlusion in rats. *Brain Research*. 1997; 760(1-2):42-51.

141. Dijkhuizen RM, Knollema S, van der Worp HB, Ter Horst GJ, De Wildt DJ, Berkelbach van der Sprenkel JW, Tulleken KA, Nicolay K. Dynamics of cerebral tissue injury and perfusion after temporary hypoxia-ischemia in the rat: evidence for region-specific sensitivity and delayed damage. *Stroke*. 1998; 29(3):695-704.

142. Fiehler J, Foth M, Kucinski T, Knab R, von Bezold M, Weiller C, Zeumer H, Rother J. Severe ADC decreases do not predict irreversible tissue damage in humans. *Stroke*. 2002; 33(1):79-86.

143. Barber PA, Parsons MW, Desmond PM, Bennett DA, Donnan GA, Tress BM, Davis SM. The use of PWI and DWI measures in the design of "proof-of-concept" stroke trials. *Journal of Neuroimaging*. 2004; 14(2):123-132.

144. Rose SE, Chalk JB, Griffin MP, Janke AL, Chen F, McLachan GJ, Peel D, Zelaya FO, Markus HS, Jones DK, Simmons A, O'Sullivan M, Jarosz JM, Strugnell W, Doddrell DM, Semple J. MRI based diffusion and perfusion predictive model to estimate stroke evolution. *Magnetic Resonance Imaging*. 2001; 19(8):1043-1053.

145. Davis SM, Donnan GA. Using Mismatch on MRI to Select Thrombolytic Responders. An Attractive Hypothesis Awaiting Confirmation. *Stroke*. 2005; 36(5):1100-1101.

146. Sobesky J, Zaro WO, Lehnhardt FG, Hesselmann V, Neveling M, Jacobs A, Heiss WD. Does the Mismatch Match the Penumbra? Magnetic Resonance Imaging and Positron Emission Tomography in Early Ischemic Stroke. *Stroke*. 2005; 36(5):980-985.

147. Parsons MW, Yang Q, Barber PA, Darby DG, Desmond PM, Gerraty RP, Tress BM, Davis SM. Perfusion magnetic resonance imaging maps in hyperacute stroke: relative cerebral blood flow most accurately identifies tissue destined to infarct. *Stroke*. 2001; 32(7):1581-1587.

148. Schellinger PD, Fiebach JB. Perfusion-Weighted Imaging/Diffusion-Weighted Imaging Mismatch on MRI Can Now Be Used to Select Patients for Recombinant Tissue Plasminogen Activator Beyond 3 Hours. Pro. *Stroke*. 2005; 36(5):1098-1101.

149. Butcher K, Parsons M, Baird T, Barber A, Donnan G, Desmond P, Tress B, Davis S. Perfusion thresholds in acute stroke thrombolysis. *Stroke*. 2003; 34(9):2159-2164.

150. Rohl L, Ostergaard L, Simonsen CZ, Vestergaard-Poulsen P, Andersen G, Sakoh M, Le Bihan D, Gyldensted C. Viability thresholds of ischemic penumbra of hyperacute stroke defined by perfusion-weighted MRI and apparent diffusion coefficient. *Stroke*. 2001; 32(5):1140-1146.

151. Barber PA, Davis SM, Darby DG, Desmond PM, Gerraty RP, Yang Q, Jolley, D, Donnan GA, Tress BM. Absent middle cerebral artery flow predicts the presence and evolution of the ischemic penumbra. *Neurology*. 1999; 52(6):1125-1132.

152. Barnett HJM, Mohr JP, Stein BM, Yatsu FM. Stroke. Pathophysiology, Diagnosis, and Management. 3rd edition. 1998. Churchill Livingstone, Philadelphia, U.S.A.

153. Müller TB, Haraldseth O, Jones RA, Sebastiani G, Godtliebsen F, Lindboe CF, Unsgard G. Combined perfusion and diffusion-weighted magnetic resonance imaging in a rat model of reversible middle cerebral artery occlusion. *Stroke*. 1995; 26(3):451-457.

154. Hasegawa Y, Fisher M, Latour LL, Dardzinski BJ, Sotak CH. MRI diffusion mapping of reversible and irreversible ischemic injury in focal brain ischemia. *Neurology*. 1994; 44(8):1484-1490.

155. Rivers CS, Wardlaw JM. What has diffusion imaging in animals told us about diffusion imaging in patients with ischaemic stroke? *Cerebrovascular Diseases*. 2005; 19(5):328-336.

156. Sandercock PAG, Algra A, Anderson C, Bath P, Bereczki D, Berge E, Bowen A, Candelise L, Forster A, Fraser HW, Hankey G, Langhorne P, Lewis S, McInnes A, Prasad K, Thomas B. Stroke Group. About the Cochrane Collaboration (Collaborative Review Groups (CRGs)). *The Cochrane Library*. 2005; 2:STROKE.

157. Paul R, Zhang ZG, Eliceiri BP, Jiang Q, Boccia AD, Zhang RL, Chopp M, Cheresh DA. Src deficiency or blockade of Src activity in mice provides cerebral protection following stroke. *Nature Medicine*. 2001; 7(2):222-227.

158. Xue R, Sawada M, Goto S, Hurn PD, Traystman RJ, van Zijl PC, Mori S. Rapid three-dimensional diffusion MRI facilitates the study of acute stroke in mice. *Magnetic Resonance in Medicine*. 2001; 46(1):183-188.

159. Shi J, Bui JD, Yang SH, He Z, Lucas TH, Buckley DL, Blackband SJ, King MA, Day AL, Simpkins JW. Estrogens decrease reperfusion-associated cortical ischemic damage: an MRI analysis in a transient focal ischemia model. *Stroke*. 2001; 32(4):987-992.

160. Bebarta V, Luyten D, Heard K. Emergency medicine animal research: Does use of randomization and blinding affect the results? *Academic Emergency Medicine*. 2003; 10(6):684-687.

161. Jacobs MA, Knight RA, Soltanian-Zadeh H, Zheng ZG, Goussev AV, Peck DJ, Windham JP, Chopp M. Unsupervised segmentation of multiparameter MRI in experimental cerebral ischemia with comparison to T2, diffusion, and ADC MRI parameters and histopathological validation. *Journal of Magnetic Resonance Imaging*. 2000; 11(4):425-437.

162. Ringer TM, Neumann-Haefelin T, Sobel RA, Moseley ME, Yenari MA. Reversal of early diffusion-weighted magnetic resonance imaging abnormalities does not necessarily reflect tissue salvage in experimental cerebral ischemia. *Stroke*. 2001; 32(10):2362-2369.

163. Detre JA, Zager EL, Alsop DC, Harris VA, Welsh FA. Correlation of diffusion MRI and heat shock protein in a rat embolic stroke model. *Journal of the Neurological Sciences*. 1997; 148(2):163-169.

164. Grohn OH, Lukkarinen JA, Silvennoinen MJ, Pitkanen A, van Zijl PC, Kauppinen RA. Quantitative magnetic resonance imaging assessment of cerebral ischemia in rat using on-resonance T(1) in the rotating frame. *Magnetic Resonance in Medicine*. 1999; 42(2):268-276.

165. Kokubo Y, Matson GB, Liu J, Mancuso A, Kayama T, Sharp FR, Weinstein PR. Correlation between changes in apparent diffusion coefficient and induction of heat shock protein, cell-specific injury marker expression, and protein synthesis reduction on diffusion-weighted magnetic resonance images after temporary focal cerebral ischemia in rats. *Journal of Neurosurgery*. 2002; 96(6):1084-1093.

166. Liu KF, Li F, Tatlisumak T, Garcia JH, Sotak CH, Fisher M, Fenstermacher JD. Regional variations in the apparent diffusion coefficient and the intracellular distribution of water in rat brain during acute focal ischemia. *Stroke*. 2001; 32(8):1897-1905.

167. Müller TB, Haraldseth O, Jones RA, Sebastiani G, Lindboe CF, Unsgard G, Oksendal AN. Perfusion and diffusion-weighted MR imaging for in vivo evaluation of treatment with U74389G in a rat stroke model. *Stroke*. 1995; 26(8):1453-1458.

168. Sutherland GR, Perron JT, Kozlowski P, McCarthy DJ. AR-R15896AR reduces cerebral infarction volumes after focal ischemia in cats. *Neurosurgery*. 2000; 46(3):710-719.

169. Keir SL, Wardlaw JM. Systematic review of diffusion and perfusion imaging in acute ischaemic stroke. *Stroke*. 2000; 31(11):2723-2731.

170. Stroke Therapy Academic Industry Roundtable (STAIR). Recommendations for standards regarding preclinical neuroprotective and restorative drug development. *Stroke*. 1999; 30(12):2752-2758.

171. Brott T, Adams HP, Olinger CP, Marler JR, Barsan WG. Measurements of acute cerebral infarction: a clinical examination scale. *Stroke*. 1989; 20(7):864-870.

172. Rankin J. Cerebral vascular accidents in patients over the age of 60. II. Prognosis. *Scottish Medical Journal*. 1957; 2(5):200-215.

173. Bonita R, Beaglehole R. Recovery of motor function after stroke. *Stroke*. 1988; 19(12):1497-1500.

174. Basser PJ, Pierpaoli C. A simplified method to measure the diffusion tensor from seven MR images. *Magnetic Resonance in Medicine*. 1998; 39(6):928-934.

175. Jenkinson M, Smith S. A global optimisation method for robust affine registration of brain images. *Medical Image Analysis*. 2001; 5(2):143-156.

176. Basser PJ, Mattiello J, LeBihan D. Estimation of the effective self-diffusion tensor from the NMR spin echo. *Journal of Magnetic Resonance Series B*. 1994; 103(3):247-254.

177. Ostergaard L, Sorensen AG, Kwong KK, Weisskoff RM, Gyldensted C, Rosen BR. High resolution measurement of cerebral blood flow using intravascular tracer bolus passages. Part II: Experimental comparison and preliminary results. *Magnetic Resonance in Medicine*. 1996; 36(5):726-736.

178. Oppenheim C, Grandin C, Samson Y, Smith A, Duprez T, Marsault C, Cosnard G. Is there an apparent diffusion coefficient threshold in predicting tissue viability in hyperacute stroke? *Stroke*. 2001; 32(11):2486-2491.

179. Smith AM, Grandin CB, Duprez T, Mataigne F, Cosnard G. Whole brain quantitative CBF, CBV, and MTT measurements using MRI bolus tracking:

implementation and application to data acquired from hyperacute stroke patients. *Journal of Magnetic Resonance Imaging*. 2000; 12(3):400-410.

180. Hacke W, Warach S. Diffusion-weighted MRI as an evolving standard of care in acute stroke. *Neurology*. 2000; 54(8):1548-1549.

181. Bastin ME, Rana AK, Wardlaw JM, Armitage PA, Keir SL. A study of apparent diffusion coefficient of grey and white matter in human ischaemic stroke. *Neuroreport*. 2000; 11(13):2867-2874.

182. Baird AE, Warach S. Magnetic resonance imaging of acute stroke. *Journal of Cerebral Blood Flow & Metabolism*. 1998; 18(6):583-609.

183. Kidwell CS, Alger JR, Saver JL. Beyond mismatch: evolving paradigms in imaging the ischemic penumbra with multimodal magnetic resonance imaging. *Stroke*. 2003; 34(11):2729-2735.

184. Lovblad KO, Wetzel SG, Somon T, Wilhelm K, Mehdizade A, Kelekis A, El Koussy M, El Tatawy S, Bishof M, Schroth G, Perrig S, Lazeyras F, Sztajzel R, Terrier F, Rufenacht D, Delavelle J. Diffusion-weighted MRI in cortical ischaemia. *Neuroradiology*. 2004; 46(3):175-182.

185. Sorensen AG, Wu O, Copen WA, Davis TL, Koroshetz WJ, Reese T, Rosen BR. Human acute cerebral ischaemia: detection of changes in water diffusion anisotropy by using MR imaging. *Radiology*. 1999; 212(3):785-792.

186. Bland JM, Altman DG. Statistical methods for assessing agreement between two methods of clinical measurement. *Lancet*. 1986; 1(8476):307-310.

187. Perkins DO, Wyatt RJ, Bartko JJ. Penny-Wise and Pound-Foolish: The Impact of Measurement Error on Sample Size Requirements in Clinical Trials. *Biological Psychiatry*. 2000; 47(8):762-766.

188. Zivin JA, Holloway RG. Weighing the evidence on DWI: caveat emptor. *Neurology*. 2000; 54(8):1552.

189. Shenkin SD, Bastin ME, MacGillivray TJ, Deary IJ, Starr JM, Wardlaw JM. Childhood and current cognitive function in healthy 80-year-olds: a DT-MRI study. *Neuroreport*. 2003; 14(3):345-349.

190. Davis SM, Donnan GA. Advances in penumbra imaging with MR. *Cerebrovascular Diseases*. 2004; 17(Suppl 3):23-27.

191. Karonen JO, Liu Y, Vanninen RL, Ostergaard L, Kaarina Partanen PL, Vainio PA, Vanninen EJ, Nuutinen J, Roivainen R, Soimakallio S, Kuikka JT, Aronen HJ.

Combined perfusion- and diffusion-weighted MR imaging in acute ischemic stroke during the 1st week: a longitudinal study. *Radiology*. 2000; 217(3):886-894.

192. Teng MM, Cheng HC, Kao YH, Hsu LC, Yeh TC, Hung CS, Wong WJ, Hu HH, Chiang JH, Chang CY. MR perfusion studies of brain for patients with unilateral carotid stenosis or occlusion: evaluation of maps of "time to peak" and "percentage of baseline at peak". *Journal of Computer Assisted Tomography*. 2001; 25(1):121-125.

193. Parsons MW, Barber PA, Chalk J, Darby DG, Rose S, Desmond PM, Gerraty RP, Tress BM, Wright PM, Donnan GA, Davis SM. Diffusion- and perfusion-weighted MRI response to thrombolysis in stroke. *Annals of Neurology*. 2002; 51(1):28-37.

194. Simonsen CZ, Rohl L, Vestergaard-Poulsen P, Gyldensted C, Andersen G, Ostergaard L. Final infarct size after acute stroke: prediction with flow heterogeneity. *Radiology*. 2002; 225(1):269-275.

195. Butcher KS, Parsons M, Macgregor L, Barber PA, Chalk J, Bladin C, Levi C, Kimber T, Schultz D, Fink J, Tress B, Donnan G, Davis S. Refining the Perfusion-Diffusion Mismatch Hypothesis. *Stroke*. 2005; 36(6):1153-1159.

196. Hacke W, Albers G, Al Rawi Y, Bogousslavsky J, Davalos A, Eliasziw M, Fischer M, Furlan A, Kaste M, Lees KR, Soehngen M, Warach S. The Desmoteplase in Acute Ischemic Stroke Trial (DIAS): a phase II MRI-based 9-hour window acute stroke thrombolysis trial with intravenous desmoteplase. *Stroke*. 2005; 36(1):66-73.

197. Barber PA, Davis SM, Infeld B, Baird AE, Donnan GA, Jolley D, Lichtenstein M. Spontaneous reperfusion after ischemic stroke is associated with improved outcome. *Stroke*. 1998; 29(12):2522-2528.

198. Vang C, Dunbabin D, Kilpatrick D. Effects of spontaneous recanalization on functional and electrophysiological recovery in acute ischemic stroke. *Stroke*. 1999; 30(10):2119-2125.

199. Jansen O, Schellinger PD, Fiebach JB, Hacke W, Sartor K. Early recanalisation in acute ischaemic stroke saves tissue at risk defined by MRI. *Lancet*. 1999; 353(9169):2036-2037.

200. Matthews JN, Altman DG, Campbell MJ, Royston P. Analysis of serial measurements in medical research. *British Medical Journal*. 1990; 300(6719):230-235.

201. Geijer B, Lindgren A, Brockstedt S, Stahlberg F, Holtas S. Persistent high signal on diffusion-weighted MRI in the late stages of small cortical and lacunar ischaemic lesions. *Neuroradiology*. 2001; 43(2):115-122.

202. Schulz UGR, Briley D, Meagher T, Molyneux A, Rothwell PM. Abnormalities on diffusion weighted magnetic resonance imaging performed several weeks after a minor stroke or transient ischaemic attack. *Journal of Neurology, Neurosurgery, & Psychiatry*. 2003; 74(6):734-738.

203. Smith SM. Fast robust automated brain extraction. *Human Brain Mapping*. 2002; 17(3):143-155.

204. Zhang Y, Brady M, Smith S. Segmentation of brain MR images through a hidden Markov random field model and the expectation-maximization algorithm. *IEEE Transactions on Medical Imaging*. 2001; 20(1):45-57.

205. Wardlaw JM, Sellar RJ. A simple practical classification of cerebral infarcts on CT and its interobserver reliability. *American Journal of Neuroradiology*. 1994; 15(10):1933-1939.

206. Rueckert D, Frangi AF, Schnabel JA. Automatic construction of 3-D statistical deformation models of the brain using nonrigid registration. *IEEE Transactions on Medical Imaging*. 2003; 22(8):1014-1025.

14. Appendix 1 – Abbreviations

Abbreviation	Definition
ADC	Apparent diffusion coefficient
ADCr	'Relative' ADC
AIF	Arterial input function
ANOVA	Analysis of variance
ASL	Arterial spin labelling
ATP	Adenosine triphosphate
AU	arbitrary units
b	Diffusion weighting value (s/mm^2)
B_0	Magnetic field
BBB	Blood brain barrier
CBF	Cerebral blood flow
CBF_a	'Absolute' cerebral blood flow
CBF_i	'Index' cerebral blood flow
CBFr	'Relative' cerebral blood flow
CBV	Cerebral blood volume
CBV_a	'Absolute' cerebral blood volume
CBV_i	'Index' cerebral blood volume
CBVr	'Relative' cerebral blood volume
CCAO	Common carotid artery occlusion
CSF	Cerebrospinal fluid
CT	Computed tomography
D	Apparent diffusion tensor of water
d	days
DSC	Dynamic susceptibility contrast
DT	Diffusion tensor
DW	Diffusion-weighted
DWI	Diffusion-weighted magnetic resonance imaging
e	Base of natural logarithm (Euler's constant)
EP	Echo planar
FID	Free induction decay
FOV	Field-of-view
GFAP	Glial fibrillary acidic protein
GLM	General linear model
h	hours
H&E	Haematoxylin and eosin
hsp72	Heat shock protein 72
ICAO	Internal carotid artery occlusion
LACI	Lacunar infarct
MAP-2	Microtubule associated protein 2
MCA	Middle cerebral artery

Abbreviation	Definition
MCAO	Middle cerebral artery occlusion
min	minutes
MR	Magnetic resonance
MRI	Magnetic resonance imaging
mRS	Modified Rankin score
MTT	Mean transit time
MTT_a	'Absolute' mean transit time
MTT_i	'Index' mean transit time
MTTr	'Relative' mean transit time
n	Number of subjects
NIHSS	National Institutes of Health Stroke Scale
NS	Not significant ($p > 0.05$)
OCSP	Oxfordshire Community Stroke Project
p	Observed significance level
PACI	Partial anterior circulation infarct
POCI	Posterior circulation infarct
PWI	Perfusion-weighted magnetic resonance imaging
r	Pearson's product moment correlation coefficient
RF	Radiofrequency
rtPA	Recombinant tissue plasminogen activator
S	Signal
S_0	Signal without diffusion effects
SBIRCS	SHEFC Brain Imaging Research Centre for Scotland
SD	Standard deviation
SE	Spin echo
SGAT	SBIRCS grid analysis tool
SHEFC	Scottish Higher Education Funding Council
SI	Signal intensity
T_1W	T_1-weighted
T_2W	T_2-weighted
T_2WI	T_2-weighted imaging
TACI	Total anterior circulation infarct
TE	Time to echo
TIA	Transient ischaemic attack
TR	Repetition time
TTP	Time-to-peak
vs.	Versus
γ	Gyromagnetic ratio
ρ	Spearman's rank correlation coefficient
$\chi 2$	Chi-square test
ω	Larmor frequency
κ	Cohen's reliability coefficient

15. Appendix 2 – Published animal review

Permission to reproduce this paper within this thesis has been granted by the publisher (S. Karger AG, Basel, Switzerland) and the co-author (JMW).

Original Paper

Cerebrovascular Diseases

Cerebrovasc Dis 2005;19:328–336
DOI: 10.1159/000084691

Received: December 8, 2004
Accepted: January 2, 2005
Published online: March 24, 2005

What Has Diffusion Imaging in Animals Told Us about Diffusion Imaging in Patients with Ischaemic Stroke?

Carly S. Rivers Joanna M. Wardlaw

Division of Clinical Neurosciences, Western General Hospital, Edinburgh, UK

Key Words
Ischaemic stroke · Diffusion-weighted imaging · Animal model · Histology · Systematic review

Abstract

Background and Purpose: In acute ischaemic stroke, the amount (and type) of cellular damage underlying diffusion-weighted imaging (DWI) lesion appearances is unclear. We summarized all information from experimental studies of DWI in focal ischaemia models. ***Methods:*** We systematically reviewed all published studies of DWI in focal ischaemic stroke models. We extracted key experimental details to determine correlations between histological features and DWI lesion characteristics. ***Results:*** Of 141 potentially eligible papers (including more than 2,817 animals, mostly rats), details of key experimental methods were unfortunately often omitted. Consistent findings amongst high-quality studies with blinded analysis included: neuronal damage persists or progresses despite early DWI lesion 'normalisation'; the apparent diffusion coefficient is not very sensitive to the amount of neuronal damage; the 'brighter' the DWI lesion, the greater the neuronal damage; and the DWI lesion may reflect glial more than neuronal changes. Anaesthesia and fixation techniques may inadvertently affect these findings. ***Conclusions:*** The relationship between cellular damage and DWI lesion appearance, particularly recovery patterns in reperfusion experiments, remains imprecise. Key experimental details could be reported more completely and consistently. Potential problems from repeated anaesthetics need to be addressed. Early DWI lesion 'recovery' in acute stroke patients may largely reflect glial rather than neuronal 'recovery'.

Copyright © 2005 S. Karger AG, Basel

Introduction

Magnetic resonance (MR) diffusion-weighted (DWI) and perfusion-weighted (PWI) imaging are very sensitive to early ischaemic changes and may distinguish permanently from transiently damaged brain. MR lesion appearance might be a surrogate marker for the effectiveness of new treatments [1]. Although DWI has been available for a decade, the relationship between DWI lesion characteristics and tissue viability remains unclear.

The 'ischaemic cascade' (stages of neuronal damage occurring as cerebral blood flow falls) includes disruption of energy metabolism, ion pump failure, accumulation of intracellular water (cytotoxic oedema [2]), and neuronal and other cell death. DWI is extremely sensitive to water

KARGER
Fax +41 61 306 12 34
E-Mail karger@karger.ch
www.karger.com

© 2005 S. Karger AG, Basel
1015–9770/05/0195–0328$22.00/0

Accessible online at:
www.karger.com/ced

Prof. J.M. Wardlaw
Division of Clinical Neurosciences, Bramwell Dott Building
Western General Hospital, Crewe Road
Edinburgh EH4 2XU (UK)
Tel. +44 131 537 3110, Fax +44 131 332 5150, E-Mail jmw@skull.dcn.ed.ac.uk

molecule movement, showing cytotoxic oedema, and thus very early ischaemic changes [3], within minutes of injury [4]. However the precise point in the ischaemic cascade where lesions become visible on DWI, and the point of no recoverability, is not known. PWI uses the magnetic properties of flowing blood, or the injection of a contrast agent, to visualize where, and to what degree, cerebral blood flow has been compromised [5]. Combining DWI and PWI demonstrates the 'mismatch' which may be potentially salvageable tissue [6]. If correct, the 'mismatch' might help determine the use of potentially dangerous therapies like thrombolysis.

Animal studies of focal ischaemia as a model of human ischaemic stroke provide an opportunity to investigate the pathological cellular changes behind lesion appearance on MR imaging [7]. We aimed to identify information available about the histology underlying DWI and/or PWI lesion appearances in experimental studies, to inform the interpretation of DWI/PWI lesion appearance and tissue salvageability in stroke patients. We therefore performed a systematic review of all experimental studies of DWI and PWI in animal models of focal ischaemic stroke to put together all the information available on the histological correlates of DWI/PWI lesion appearances, and the likelihood of permanent tissue damage or recovery in the presence of particular DWI and/or PWI lesion appearances.

Methods

The methodology of this systematic review was adapted from that used in the Cochrane Database of Systematic Reviews [8]. Although developed for systematic reviews of randomized controlled trials, the same principles apply to, and have been successful in, several systematic reviews of observational and diagnostic studies.

Search Strategy

We searched for published articles of DWI, PWI, or a combination of the two in animal models of ischaemic stroke in the English and non-English language literature on MEDLINE and EMBASE from 1966 to December 31, 2002 (for a complete list of search terms see Appendix 1). To validate the search strategy (in accordance with established systematic review methodology [8]), we also handsearched the last 5 years (January 1998 to December 2002) of the three journals that contributed the most papers from the literature search *(Brain Research, Journal of Cerebral Blood Flow and Metabolism,* and *Stroke)*, and reference lists in all included articles.

Inclusion Criteria

We included studies published in full of DWI, PWI, or a combination of the two, in mammalian models of focal ischaemic stroke, with histology performed within a maximum of 24 h of the last MR imaging. One reviewer identified the abstracts and excluded articles not relevant to this review. Papers were reviewed by the second reviewer and final decisions made by discussion.

Exclusion Criteria

Studies without DWI or PWI, non-mammalian animal models, non-focal models of stroke, global models of ischaemic insult, non-ischaemic models of brain injury, no histology performed, and histology performed more than 24 h after the last MR imaging were excluded as the dynamic nature of ischaemic stroke would prevent histological results being related to imaging appearance after a long time lapse between imaging and histology. Reviews, conference papers, studies only appearing as an abstract and publication of duplicate data were excluded. Where the inclusion of a paper was in question, a consensus was reached between the two reviewers.

Methodological Quality Scoring

A methodological score system was devised to reflect key aspects of the experimental methods used (table 1). Aspects of the animal model, imaging and histology methods, blinding, and method of comparison of histology with imaging were assessed for all papers. These criteria were drawn up in advance of evaluating the identified papers, as part of the primary methodology of the review and in accordance with Cochrane methods [8].

Data Extraction

One reviewer extracted information on the study year, number and type of animals (species, strain, and sex), ischaemia model (method and duration of occlusion, whether permanent or transient), MR imaging (make, model, strength of scanner, scanning protocol), anaesthetic and animal life support in scanner, time from imaging to sacrifice, histological protocol (details of fixation and analysis of histological slices, including how the histological slices were matched to the MR slices for analysis), MR image analysis [lesion volume, apparent diffusion coefficient (ADC) values], blinding of image and histological analysis, and what MR imaging appearance corresponded to what macroscopic or histological state. Data extraction was verified by the second reviewer.

Studies explicitly stating that the analysis of the histological lesion was blind to the DWI lesion and vice versa, and/or studies achieving a quality score of 6 or more were examined further to extract specific information about the relationship between DWI appearance and histological damage. We aimed to undertake analyses of the odds of DWI/PWI appearances being associated with histological features, if such information was available.

Results

The search yielded 1,420 articles on MEDLINE and 1,243 articles on EMBASE, between 1966 and December 2002, totalling 2,663 papers, 943 of which were repeats, leaving an initial database of 1,720 articles. Of these, 1,579 papers were excluded (reasons given in table 2), mostly because the injury model was not appropriate (e.g. global not focal).

Table 1. Methodological quality scoring system

Question	Issue	1/2 mark	1 mark (in addition to 1/2 mark requirements)
1	Animal ischaemia model reproducible?	method (e.g. MCAO) with reference to original procedure	anaesthetic type/dose, surgical procedure, sham/experimental groups described
2	Animal subjects reproducible?	species, strain, sex	source, average weight, housing and feeding details
3	MR imaging reproducible?	make, model and strength of MR scanner, B value	DWI performed in 3 orthogonal directions, method of analysis reproducibly described
4	Histological procedure reproducible?	fixatives and stains listed without specific values and concentrations	concentration of fixatives and stains, size/location brain slices, method of analysis reproducibly described
5	Histological time	<24 h from last imaging session	<6 h from last imaging session
6	Blinding of image analysis to histology	implied (e.g. user independent)	specifically mentioned blinding in text
7	Blinding of histology analysis to imaging	implied (e.g. user independent)	specifically mentioned blinding in text
8	Imaging/histology comparison	'correlated well' on visual exam	in-depth investigation with reproducible methods listed
9	Sub-region analysis	done on either imaging *or* histology	if performed on both imaging and histological results
10	Aim		clear hypothesis with discussion of how results relate

Table 2. Reasons for excluding papers

Reason for exclusion	Papers	%
Not stroke model	649	41.1
Not animal model	99	6.3
Global ischaemia	162	10.2
Inappropriate injury models (e.g., head trauma, aneurysm)	136	8.6
Reviews, letters, conference papers	153	9.7
No DWI	297	18.8
No histology[1]	83	5.3
Total	1,579	100.0

[1] Including 11 papers with histology >24 h from MR imaging.

The remaining 141 studies, concerning the use of DWI, PWI, or the combination of the two, were included. The total number of animals in these papers was over 2,817 (two studies did not report animal numbers [9, 10]), giving a mean of 21 animals per paper (median 18).

General Details of Included Studies

Of the 141 papers, 108 papers (76.7%, n = 2,255, 80.2% of animals) used rats, 19 used cats (13.5%, n = 315, 11.1% of animals), 8 used mice (5.7%, n = 178, 6.3% of animals), 3 used pigs (2.1%, n = 31, 1.1% of animals), 2 used rabbits (1.4%, n = 36, 1.3% of animals), and 1 used non-human primates (0.7%, n = 2, 0.1% of animals) (fig. 1).

A middle cerebral artery occlusion model (MCAO) was used in 130 (92%, n = 2,641) studies, an internal carotid artery occlusion model (ICAO) in 4 (3%, n = 63) studies, a common carotid artery occlusion model (CCAO) in 3 (2%, n = 48) studies, the Rose-Bengal cortex lesion model in 3 (2%, n = 52) studies, and a middle cerebral artery and common carotid artery occlusion model (CCA & MCAO) in 1 (1%, n = 33) study (fig. 2). Some studies sacrificed animals immediately after a period of artery occlusion and therefore were non-reperfusion models; others allowed the animals to survive for some time (from several hours up to 1 week) after a period of occlusion and therefore were reperfusion models.

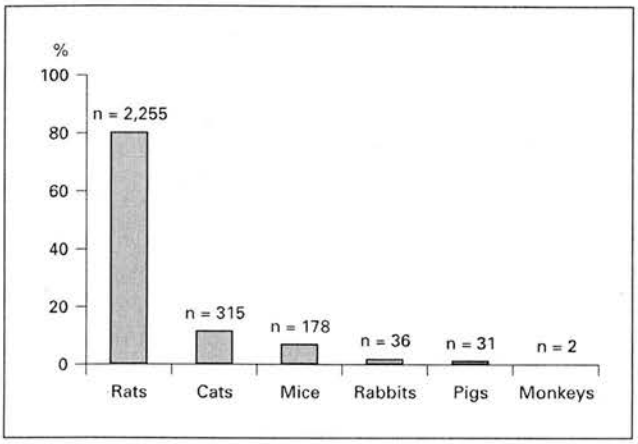

Fig. 1. Percentage of total animals by species in the studies considered in the review. Mean n = 21, median n = 18, total n >2,500.

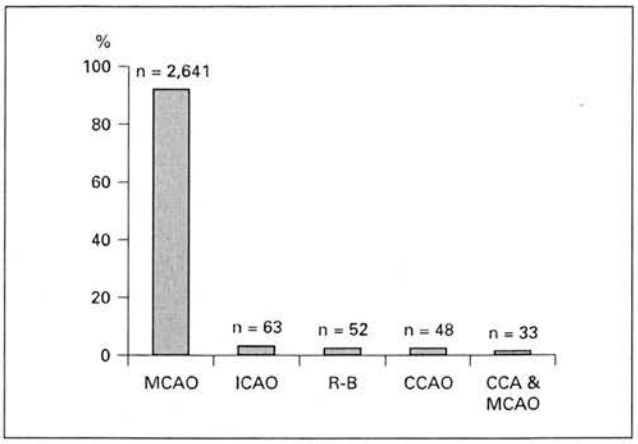

Fig. 2. Percentage of lesion models in the studies in the review. MCAO = Middle cerebral artery occlusion; ICAO = internal carotid artery occlusion; R-B = Rose-Bengal cortex lesion; CCAO = common carotid artery occlusion; CCA & MCAO = common carotid and middle cerebral artery occlusion.

Table 3. Average scores on the methodological quality scoring system

Quality score question	Average score	No. of papers (/141) scoring 1/1	Percent scoring 1/1
1	0.920	119	84.4
2	0.468	13	9.2
3	0.614	34	24.1
4	0.850	102	72.3
5	0.850	98	69.5
6	0.250	9	6.4
7	0.093	9	6.4
8	0.511	31	22.0
9	0.168	18	12.8
10	0.879	124	87.9
Overall (/10)	5.727	0[1]	0[1]

[1] No papers scored 10/10.

Methodological Quality Scores

In general, methods were not reported in detail. The total average score was 5.7 out of 10 (table 3). Only 13 (9.2%) papers adequately described their animal subjects. Basic differences in animal strain and sex can make a large difference in results (e.g. the apparently neuroprotective effects of oestrogen in an MCAO model of ischaemia in female rats [11]). Only 34 (24%) papers adequately described the MR procedures well enough that they might be reproduced. Many papers did not mention measurement of DWI in three orthogonal directions (necessary to obtain reliable and reproducible quantitation of diffusion and ADC values [12]). Few studies mentioned blinding of the image and histological analysis to each other. Failure to employ blinding and randomization in animal studies of drug effects is known to increase the likelihood of a positive result [13]. Over half (n = 71, 51%) of the studies did not mention blinding of any of the analyses at all. Only 3 studies (n = 51 animals, 2% of total animals), explicitly stated that histological analysis was blind to DWI analysis and vice versa [14–16], so we can only be sure that data from 2% of the animals were analyzed completely free of bias. The way in which the MR images and analyses were compared to histological data generally lacked detail, with only 31 (22%) studies comparing DWI and histological slices any further than simply saying they 'correlated well'. However, the precise meaning of a 'good correlation' was not given, and explicit mention of how the histological slices were matched to MR slices for analysis was either lacking or described only as being 'eyeballed' for a best fit. Only 18 (13%) studies examined any sub-regions of the DWI lesion or histological abnormality.

Perfusion values were obtained and reported in some papers, but in such different ways that it was not possible to extract the information as to the relationship between perfusion parameters, DWI and histology in ways that allowed data synthesis. We have therefore concentrated on the DWI and histology correlations.

Table 4. Details of the 13 papers scoring >6 on the methodological scoring system; histological features in regions of imaging abnormality

Study	n	Magnet (T)	Occlusion time	Duration of reperfusion	Imaging results	Histological feature studied	Histological results
Detre et al. [17]	6	4.7	120 min	No reperfusion[1]	'center' ADCr 35% < and 'edge' ADCr 77% < of initial ADC	hsp70 expression	hsp70 +ve in 'penumbra' indicating permanent damage
Grohn et al. [18]	12	4.7	90 min	24 h	DWI normalizes but DWI abnormality recurs at 24 h	scoring % of neuronal damage	tissue dead despite DWI renormalisation
Jacobs et al. [14]	22	2.0	4–8 h 16–24 h 48–168 h	No reperfusion[1]	DWI 14%, ADC 14% lesion volume difference to histology DWI 17%, ADC 14% lesion volume difference to histology DWI 13%, ADC 10% lesion volume difference to histology	inspection of H&E-stained slices for signs of ischaemic damage	DWI lesion < histological lesion, ADC not significantly different ADC and DWI lesions significantly correlated with histology but which was larger (ADC/DWI or histology volume) not specified
Kokubo et al. [19]	6	7.0	60 min	23 h	'caudate' ADCr 65% < initial ADC 'cortex' ADCr 80% < initial ADC	hsp70 expression	hsp70 –ve in caudate – 'irreversible damage' hsp70 +ve in cortex – 'reversible damage'
Li et al. [20]	14	2.0	30 min	12 h	'caudate' ADC 45 × 10^{-5} mm^2/s 'cortex' ADC 46–47 × 10^{-5} mm^2/s	scoring % of neuronal damage	'caudate' >50% neuronal necrosis 'cortex' <10% neuronal necrosis
Li et al. [21]	16	2.0	10 min 30 min	72 h 72 h	ADC initial decrease, then complete recovery ADC decrease, recovery, secondary decrease at 12 h pseudo-normalisation at 24–48 h	scoring % of neuronal damage scoring % of neuronal damage	17% neuronal necrosis in lesion despite ADC renormalisation 95% neuronal necrosis in lesion despite ADC renormalisation
Li et al. [22]	18	2.0	30 min	12 h	ADC 25% < normal at 0–1 h ADC normalizes at 1.5 h ADC 25% < normal at 12 h	scoring % of neuronal damage	92% neuronal necrosis, most astrocytes swollen at 12 h 94% neuronal necrosis, astrocyte disintegration at >12 h
Liu et al. [23]	10	2.0	90 min	No reperfusion[1]	ADC contralateral cortex normal ADC ipsilateral frontoparietal cortex 25% < initial ADC ADC ipsilateral caudoputamen 45% < initial ADC	scoring % of neuronal damage	contralateral cortex – no neuronal damage ipsilateral frontoparietal cortex – 62% of neurons shrunken ipsilateral caudoputamen – 46% of neurons shrunken
Müller et al. [6]	8	2.35	45 min 120 min	70 min 2 h	DWI lesion 9.9% of hemispheric area DWI lesion 29.1% of hemispheric area	size unstained H&E lesion	histological lesion < DWI lesion histological lesion < DWI lesion
Müller et al. [24]	9	2.35	120 min	2 h	15% increase of DWI hyperintensity in 19% of hemisphere area	size unstained H&E lesion	histological lesion (25% of hemisphere) > DWI lesion (19% of hemisphere)
Neumann-Haefelin et al. [15]	19	2.0	30 min 60 min 150 min	7 days	DWI lesion disappeared, but recurred at 24 h DWI lesion disappeared, but recurred at 24 h DWI lesion remained without reversal	size unstained H&E lesion	damage present with no significant difference between groups at 7 days despite different patterns of DWI changes
Ringer et al. [16]	10	2.0	30 min	4.5 h or 7 days	DWI abnormalities reversed at 3–5 h, recurred at 1 day	MAP-2, hsp72, GFAP expression	30% loss MAP-2 reactivity, extensive hsp72 reactivity, 'astrocytes normal' on GFAP
Sutherland et al. [25]	10	7.0	90 min	6.5 h	DWI lesion area > T_2 lesion area	size of unstained H&E lesion	histological lesion < T_2 lesion < DWI lesion

ADC = Apparent diffusion co-efficient; ADCr = ratio of stroke lesion ADC to contralateral normal brain ADC; H&E = haematoxylin and eosin; n = number of animal subjects in study.

[1] No reperfusion = animals were sacrificed at end of occlusion period.

Data Extracted on DWI and Histopathological Lesion Appearances

Although all 141 papers were examined, papers with a quality score of less than 6 consistently did not provide data on the relationship between DWI appearance and histological findings. We therefore focused on papers scoring ≥6, and papers with explicit mention of blinding of histological and imaging analyses. Fifty-one papers achieved a quality score of ≥6, yet only 13 contained information on the relationship of DWI lesion appearance to histology (table 4), including the 3 that explicitly mentioned blinding of image to histological analysis [14–16].

Only 1 of the 13 papers explicitly described the method of aligning histological slices to MR slices for analysis [14]; the other 12 papers either did not mention how histological slices were matched to MR slices or simply used 'eyeballing' to match up the DWI and histology slices.

Three Papers with Explicit Blinding of Histology to DWI and vice versa

As these 3 papers provide the least biased comparison of DWI to histology, we examined their results in detail. Jacobs et al. [14] used a permanent occlusion model in rats, with unsupervised, automated tissue segmentation technique (ISODATA) to outline the lesion from a composite of T_2 and ADC data. The ISODATA regions were co-registered and compared to manually outlined haematoxylin and eosin (H&E)-stained histological slices at acute (4–8 h), sub-acute (16–24 h) and chronic (48–168 h) times after initiating arterial occlusion. Histological damage, including swollen and shrunken neurons, was seen beyond the edges of the 'bright' DWI lesion at 4 h, showing that at acute stages DWI underestimated cortical ischaemia. The ADC image was poorer than the DWI image at assessing tissue damage extent as seen histologically in the acute stage of ischaemia, but better at the sub-acute and chronic stages.

Neumann-Haefelin et al. [15] compared 30 min, 1 h, or 2.5 h of transient ischaemia in rats with histology at 7 days (table 4). DWI and ADC abnormalities reversed after 30 min and 1 h (but not after 2.5 h) of vessel occlusion followed by reperfusion, but reappeared at 24 h in all groups. At 24 h, the DWI lesion in the 30 min and 1-hour occlusion groups was not as extensive as in the 2.5-hour occlusion group. However, an infarct was seen histologically at 7 days with all 3 durations of occlusion, and was not significantly different in area between the groups, even in those with complete initial DWI lesion disappearance after reperfusion.

Ringer et al. [16] used a transient 30-min MCAO model with DWI during, at 3–5 h, 1 day, and 7 days, and neuronal [microtubule associated protein 2 (MAP 2)], astrocytic [glial fibrillary acidic protein (GFAP)], heat shock protein 72 (hsp72), and cresyl violet stained histology at 5 h and 7 days. The DWI abnormalities visible at 30 min reversed at 3–5 h after reperfusion but recurred at 24 h. When the DWI was normal at 5 h, there was a significant decrease in MAP-2 immunoreactivity in 30% of the initial DWI lesion, GFAP was normal, hsp72 staining was extensive and, together with cresyl violet staining extent, corresponded to the initial DWI lesion extent. Hence, the 'normalisation' of the DWI abnormality did not mean that the underlying tissue was normal, as the neurons (MAP-2) showed signs of structural damage and stress. The normal GFAP staining suggested that non neuronal cell components may be capable of more recovery, thereby partially compensating for altered fluid balances and contributing to the apparently 'normal' DWI appearance early after reperfusion.

Remaining Ten Papers Achieving a Quality Score of 6 or More

Although blinding was not explicitly mentioned in these papers, they did achieve high quality scores reflecting good methodological descriptions in other domains. Of these 10 papers, all except 1 ([25], which used cats) used rats. The intraluminal suture method of MCAO was used in all papers except by Detre et al. [17], who used fibrin-rich emboli in the MCA, and Sutherland et al. [25], who used a microaneurysm clip on the MCA. All studies sacrificed the animals immediately after the final MR imaging except 1 ([25], in which the animals were killed 2 h after the start of the final imaging session).

These 13 papers (table 4) also indicated that histological neuronal damage persisted or progressed despite the apparent waxing and waning of the DWI lesion [15, 16, 18]. They further support the observation that the resolution of the early DWI lesion after reperfusion, and its reappearance after 24 h of reperfusion, may be more due to changes in astrocytes and glial cells than a decrease in neuronal damage. A consistent comment in several papers was that it was the astrocytes that swelled (so presumably restricted the extracellular space and water movement to produce the hyperintense DWI/reduced ADC images), while the neurons shrank. Neuronal damage appeared to persist once initiated, while astrocytes swelled or deflated, which may explain the apparent 'normalisation' of the DWI lesion [16, 22, 23]. This suggests that DWI recovery and 'secondary DWI decline' are perhaps not caused by 'secondary injury' to neurons but occur due to the progression of primary damage as astrocytic swelling changes over time [16, 20, 22, 23]. The DWI lesion signal intensity ('brightness') seemed to reflect the amount of neuronal damage – after 90 min of occlusion and 24 h of reperfusion, within the DWI lesion, the more intense the DWI signal, the greater the proportion of dead neurons [18]. Acute ADC values may not be a good determinant for recoverability, as, despite great variability in acute ADC values in 30, 60, and 150 min ischemia groups, in one study all groups showed a similar degree of histological tissue damage at 7 days [15]. Also, in one group, the re-

duction in ADC after 30 min of occlusion was similar in areas with 10% of neurons dead and areas with 50% of neurons dead [20]. However, in another study, the ADC value at the end of vessel occlusion did correspond to the amount of neuronal damage, as larger decreases in the ADC occurring after 90 min occlusion correlated with increasing levels of neuronal damage after 24 h of reperfusion [18]. It was also clear that even short periods (30 min) of transient ischaemia in rats caused permanent damage to neurons [15, 20–22]. Differing degrees of damage were also seen in different parts of the brain for a given duration of occlusion; damage to the striatum (particularly the caudoputamen) was worse than damage to the cortex on both DWI and histological slices [19–22].

Discussion

MR DWI and PWI are popular in ischaemic stroke, and are generally thought of as displaying 'neuronal' damage. However, the exact degree of ischaemic damage at the cellular level demonstrated by DWI and PWI, and the likelihood of recovery, has yet to be determined [26]. Although the proportion of studies that we were able to examine in detail was disappointing (due to missing information or potential bias of results), a consistent message did emerge, suggesting that glial cell ischaemic changes are a major contributor to the initial appearance and subsequent evolution of the DWI lesion. Thus 'neuroprotection' strategies may not be best monitored with DWI, unless it is likely that the drug in question has actions on other cell types. If glial cells are responsible for much of the DWI lesion evolution, then new approaches to avoid adverse events (such as massive infarct swelling) should consider interventions in the glial cell 'ischaemic cascade'.

This review has identified several important correlations between DWI and histology, but many papers were not informative. Possibly some studies were not set up specifically to examine the relationship between DWI and histology; however, the limited description of the animals used, MR imaging, and histological analysis, combined with absence of blinding of image and histological analyses, uncertainties about how the image data were compared to the histology, and little sub-regional analyses, means that there are still many unanswered questions about the relationship of DWI/PWI lesion appearance, the pathophysiological state of the brain, and the chances of tissue recovery. Blinding of image and histology interpretation is vital if biases are to be avoided [13].

We examined all papers but found that papers scoring less than 6 on the quality score did not inform the relationship between DWI and histological appearance. In fact, frustratingly only 13 of 51 (25.5%) of papers scoring ≥ 6/10 had information on the DWI/histology relationship.

Amongst the studies achieving a higher methodological score (table 4), several potentially important methodological points became apparent which might explain some of the differing results. Firstly, several of the studies used repeated anaesthesia with isoflurane [20, 21] or very prolonged periods of anaesthesia – either might contribute to cerebral damage in areas of vulnerable ischemic brain, tipping potentially vulnerable tissue towards permanent damage and making cell damage appear worse for a given ischaemic insult than would actually have been the case without the anaesthetic. Secondly, only one study mentioned taking care to perfuse and fix the tissue for histological analysis in a way that should eliminate artefactual 'dark, shrunken' neurons [23]. How much of the neuronal damage seen on histological examination in other studies could be due, even in part, to fixation effects? Perhaps damage inflicted by tissue fixation could account for some of the inconsistency of results, as for example seen in Müller et al. [6, 24], where the lesion on DWI was larger than the histological lesion in the former, and smaller than the histological lesion in the latter. When comparing histological slices to MR slices, it is important to ensure that the same areas of the brain are being compared. It was not clear in the majority of the papers whether, and how, this histology/MR lesion 'matching' was performed, although 'eyeballing' seemed to be a commonly used method. Thus it is difficult to be sure that the histological slice was the same tissue as that of the 'matched' MR image.

Despite this, several consistent patterns emerged (table 4) with implications for studies in patients. The histological damage persists and progresses despite the DWI lesion waxing and waning, i.e. referring to reappearance of the DWI lesion after a period of normalisation as 'secondary neuronal injury' in human studies is probably not correct in pathophysiological terms. The initial ADC value is not a good index of likely recovery as similar values were obtained from tissue that subsequently mostly recovered as from other areas which were permanently damaged. However, the intensity of the DWI signal ('brightness') does seem to relate to the proportion of damaged neurons – the more abnormal ('brighter') the DWI signal, the greater the proportion of damaged neurons. Also, the DWI hyperintensity more closely identified the extent of abnormal tissue than did the hypointen-

sity on ADC. This is helpful as the intensity of the DWI signal is the most rapidly and easily interpreted information from DWI in the clinical situation – the observer can assess the lesion 'brightness' immediately, so this is probably one of the more clinically useful outputs of this work. Changes in astrocytes, rather than neurons, probably account for much of the DWI lesion waxing and waning – the neurons are said to shrink, while the astrocytes are reported to swell. If DWI signal change is at least in part the result of restricted water movement in the extracellular space, then swollen astrocytes rather than shrunken neurons (assuming the 'shrinkage' is not a fixation artefact) could be the major contributor to DWI hyperintensity/ADC reduction. In rats, even 30 min of ischaemia is lethal to some neurons, and damage (both on DWI and histologically) was worse for a given degree of ischaemia in the caudoputamen than in the cortex.

Where next? Experimental methodology could be more clearly and consistently described; occlusion methods, animals, and MR imaging should be described in a reproducible way, and blinded methods of image and histological analyses are essential to reduce bias. More information is required on how DWI abnormalities relate to cellular changes – at what degree of 'brightness' on DWI does the tissue pass the point of no recovery, and how does this change with increasing time after stroke onset? The Stroke Therapy Academic Industry Roundtable [27] discussion concluded that little animal research done to date 'has translated into effective treatment modalities for stroke in humans'. Perhaps the focus on neurons, both experimentally and in imaging studies, has deflected attention from the contribution of other important cell types to the total burden of damage, and likelihood of recovery, in ischaemic lesions as a whole. Experimental studies may help with translational research to clarify and determine mechanisms for important histopathological-imaging relationships found in clinical studies. However, the methodology should be clearly described, use a model relevant to stroke patients, and take account of important differences in proportions of cerebral cells, and their contributions to the ischaemic process, between animals and humans.

Acknowledgements

C.S.R. is funded by a Royal Society of Edinburgh/Lloyds TSB Foundation studentship. The work was conducted at the SHEFC Brain Imaging Research Centre for Scotland (www.dcn.ed.ac.uk/bic).

Appendix 1: Search Terms

Medline Search Terms:

(1) exp Magnetic Resonance Imaging/
(2) Tomography, X-Ray Computed/
(3) (mri or magnetic resonance or ct scan$ or cat scan$ or compt$ tomography).tw.
(4) 1 or 2 or 3
(5) Disease Models, Animal/
(6) Models, Animal/
(7) ((animal or stroke or experimental) adj5 model$).tw.
(8) experimental stroke.tw.
(9) exp rats/ or exp mice/ or rabbits/ or exp primates/
(10) animal/
(11) exp animals, laboratory/
(12) ((rat or mouse or mice or rabbit or primate) adj5 model$).tw.
(13) or/5–12
(14) Cerebrovascular disorders/
(15) exp Brain ischemia
(16) Carotid artery diseases/ or Carotid artery thrombosis/
(17) exp Cerebrovascular accident/
(18) exp Hypoxia-ischemia, brain/
(19) Cerebral artery diseases/ or Intracranial arterial diseases/
(20) exp 'Intracranial embolism and thrombosis'/
(21) (stroke$ or apoplex$ or cerebral vasc$ or cerebrovasc$ or cva or transient isch?emic attack$ or tia).tw.
(22) ((brain or cerebr$ or cerebell$ or vertebrobasil$ or hemispher$ or intracran$ or intracerebral or infratentorial or supratentorial or middle cerebr$ or mca$ or anterior circulation) adj5 (isch?emi$ or infarct$ or thrombo$ or emboli$ or occlus$ or hypoxi$)).tw.
(23) 14 or 15 or 16 or 17 or 18 or 19 or 20 or 21 or 22
(24) 4 and 13 and 23

Embase Search Terms:

(1) Nuclear magnetic resonance imaging/
(2) exp computer assisted tomography/
(3) (mri or ct scan or cat scan or magnetic resonance or comput$ tomography).tw.
(4) 1 or 2 or 3
(5) exp Cerebrovascular disease/
(6) (stroke$ or cerebrovasc$ or cerebral vasc$ or cva or poststroke or apoplexy or transient isch$ or tia$).tw.
(7) ((brain or cerebr$ or cerebell$ or vertebrobasilar or hemispher$ or intracran$ or intracerebral or infratentorial or supratentorial or mca$ or anterior circulation) adj5 (isch?emi$ or infarct$ or thrombo$ or emboli$ or occlus$ or hypoxi$)).tw.
(8) 5 or 6 or 7
(9) 4 and 8
(10) animal model/ or disease model/
(11) animal/ or animal experiment/ or exp experimental animal/
(12) ((animal or stroke or experimental) adj5 model$).tw.
(13) experimental stroke.tw.
(14) ((rat or mouse or mice or rabbit or cat) adj5 model$).tw.
(15) exp rat/ or exp mouse/ or rabbits/ or exp cat/
(16) or/10–15
(17) 9 and 16

References

1 Barnett HJM, Mohr JP, Stein BM, Yatsu FM: Stroke. Pathophysiology, Diagnosis, and Management, ed 3. Philadelphia, Churchill Livingstone, 1998.

2 Yang Q, Tress BM, Barber PA, Desmond PM, Darby DG, Gerraty RP, Li T, Davis SM: Serial study of apparent diffusion coefficient and anisotropy in patients with acute stroke. Stroke 1999;30:2382–2390.

3 Fisher M, Sotak CH, Minematsu K, Li L: New magnetic resonance techniques for evaluating cerebrovascular disease. Ann Neurol 1992;32: 115–122.

4 Moseley ME, Kucharczyk J, Mintorovitch J, Cohen Y, Kurhanewicz J, Derugin N, Asgari H, Norman D: Diffusion-weighted MR imaging of acute stroke: Correlation with T_2-weighted and magnetic susceptibility-enhanced MR imaging in cats. Am J Neuroradiol 1990;11: 423–429.

5 Latchaw RE, Yonas H, Hunter GJ, Yuh WT, Ueda T, Sorensen AG, Sunshine JL, Biller J, Wechsler L, Higashida R, Hademenos G: Guidelines and recommendations for perfusion imaging in cerebral ischemia: A scientific statement for healthcare professionals by the writing group on perfusion imaging, from the Council on Cardiovascular Radiology of the American Heart Association. Stroke 2003;34: 1084–1104.

6 Müller TB, Haraldseth O, Jones RA, Sebastiani G, Godtliebsen F, Lindboe CF, Unsgard G: Combined perfusion and diffusion-weighted magnetic resonance imaging in a rat model of reversible middle cerebral artery occlusion. Stroke 1995;26:451–457.

7 Hasegawa Y, Fisher M, Latour LL, Dardzinski BJ, Sotak CH: MRI diffusion mapping of reversible and irreversible ischemic injury in focal brain ischemia. Neurology 1994;44:1484–1490.

8 Cochrane Collaboration: Cochrane Stroke Group Search Strategy for Specialized Register. Cochrane Syst Rev 2000:1.

9 Paul R, Zhang ZG, Eliceiri BP, Jiang Q, Boccia AD, Zhang RL, Chopp M, Cheresh DA: Src deficiency or blockade of Src activity in mice provides cerebral protection following stroke. Nat Med 2001;7:222–227.

10 Xue R, Sawada M, Goto S, Hurn PD, Traystman RJ, van Zijl PC, Mori S: Rapid three-dimensional diffusion MRI facilitates the study of acute stroke in mice. Magn Reson Med 2001;46:183–188.

11 Shi J, Bui JD, Yang SH, He Z, Lucas TH, Buckley DL, Blackband SJ, King MA, Day AL, Simpkins JW: Estrogens decrease reperfusion-associated cortical ischemic damage: An MRI analysis in a transient focal ischemia model. Stroke 2001;32:987–992.

12 Ulug AM, Beauchamp N Jr, Bryan RN van, Zijl PC: Absolute quantitation of diffusion constants in human stroke. Stroke 1997;28: 483–490.

13 Bebarta V, Luyten D, Heard K: Emergency medicine animal research: Does use of randomization and blinding affect the results? Acad Emerg Med 2003;10:684–687.

14 Jacobs MA, Knight RA, Soltanian-Zadeh H, Zheng ZG, Goussev AV, Peck DJ, Windham JP, Chopp M: Unsupervised segmentation of multiparameter MRI in experimental cerebral ischemia with comparison to T_2, diffusion, and ADC MRI parameters and histopathological validation. J Magn Reson Imaging 2000;11: 425–437.

15 Neumann-Haefelin T, Kastrup A, de Crespigny A, Yenari MA, Ringer T, Sun GH, Moseley ME: Serial MRI after transient focal cerebral ischemia in rats: Dynamics of tissue injury, blood-brain barrier damage, and edema formation. Stroke 2000;31:1965–1972.

16 Ringer TM, Neumann-Haefelin T, Sobel RA, Moseley ME, Yenari MA: Reversal of early diffusion-weighted magnetic resonance imaging abnormalities does not necessarily reflect tissue salvage in experimental cerebral ischemia. Stroke 2001;32:2362–2369.

17 Detre JA, Zager EL, Alsop DC, Harris VA, Welsh FA: Correlation of diffusion MRI and heat shock protein in a rat embolic stroke model. J Neurol Sci 1997;148:163–169.

18 Grohn OH, Lukkarinen JA, Silvennoinen MJ, Pitkanen A, van Zijl PC, Kauppinen RA: Quantitative magnetic resonance imaging assessment of cerebral ischemia in rat using on-resonance T(1) in the rotating frame. Magn Reson Med 1999;42:268–276.

19 Kokubo Y, Matson GB, Liu J, Mancuso A, Kayama T, Sharp FR, Weinstein PR: Correlation between changes in apparent diffusion coefficient and induction of heat shock protein, cell-specific injury marker expression, and protein synthesis reduction on diffusion-weighted magnetic resonance images after temporary focal cerebral ischemia in rats. J Neurosurg 2002; 96:1084–1093.

20 Li F, Silva MD, Liu KF, Helmer KG, Omae T, Fenstermacher JD, Sotak CH, Fisher M: Secondary decline in apparent diffusion coefficient and neurological outcomes after a short period of focal brain ischemia in rats. Ann Neurol 2000;48:236–244.

21 Li F, Liu KF, Silva MD, Omae T, Sotak CH, Fenstermacher JD, Fisher M, Hsu CY, Lin W: Transient and permanent resolution of ischemic lesions on diffusion-weighted imaging after brief periods of focal ischemia in rats: Correlation with histopathology. Stroke 2000;31: 946–954.

22 Li F, Liu KF, Silva MD, Meng X, Gerriets T, Helmer KG, Fenstermacher JD, Sotak CH, Fisher M: Acute postischemic renormalisation of the apparent diffusion coefficient of water is not associated with reversal of astrocytic swelling and neuronal shrinkage in rats. Am J Neuroradiol 2002;23:180–188.

23 Liu KF, Li F, Tatlisumak T, Garcia JH, Sotak CH, Fisher M, Fenstermacher JD: Regional variations in the apparent diffusion coefficient and the intracellular distribution of water in rat brain during acute focal ischemia. Stroke 2001; 32:1897–1905.

24 Müller TB, Haraldseth O, Jones RA, Sebastiani G, Lindboe CF, Unsgard G, Oksendal AN: Perfusion and diffusion-weighted MR imaging for in vivo evaluation of treatment with U74389G in a rat stroke model. Stroke 1995; 26:1453–1458.

25 Sutherland GR, Perron JT, Kozlowski P, McCarthy DJ: AR-R15896AR reduces cerebral infarction volumes after focal ischemia in cats. Neurosurgery 2000;46:710–719.

26 Keir SL, Wardlaw JM: Systematic review of diffusion and perfusion imaging in acute ischaemic stroke. Stroke 2000;31:2723–2731.

27 Stroke Therapy Academic Industry Roundtable (STAIR). Recommendations for standards regarding preclinical neuroprotective and restorative drug development. Stroke 1999;30: 2752–2758.